

Winter 1992

Diapycnal Mixing and Mass Transfer in Western Boundary Currents

Jose Luis Pelegri Llopart
Old Dominion University

Follow this and additional works at: https://digitalcommons.odu.edu/oeas_etds



Part of the [Oceanography Commons](#)

Recommended Citation

Llopart, Jose L.. "Diapycnal Mixing and Mass Transfer in Western Boundary Currents" (1992). Doctor of Philosophy (PhD), Dissertation, Ocean & Earth Sciences, Old Dominion University, DOI: 10.25777/mk4h-my81

https://digitalcommons.odu.edu/oeas_etds/145

This Dissertation is brought to you for free and open access by the Ocean & Earth Sciences at ODU Digital Commons. It has been accepted for inclusion in OES Theses and Dissertations by an authorized administrator of ODU Digital Commons. For more information, please contact digitalcommons@odu.edu.

DIAPYCNAL MIXING AND MASS TRANSFER
IN WESTERN BOUNDARY CURRENTS

by

José Luis Pelegrí Llopart

M.Sc., December 1984, Oregon State University, Corvallis, U.S.A.

M.Sc., June 1980, University of Wales, Bangor, Great Britain

Licenciatura, June 1978, Universidad Simón Bolívar, Caracas, Venezuela

A Dissertation submitted to the Faculty of
Old Dominion University in Partial Fulfillment of the
Requirement for the Degree of

DOCTOR OF PHILOSOPHY

OCEANOGRAPHY

OLD DOMINION UNIVERSITY

December, 1992

Approved by:

Gabriel T. Csanady (Director)

Larry P. Atkinson

John M. Bane

A. D. Kirwan, Jr.

Abstract

DIAPYCNAL MIXING AND MASS TRANSFER IN WESTERN BOUNDARY CURRENTS

José Luis Pelegrí Llopart
Old Dominion University, 1992
Director: Prof. Gabriel T. Csanady

The distribution of nutrient flux in five sections across the Gulf Stream (from the Florida Straits to $35^{\circ}W$) is characterized by an intense core, centered at the depth of the $26.8 \sigma_t$ isopycnal surface. This 'Nutrient Stream' transports nutrients of $O(10^3 \text{ kmol s}^{-1})$ of nitrate and proportional amounts of other nutrients. Water mass and nutrient balances of nine isopycnal layers reveal significant diapycnal mixing between upper-thermocline and surface waters in the sector of the Stream between the Florida Straits and the Mid-Atlantic Bight. A two-box model of the nutrient-depleted surface layers ($\sigma_t < 26.8$) and the nutrient-rich thermocline layers ($26.8 < \sigma_t < 27.5$) shows upward one-way transfer and two-way exchange, both at a rate at about $1.6 \text{ m}^2 \text{ s}^{-1}$ per unit length of the Stream.

We use isopycnic coordinates to analyze a hydrographic section across the Gulf Stream off the Mid-Atlantic Bight. The analysis shows that the Nutrient Stream is characterized by low Richardson numbers, matched by a signature of mixing in the nutrient distribution on isopycnal layers. Analysis of the Jacobian, $J = dz/d\rho$ (with z the depth and ρ the potential density), total vorticity and

potential vorticity fields, shows that this region has low Jacobians associated with high potential vorticity values, as required theoretically for the case of dominant diapycnal mixing. The diapycnal velocity is calculated from the vertical gradient of the Reynolds density flux, this parameterized as density eddy diffusivity divided by the Jacobian. Regions of large negative diapycnal gradients of the diapycnal velocity coincide with the location of the low Jacobians, suggesting that diapycnal mixing is the consequence of frontogenetically produced anomalies.

Fine-scale details of the density distribution in the Nutrient Stream show a 'staircase' structure. We propose a simple model to account for mixed-layer formation in previously stratified regions, once the Richardson number becomes subcritical. Our time scale estimate for the duration of mixing events is of only a few hours. Such events are possibly triggered by enhanced diapycnal gradients of the horizontal velocities in strongly stratified regions, during frontogenesis in Gulf Stream meanders. This process appears responsible for two-way exchange in the Nutrient Stream.

a Laura, Ana y Mónica

Acknowledgements

*I thank the Lord, because he is good,
because his love lasts forever.*

Psalm 136

These years at the Oceanography Department of ODU have been a fulfilling experience. They have meant numerous trials, errors and achievements, both in the personal and scientific dimensions. They have taught me that science, as well as humanity, must be searched with endurance, serenity and joy. Endurance to overcome never-ending errors, serenity to think, and joy to appreciate not only the final achievements but also the whole process of learning. I could not have endured these years, and this work, without the unselfish help of many people, and I'm delighted to acknowledge them.

During the last four years, Gabe Csanady has been a continuous example in the enjoyment of science and life. Gabe first gave me the opportunity to come to ODU, and then guided me, with the full meaning of this word. His physical insight became evident from our very first meeting, when he advised me to look at the nutrient transport by the Gulf Stream. Rather than concentrating on the mathematics, Gabe has always suggested directions of research and has emphasized the physics imbedded in a problem. He has appreciated and encouraged each of my small scientific triumphs and warned me about my misdirections. He has never pressed me for quick results, rather he has been extremely patient and has taught me to search through mature understanding. For all these reasons, for teaching me how to do independent research and for the enjoyable and fruitful experience of working together, I am now happy to thank Gabe. I also want to sincerely thank Joyce Csanady, for the appreciation she has shown to me, my wife and children, from the very beginning she made us part of her family. Joyce and Gabe Csanady have always been very kind to me and my family, and they have made me feel that I am not only their student, but also their friend.

I feel very lucky to have had a number of excellent people and scientists in my committee and as teachers. Denny Kirwan has been a model of respect towards the people around him, specially his students, and a scientist with the highest standards of excellence. Larry Atkinson is a genuine educator, always finding time and ideas to share. John Klinck has renovated my faith in numerical modelers, preaching that numerical methods must go by the hand of physics, and he himself has been a model of friendship and availability. I want to thank them all for their support and encouragement.

I am indebted to Peter Hamilton for making available the MASAR data, which I started looking shortly after my arrival to ODU, and to Mike McCartney for letting me use the data from five oceanographic sections across the Gulf Stream, which became the base of the data analysis in this dissertation. I am thankful to John Bane for letting me use his 1979 AXBT data off the North Carolina coast. Looking at these data helped me develop some of the hypotheses discussed in this work, which I plan to pursue in the next future. I also want to thank him for accepting to be part of my dissertation committee. I am grateful to Nick Fofonoff and Tom Rossby for providing me with additional data sets, which I have not yet been able to analyze. I also wish to thank Ruth Curry, Sara Haines, Steve Lockhart and Sandy Fontana, whom were involved in making available the above data sets. I am grateful to Jenifer Clark for providing the processed satellite images.

I thank Andras Kapolnai and John Moisan for listening to my confusions and sparkling fruitful ideas, and to Wayne Schroll, Bill Chandler and Peter Becker for their unconditional help with the computer system. I also thank Eileen Hofmann, William Dunstan, Jack Ludwick, Greg Cutter, Tony Provenzano, Ron Johnson, Jim Churchill, Ana Martins, Scott Condie, Eiichi Oka, Bill Indest, Julie McClean, Cisco Werner and Randy Watts, for their help at several stages during these years.

I am obliged to the staff of the Oceanography Department, Faye Carrington, Billie Fedyszyn, and Karen Calogrides, and specially to the staff at CCPO, Karal Gregory, Carole Hannah, Beverly Mitchels and Julie Rea, for their help in all those details that are so important. I also want to thank Sue Cooke and Don Emminger from the Graphics Department, for skillfully drawing a number of schematic figures and adapting several figures from other publications.

I am thankful to all my past and present fellow students, in particular those at CCPO, for their constant sharing of experiences and hopes. Being among them, participating in their enthusiasm, has been the basis to develop my esteem for ODU and my passion for Oceanography. They are what make the Oceanography Department and the CCPO such a special place.

I express my gratitude to my friends and family in Venezuela and Spain, for their continuous support and prayers. To my parents, for being always where I needed them, and to my brothers, for staying together despite the distances.

Finally, I thank my wife, Mónica, for her supporting love and strength, for her endurance to all the difficulties, and for believing in me, in this manner she made possible this dream. And I also thank her and our two daughters, Ana and Laura, for being the most wonderful part of the dream.

The work described in this dissertation has been funded by the Department of Energy under a grant entitled "The role of continental margin processes in the nutrient bearing stratum of the North Atlantic", and by the Commonwealth Center for Coastal Physical Oceanography.

Table of Contents

	Page
List of Tables	vii
List of Figures	viii
1. Introduction	1
2. The Western Edge of the Subtropical Gyre	6
2.1 Thermocline circulation	6
2.2 Western boundary upwelling	19
2.3 The nutrient bearing stratum	21
2.4 Tracer anomalies and diapycnal mixing in the Gulf Stream	22
3. Hydrographic Observations	27
3.1 MASAR data	28
3.2 Five sections across the Gulf Stream	38
3.3 Section 36N	38
4. The Gulf Stream and the Nutrient Stream	81
4.1 The Nutrient Stream	81
4.2 Changes in water mass and nutrient transports	122
5. Water Mass and Nutrient Balances	133
5.1 Nutrient anomalies	133
5.2 A kinematic model for water and nutrient balances	135
5.3 Recirculation and mixing	137
5.4 Estimates of mean transports	139
6. Equations in Isopycnic Coordinates	144
6.1 The 'mean' diapycnal velocity	145
6.2 Isopycnic equations with diapycnal mixing	147
6.3 Vorticity balance	149
7. Dynamical Analysis of Section 36N	153
7.1 The Jacobian and the Richardson number	153
7.2 Vorticity anomalies in the Nutrient Stream	167

	Page
8. Diapycnal Fluxes of Mass and Potential Vorticity	175
8.1 Estimating the diapycnal velocity	176
8.2 Diapycnal velocities and diapycnal convergence	183
9. Two-Way Exchange	199
9.1 Frontogenesis and mixing	199
9.2 A simple model of diapycnal mass transfer	207
9.3 Estimates of tilting and torque terms	213
10. The Upper Level Atmospheric Jet Stream Analogy	218
11. Conclusions	224
Bibliography	229
Autobiographical Statement	238

List of Tables

Table	Page
1	Total water mass (sverdrups), nutrient ($kmol s^{-1}$), and DO ($l m^{-2} s^{-1}$) transports across the Florida Straits according to Brewer and Dyrssen (1987) and our calculations (FS and 24N, respectively). Also shown are the partial transports going across section 7S.
	127
2	Total and partial water mass (sverdrups), nutrient ($kmol s^{-1}$) and DO ($l m^{-2} s^{-1}$) transports, and nutrient ($\mu mol l^{-1}$) and DO ($ml l^{-1}$) concentrations in sections 24N and 36N.
	130
3	Estimates for inflow and mixing water mass transports (sverdrups) between sections 24N and 36N, obtained from the two-box model. ...
	138
4	Water mass (sverdrups) and nitrate transports ($kmol s^{-1}$) in the surface s ($\sigma_t < 26.8$), thermocline t ($26.8 < \sigma_t < 27.5$), and deep strata d ($27.5 < \sigma_t < 27.8$) of sections 24N, 36N, 64W, 53W, and 35W.
	141
5	Estimates for quantities involved in maximum contributions to the vorticity balance, within the Nutrient Stream. The upper row gives the results as calculated from the smoothed density data. The lower row gives the estimates as obtained from our simple model of diapycnal mass transfer.
	214

List of Figures

Figure	Page
1	(a) Relative topography of 100 <i>db</i> relative to 1500 <i>db</i> (units in dynamic millimeters). (b) Relative topography of 1500 <i>db</i> relative to 3000 <i>db</i> (units in dynamic millimeters - 600). Reproduced from Stommel et al. (1978).8
2	(a) Annual mean vertical Ekman pumping velocity (positive values are upward, units in $10^{-7} m s^{-1}$). (b) Contours of annual mean geostrophic water mass transport (units in sverdrups). Reproduced from Leetma and Bunker (1978). 10
3	Property distributions on selected isopycnal surfaces in winter. Areas shaded indicate no water of this density present during winter. Units are TU (1 tritium atom per 10^{18} hydrogen atoms) for tritium, and $10^{-11} m s^{-1}$ for potential vorticity. Reproduced from Sarmiento et al. (1982). 11
4	Lines of wintertime outcrops for selected layers. Hatched areas are of positive (upwards) vertical Ekman pumping velocities. Reproduced from Kawase and Sarmiento (1983). 15
5	Potential vorticity section in isopycnic coordinates, obtained from the KNORR 104 cruise, which approximately followed the $40^{\circ}W$ meridian. Reproduced from Keffer (1985). 16
6	Depth (meters) and nitrate concentration ($\mu mol kg^{-1}$) on selected isopycnal layers. Areas stippled indicate no water of this density present during winter. Hatched areas are regions with relatively large error. Reproduced from Kawase and Sarmiento (1985). 18
7	(a) Nitrate and (b) phosphate concentrations as a function of density (σ_t). Circles and triangles represent observations taken in the Sargasso Sea and the Gulf Stream, respectively. Reproduced from Stefánsson and Atkinson (1971). 24
8	(a) Oceanographic thermal analysis map for September 9, 1985 (done by Jenifer Clark, NOAA) for the MASAR area. (b) Location of the MASAR sections during cruise 7, made between September 6 and 9, 1985 (adapted from Brown et al. 1987). 30
9	Temperature, salinity, density (σ_t), and nitrate, phosphate, silicate and DO concentrations in section 7S. 31

Figure

Page

10	Hydrographic and nutrient sections employed to calculate water mass and nutrient transports from the Florida Straits to the North Atlantic Ocean. The dashed lines indicate the approximate contours for the Nutrient Stream as defined by the specified nutrient flux values.	39
11	Temperature, salinity, density (σ_t), and nitrate, phosphate, silicate and DO concentrations in section 24N.	40
12	Temperature, salinity, density (σ_t), and nitrate, phosphate, silicate and DO concentrations in section 36N.	47
13	Temperature, salinity, density (σ_t), and nitrate, phosphate, silicate and DO concentrations in section 64W.	54
14	Temperature, salinity, density (σ_t), and nitrate, phosphate, silicate and DO concentrations in section 53W.	61
15	Temperature, salinity, density (σ_t), and nitrate, phosphate, silicate and DO concentrations in section 35W.	68
16	Detailed location of section 36N, occupied in the offshore direction between June 12 and 14, 1981.	75
17	Frontal analysis maps for the region of interest, during June 10 and 15, 1981 (adapted from originals courtesy of Jenifer Clark, NOAA). ...	76
18	Overview of temperature, salinity and sigma-theta profiles, using the unsmoothed data of station 15 in section 36N. Also shown is the smoothed and interpolated density-depth profile (dashed line).	78
19	16 m-averaged (smoothed) sigma-theta, σ_θ , in section 36N.	79
20	Smoothed and interpolated depth, z , in section 36N.	80
21	Velocity, and nitrate, phosphate, silicate and DO fluxes in section 7S.	83
22	Velocity, and nitrate, phosphate, silicate and DO fluxes in section 24N.	88
23	Density (σ_t), velocity, nitrate concentration, and nitrate, phosphate, silicate and DO fluxes in section 36N, down to 2000 m.	93
24	Density (σ_t), velocity, nitrate concentration, and nitrate, phosphate, silicate and DO fluxes in section 64W, down to 2000 m.	100
25	Density (σ_t), velocity, nitrate concentration, and nitrate, phosphate, silicate and DO fluxes in section 53W, down to 2000 m.	107
26	Density (σ_t), velocity, nitrate concentration, and nitrate, phosphate, silicate and DO fluxes in section 35W, down to 2000 m.	114
27	Nitrate concentration, c_{NO_3} , in section 36N as a function of σ_t and cross-stream distance.	123
28	DO concentration, c_{O_2} , in section 36N as a function of σ_t and cross-stream distance.	124
29	Variation of total water mass and nutrient transports with along-stream distance. The three scales in the right margin correspond to nitrate, phosphate, and silicate transport, respectively.	128

Figure	Page
30	Relative increase between sections 24N and 36N of water mass transport in isopycnal layers.132
31	Schematic representation of the main elements for the two-box model of the Gulf Stream between sections 24N and 36N.136
32	Schematic illustration of the overall mass transfer rates (in units of m^2s^{-1}), off the Mid-Atlantic Bight.140
33	Separation index, $j = \rho J$, in section 36N.154
34	Sigma-theta, σ_θ , for the top 1000 m of the Gulf Stream in section 36N. For $\sigma_\theta > 26.5$, the areas corresponding to $j < 3 \times 10^5 m$ have been hatched.156
35	Montgomery potential, ϕ , referred to the $27.8\sigma_\theta$ -surface, in section 36N.157
36	Along-stream geostrophic velocity, v , referred to the $27.8\sigma_\theta$ -surface, in section 36N.159
37	Richardson number, Ri , in section 36N.161
38	Separation index, $j = \rho J$, for the top 1000 m of the Gulf Stream, from the unsmoothed density field in section 36N. 0 stands for 10^0 units ($10^5 m$), and 3 for 10^3 units ($10^8 m$).163
39	J as a function of σ_θ , for both the smoothed and unsmoothed density fields, in section 36N (the data for this figure is from stations 14, 15, and 16). (a) Complete range of values for the unsmoothed data, with absolute values greater than $10^5 m^4 kg^{-1}$ being replaced by this limit. (b) Detail of the region with Jacobian values between 0 and $10^4 m^4 kg^{-1}$; each of the three solid lines corresponds to the smoothed field for a different station, the dots correspond to the unsmoothed values.164
40	Nitrate concentration, c_{NO_3} , in section 36N, as a function of σ_θ and cross-stream distance.166
41	Absolute vorticity, $\zeta + f$, in section 36N. Planetary vorticity at this location is about $8.7 \times 10^{-5} s^{-1}$168
42	Potential vorticity, q , in section 36N.169
43	Montgomery potential AP (units of dynamic meters) referenced to $\sigma_\theta = 27.85$, potential temperature θ ($^{\circ}C$), dissolved oxygen O_2 ($ml l^{-1}$), and potential vorticity $PV = (f/\rho) \partial\rho/\partial z$ ($10^{-12} m^{-1} s^{-1}$), for four sections across the Gulf Stream. The longitudes of the sections are (a) $68^{\circ}30'W$, (b) $64^{\circ}30'W$, (c) $56^{\circ}30'W$, and (d) $54^{\circ}30'W$. Reproduced from Bower et al. (1985).171
44	Square of the diapycnal velocity gradient, $(\partial v/\partial \rho)^2$, in section 36N. ..174
45	Density, density eddy diffusivity, vertical Reynolds density flux, and diapycnal velocity, for two idealized situations leading to two-way exchange (solid line) and one-way transfer (dotted line).178

46	Variation of the ratio K_H/K_{H0} with Richardson number. Data reported by Ueda et al. (1981) for the atmospheric boundary layer are shown. The dotted line is Ueda et al.'s (1981) interpolation formula for laboratory data of Komori et al. (1983). The dashed and solid lines correspond to Munk and Anderson's (1948) expression with $\beta = 10/3$ and 10, respectively.	181
47	Diapycnal velocity, w_ρ , in section 36N. Solid and dashed lines refer to positive and negative values, respectively. Only the contours with $(\pm) 10^{-7} K_0$ [$2.6 \times 10^{-10} \text{ kg m}^{-3} \text{ s}^{-1} \simeq 2.6 \times 10^{-10} \sigma_\theta \text{ s}^{-1}$] are labeled. Additional contours, changing by $(\pm) 2 \times 10^{-7} K_0$ [$5.2 \times 10^{-10} \text{ kg m}^{-3} \text{ s}^{-1} \simeq 5.2 \times 10^{-10} \sigma_\theta \text{ s}^{-1}$], are shown.	184
48	Entrainment velocity, w_e , in section 36N. Solid and dashed lines refer to positive and negative values, respectively. Only the contours with $(\pm) 5 \times 10^{-5} K_0$ [$1.3 \times 10^{-7} \text{ m s}^{-1}$] are labeled. Additional contours, changing by $(\pm) 5 \times 10^{-5} K_0$ [$1.3 \times 10^{-7} \text{ m s}^{-1}$], are shown.	186
49	Diapycnal divergence, $\partial w_\rho / \partial \rho$, in section 36N. Solid and dashed lines refer to positive and negative values, respectively. Only the contours with $(\pm) 10^{-5} K_0$ [$2.6 \times 10^{-8} \text{ s}^{-1}$] are labeled. Additional contours, changing by $(\pm) 10^{-5} K_0$ [$2.6 \times 10^{-8} \text{ s}^{-1}$], are shown.	187
50	Nitrate flux in isopycnic coordinates (compare with Fig. 23), defining the location of the lower portion of the Nutrient Stream.	188
51	Contributions to the diapycnal velocity (equation 45), w_ρ^r and w_ρ^j , within the Nutrient Stream in section 36N. Solid and dashed lines refer to positive and negative values, respectively.	190
52	Diapycnal velocity, w_ρ , within the Nutrient Stream in section 36N. Solid and dashed lines refer to positive and negative values, respectively.	192
53	Entrainment velocity, w_e , within the Nutrient Stream in section 36N. Solid and dashed lines refer to positive and negative values, respectively.	193
54	Diapycnal divergence, $\partial w_\rho / \partial \rho$, within the Nutrient Stream in section 36N. Solid and dashed lines refer to positive (divergence) and negative (convergence) values, respectively.	194
55	Separation index, $j = \rho J$, within the Nutrient Stream in section 36N.	196
56	Density eddy diffusivity, K , within the Nutrient Stream in section 36N.	197
57	Details of the temperature, salinity and sigma-theta profiles, using the unsmoothed data of station 15 (see Fig. 18). (a) A highly stratified region centered at $\sigma_\theta = 26.73$, and (b) the underlying step-like structure.	201

Figure	Page
58 High resolution temperature and temperature gradient in a station taken near the middle of the Gulf Stream, at about $38^{\circ}N$, $69^{\circ}W$. Also shown are the horizontal velocities (vertical resolution of about 8 m) and the 50 m -averaged Richardson numbers (adapted from Gregg and Sanford 1980).	203
59 Vertical Reynolds density flux, diapycnal velocity and its diapycnal gradient, as calculated from the smoothed data of stations 15 and 16, within the Nutrient Stream in section 36N. The dotted line is the calculated $\overline{w'\rho'} = K/J$ distribution, and the dashed and solid lines are the corresponding w_{ρ} and $\partial w_{\rho}/\partial\rho$ profiles.	205
60 Temperature distribution (dashed lines; solid lines are for $T = 15$ and $18^{\circ}C$) and regions with high phytoplankton concentration (shaded areas) for two nearby transects across the Gulf Stream (adapted from Arnone et al. 1990). The transect in (a) was approximately taken across the inflection point between a crest and the subsequent trough, the transect in (b) was taken slightly before the subsequent crest.	206
61 Simple model for the vertical Reynolds density flux, $\overline{w'\rho'}$, at the location of the Nutrient Stream, both (a) before and (b) after mixing. The dotted line is the hypothetical $\overline{w'\rho'}$ distribution, the dashed and solid lines are the corresponding w_{ρ} and $\partial w_{\rho}/\partial\rho$ profiles.	209
62 (a) Jacobian, J , and (b) depth, z , profiles corresponding to the original (before mixing, solid line) and modified (after mixing, dotted-dashed line) vertical Reynolds density flux $\overline{w'\rho'}$. The dotted vertical line in the Jacobian distribution indicates the value of J_c	210
63 Shapiro's (1976) representation of turbulence in upper level atmospheric jet stream systems. (a) Regions of clear-air turbulence in the vicinity of the jet stream are stippled; the solid and dashed lines are contours of potential temperature and wind speed, respectively. (b) The postulated vertical Reynolds potential temperature flux is shown as a function of height; the crosses indicate observed values.	220
64 (a) Richardson number and (b) potential vorticity (units of $10^{-7}\text{ K s}^{-1}\text{ mb}^{-1}$), in isobaric coordinates, for a section across the upper level atmospheric jet stream system (reproduced from Shapiro 1978). The dashed line indicates the flight path taken during the observations.	221

Chapter 1. Introduction

*In my youth I had hoped that the
better scrutiny of the heavens, which
we need, would be achieved by me.
In my old age I despair, but I still
hope that my words will induce
someone to carry on the search.*

Averroes (1126-1198)

The idea of a “cellular” structure of circulation, where properties are approximately conserved, goes back to Carl-Gustaf Rossby’s (1936, p. 5) seminal paper.

On it he says:

“Since the vertical circulation does not extend all the way down it may be argued that the water, because of its stratification, has a cellular structure, each cell being separated through approximately horizontal surfaces of discontinuity from the cells above and below. Each boundary surface would then act as a ‘false’ bottom and each cell would have a practically independent circulation.”

Rossby supported these ideas using temperature-salinity-oxygen correlations between the shallow waters on the coastal side of the Gulf Stream and the deeper layers on its offshore side. Alfred Redfield (1936) immediately pointed out the important ecological consequences of along-isopycnal water transfer in the Gulf Stream. He indicated that such upward and shoreward transfer should take place “along isopycnics, which are known to slope sharply as they cross the Gulf Stream”. He further substantiated these results using Seiwel’s (1934) observations on the oxygen and phosphate distributions.

However, the father of isopycnal thinking in oceanography is undoubtedly

Raymond Montgomery. Working on his thesis under Rossby's supervision, he wrote first a short note (Montgomery 1937) in which he introduced "isentropic" charts, common in atmospheric sciences, to oceanography. In this note he described a method to calculate geostrophic shear in isopycnic coordinates. He (Montgomery 1938) and Parr (1938) were the first ones, and apparently the only ones during five lustra, to use this method. Montgomery (1938, p. 5) justified the utility of the isopycnal representation with the following statement:

"... there is no potent mechanism for altering the potential density of any water element below the layer of direct surface influences. Hence there can be no flow of major proportions across surfaces of constant potential density. For these reasons it is now generally accepted that flow takes place essentially parallel to these surfaces. It follows that the major sources for the water on each surface of constant potential density are to be found along its intersection with the sea surface in higher latitudes."

Surprisingly, Montgomery's application of isopycnic dynamical analysis was not resumed until the mid-sixties, with the works by Kirwan (1963), Reid (1965), Tsuchiya (1968), and Buscaglia (1971) (for a review see Reid 1981). Riley's (1951) comprehensive analysis of the circulation in the Atlantic was carried out using the dynamic method on horizontal levels and interpolating over selected isopycnal surfaces. Perhaps even more striking, Montgomery's idea of water sources at the sea surface intersection of the isopycnal surfaces, would take more than forty years to develop as a realistic model for the thermocline circulation. The analytical models of thermocline circulation due to Rhines and Young (1982a,b) and Luyten et al. (1983), have finally provided much needed insight into how the interior of subtropical gyres works. However, the dynamics of the crucial western end of these gyres remains obscure. The rise of the thermocline near the western boundary, the separation of the current from the coast and its adjustment to the increasing

planetary vorticity, have not been fully accounted for. An understanding of the dissipation mechanisms involved is necessary to produce fully realistic models of the subtropical gyres. Apart from their crucial dynamical role, boundary currents transport a vast amount of heat poleward, as well as a large load of nutrients, two important factors in climate and in the global biogeochemical cycle.

One of the possible dissipative mechanisms in western boundary currents, which has received very little attention in the literature, is diapycnal mixing. Henry Stommel's early monograph on the Gulf Stream (1965, p. 115) is the only reference, to my knowledge, where diapycnal mixing is considered as a likely phenomenon for the Gulf Stream. Talking in terms of the internal Froude number (the square of the inverse bulk Richardson number), he showed that a simple potential vorticity conserving model allows supercritical Froude numbers. He suggested that (Stommel 1965, p. 116):

"... the real Gulf Stream approaches critical internal Froude flow, and it is quite conceivable that as a result there are internal hydraulic jumps and other interesting small-scale phenomena, such as oblique shock fronts, along the left-hand, inshore edge of the Stream."

This dissertation will show that Stommel's physical intuition was again right.

Gregg and Sanford (1980) analyzed several profiles of temperature and velocity shear in the Gulf Stream and concluded that shear-induced mixing was possible, although they thought it was probably less important than thermohaline intrusions. The possibility of mixing in high-shear regions of these oceanic baroclinic Streams (that could provide Montgomery's "potent mechanism for altering the potential density of any water element below the layer of direct surface influences"), deserves further analysis. Such high-shear regions may be of intermittent character, possibly related to some phase of the meanders. Diapycnal mixing, if

intense, may modify the distribution of isopycnal surface height and other dynamical quantities, such as the isopycnal potential vorticity. Furthermore, when taking place in the upper-thermocline layers, diapycnal mixing may be responsible for the exchange of nutrient-rich thermocline and nutrient-depleted surface waters.

In this work we first look at the supply of nutrients by the Gulf Stream to the North Atlantic Ocean. We show that this nutrient flux takes place along the upper thermocline layers, in what is to be called the ‘Nutrient Stream’. Then, we calculate the along-shore variations in the water and nutrient transports, both in terms of total transport and vertical structure. Analysis of the balances of water and nutrient transports permits us to estimate the isopycnal input and diapycnal mixing that occurs along the Gulf Stream, on its way from the Florida Straits to the northern North Atlantic Ocean.

Isopycnal coordinates, with potential density ρ used as the vertical coordinate, is the natural framework for studying diapycnal mixing. In this framework, we review the kinematics of diapycnal mixing, and the equations of motion in isopycnal coordinates in the presence of diapycnal mixing. The Jacobian of the transformation from cartesian to isopycnal coordinates, $J = dz/d\rho$, is an important parameter in this analysis. We investigate conditions necessary for the material tendency of the Jacobian, and of potential vorticity, to be controlled by diapycnal gradients of the diapycnal velocity.

The theory is tested with data from a Gulf Stream hydrographic section off the Mid-Atlantic Bight. We examine several pieces of evidence, such as the distribution of the Richardson number, indicative of shear-mixing in the Gulf Stream. Next, we look at the distribution of the Jacobian, total vorticity and potential

vorticity in isopycnic coordinates. We show that the Nutrient Stream is the locus of low Jacobian values responsible for associated high values of potential vorticity. We argue that in these conditions diapycnal transfer is dominant, so that both the mass-conservation and potential vorticity equations reduce to simple forms. Assuming that diapycnal mixing is the result of shear-induced small-scale instabilities, we then relate diapycnal velocity to Richardson number and Jacobian. We show that regions with small Jacobian (large potential vorticity) values imply large diapycnal convergence that tends to eliminate these anomalies. This leads us to the view that diapycnal mixing is the consequence of anomalies produced during frontogenesis in Gulf Stream meanders. We end by proposing a simple model for turbulence and mixing within the Nutrient Stream, and by comparing our results with analogous observations in the upper level atmospheric jet stream.

Chapter 2. The Western Edge of the Subtropical Gyre

*Thereupon I began to reflect, whether
or not that which is concealed from us
a priori by chance, can at least
become known to us a posteriori,
by an event observed many times
in similar instances.*

Jacob Bernoulli (1654-1705)

In this chapter we present a summary of how thinking on the thermocline circulation problem, including its western boundary component, has evolved during the last decades. We look with some detail at the associated nutrient transport, both because of its biological implications and because of the clues it may provide as a tracer, particularly on diapycnal mixing in western boundary currents.

2.1 Thermocline circulation

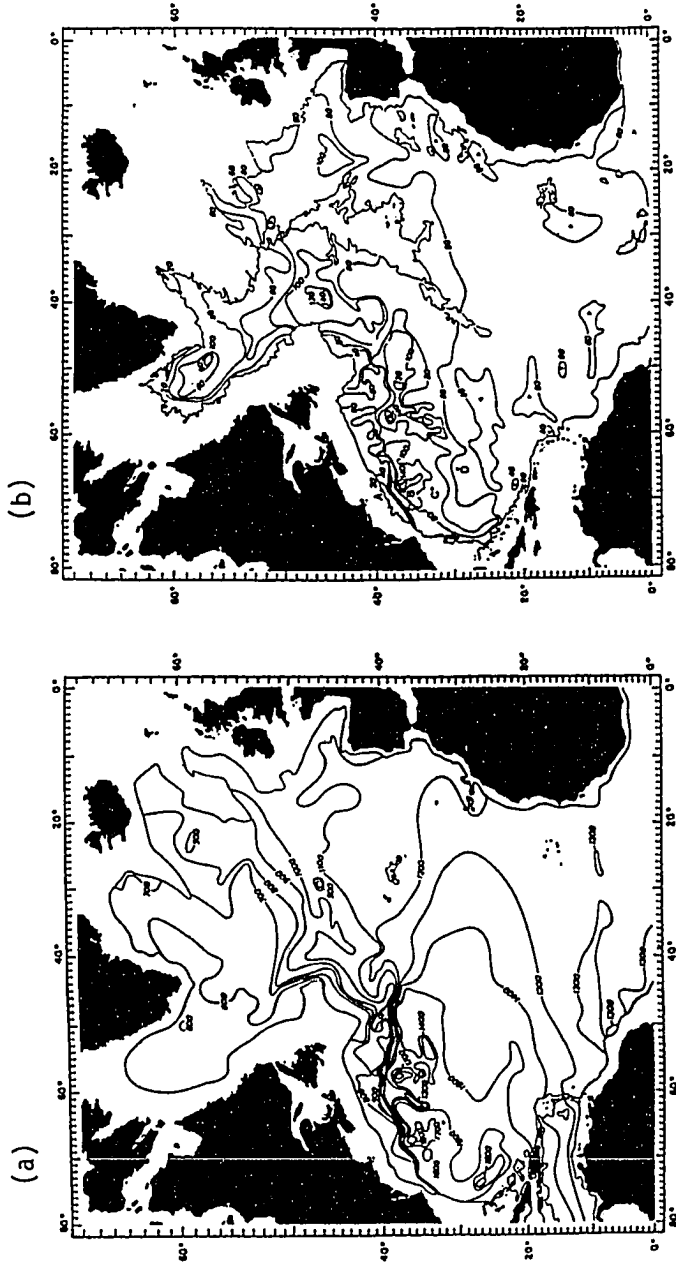
A number of attempts (for an early review see Veronis 1969) were made during several decades, to tackle the thermocline circulation problem, some of them taking into account the relation between thermocline circulation and ventilation (e.g. Welander 1959). However, it was not until the late 70's that enough was known empirically to describe the pattern of thermocline circulation. Worthington (1976) calculated the geostrophic velocities in the Gulf Stream system and interpolated the results to isopycnal surfaces, which allowed him to infer characteristics of "recirculation" in the North Atlantic. He reported a maximum water

mass transport (relative to the bottom) of about 140 sverdrups. In particular, he found that the recirculation gyre becomes narrower with depth. Similarly, Stommel et al. (1978) found clear evidence for a narrow baroclinic recirculation in the thermocline and deep layers, located somewhat to the south of the surface expression of the Gulf Stream (Fig. 1). Their results also point at the existence of related barotropic recirculation, both near the surface and in deeper layers. For the upper 800 *m* they suggested that barotropic recirculation could account for about 30 – 50% of the mass transport imbalance in upper layers. These values may be arguable, due to the seasonal variability of the mass transport through the Florida Straits (Niiler and Richardson 1973).

Stommel et al. (1978) estimated that the barotropic recirculation in the thermocline and deeper layers can account for some 50-70 sverdrups. This value is similar to the difference between Worthington's (1976) geostrophic transports (with a maximum of 140 sverdrups) and Barret and Schmitz's (1971) direct measurements using floats near 67°W (with a maximum of 203 sverdrups). It appeared clear, however, that the barotropic contribution is considerably smaller than the baroclinic transport. This was supported by Reid's (1981) analysis of thermocline circulation using acceleration potentials, which shows good agreement with salinity, oxygen and nutrient distributions, and it was confirmed by Wunsch's (1978) inverse calculations, which indicate that no significant ageostrophic flow is required to obtain a solution for the North Atlantic circulation west of 50°W.

Leetma et al. (1977) and Leetma and Bunker (1978) calculated the mean Ekman pumping velocities for the North Atlantic, from which they estimated the geostrophic circulation as obtained from the Sverdrup relation (Sverdrup minus

Figure 1. (a) Relative topography of 100 *db* relative to 1500 *db* (units in dynamic millimeters). (b) Relative topography of 1500 *db* relative to 3000 *db* (units in dynamic millimeters - 600). Reproduced from Stommel et al. (1978).



Ekman transport; Fig. 2). They found remarkably good agreement between this circulation and that inferred from Stommel et al.'s (1978) dynamic heights at 100 *m* relative to 1500 *m*. In particular, Leetma and Bunker (1978) concluded that the northward flow through the Florida Straits appears to be in balance with the southward Sverdrup transport at 31°*N*. This was supported by Leetma et al. (1977) and Stommel and Schott (1977), whose analyses for the southeastern portion of the gyre (the beta triangle) imply that the dynamics there is Sverdrupian.

The relation between thermocline circulation and the outcropping of the isopycnal surfaces became clear in Sarmiento et al.'s (1982) isopycnic analysis of the North Atlantic salinity, tritium and potential vorticity distribution (Fig. 3). The potential vorticity distribution shows homogenized values in large recirculation regions in the upper thermocline layers, $\sigma_\theta = 26.5$ to 26.8, smaller at $\sigma_\theta = 27.1$. The salinity distribution in all isopycnals showed a tongue-like maximum associated with the outcrop areas, except in the deepest isopycnal analyzed ($\sigma_\theta = 27.4$) where the association was with the outflow from the Mediterranean. The tritium distribution is in agreement with the salinity distribution, but it provides additional information about mixing processes and the time-scale of the motions. It shows the upper layers (down to $\sigma_\theta = 26.5$) with rather high tritium values possibly due to vertical mixing. The upper-thermocline layers, $\sigma_\theta = 26.8$ and 27.1, present large northeast-southwest gradients, which reflect the input of high tritium concentration waters from the outcrop regions. The time scale suggested by this gradient is of $O(10\text{ yrs})$, which is in agreement with recirculating velocities of $O(0.01\text{ m s}^{-1})$. Sarmiento et al. (1982) also observed large gradients

Figure 2. (a) Annual mean vertical Ekman pumping velocity (positive values are upward, units in 10^{-7} m s^{-1}). (b) Contours of annual mean geostrophic water mass transport (units in sverdrups). Reproduced from Leetma and Bunker (1978).

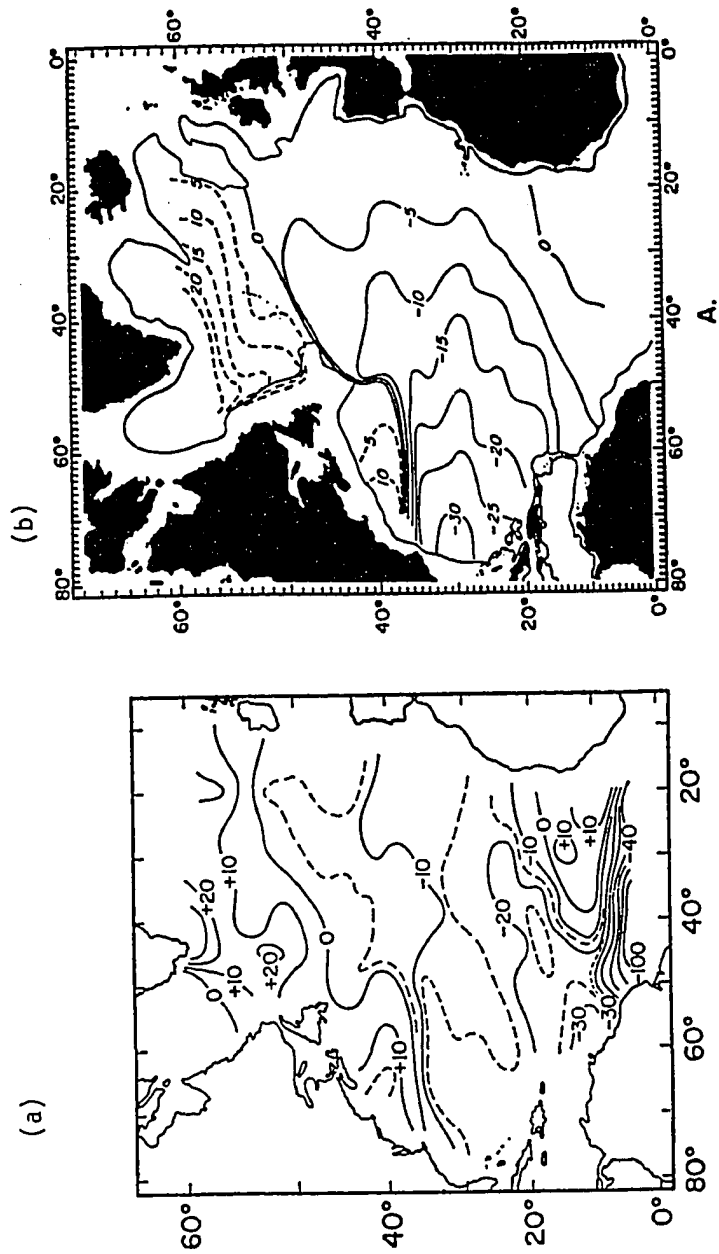
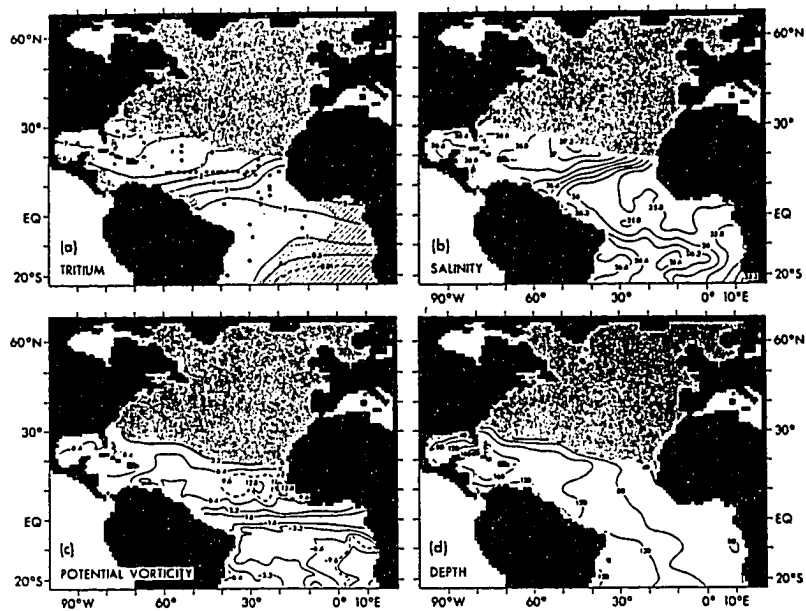
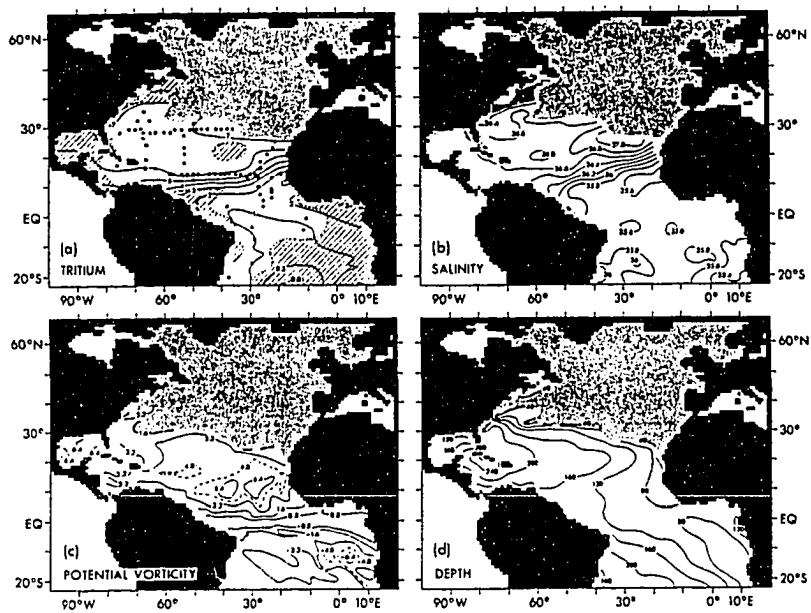


Figure 3. Property distributions on selected isopycnal surfaces in winter. Areas shaded indicate no water of this density present during winter. Units are TU (1 tritium atom per 10^{18} hydrogen atoms) for tritium, and $10^{-11} \text{ m s}^{-1}$ for potential vorticity. Reproduced from Sarmiento et al. (1982).

$\sigma_\theta = 25.6$

 $\sigma_\theta = 26.2$


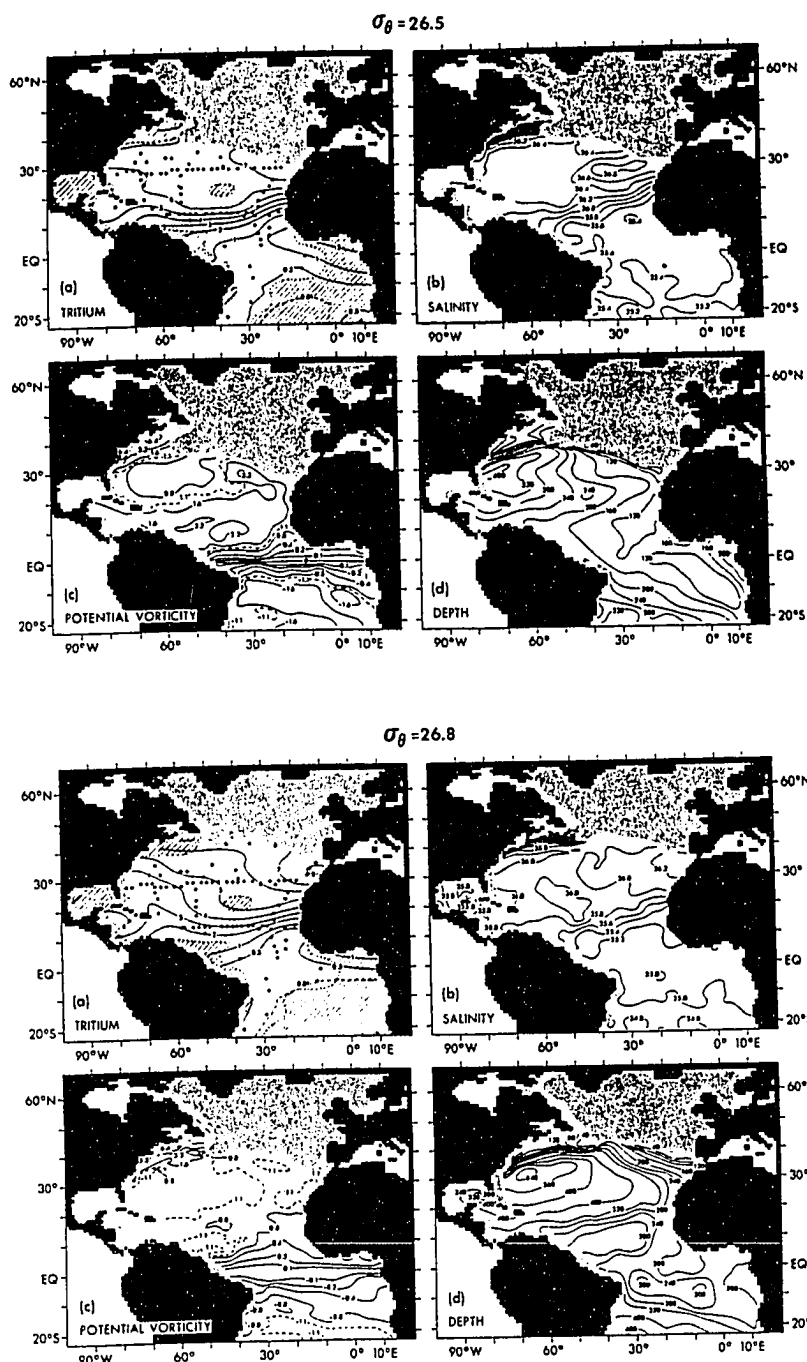


Figure 3 (continued)

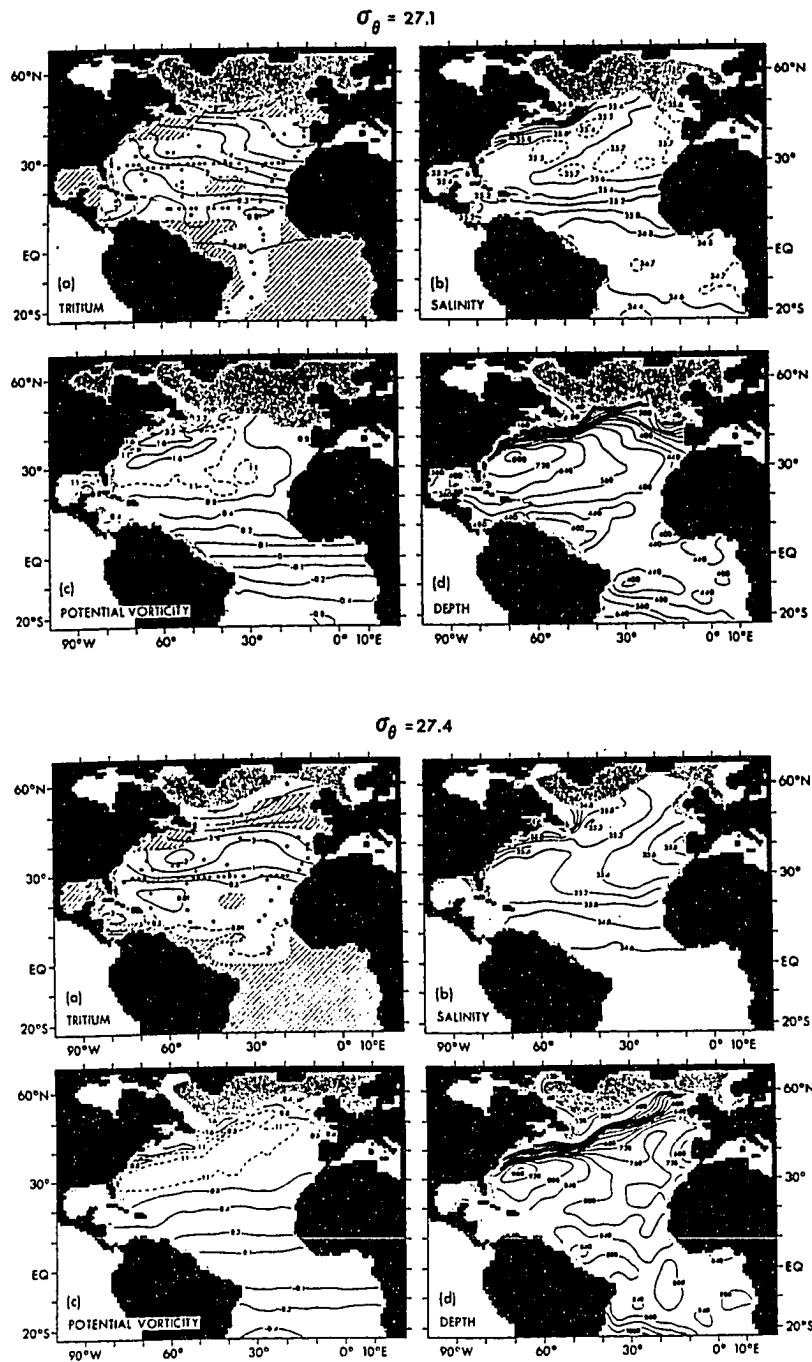


Figure 3 (continued)

of tritium concentration in the southeastern region of the subtropical gyre.

The above picture is consistent with the relation between the location of the winter outcrops for several isopycnals, and the regions of positive and negative Ekman pumping velocities (see Fig. 4, reproduced from Kawase and Sarmiento 1985; see also Fig. 2). In the northeastern portion of the subtropical gyre, the upper thermocline layers (down to $\sigma_\theta = 27.1$) outcrop in regions of negative Ekman pumping. Sarmiento (1983), using tritium as a tracer, showed that the downward Ekman pumping in these regions was far too small to account for the water flux between the surface and the thermocline layers. He suggested that other exchange processes at the outcrop regions, such as mixing and convective overturning, should be dominant. Jenkins (1987) using tritium and its inert daughter ^3He , reached a similar conclusion for the beta triangle. His results showed that this region was indeed ventilated, with most water coming from the outcrop regions and the along-isopycnal flow consistent with the geostrophic velocities.

McDowell et al. (1982) and Keffer (1985) presented additional potential vorticity maps and sections in isopycnic coordinates in agreement with Sarmiento et al. (1982) results. Fig. 5 (from Keffer 1985) shows a section of potential vorticity, drawn in isopycnic coordinates, approximately taken along 40°W . This figure shows the northern outcropping of the isopycnals and how, at high latitudes, the lines of constant potential vorticity are approximately parallel to the isopycnals. However, towards the equator they clearly cross the isopycnals, which indicates that in this region the flow cannot be meridional. Notice also the region of homogenized potential vorticity values, centered at $\sigma_\theta = 26.8$ and 30°N , which corresponds to the region of thermocline recirculation. Maps of nutrients for the

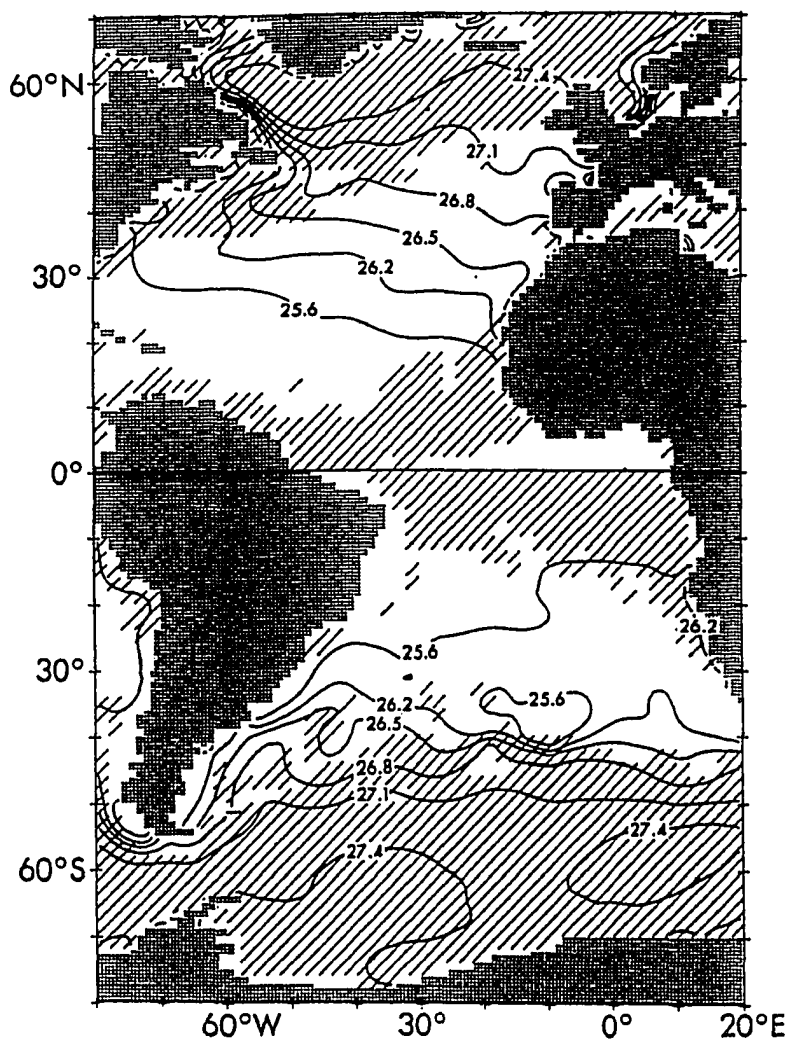
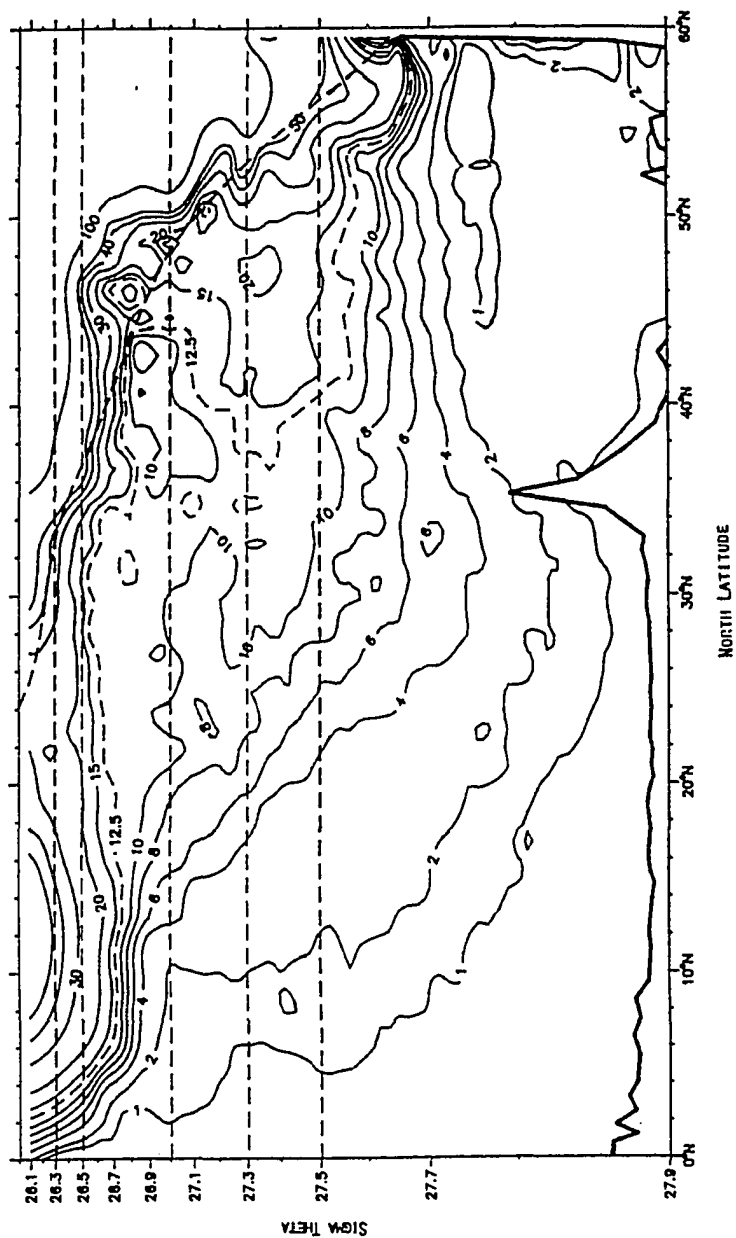


Figure 4. Lines of wintertime outcrops for selected layers. Hatched areas are of positive (upwards) vertical Ekman pumping velocities. Reproduced from Kawase and Sarmiento (1983).

Figure 5. Potential vorticity section in isopycnic coordinates, obtained from the KNORR 104 cruise, which approximately followed the $40^{\circ}W$ meridian. Reproduced from Keffer (1985).

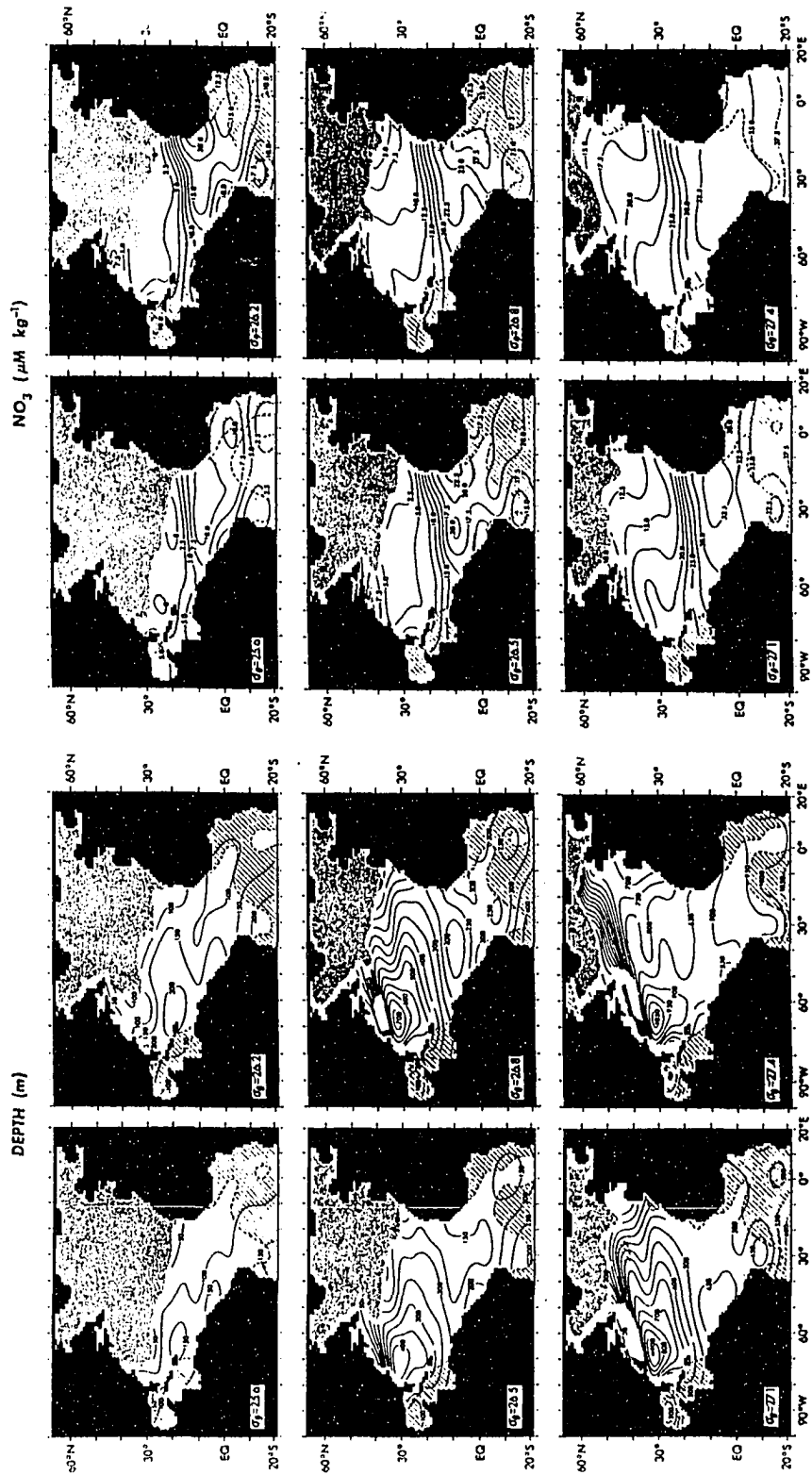


thermocline (see Fig. 6, reproduced from Kawase and Sarmiento 1985, for nitrate) showed NE-SW concentration gradients consistent with this recirculation pattern.

Simultaneous with this developing observational picture, came also a better understanding of the physical mechanisms that cause it. Stommel (1979) was the first to combine Sverdrup dynamics with Montgomery's (1938) isopycnal view of circulation. He argued that continuity was satisfied between the Ekman pumping vertical velocity at the base of the Ekman layer and the along-isopycnal flow at a depth of about 150 *m*. Furthermore, since the zonal movement of outcropping isopycnals is faster than the downward water movement, only the late winter water at the outcrop can effectively penetrate the thermocline. It was Luyten, Pedlosky and Stommel's (1983) paper which finally formulated the theory of Sverdrupian circulation in the thermocline. The theory showed three regions: a region "ventilated" through water input via negative Ekman-pumping at the outcrop of the isopycnals; a "closed", unventilated region, in the western portion of the ocean; and a "shadow" region which cannot be reached by the parcel trajectories, in the southeastern portion of the gyre. The closed region was anticipated in Rhines and Young (1982a,b) papers, first under conditions of large forcing of the thermocline layers through frictional coupling with the surface layer, later by "homogenization" of potential vorticity through sustained recirculation and along-isopycnal mixing.

The above quoted models have provided much insight into thermocline circulation, but they are in various ways overidealized. More recent works based on these models have been able to combine some of their features and remove some of their limitations: see Pedlosky and Young (1983), which coupled Rhines and Young (1982a,b) and Luyten et al. (1983) theories, also Luyten and Stommel

Figure 6. Depth (meters) and nitrate concentration ($\mu\text{mol kg}^{-1}$) on selected isopycnal layers. Areas stippled indicate no water of this density present during winter. Hatched areas are regions with relatively large error. Reproduced from Kawase and Sarmiento (1985).



(1986) and Veronis (1988), which included forcing through heat flux at the ocean's surface. Layered numerical models with high spatial resolution, using either the quasigeostrophic approximation (Holland et al. 1984) or primitive equations (Cox 1985), have reproduced the main features of the above three regions, illustrating, in particular, the importance of mesoscale eddies in diffusing potential vorticity.

In the ventilated thermocline layers of the North Atlantic, the water properties must reset themselves in every recirculation. Water flows along these layers in route to the western edge of the gyre, where they are recruited by the Gulf Stream. There they flow northward and upward, to reach the surface layers of the northern North Atlantic. These waters are yet subducted once again, after having reset their properties, including potential vorticity. One of our interests in this work is in appreciating how diapycnal mixing may provide a mechanism for these recirculating waters to get up near the surface in western boundary currents.

Considerations of this type are also important in closing the nutrient balance for the subtropical gyre and the whole North Atlantic Ocean. Brewer and Dyrssen (1987) obtained gross estimates for the nitrate and phosphate transport across the Florida Straits and suggested that the Gulf Stream is a principal source of nutrients for the North Atlantic. Here we will carry this analysis further to estimate how the transport of nutrients by the Gulf Stream is modified along its path, and how much reaches the northern North Atlantic ocean.

2.2 Western boundary upwelling

Despite the advances in the understanding of the thermocline problem the western end of these theories remains unclear. In particular, how is the nutrient transport balance closed in the western boundary regions and what characterizes

along-isopycnal circulation there? Circulation maps for the North Atlantic (Worthington 1976, Stommel et al. 1978) close the water transport balance through western boundary currents at all isopycnal surfaces, but do not indicate how this takes place. Rossby's (1936) argument on the cause of western boundary upwelling was rejected by Defant (1937), Ekman (1939) and Stommel (1965). The physical processes operating in western boundary currents remain to be fully explored. What is clear is that these processes have to depend on the overall circulation of the subtropical gyre, and must balance the vorticity and energy input of the winds to the subtropical gyre. We are still a long way from a full understanding of western boundary current dynamics. Recent work by Gabriel Csanady (1989) has, however, begun to define the outlines of a solution.

Csanady's (1989) theory of western boundary upwelling is based on the idea that energy dissipation in oceanic gyres is concentrated in western boundary currents, and that the first phase of dissipation is the release of potential energy to the "primary" eddies and meanders growing on the current. The first phase involves the upward movement of relatively light fluid along isopycnals, across the direction of the mean current, in accordance with the baroclinic instability mechanism. The eddy energy is eventually transmitted to the environment and dissipated (for example, through the radiation of topographic waves). The dissipation makes the rise of the light fluid permanent. Since current measurements with isopycnal floats (Bower and Rossby 1989) show no significant along-isopycnal mean vertical currents under the Gulf Stream, Csanady proposed that western boundary upwelling is effected through Reynolds mass flux (correlation between layer depth and cross-stream depth).

From an analysis of data on the formation and disappearance of the Mid-Atlantic Bight slope water pycnocline, Csanady and Hamilton (1988) have found evidence that a significant portion of the along-isopycnal flow crosses the western boundary current and reaches the Slope Sea of the Mid-Atlantic Bight. The layers involved in this cross-stream exchange correspond to the upper thermocline ($26.8 < \sigma_\theta < 27.3$), at depths of about 800 m in the Sargasso Sea and rising some 600 m under the Gulf Stream to occupy the top few hundred meters in the Slope Sea. Csanady and Hamilton (1988) estimated the average upwelling rate for these layers to be about $4 \text{ m}^2 \text{ s}^{-1}$ per unit length of the Stream.

2.3 The nutrient bearing stratum

Riley (1951) analyzed the distribution of oxygen and nutrients (nonconservative properties) in the Atlantic Ocean with the help of a numerical model. The input circulation pattern for his model was obtained from salinity and temperature data. According to Reid (1981), if it had not been that Riley's analysis came just after Munk's (1950) work on western boundary currents, "it might have stimulated a more thorough investigation, even with those limited data, of the variation of flow patterns with depth that might have been carried out concurrently with the studies of total transport." The fact is that this type of approach did not get restarted until last decade, with the works of Bolin et al. (1983, 1987), Schiltzer (1988, 1989) and Thiele and Sarmiento (1990). One of the most striking features arising from Riley's (1951) early analysis is the presence of nutrient-rich and oxygen-poor layers in the mid-thermocline, approximately between the isopycnals $\sigma_\theta = 26.8$ and 27.5. These layers correspond to Worthington's (1976) mid-thermocline waters, and have been called the "nutrient bearing stratum" of the North Atlantic by

Csanady (1990b).

Modern data reveal the extent and permanence of the nutrient bearing stratum. For example, the transatlantic sections in Roemmich and Wunsch (1985) show how this stratum extends zonally over the whole North Atlantic Ocean with uniform concentrations. Its meridional extent, as seen in Kawase and Sarmiento (1985) isopycnal maps (Fig. 6), is also large. These maps show that the thermocline waters of the subtropical gyre are enriched in nutrients during their southward and westward trip, supposedly through rain down and decomposition of organic particles from above.

In the Slope Sea and at the edge of the continental shelf the nutrient bearing stratum approaches the sea surface and mixing is enhanced. As Redfield (1936) originally suggested, this is the source of nutrients for the high biological production in these areas (Yentsch 1974, Riley 1975, Nakao 1977, Brown et al. 1984, Atkinson et al. 1987). If, however, nutrient-rich thermocline waters rise to the surface within the Gulf Stream, then high productivity will not necessarily be confined to shallower regions on the cyclonic side of the Gulf Stream. In this case high phytoplankton concentrations may occur over the Stream itself and, principally, in the surface waters of the northern North Atlantic Ocean fed by the Nutrient Stream. A clear manifestation of this may be seen in satellite pictures showing high chlorophyll pigment concentrations during the occurrence of the North Atlantic spring bloom (Esaias et al. 1987, NSF/NASA 1989).

2.4 Tracer anomalies and diapycnal mixing in the Gulf Stream

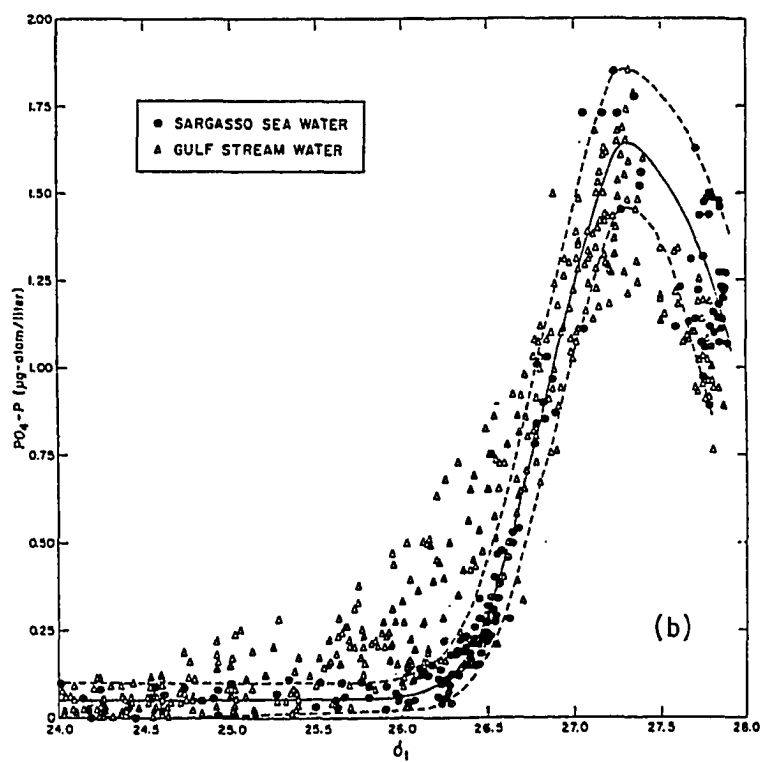
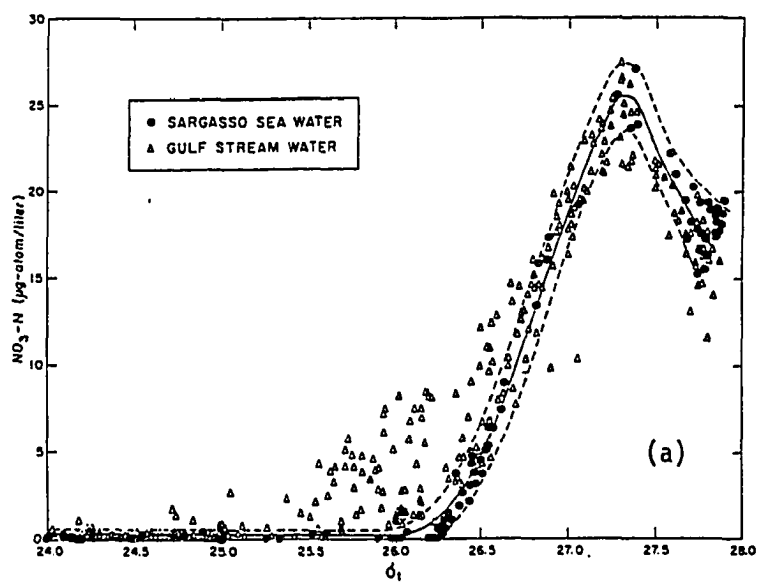
The distribution of nutrients, or of chemical tracers such as tritium, in the upwelling layers of the Gulf Stream may be used to provide information on the

origin and rates of water input along and across isopycnals. As indicated above, Rossby (1936) and Redfield (1936) pioneered the idea of along-isopycnal water input into western boundary currents, based in the continuity of oxygen and nutrient distributions. Richards and Redfield (1955) studied the evolution of oxygen anomalies, as compared with Sargasso Sea waters, along the course of the Gulf Stream. They reported relatively large and patchy negative oxygen anomalies, mostly in the $26 - 26.5 \sigma_t$ range but extending down to $\sigma_t = 27$, which they related to the low oxygen content of water arriving through the Florida Straits. They speculated that the patchiness in the oxygen anomalies may be due to the Gulf Stream having several branches.

Stefánsson and Atkinson (1971) studied the nutrient anomalies in the Gulf Stream, again as compared with Sargasso Sea waters (Fig. 7). They observed positive nutrient anomalies in the $25.0 - 26.6 \sigma_t$ stratum, which they ascribed to nutrient-rich waters of Caribbean origin. Their results, however, also show significant negative nutrient anomalies in the $27.0 - 27.5 \sigma_t$ stratum. These cannot be attributed to waters of southern origin, because Caribbean thermocline waters have higher nutrient concentrations (Fig. 6; see also the hydrographic sections described in Chapter 3). Densities in the Florida Straits do get at least as large as $\sigma_t = 27.3$, and one would expect that these waters would carry positive nutrient anomalies in the thermocline.

Richards and Redfield (1955) tried to explain the negative surface oxygen anomalies in the Gulf Stream by arguing that the surface stratum ($26.0 - 26.5 \sigma_t$) corresponds to the swiftest flowing waters. This idea, if true, could provide an explanation for the positive surface nutrient anomalies, but not so for the neg-

Figure 7. (a) Nitrate and (b) phosphate concentrations as a function of density (σ_t). Circles and triangles represent observations taken in the Sargasso Sea and the Gulf Stream, respectively. Reproduced from Stefánsson and Atkinson (1971).



ative upper-thermocline anomalies. Furthermore, Richards and Redfield did not consider the nutrient anomaly flux, which should be the important parameter to consider. In particular, we will show later that the nutrient flux is centered in the $26.8 - 27.1 \sigma_t$ range, with similar values both at $\sigma_t = 26.5$ and 27.3 .

A plausible explanation for the patchy nutrient anomalies, positive in the surface layers and negative in the upper thermocline, is intermittent two-way exchange, noticing that surface layers in the Sargasso Sea are much poorer in nutrients than deeper layers. Positive anomalies at the surface and negative anomalies below simply means a reduced gradient, consistent with the idea of diapycnal mixing.

How could diapycnal mixing arise? Stommel (1965) used a one and a half layer potential vorticity conserving model, to simulate the Gulf Stream frontal system. He pointed out that when the upper layer depth, D , becomes shallow enough ($D/D_0 < 0.38$, where D_0 is the upper layer depth far from the front), the internal Froude number exceeds unity, and the flow becomes supercritical. Looking at a hydrographic section from Worthington (1954), Stommel (1965, p. 115) pointed out that “it is interesting to note that this is where the point of inflection in the depth of the 10°C isotherm actually occurs”. In the hydrographic section analyzed below (Chapters 7 and 8) this is also the point where the shrinking of the isopycnal layers is a maximum.

Further support for the idea of diapycnal mixing comes from the analysis of tritium distributions by Jenkins (1980) and Sarmiento et al. (1982). They observed large upper thermocline tritium concentrations in the northwest portion of the subtropical gyre, which can only be due to enhanced mixing between the

surface and upper thermocline layers.

In this work we look at oxygen and nutrient anomalies in several sections across the Gulf Stream, and use them to analyze mixing processes in western boundary currents. We also enlist the help of a dynamical tracer, potential vorticity. Recently Haynes and McIntyre (1987, 1990) have thoroughly explored the similarities and differences between potential vorticity and chemical tracers. Here we show how potential vorticity is modified within shrinking and stretching isopycnal layers by diapycnal mixing.

Chapter 3. Hydrographic Observations

*Aristotle taught me to fix my
judgement on that which is grounded
upon reason, and not on the bare
authority of the master.*

Galileo Galilei (1564-1642)

Western boundary currents have been the subject of many and diverse studies. The Gulf Stream, a sample western boundary current, is probably the best studied current in the world ocean. XBT and oxygen sections were already available to C. G. Rossby and A. C. Redfield in the 30's (Seiwell 1934, Rossby 1936, Redfield 1936). Early works on western boundary currents include Stommel's (1958, 1965) monograph on the Gulf Stream, von Arx's (1962) description of its variability, and Stommel and Yoshida's (1972) collection of papers on the Kuroshio current. More recent review articles on the Gulf Stream are those by Fofonoff (1981) and Watt (1983).

Fuglister (1963) carried out a comprehensive study of the Gulf Stream in 1960, which served as the basis for much subsequent work (e.g. Stommel et al. 1978, Bower et al. 1985). Since then, many other sections have been taken, such as those compiled and analyzed by Worthington (1976) and Stommel et al. (1978). With the advent of autoanalyzer techniques, subsurface nutrient data became easier to obtain in the late 60's (Stefánsson and Atkinson 1971). High resolution CTD sections became standard in the 70's. Aerial XBT surveys were undertaken in

the late 70's (Bane et al. 1981, Brooks and Bane 1981, 1983). Spain et al. (1981) developed free-falling instruments, named PEGASUS, capable of measuring both temperature and horizontal currents. Halkin and Rossby (1985) and Leaman et al. (1989) have employed these in obtaining Gulf Stream sections.

Fuglister (1972) and Kirwan et al. (1976) were the first to deploy surface lagrangian floats in the Gulf Stream. Richardson et al. (1981) first developed sub-surface SOFAR drifters, which Shaw and Rossby (1984) used for the Gulf Stream region. Shortly after, Rossby et al. (1985) and Levine et al. (1986) developed constant-density or isopycnal RAFOS floats, which they used to study the Gulf Stream. Acoustic Doppler Current Profilers (ADCP) are presently used as standard equipment in many ships sampling the Stream.

The data used in this work come from two sources. The first one is the MASAR (Mid-Atlantic Bight Slope and Rise) experiment, which explored the Slope Sea and the inshore edge of the Gulf Stream during 1984 and 1985. The second is a set of five hydrographic sections covering the entire Gulf Stream system, from the Florida Straits to the North Atlantic current (beyond the Grand Banks), taken between 1981 and 1985. Both data sets contain high quality CTD, XBT and nutrient data, previously analyzed and used in several reports and publications. These data sets were obtained with standard technology, having the advantage of proven good quality. On the other hand, their spatial resolution was not as good as is possible with more up-to-date techniques.

3.1 MASAR data

The MASAR experiment was sponsored by the Minerals Management Service (MMS) and it is carefully described in Brown et al. (1987); see also Csanady and

Hamilton (1988) and Bane et al. (1988). It included the deployment of a number of mooring arrays with current meters in two sections across the slope and rise of the Mid-Atlantic Bight, maintained between February 1984 and December 1985. During this period there were also eight cruises, at intervals of about three months, and during each of them (except the last one) two hydrographic sections ("northern" and "southern") were taken in the offshore direction. The data collected included CTD and XBT profiles, and subsurface water samples of dissolved oxygen (DO), nitrate, phosphate and silicate. They were provided to us in processed and verified form by P. Hamilton, of Science Applications International Corporation.

As part of the present work we looked at all (15) offshore sections. The Gulf Stream usually passed outside the range of these sections. The Stream did partially cross the southern section during cruises 1 (March 1984), 5 (February 1985), 6 (May 1985) and 7 (September 1985). Of these, cruise 7 provided the most complete picture of the Gulf Stream (hereafter called section 7S). It is the only one that we will analyze.

Fig. 8 shows the location of section 7S, together with the simultaneous position of the Gulf Stream, as it appeared in a satellite image (courtesy of Jenifer Clark, NOAA, adapted from Brown et al. 1987). The satellite image confirms that a portion of the Gulf Stream went through section 7S. Fig. 9 presents the distribution of temperature, salinity, and density for section 7S, with the upwelling isopycnals of the Gulf Stream. Also shown are the distributions for the nitrate, phosphate, silicate and DO concentrations.

Figure 8. (a) Oceanographic thermal analysis map for September 9, 1985 (done by Jenifer Clark, NOAA) for the MASAR area. (b) Location of the MASAR sections during cruise 7, made between September 6 and 9, 1985 (adapted from Brown et al. 1987).

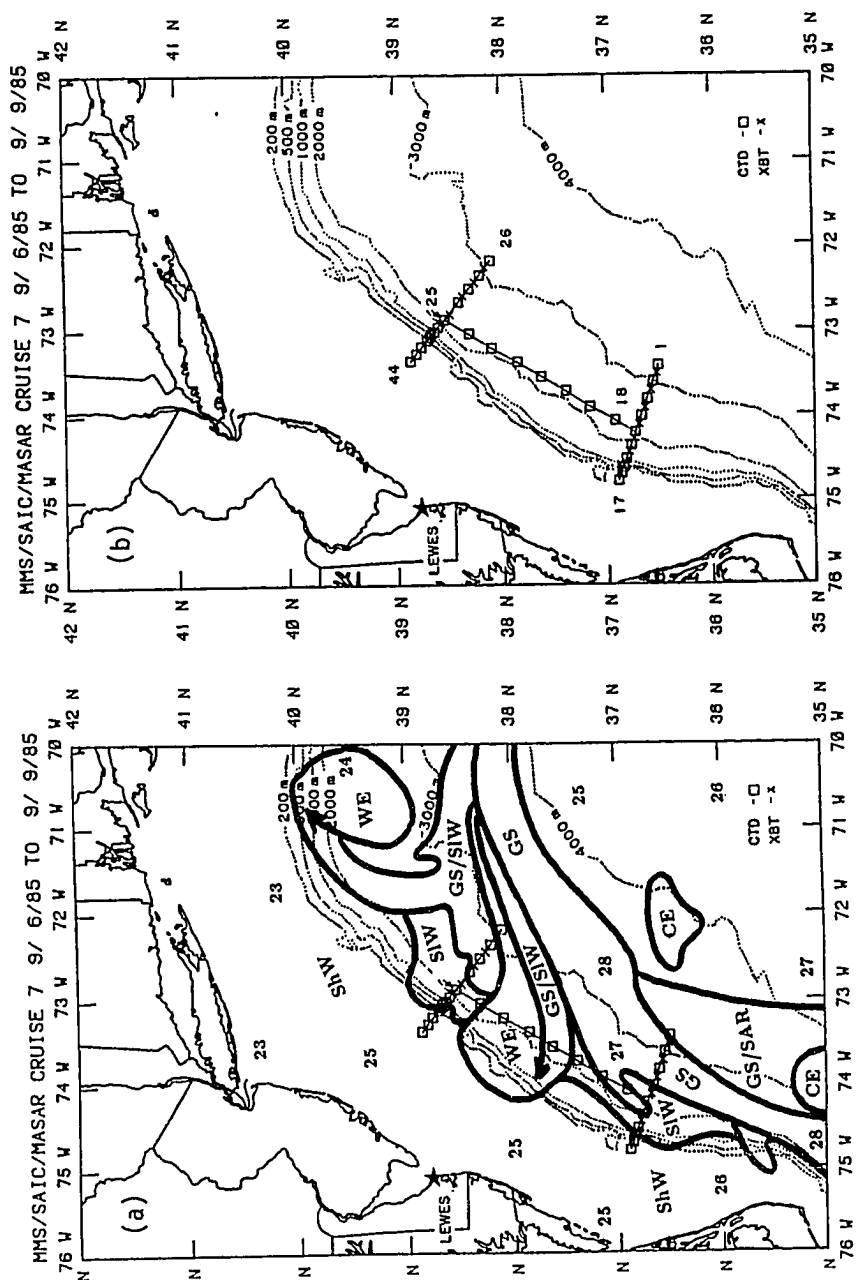
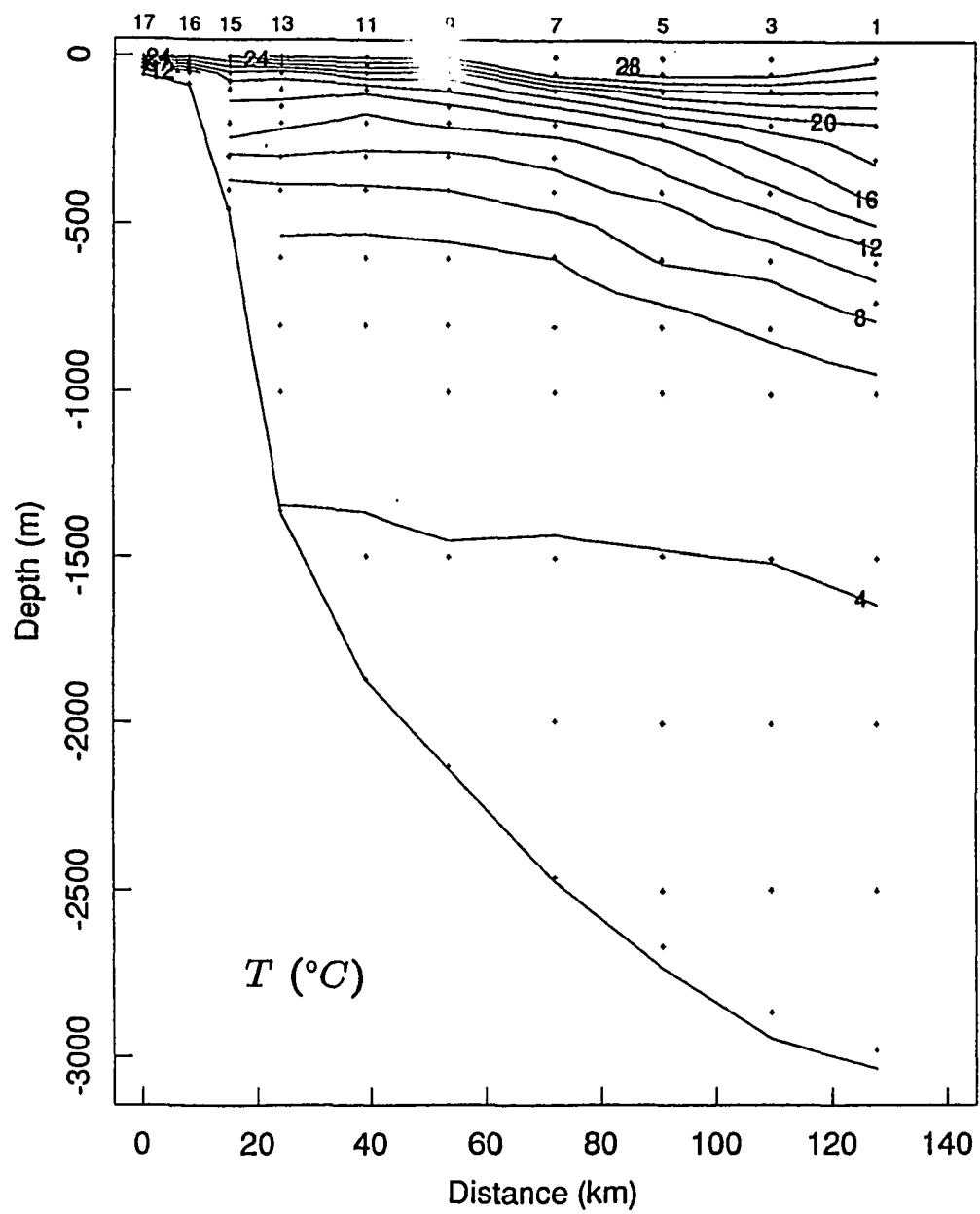


Figure 9. Temperature, salinity, density (σ_t), and nitrate, phosphate, silicate and DO concentrations in section 7S.



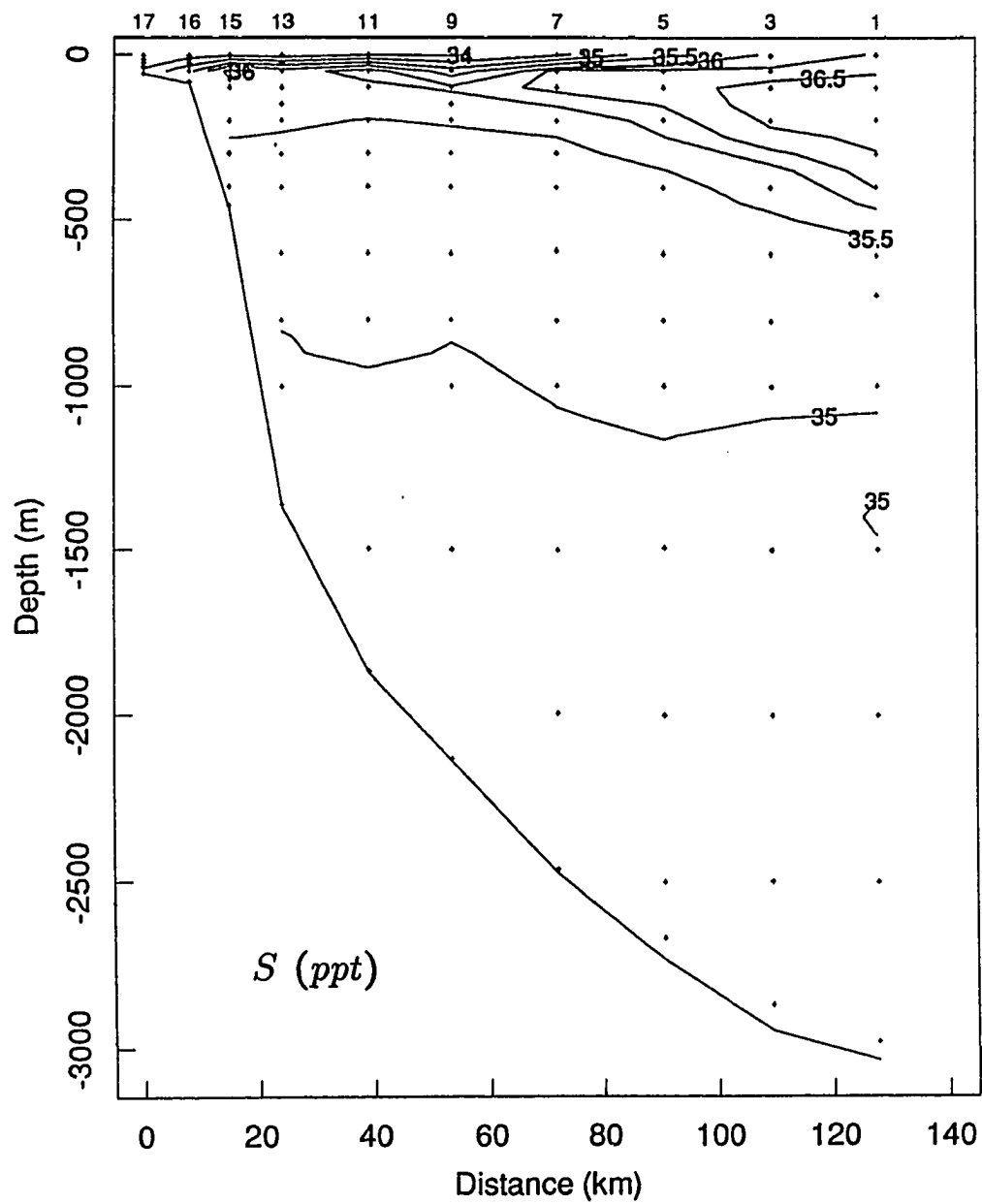


Figure 9 (continued)

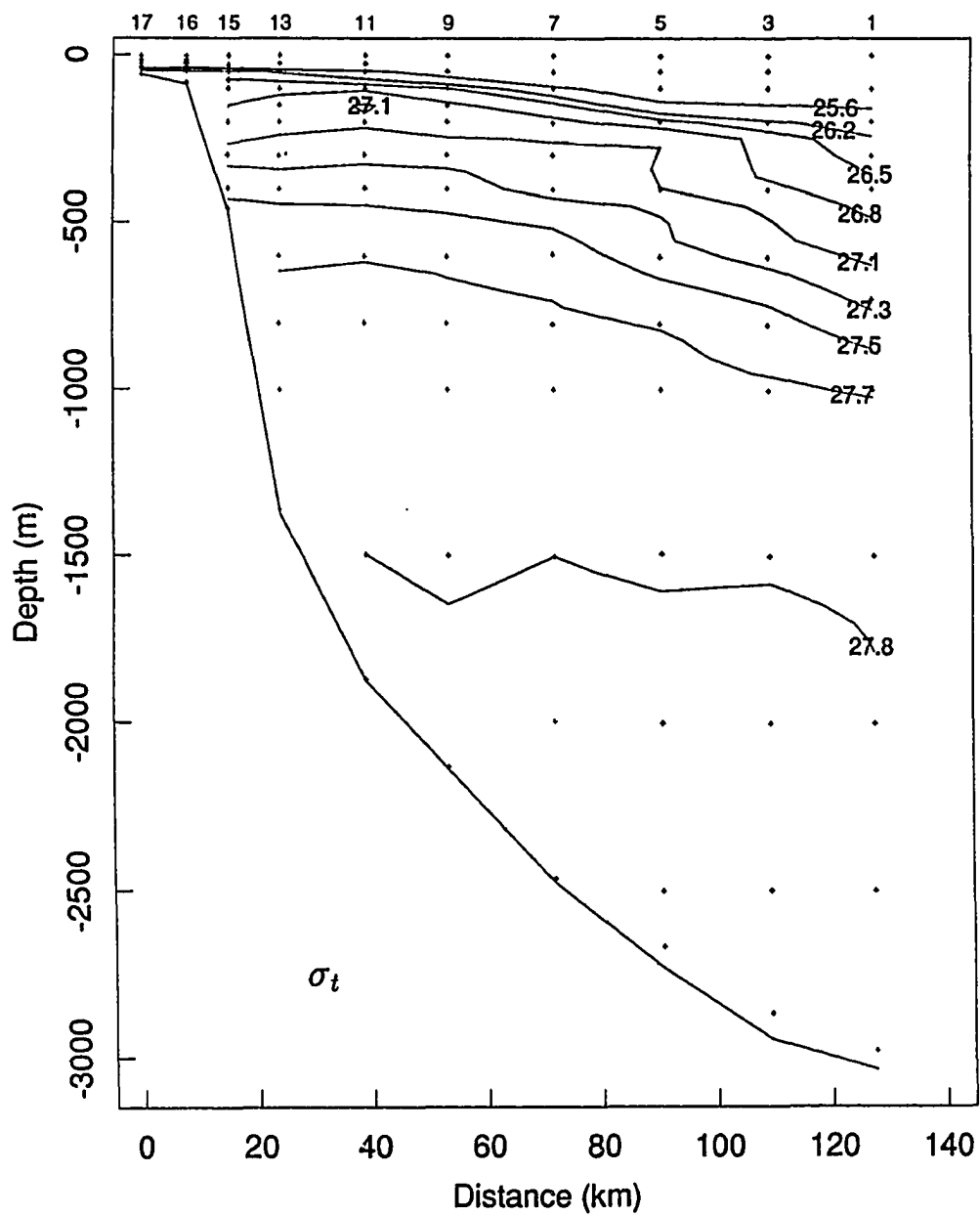


Figure 9 (continued)

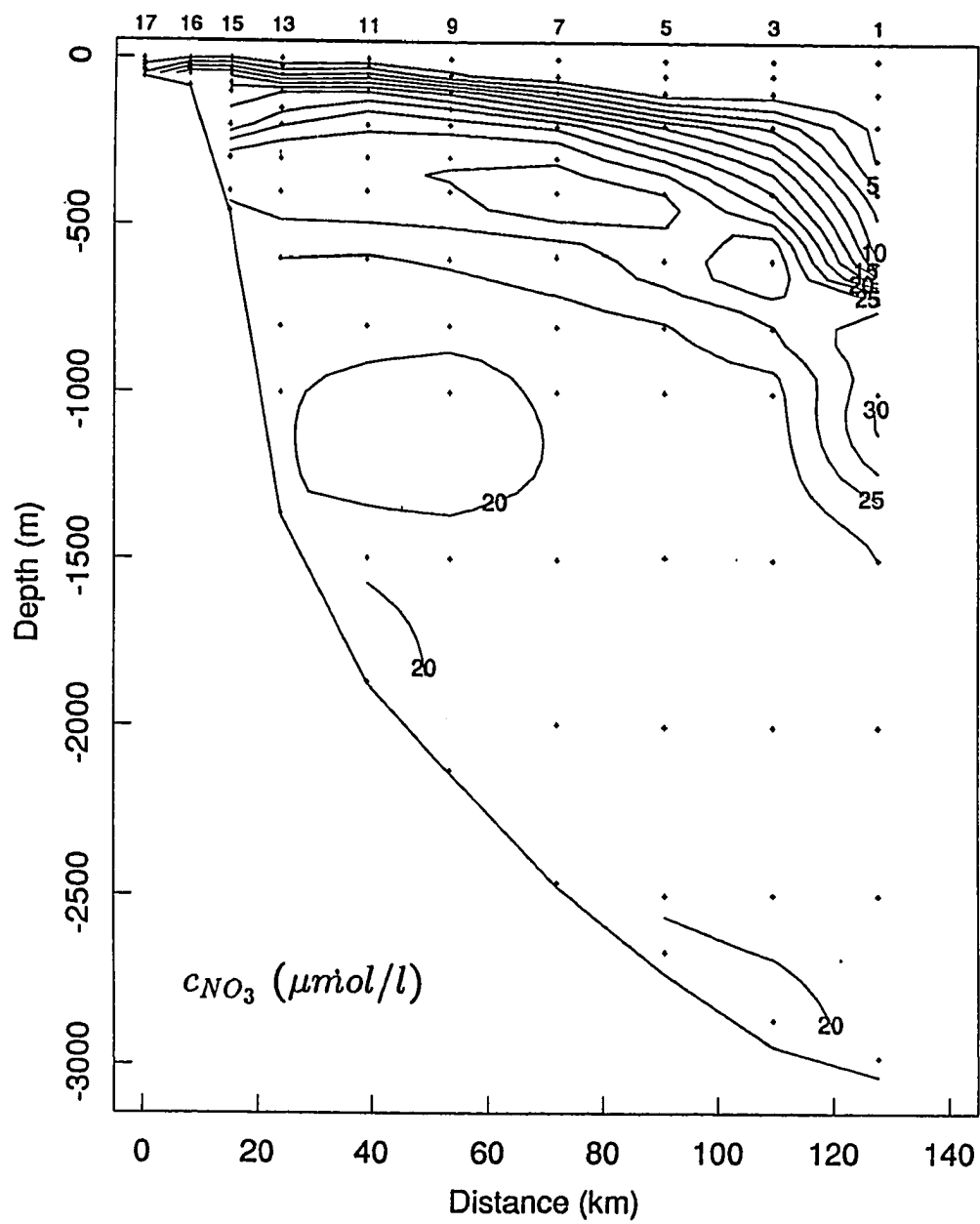


Figure 9 (continued)

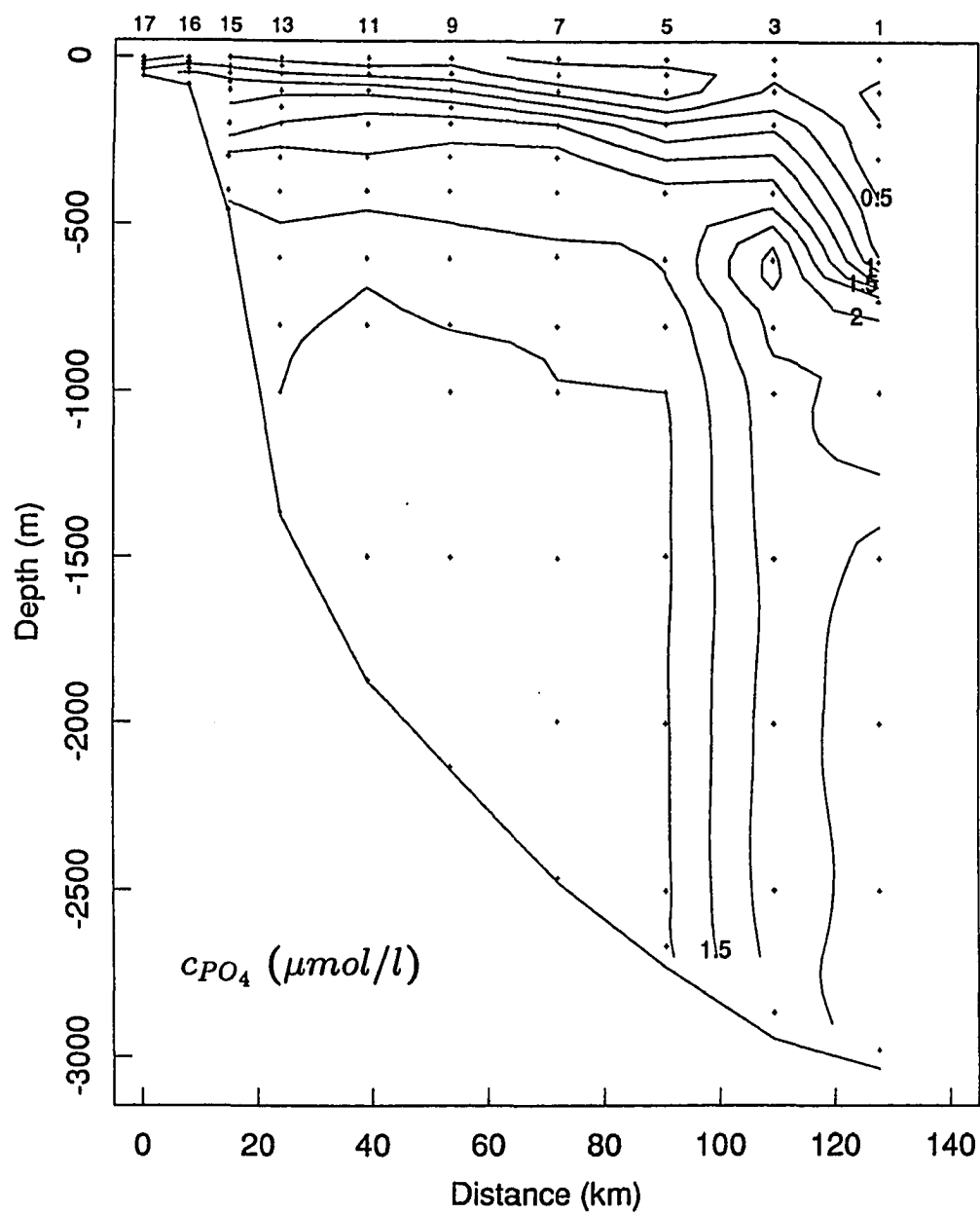


Figure 9 (continued)

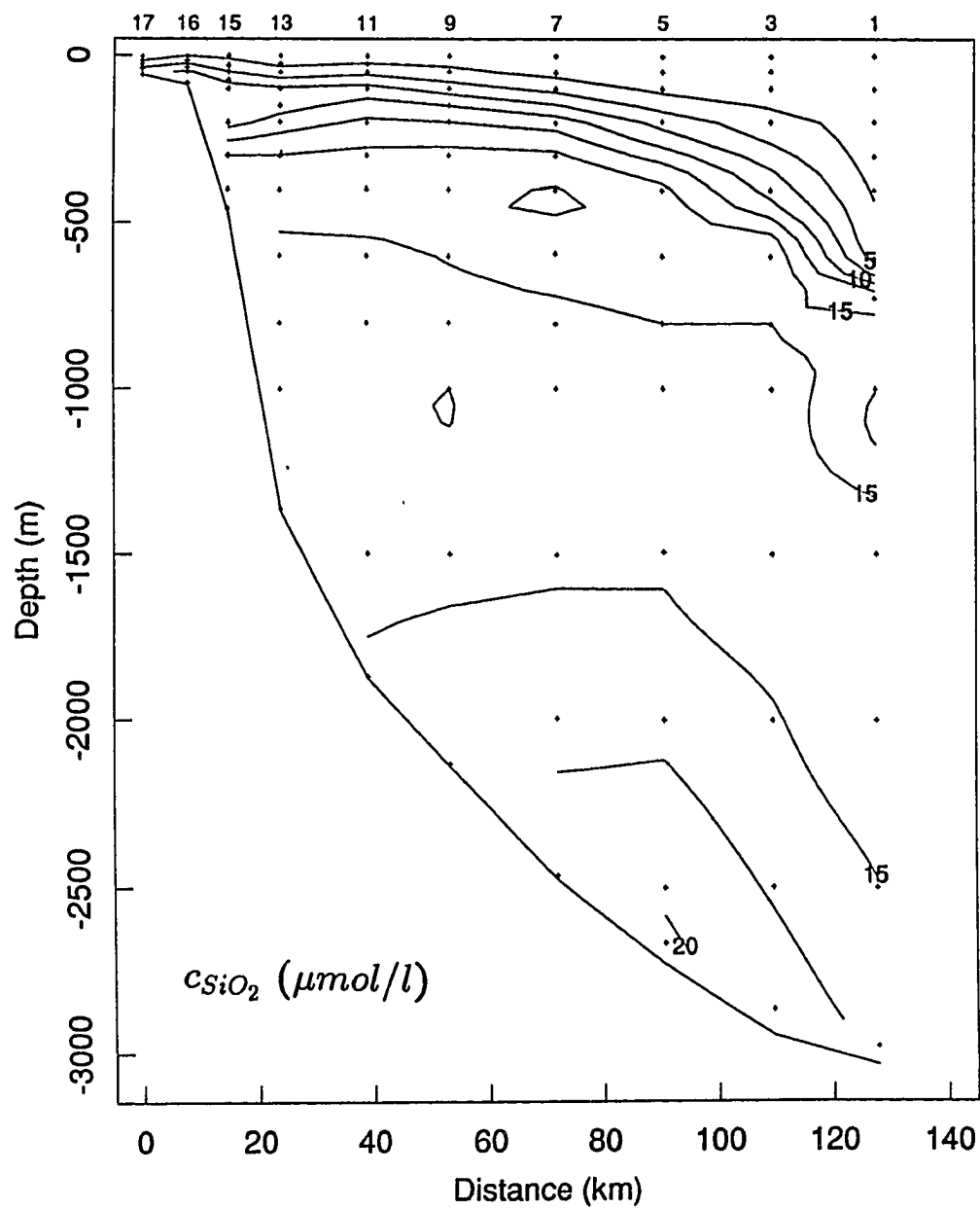


Figure 9 (continued)

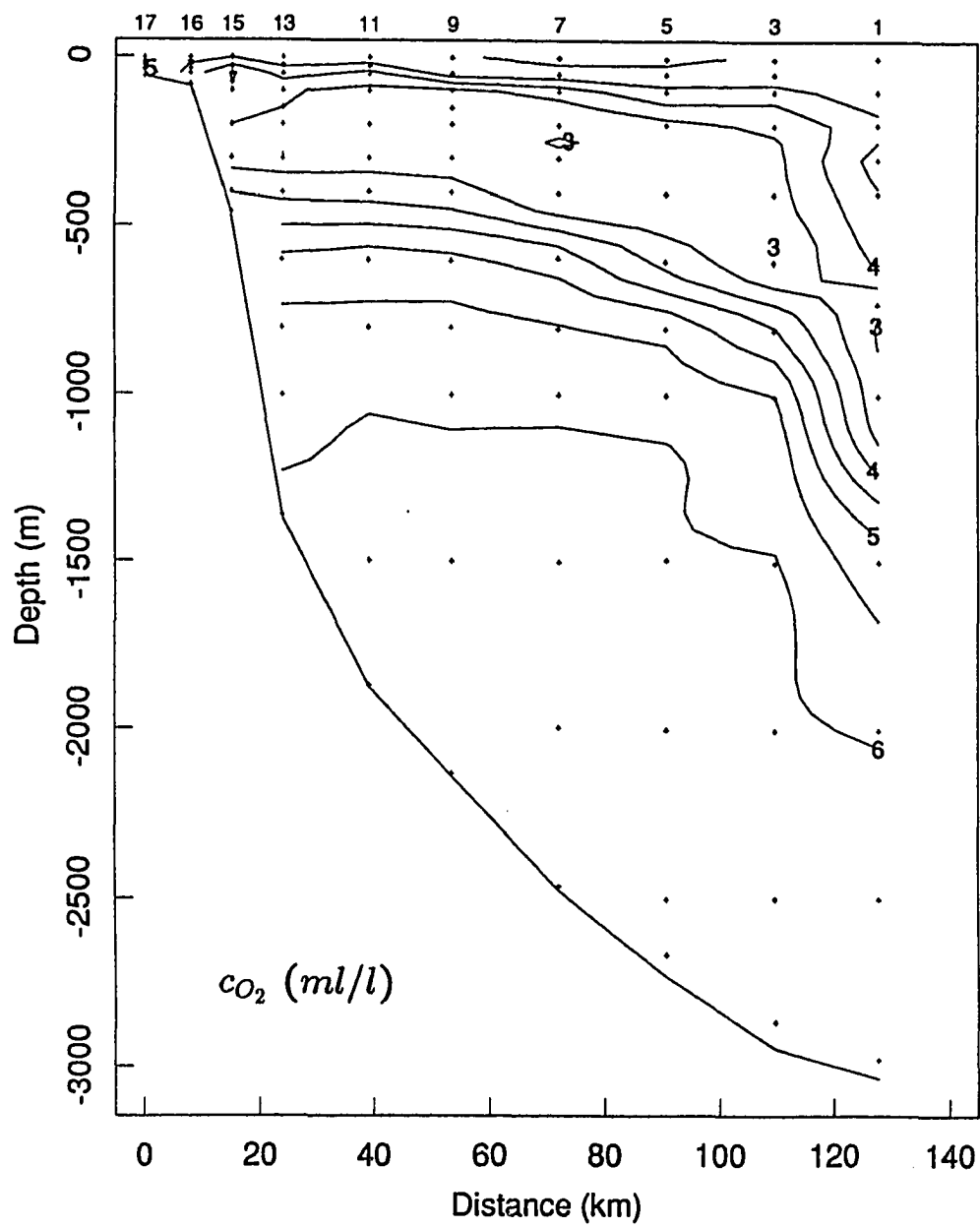


Figure 9 (continued)

3.2 Five sections across the Gulf Stream

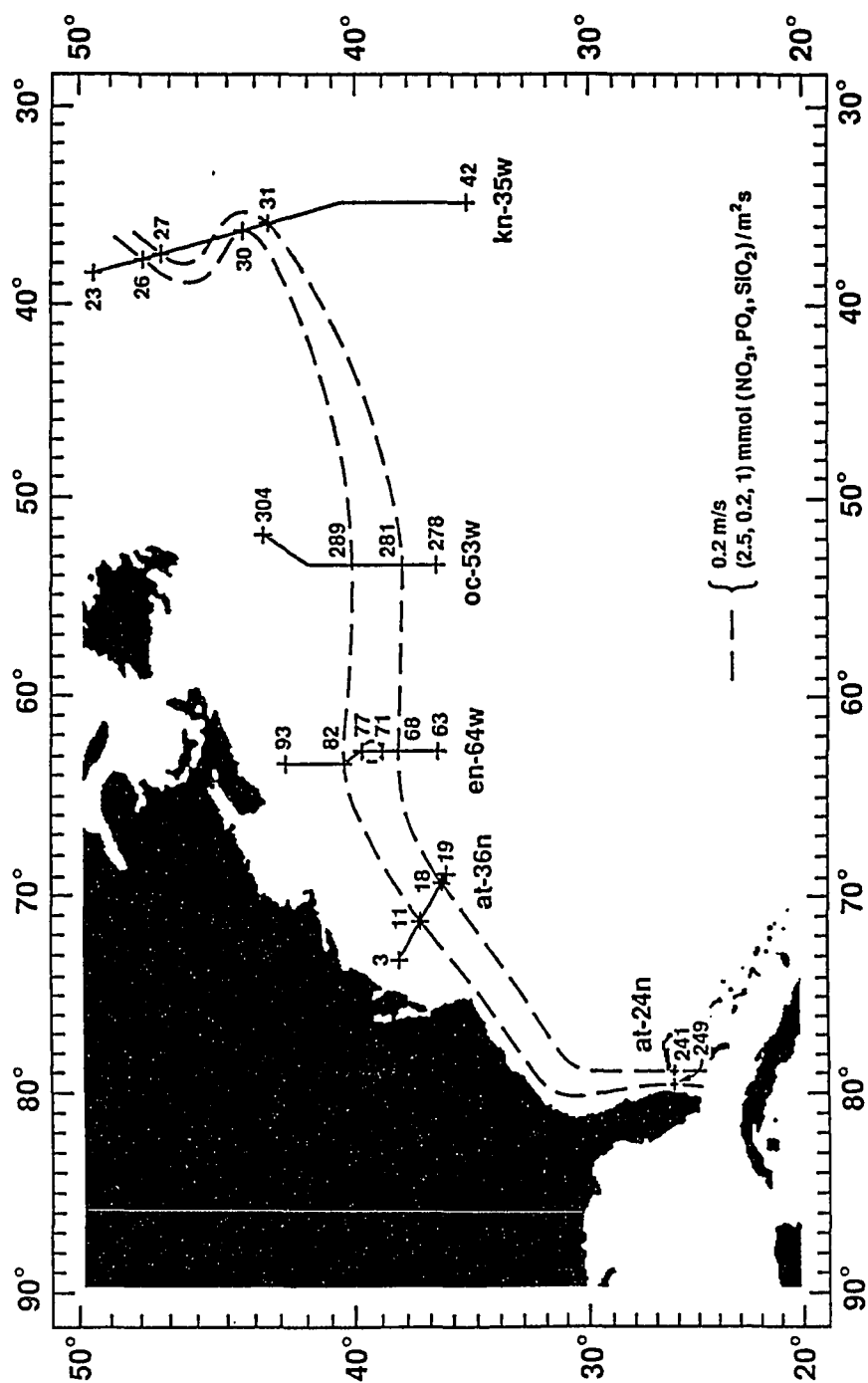
The tracks of the five Gulf Stream-North Atlantic Current hydrographic sections used in our study are shown in Fig. 10. They will be identified by the latitude or longitude approximately followed during the cruise: $24^{\circ}N$, $36^{\circ}N$, $64^{\circ}W$, $53^{\circ}W$, and $35^{\circ}W$ (hereafter, they will be called sections 24N, 36N, 64W, 53W and 35W, respectively). The dates of the sections were September 5, 1981, June 12-14, 1981, April 23-28, 1985, May 14-17, 1983, and July 28 to August 9, 1983, respectively. All sections were taken in late spring to summer, and two consecutive section pairs (24N-36N and 53W-35W) were taken in the same year, with a time lapse of only about two and a half months.

The data were made available to us in processed and verified form by M. McCartney of Woods Hole Oceanographic Institute. They included readings of temperature, salinity, nitrate, phosphate, silicate and DO. From the salinity and temperature data, we have calculated the σ_t field. Figs. 11 to 15 present these data for all sections. In all of them the north-westwards upwelling isopycnals signify the Gulf Stream. In our analysis of all five sections we used XBT as well as DO and nutrient data.

3.3 Section 36N

We have examined section 36N in greater detail than the others. For this analysis we have used both nutrient and high resolution CTD data. This section crosses the Gulf Stream off the Mid-Atlantic Bight, and it was occupied between June 12 and June 14, 1981, moving in the offshore direction (Fig. 16). Fig. 17, adapted from originals (courtesy of Jenifer Clark of NOAA), shows two Gulf Stream frontal analysis maps made over the region of consideration just before (June 10, 1981)

Figure 10. Hydrographic and nutrient sections employed to calculate water mass and nutrient transports from the Florida Straits to the North Atlantic Ocean. The dashed lines indicate the approximate contours for the Nutrient Stream as defined by the specified nutrient flux values.



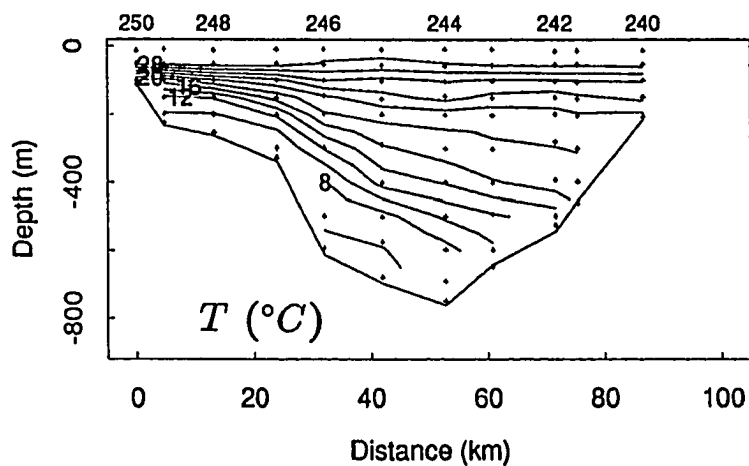


Figure 11. Temperature, salinity, density (σ_t), and nitrate, phosphate, silicate and DO concentrations in section 24N.

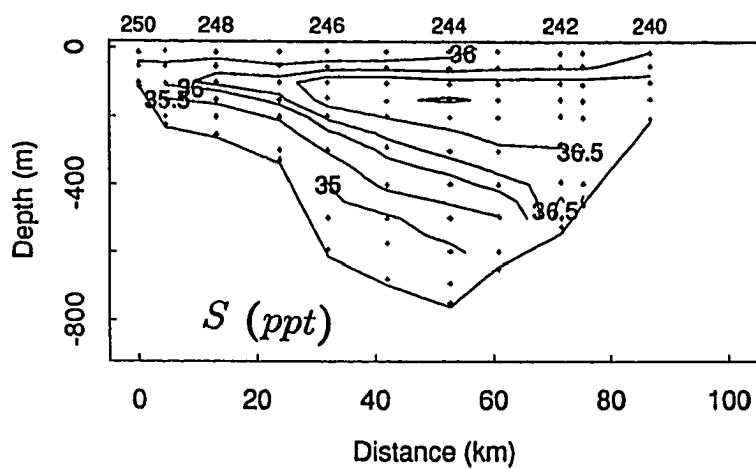


Figure 11 (continued)

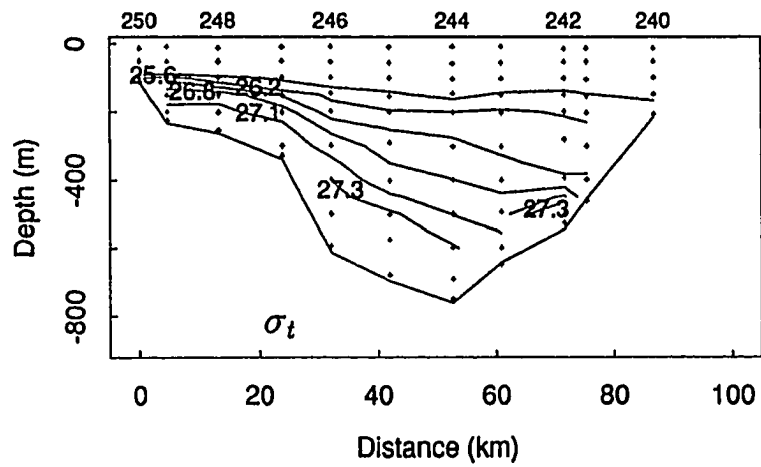


Figure 11 (continued)

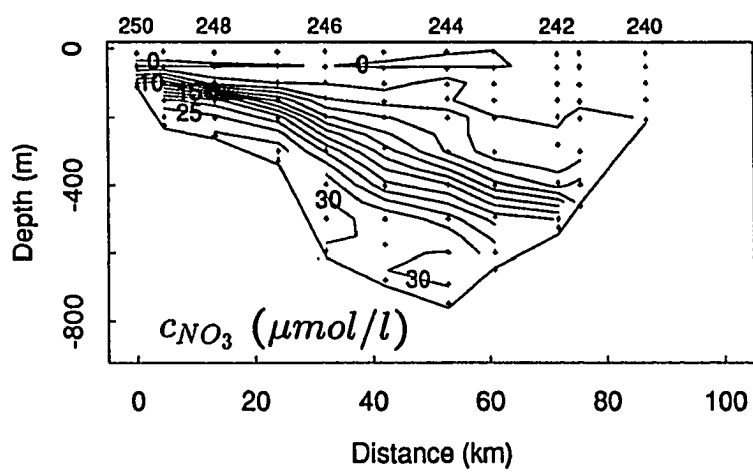


Figure 11 (continued)

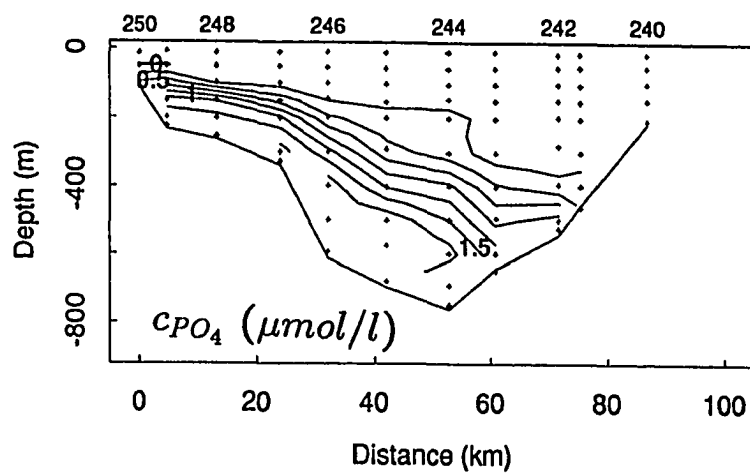


Figure 11 (continued)

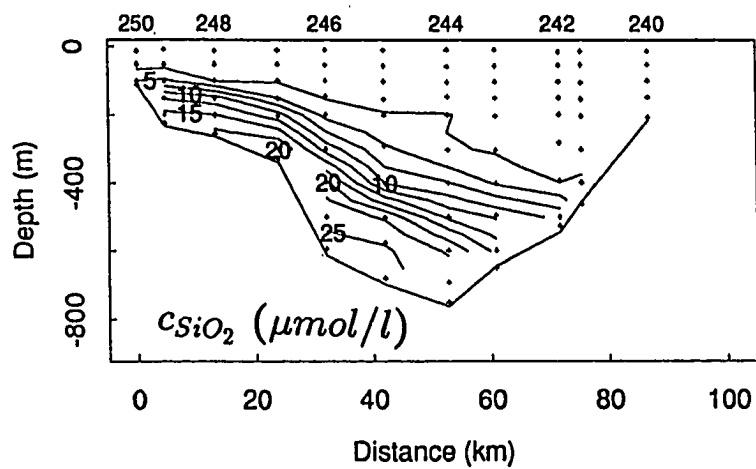


Figure 11 (continued)

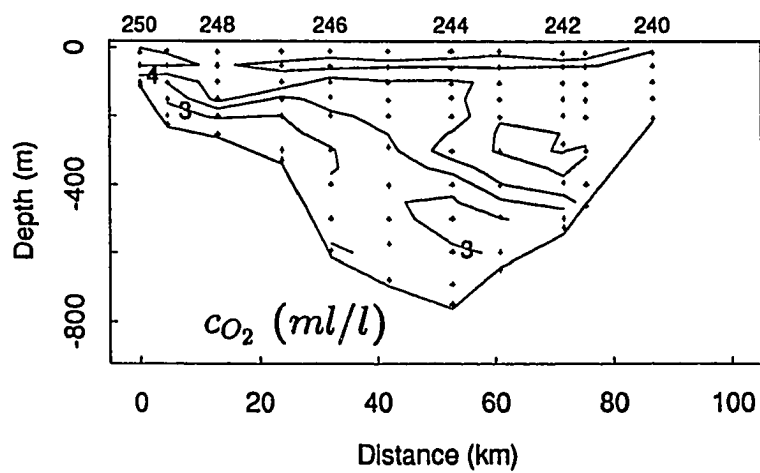
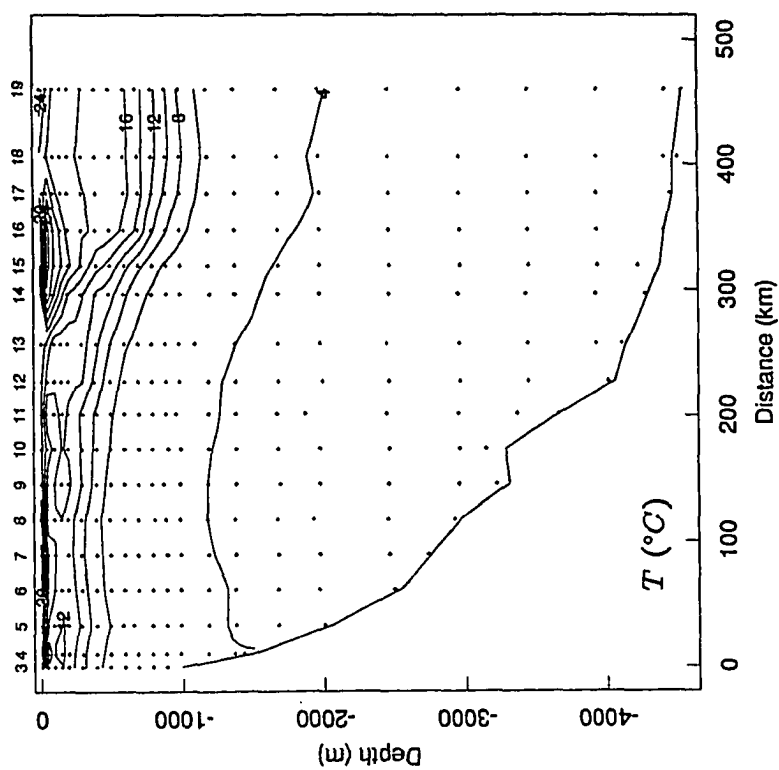


Figure 11 (continued)

Figure 12. Temperature, salinity, density (σ_t), and nitrate, phosphate, silicate and DO concentrations in section 36N.



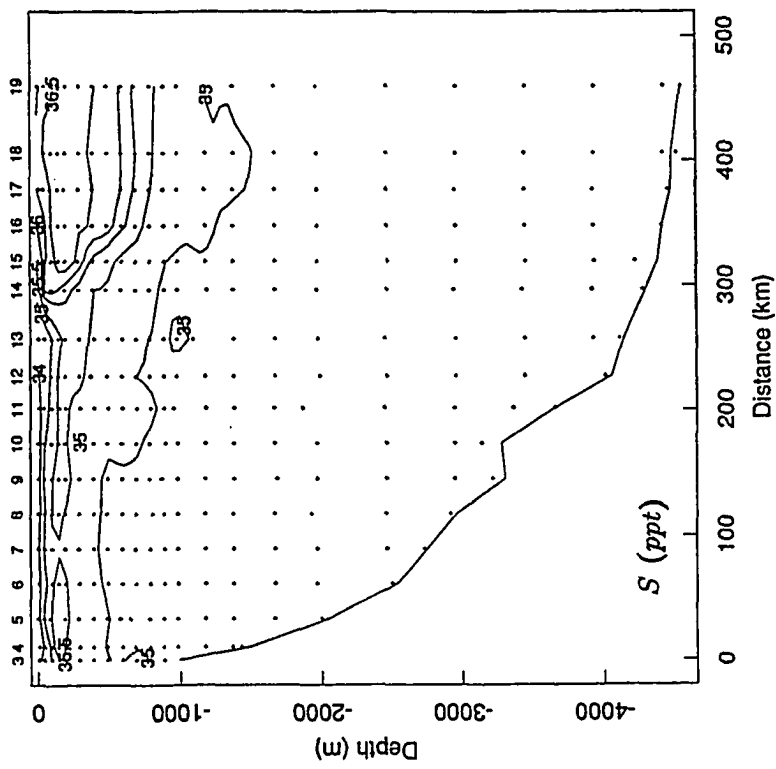


Figure 12 (continued)

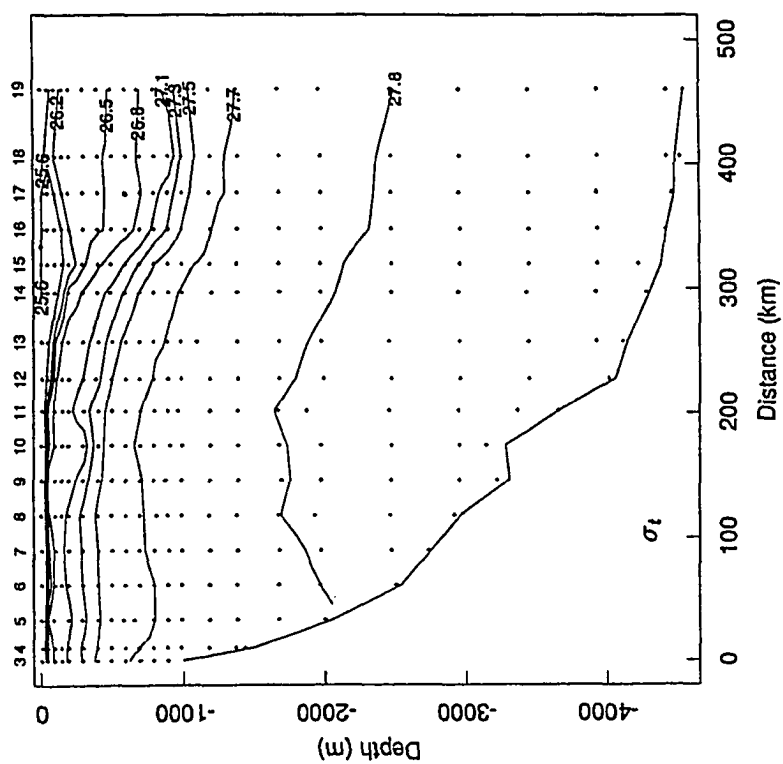


Figure 12 (continued)

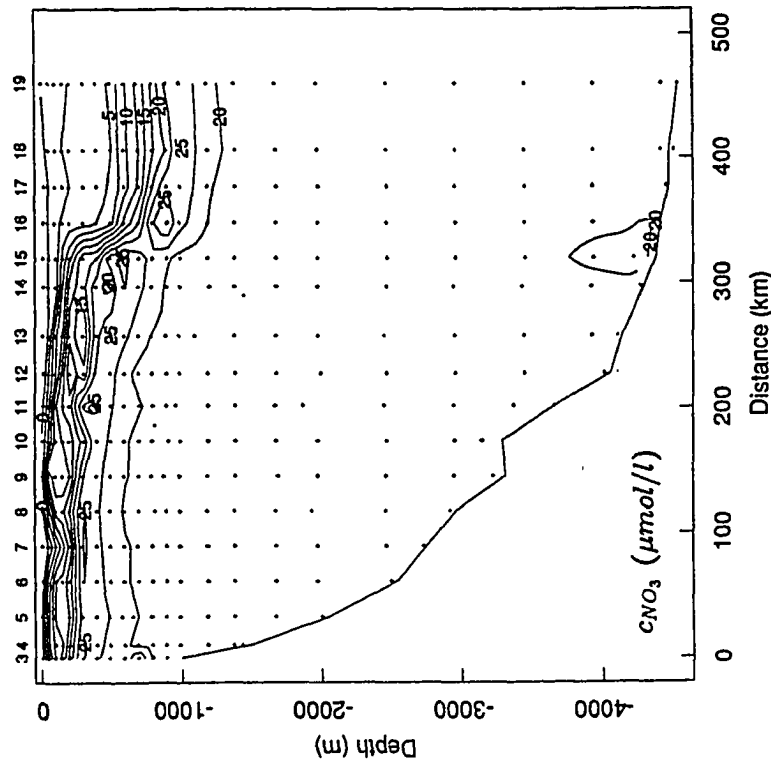


Figure 12 (continued)

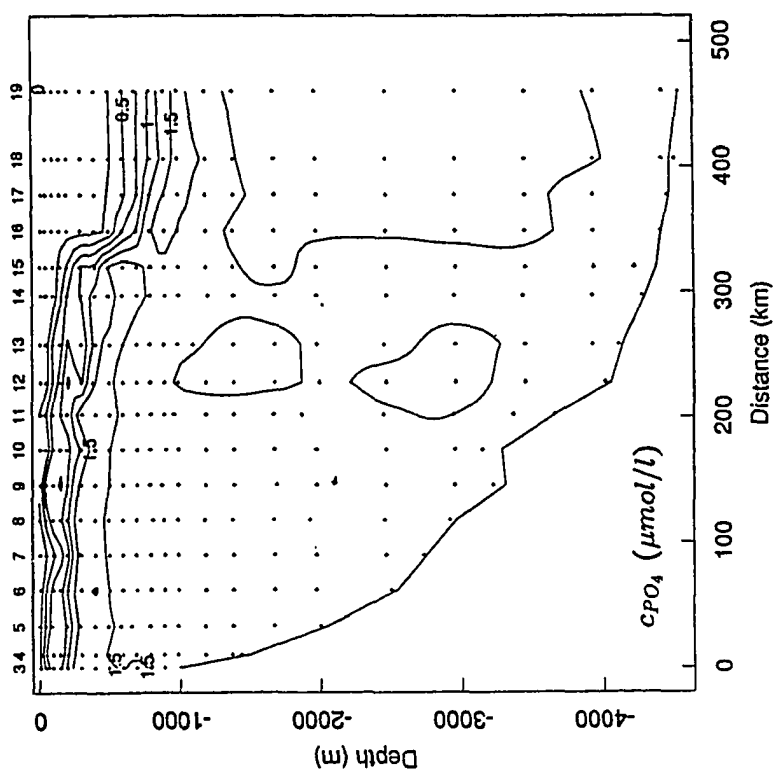


Figure 12 (continued)

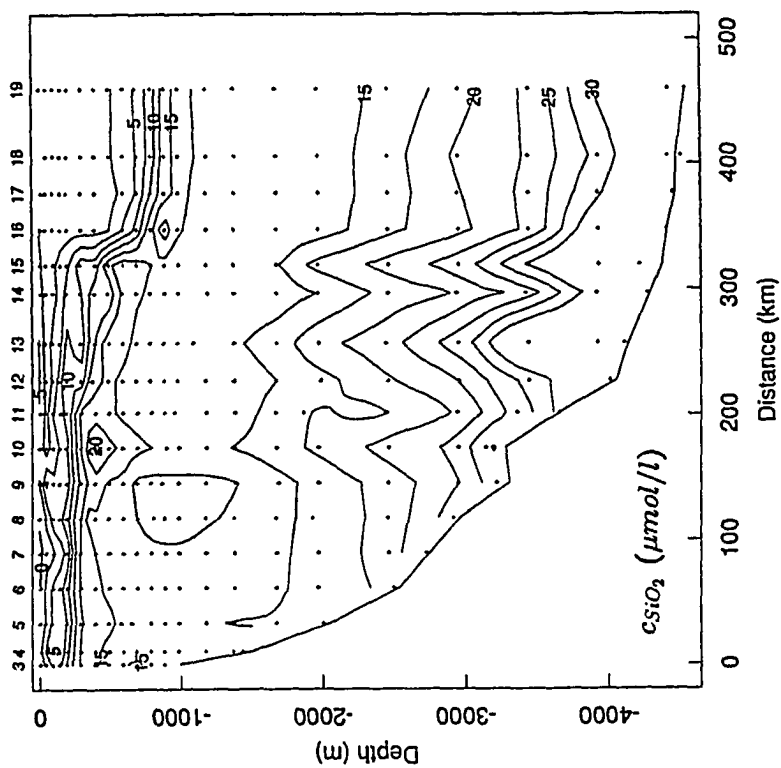


Figure 12 (continued)

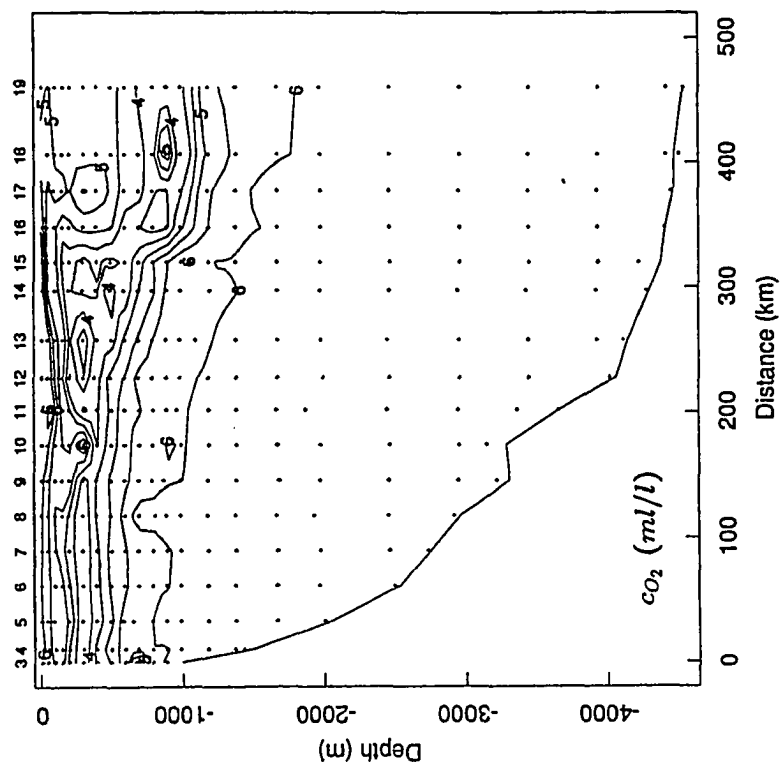
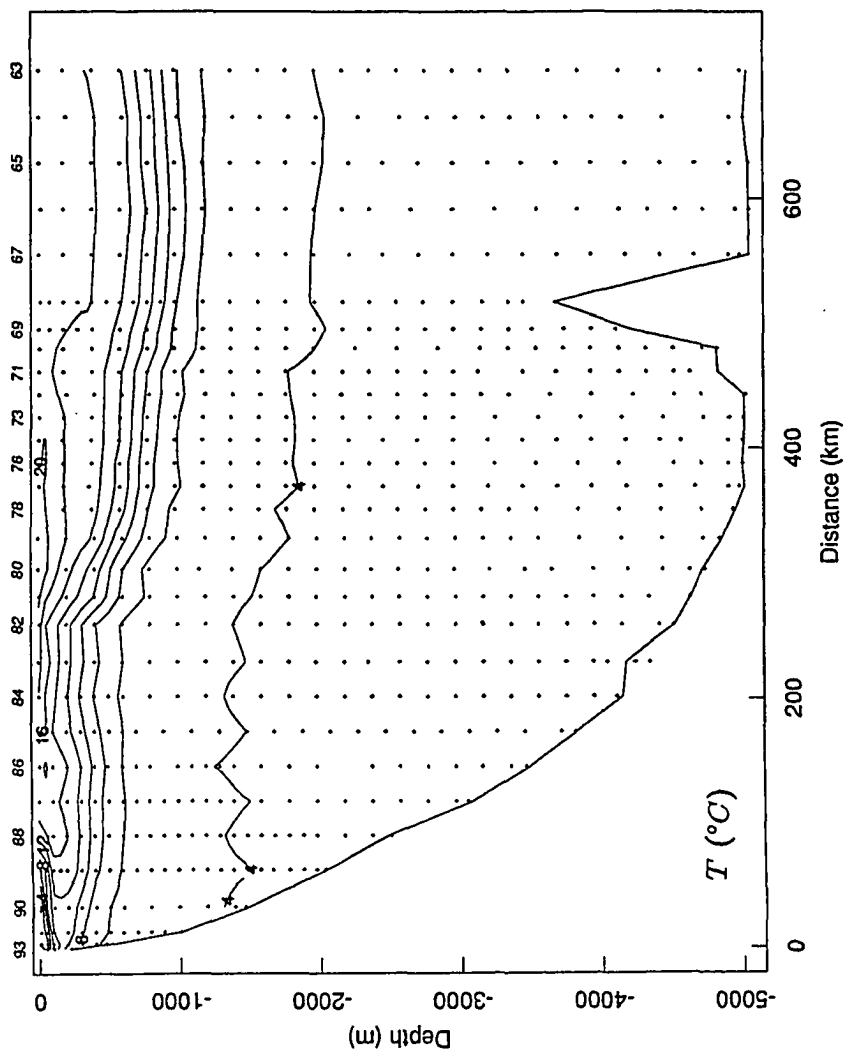


Figure 12 (continued)

Figure 13. Temperature, salinity, density (σ_t), and nitrate, phosphate, silicate and DO concentrations in section 64W.



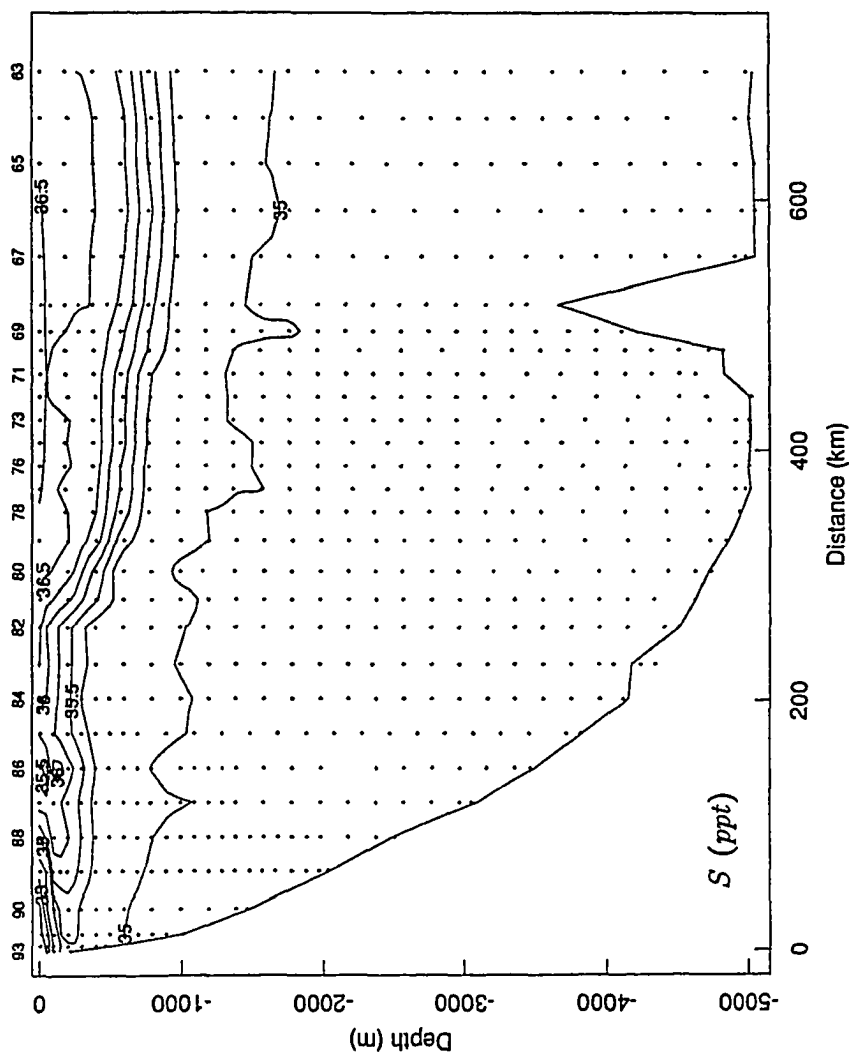


Figure 13 (continued)

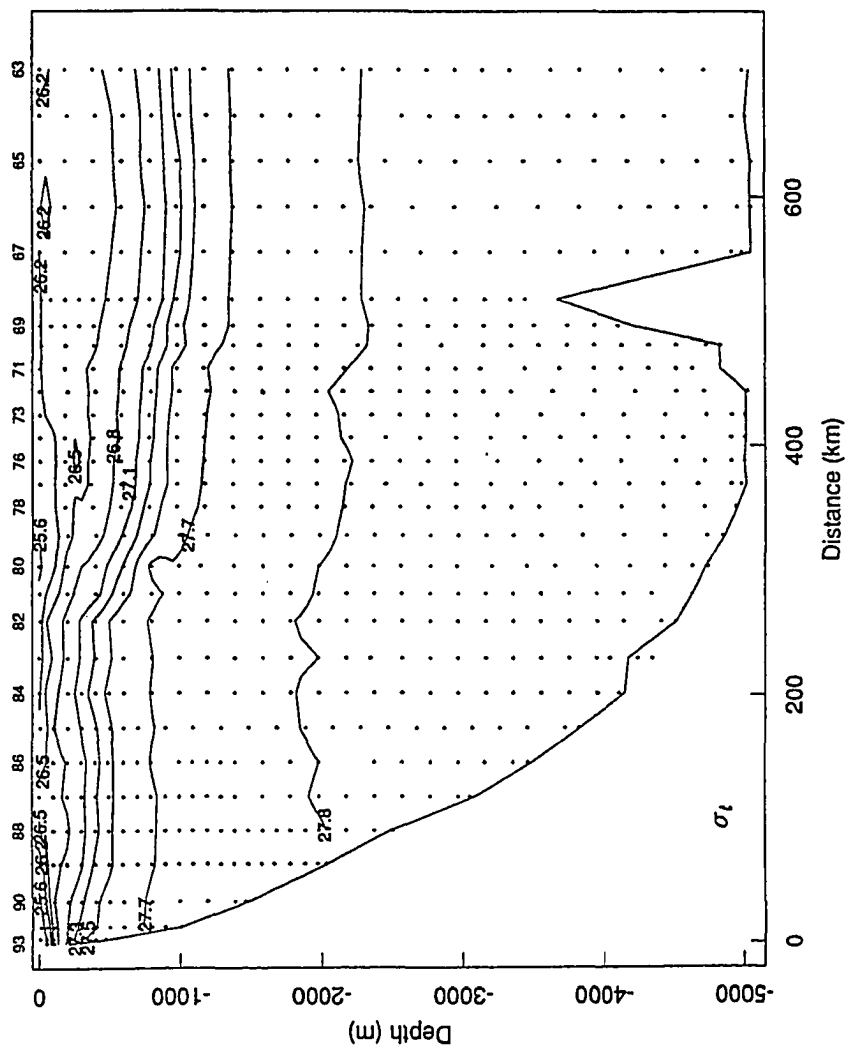


Figure 13 (continued)

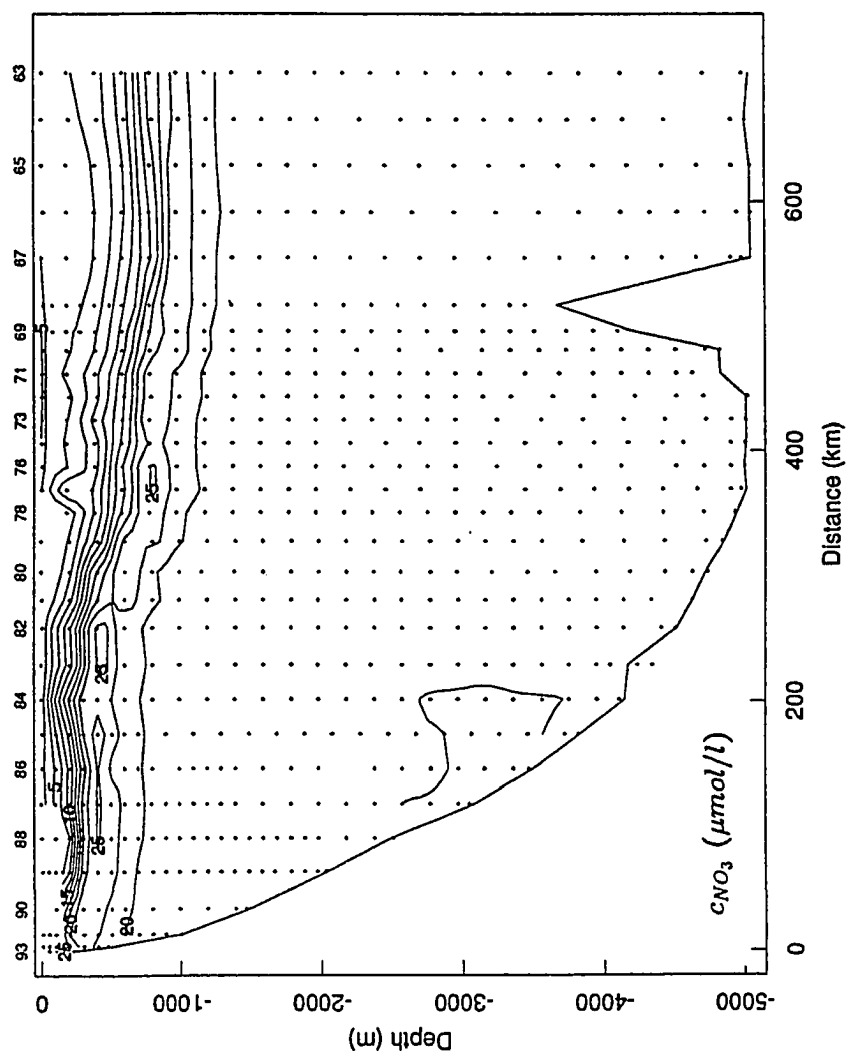


Figure 13 (continued)

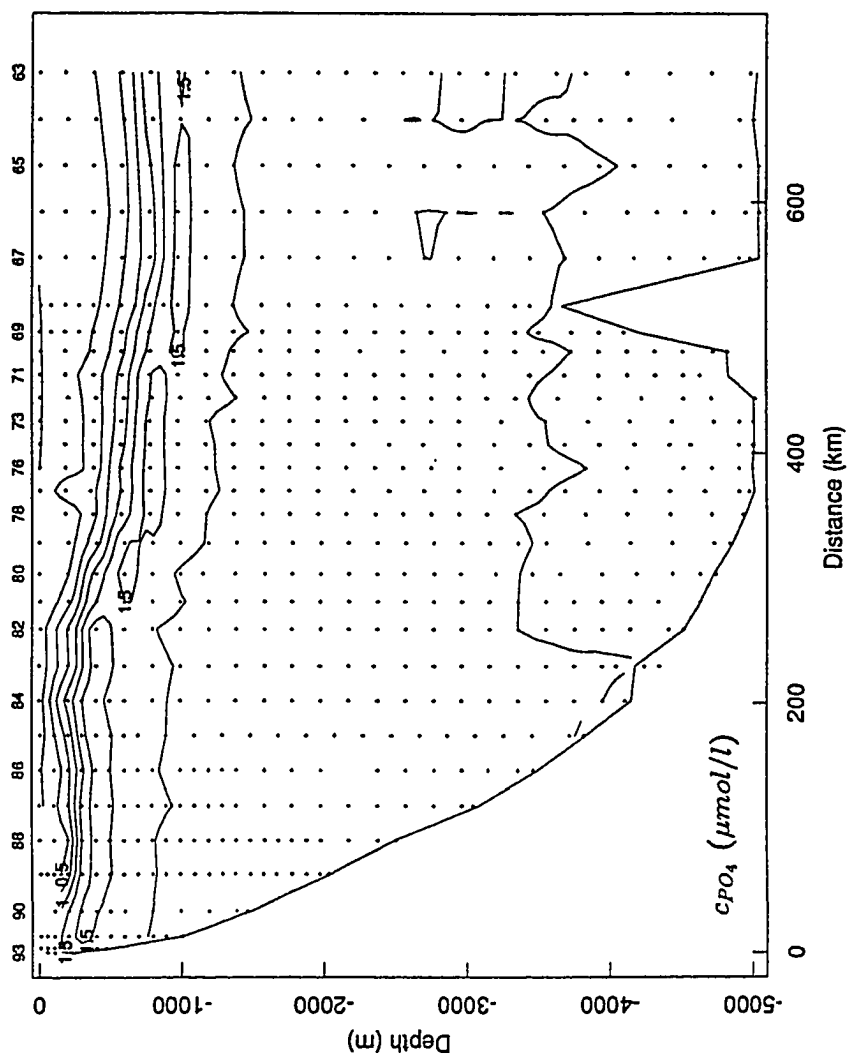


Figure 13 (continued)

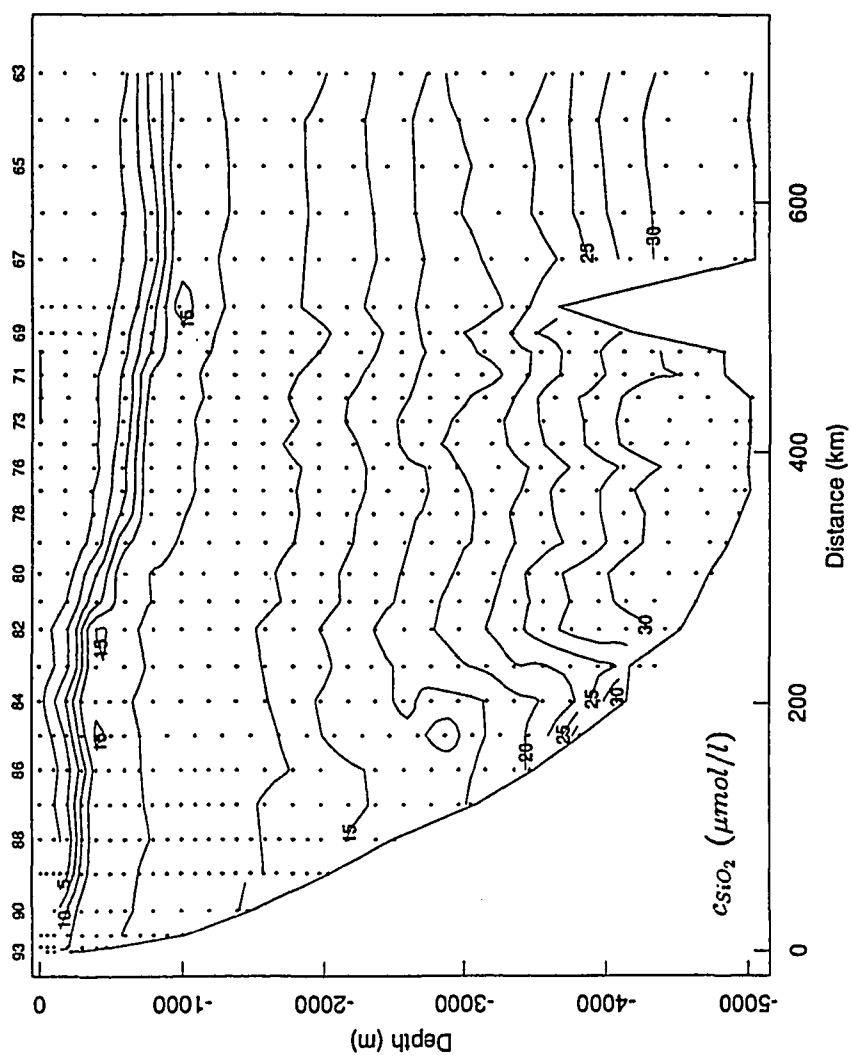


Figure 13 (continued)

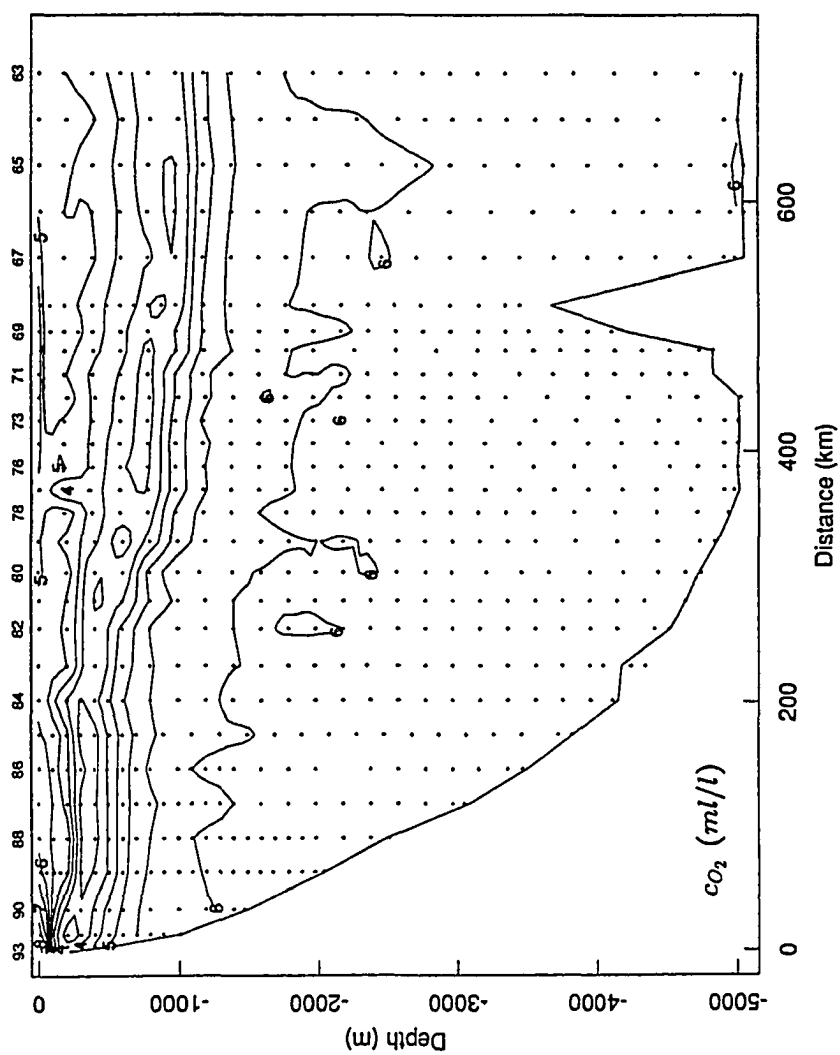
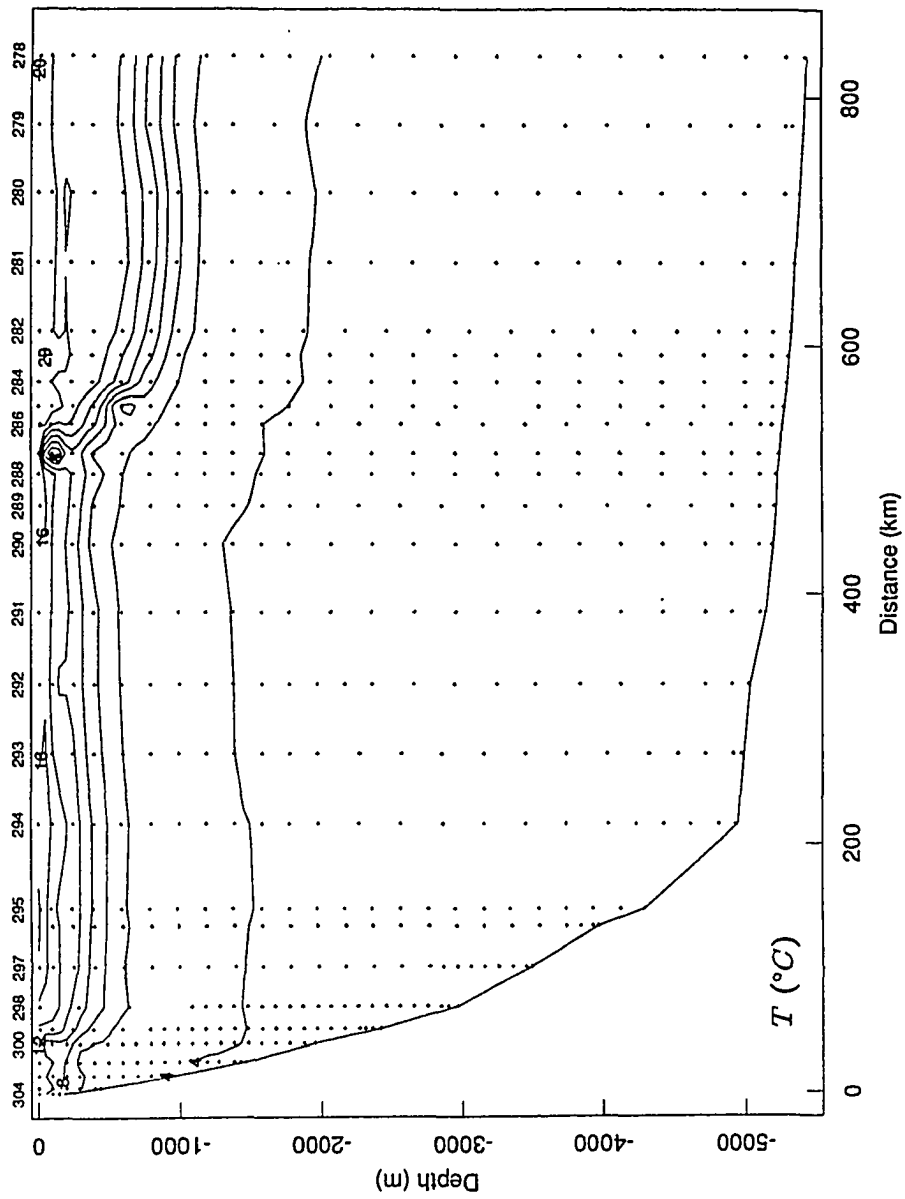


Figure 13 (continued)

Figure 14. Temperature, salinity, density (σ_t), and nitrate, phosphate, silicate and DO concentrations in section 53W.



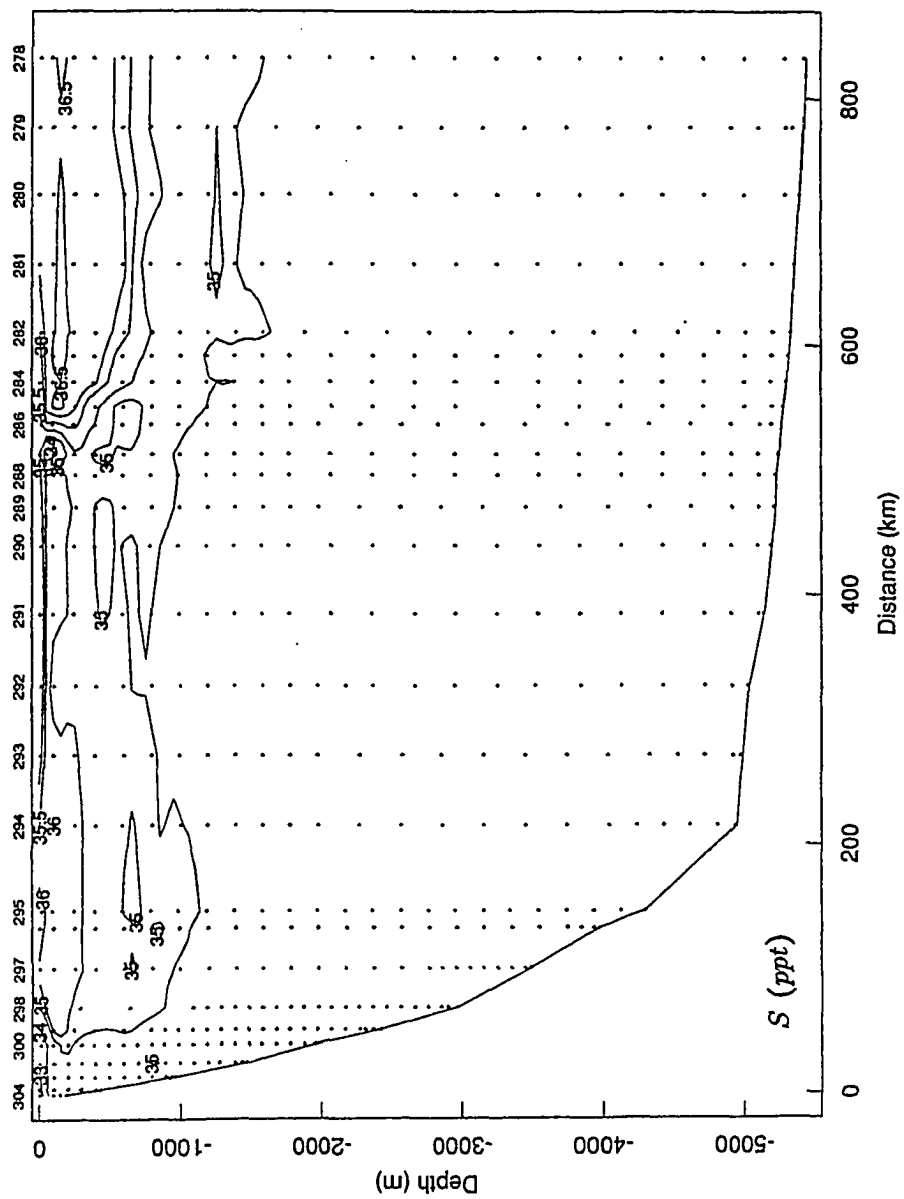


Figure 14 (continued)

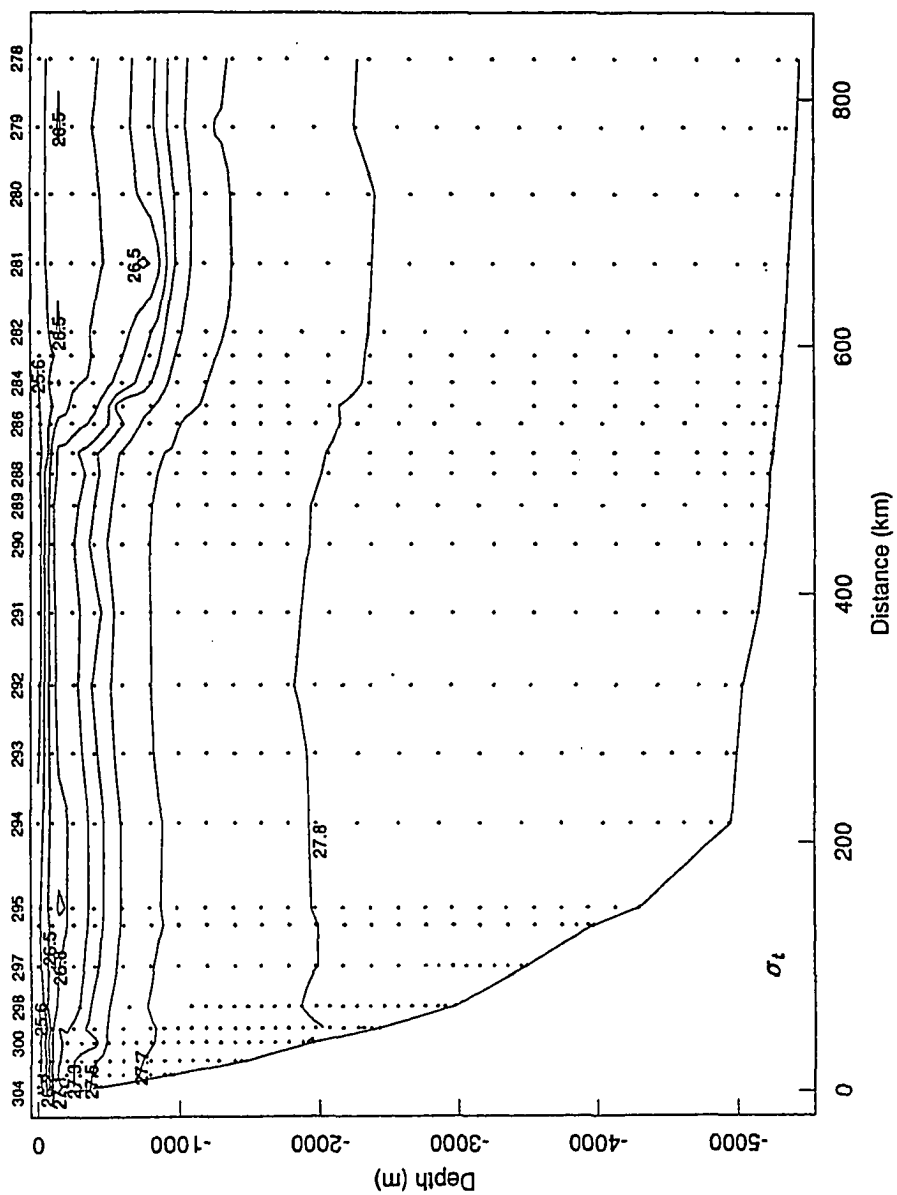


Figure 14 (continued)

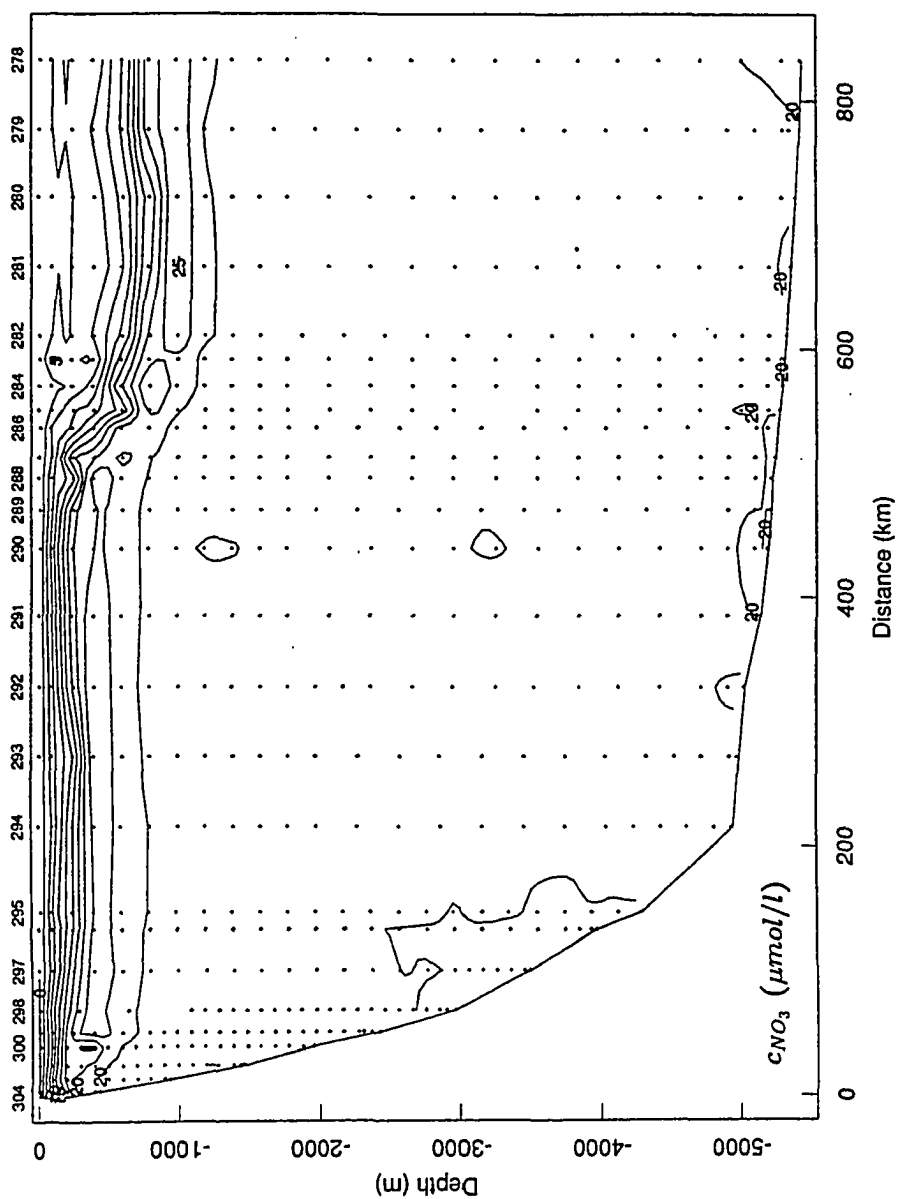


Figure 14 (continued)

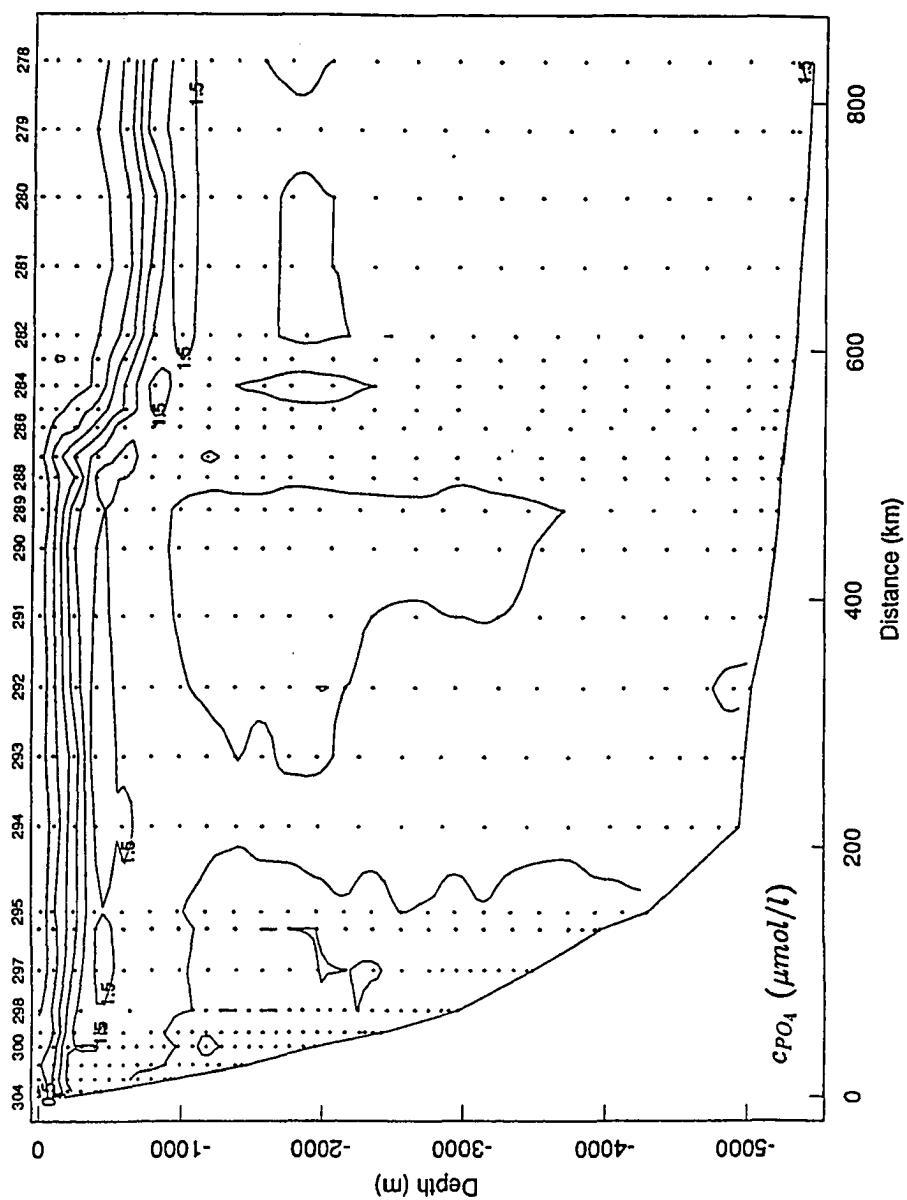


Figure 14 (continued)

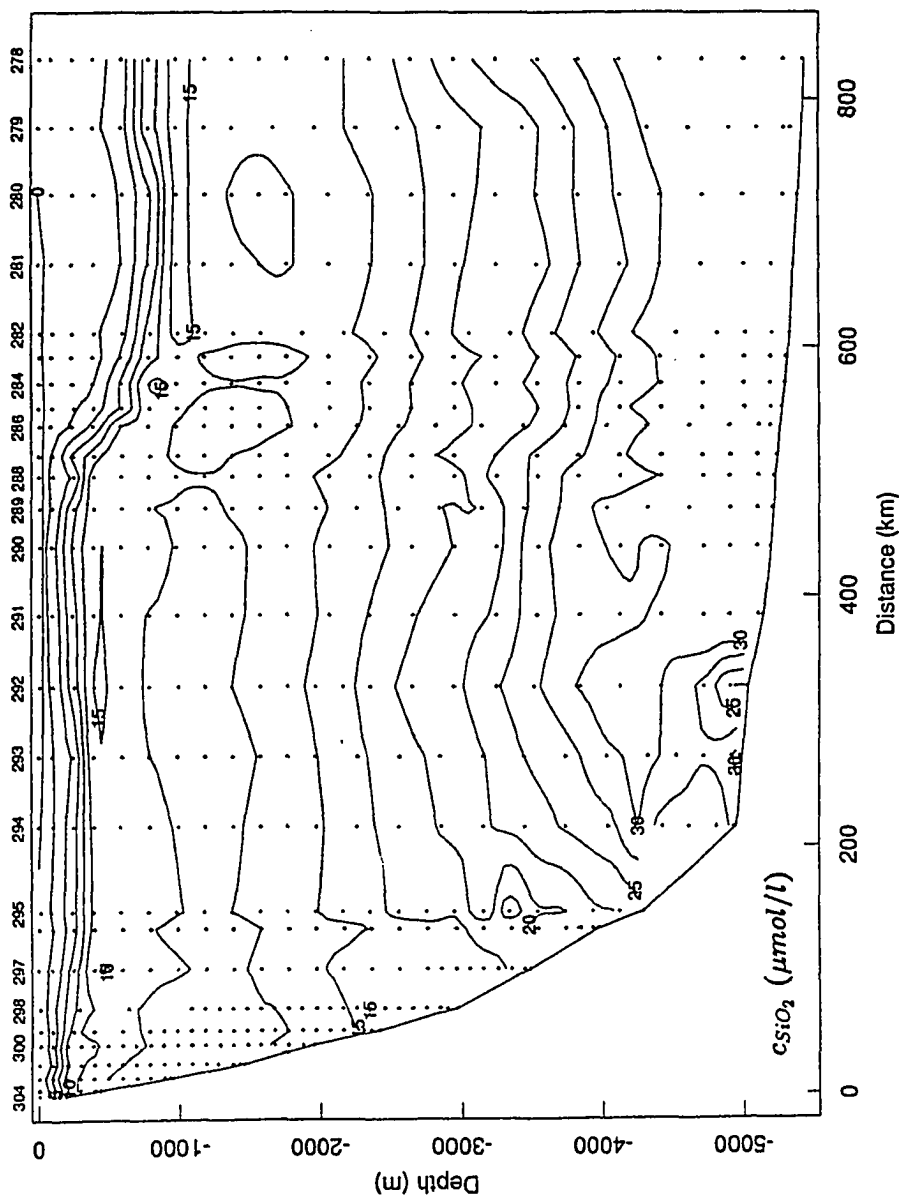


Figure 14 (continued)

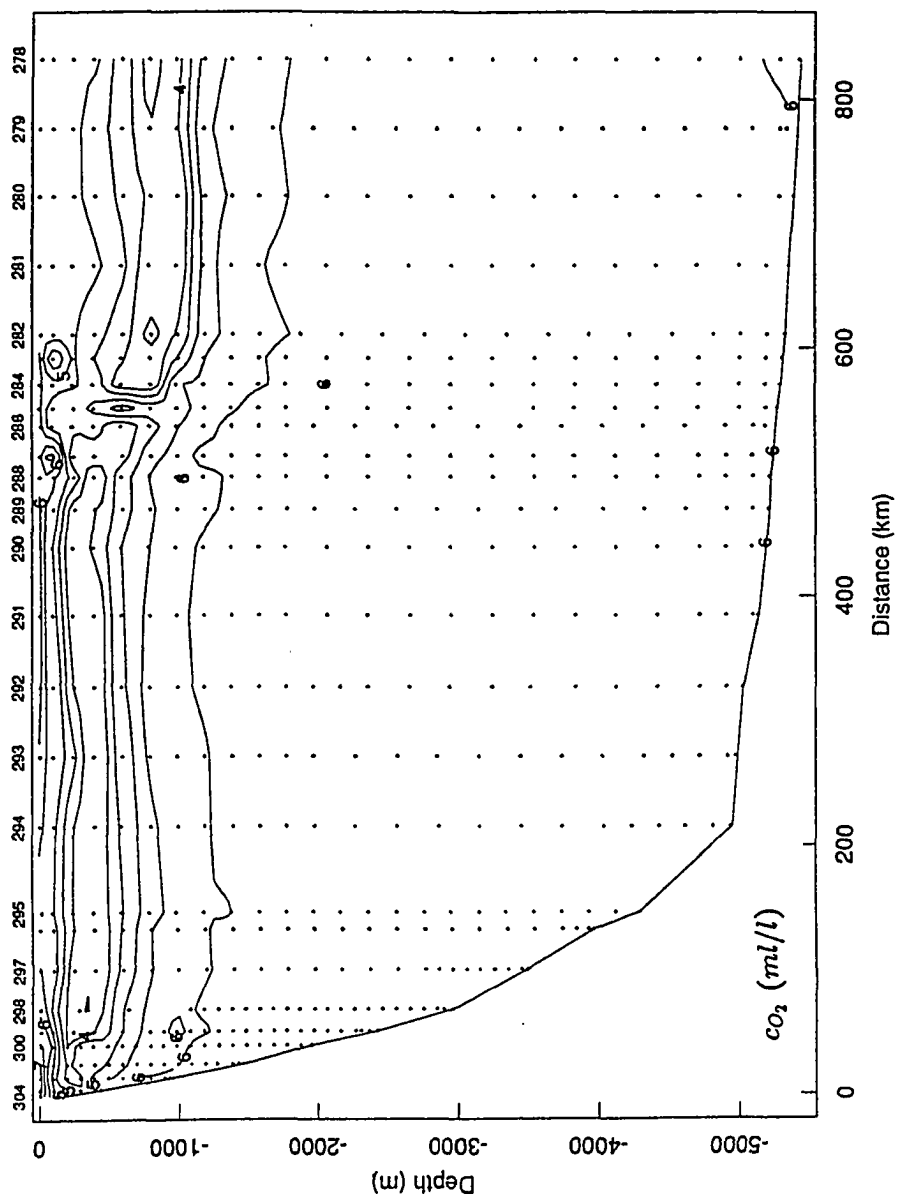
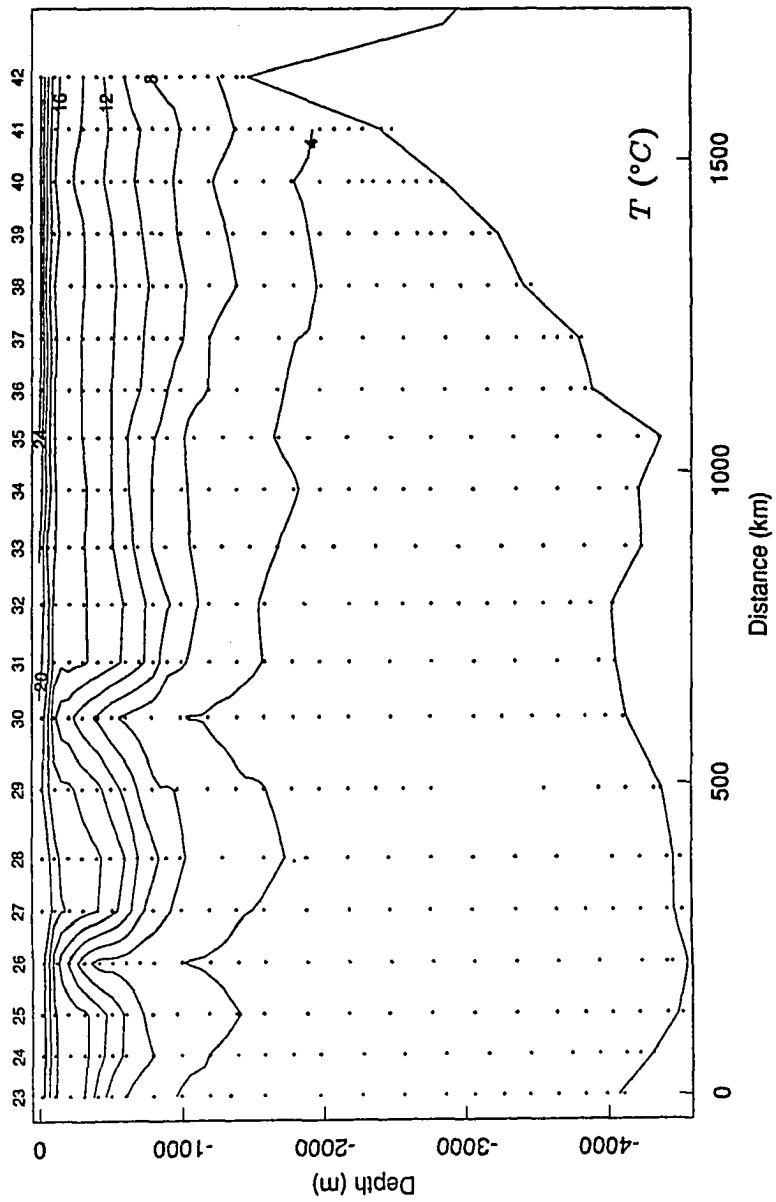


Figure 14 (continued)

Figure 15. Temperature, salinity, density (σ_t), and nitrate, phosphate, silicate and DO concentrations in section 35W.



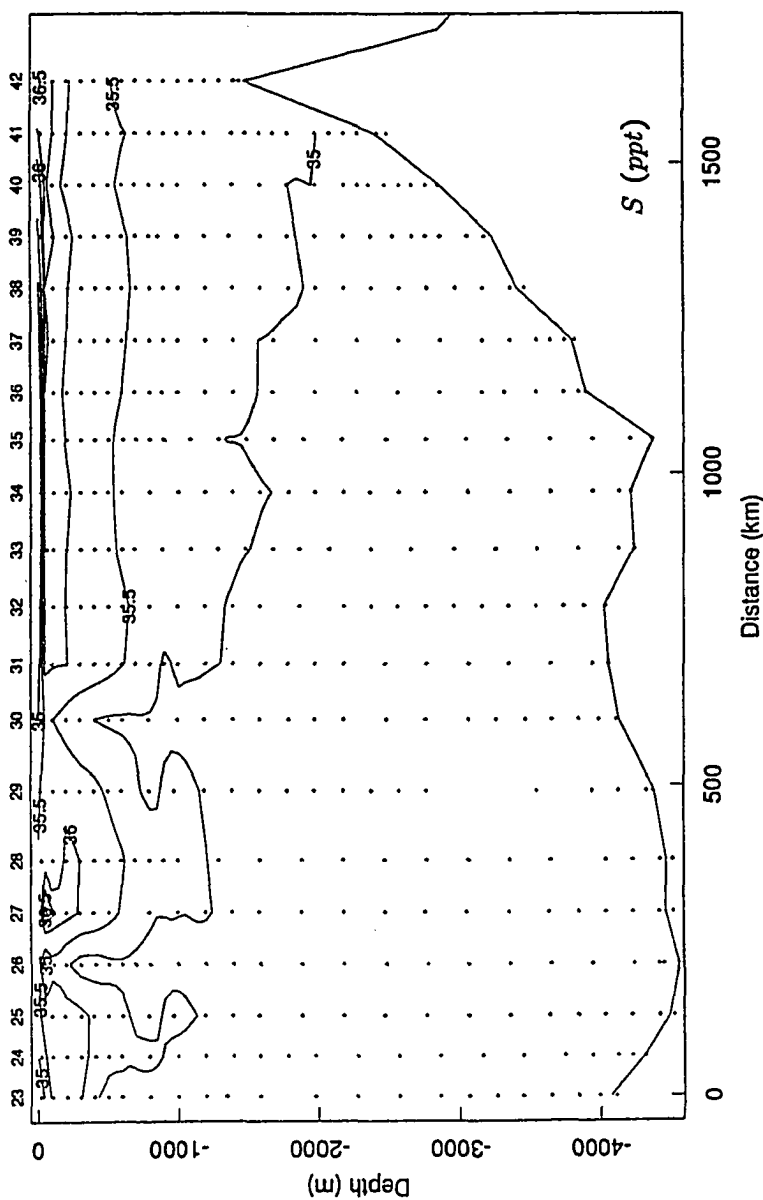


Figure 15 (continued)

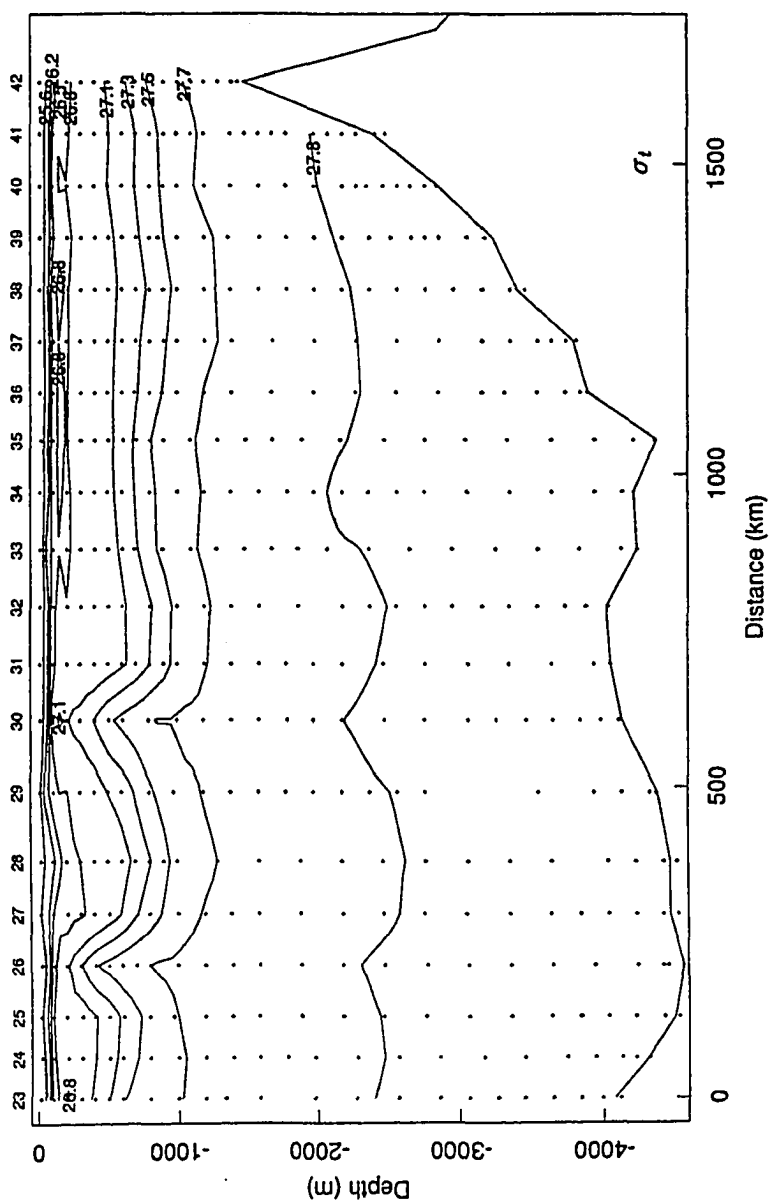


Figure 15 (continued)

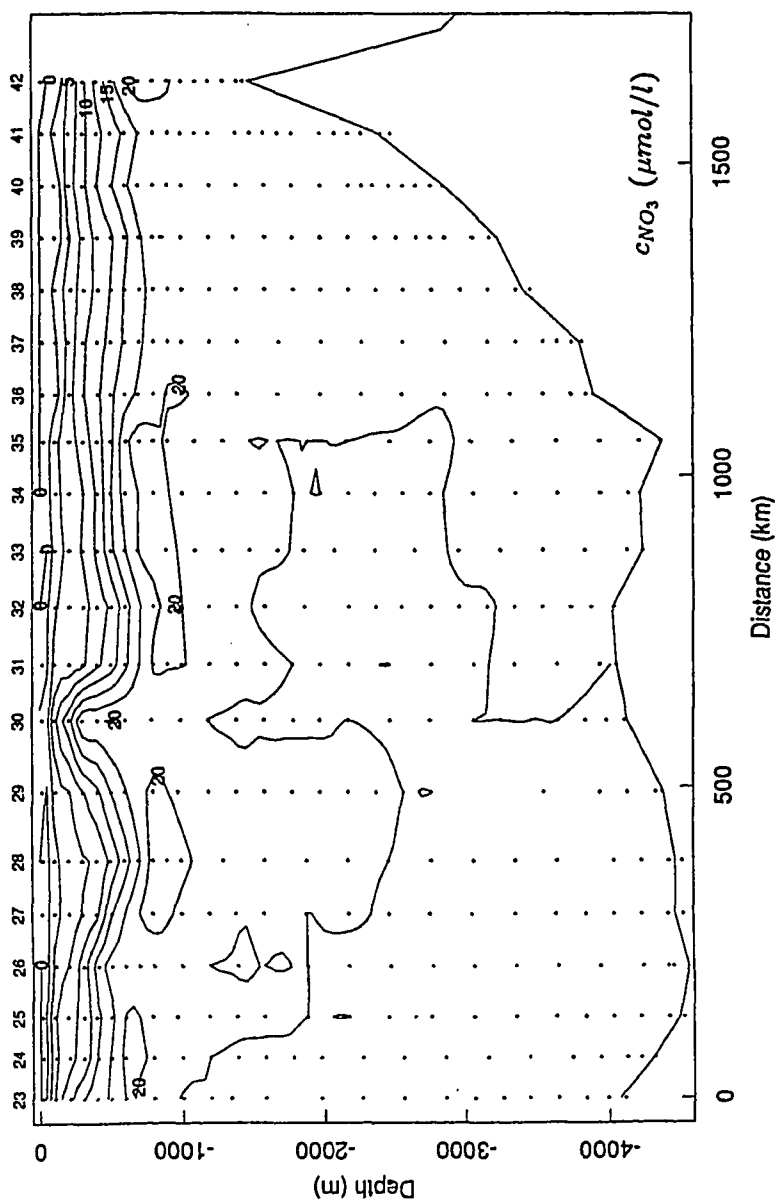


Figure 15 (continued)

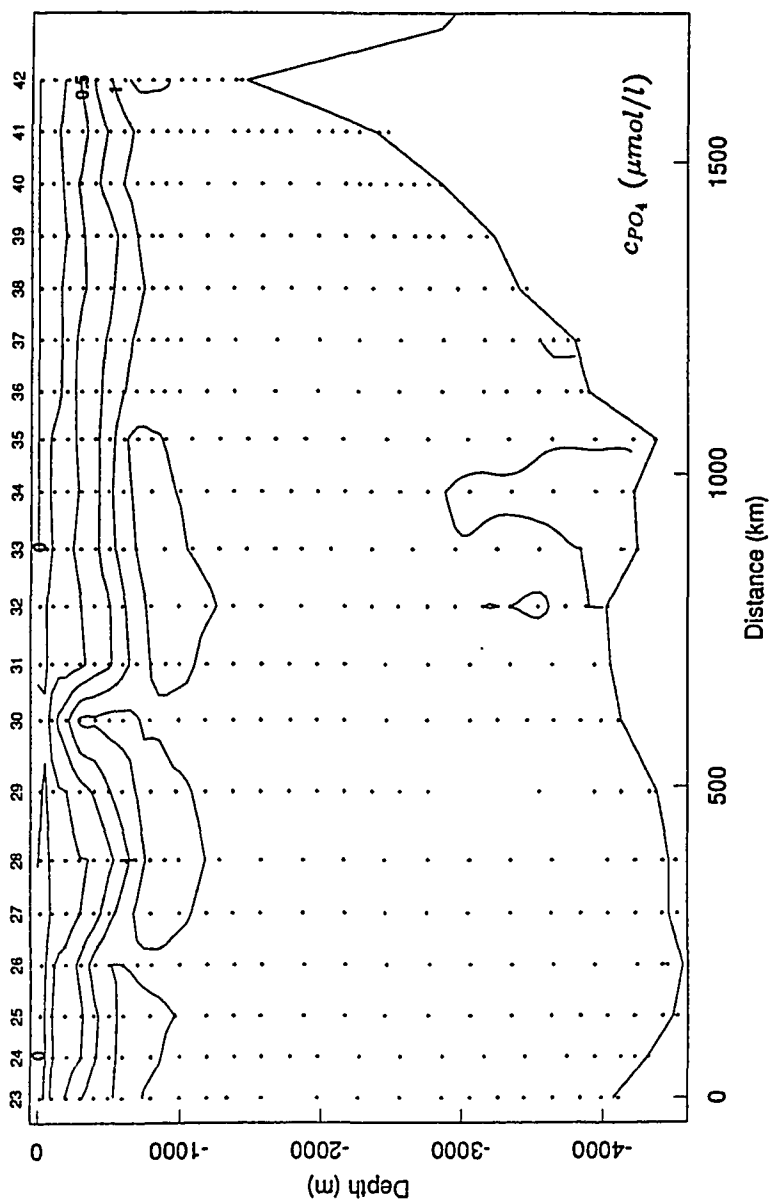


Figure 15 (continued)

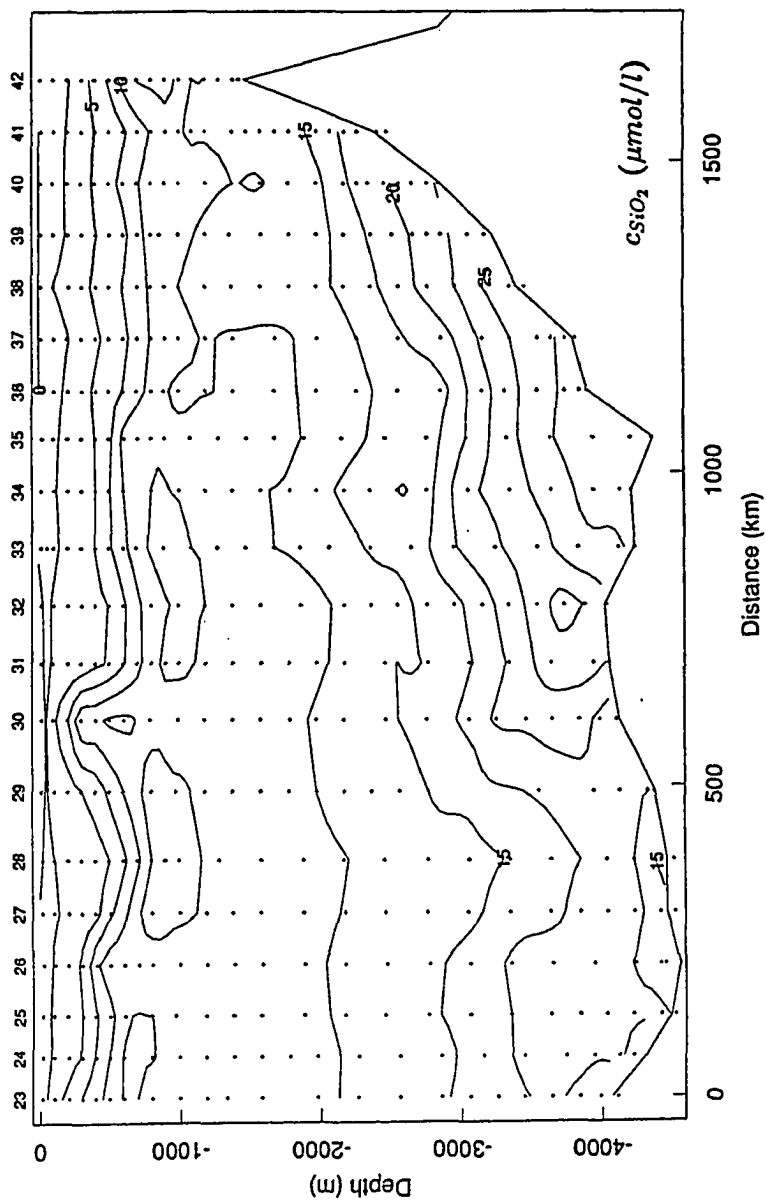


Figure 15 (continued)

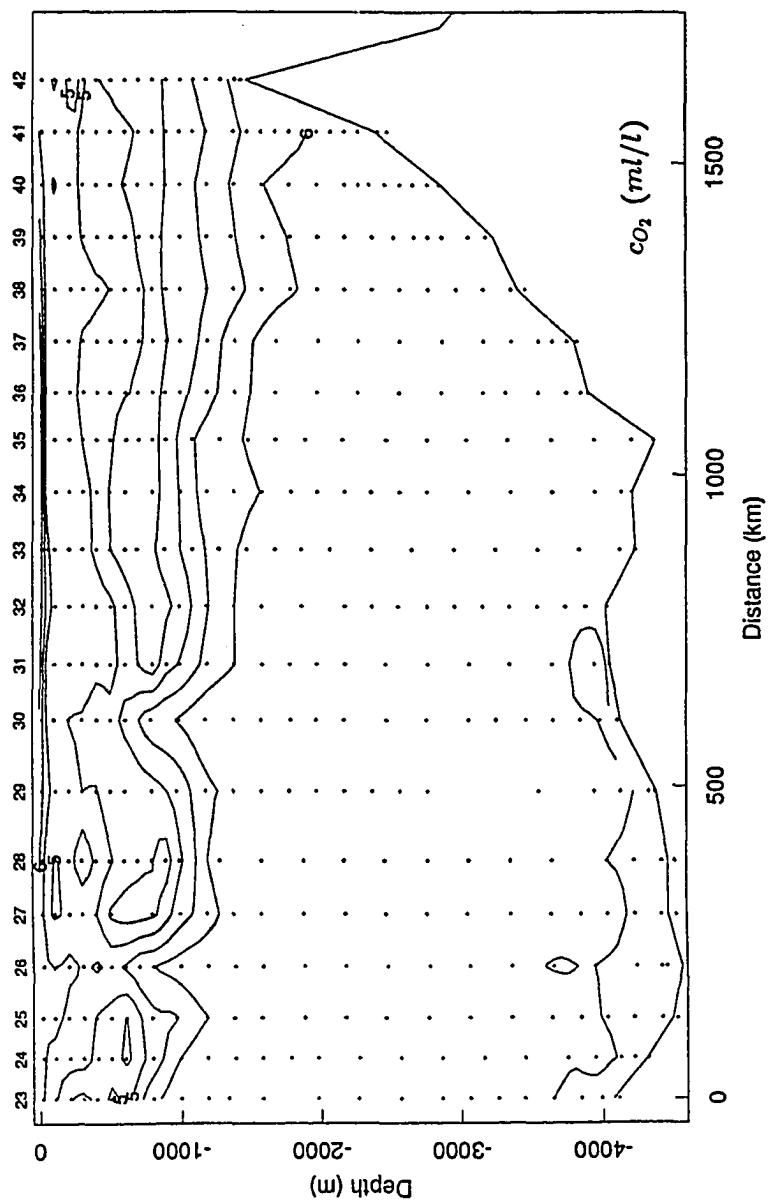


Figure 15 (continued)

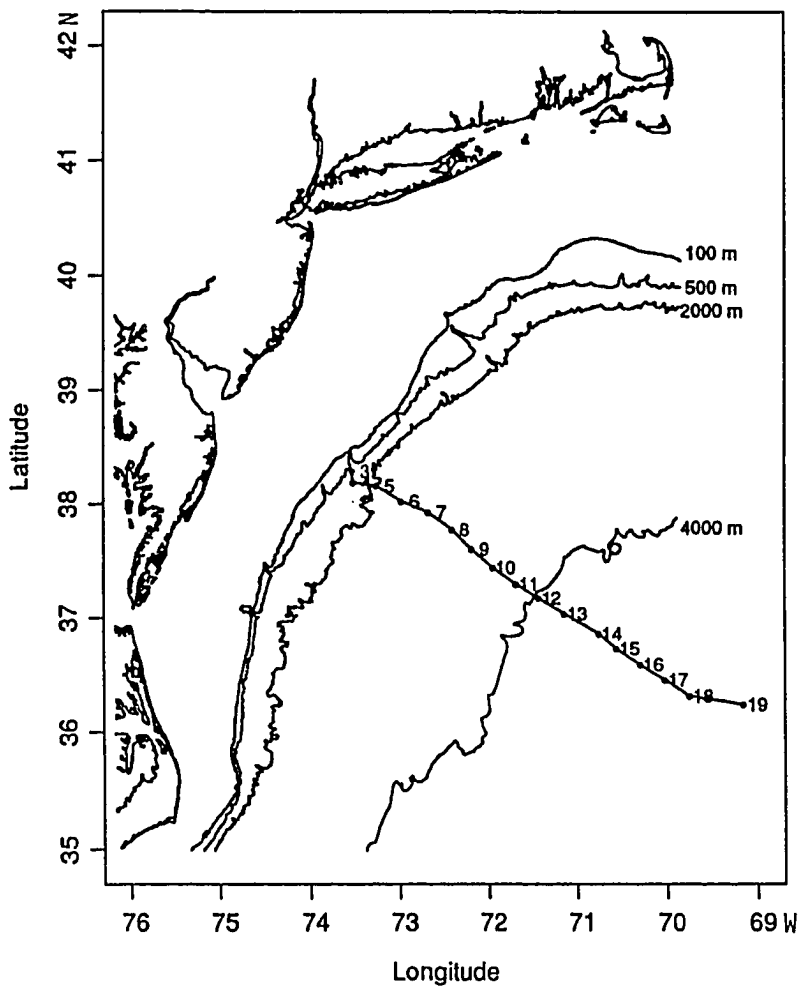
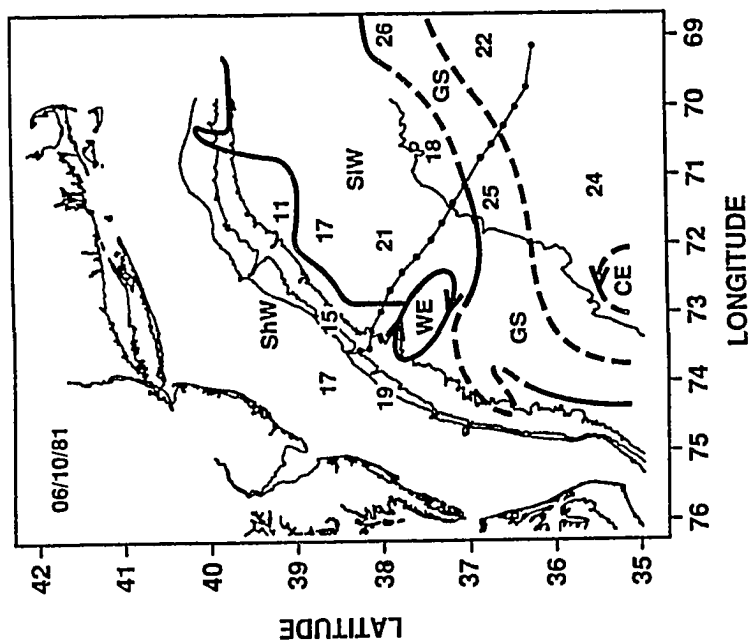
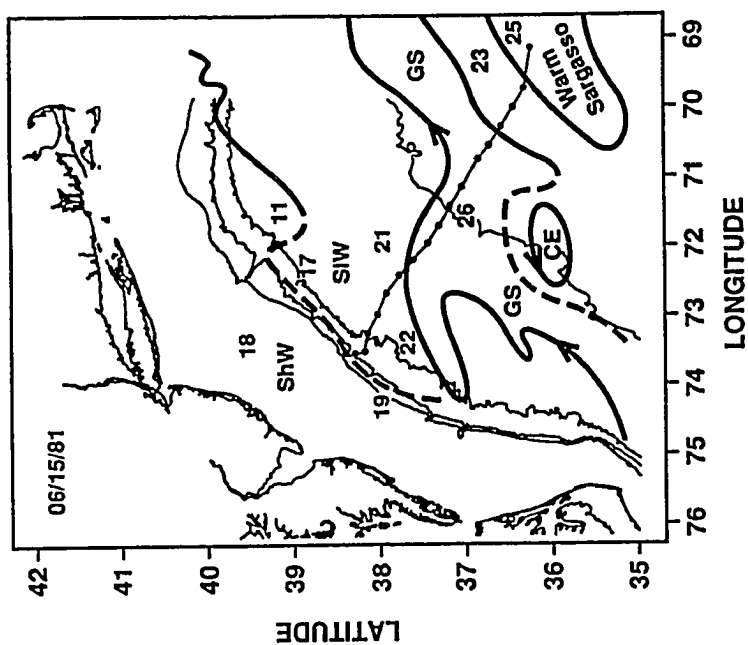


Figure 16. Detailed location of section 36N, occupied in the offshore direction between June 12 and 14, 1981.

Figure 17. Frontal analysis maps for the region of interest, during June 10 and 15, 1981 (adapted from originals courtesy of Jenifer Clark, NOAA).



and after (June 15, 1981) section 36N was taken. The location of the Gulf Stream in section 36N should be in between what the two maps in Fig. 17 indicate.

In order to use isopycnic coordinates, the CTD data, provided to us as average values over 2 *m* depth intervals, were smoothed with a running-filter to 16 *m* interval averages. This was the minimum smoothing necessary to remove all potential density inversions in the data. Subsequently, levels of sigma-theta surfaces separated by 0.01 intervals were determined by cubic-spline interpolation. Fig. 18 shows the 2 *m*-averaged original salinity, temperature and sigma-theta profiles for a portion of station 15 (located within the Gulf Stream), together with the 16 *m*-smoothed and 0.01 σ_θ -interpolated depth values.

Fig. 19 shows the smoothed σ_θ -distribution with the sea surface as the reference pressure, in the cartesian coordinate system, and Fig. 20 presents the derived depth distribution, *z*, in isopycnic coordinates. The isopycnic coordinates have not been extended above the 26.5 σ_θ -surface because near the sea surface the isopycnals are closely packed and the interpolation procedure loses accuracy. The lower limit has been chosen to correspond to the 27.8 σ_θ -surface, which for this section roughly corresponds to the 2000 *m* level. After Chapter 6, except where otherwise noted, our calculations with section 36N will always use the above 'smoothed' data (smoothed and interpolated depth field). The differences between the σ_t and σ_θ surfaces are, for our purposes, insignificant, and the results obtained in σ_θ coordinates may be directly compared to those in σ_t coordinates.

Figure 18. Overview of the temperature, salinity and sigma-theta profiles, using the unsmoothed data of station 15 in section 36N. Also shown is the smoothed and interpolated density-depth profile (dashed line).

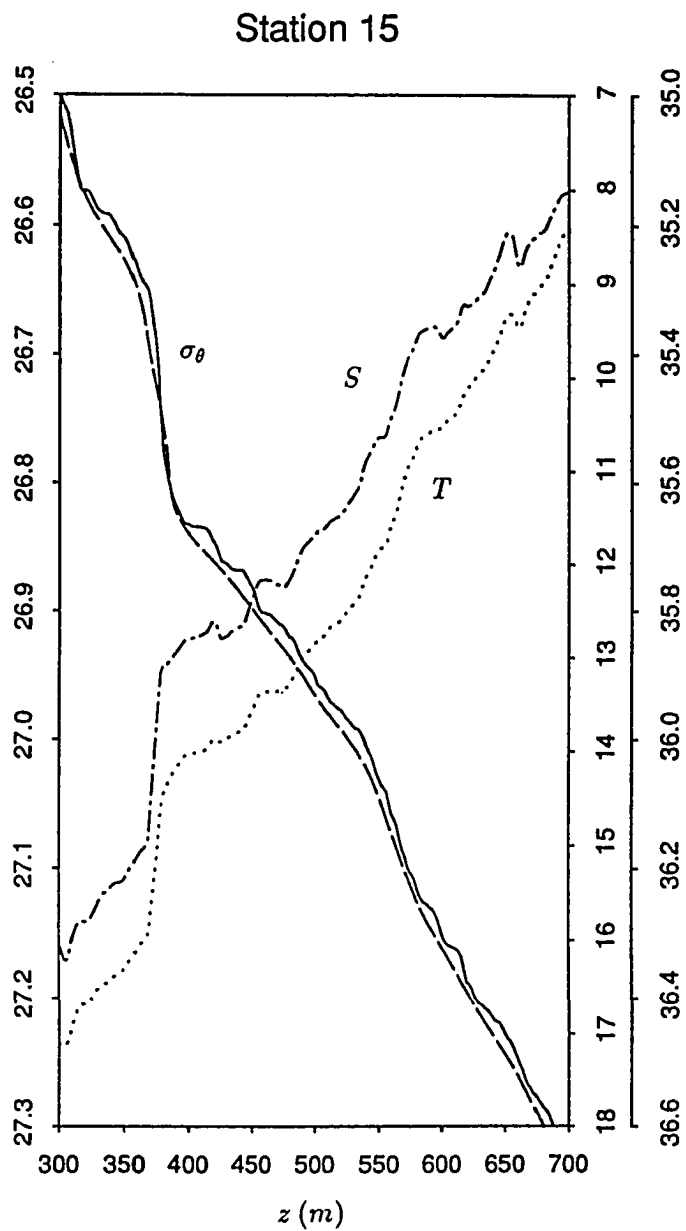
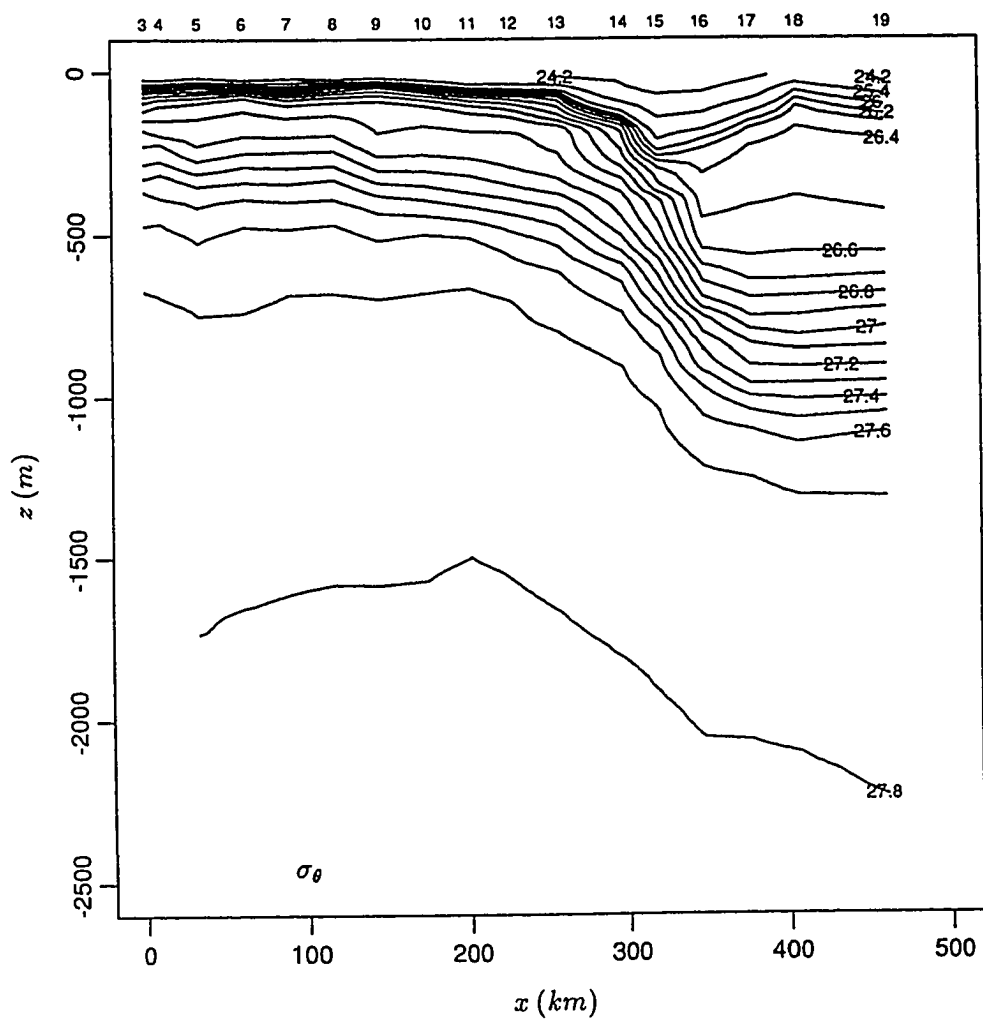


Figure 19. 16 m -averaged (smoothed) sigma-theta, σ_θ , in section 36N.



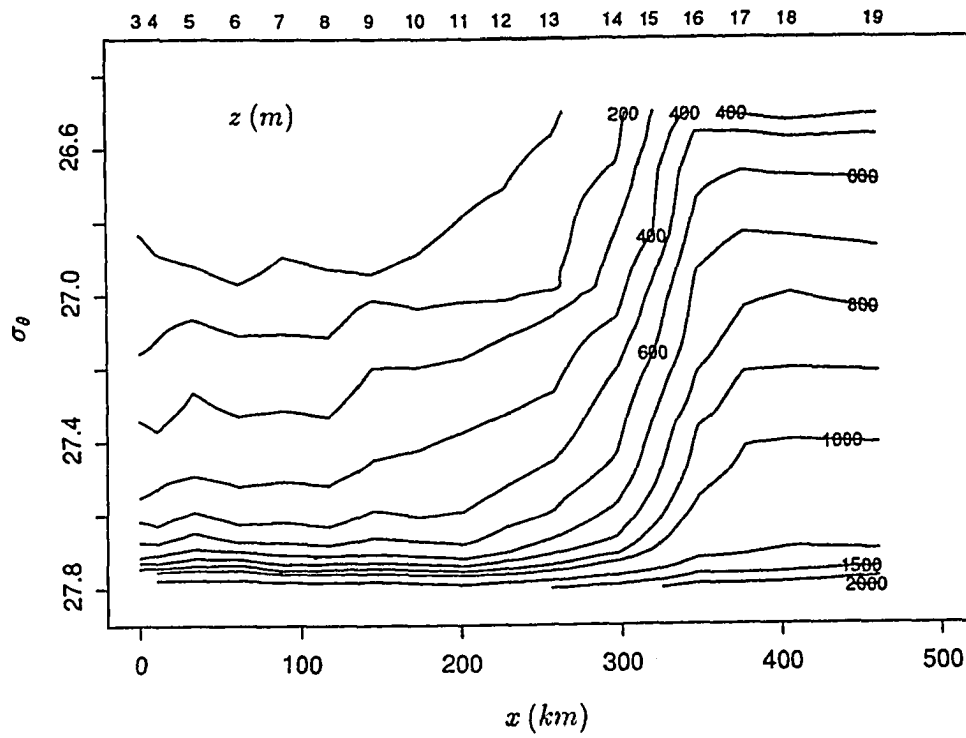


Figure 20. Smoothed and interpolated depth, z , in section 36N.

Chapter 4. The Gulf Stream and the Nutrient Stream

*The heart has its reasons which reason
does not know.*

Blaise Pascal (1623-1662)

On account of the importance of nutrient transport to the global biogeochemical cycle, it is clearly desirable to establish from observation just what the mass balance of the nutrient bearing stratum is, and how large a nutrient transport the western boundary current actually carries. Brewer and Dyrssen (1987) obtained first order estimates for the nutrient transport through the Florida Straits. Here we trace this transport further and show that it greatly increases as the Stream flows along the continental margin of North America.

In addition to estimating water mass and nutrient transports, we also examine the questions of how the transport of water mass and nutrients is distributed over the different isopycnal layers, what the downstream increase of the transport implies for the circulation of the nutrient bearing stratum in the ocean interior, and what the changing profile of nutrient transport reveals about processes within the boundary current itself.

4.1 The Nutrient Stream

From the density field we have calculated the geostrophic velocities referred to 2000 *m*, except for section 24N. Below this depth the isopycnals were flat enough

to guarantee that the relative error in the velocities and transports in the important isopycnal layers is small. The dynamic heights for regions shallower than 2000 *m* have been calculated using the method described in Csanady (1979), which assumes zero bottom along-shore velocity and uses the density anomaly values at the bottom. Since north of Cape Hatteras the Gulf Stream rapidly separates from the slope, any error caused by this approximation has little effect on our conclusions. In section 24N, we used the mean summer velocity field of Niiler and Richardson (1973) for a cross-section located about half a degree south of section 24N. This is made necessary by the importance of barotropic flow in the Florida Straits.

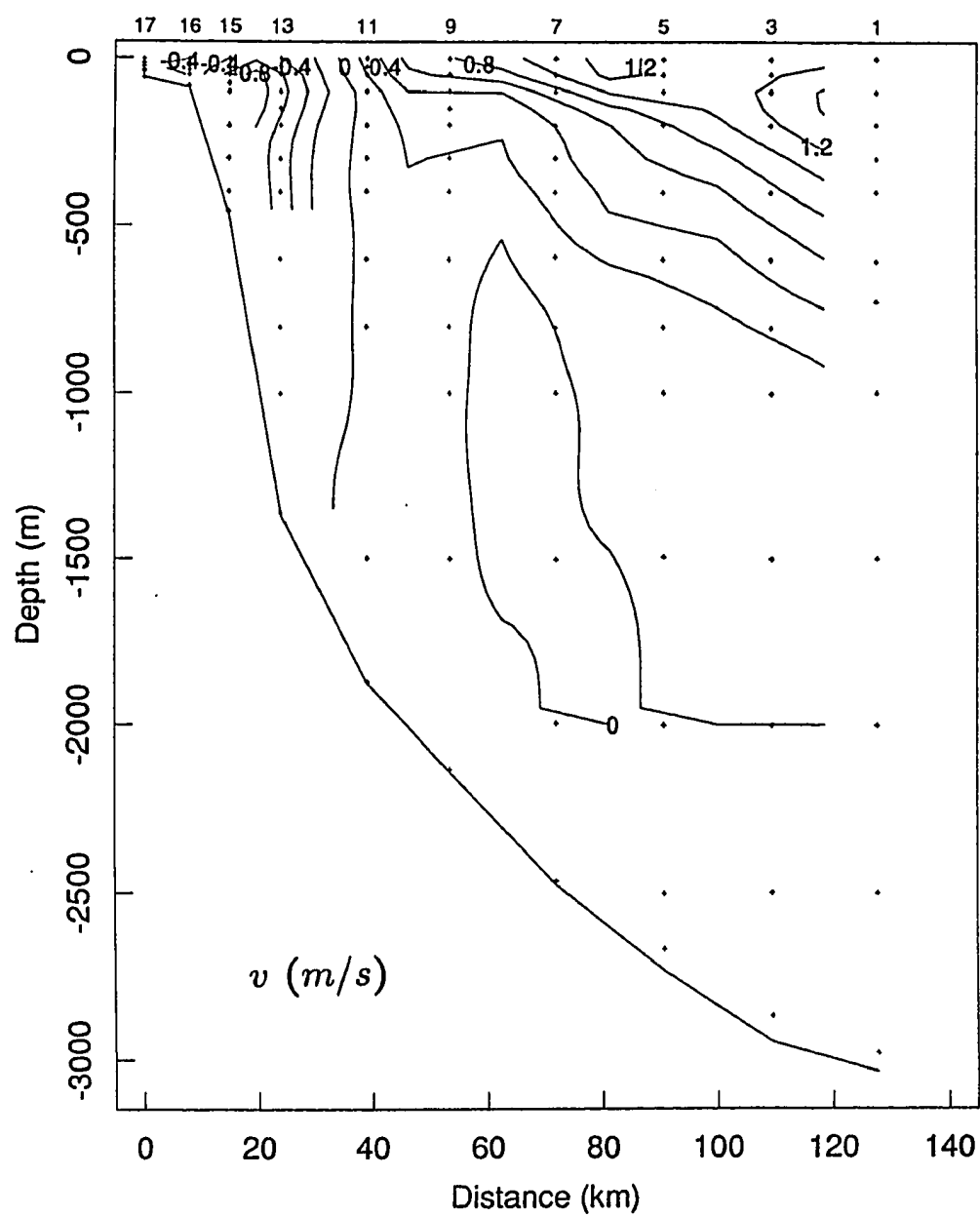
Nutrient flux t_v , or nutrient transport per unit area, is defined as the product of concentration c and velocity normal to the section v :

$$t_v = cv \quad (1)$$

The flux was calculated for the three nutrients named and DO, in all sections. The units are $\mu\text{mol l}^{-1} \equiv \text{mmol m}^{-3} \equiv 10^{-6} \text{ kmol m}^{-3}$ for nutrient concentration, $\text{mmol m}^{-2} \text{ s}^{-1} \equiv 10^{-6} \text{ kmol m}^{-2} \text{ s}^{-1}$ for nutrient flux. The units are ml l^{-1} for DO concentrations, $\text{l m}^{-2} \text{ s}^{-1}$ for DO flux.

Fig. 21 shows the velocity, and nutrient and DO fluxes for section 7S. Fig. 22 shows the velocity, and nutrient and DO fluxes for section 24N. Figs. 23 to 26 show the density, velocity, nitrate concentration, and nutrient and DO fluxes for sections 24N, 36N, 64W, 53W and 35W, down to 2000 *m*. The Gulf Stream has a width approximately ranging between 80 and 200 *km*, with velocities reaching a maximum near the surface and decreasing with depth until the assumed level of no motion. Nutrient concentrations have very small values in the surface region

Figure 21. Velocity, and nitrate, phosphate, silicate and DO fluxes
in section 7S.



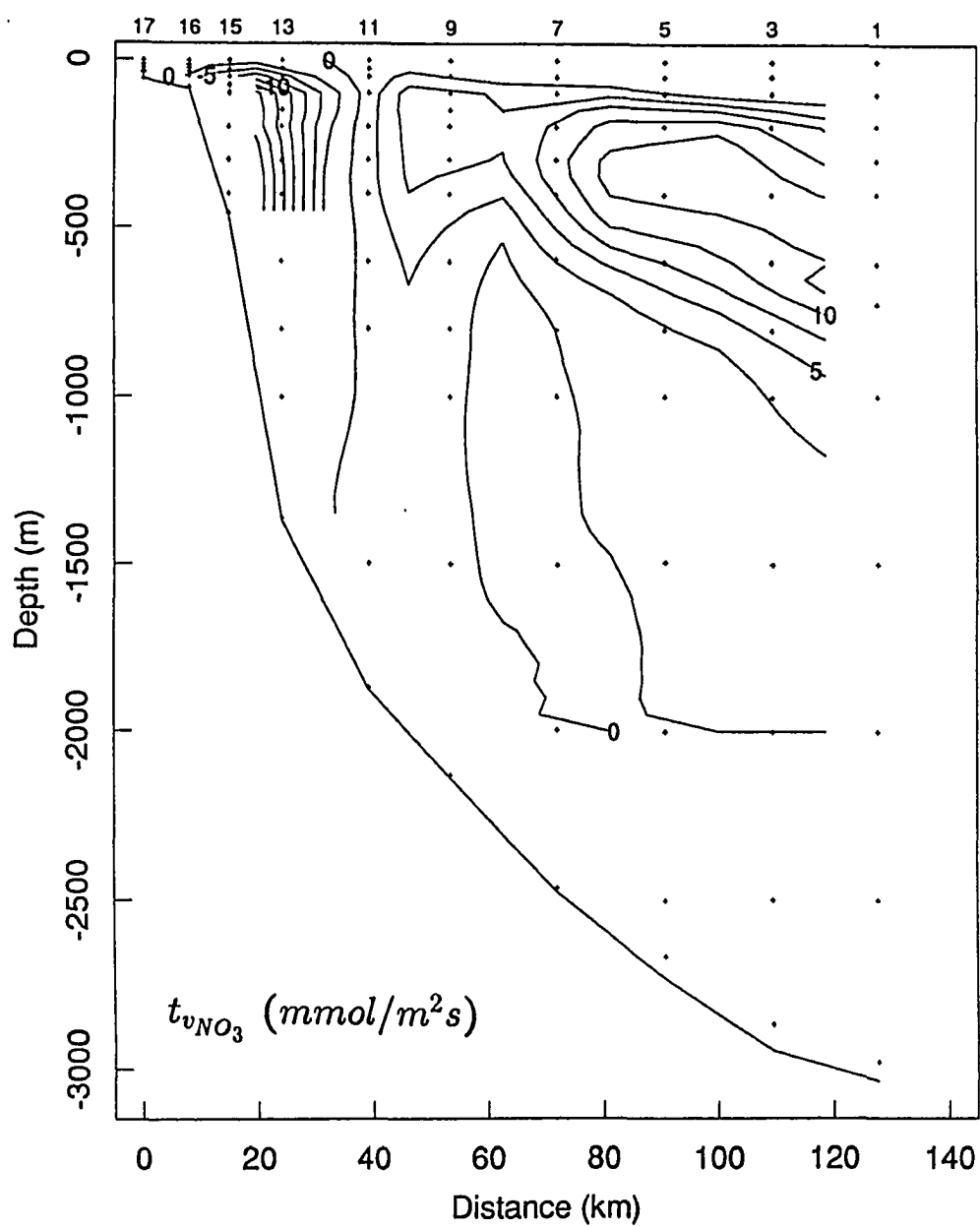


Figure 21 (continued)

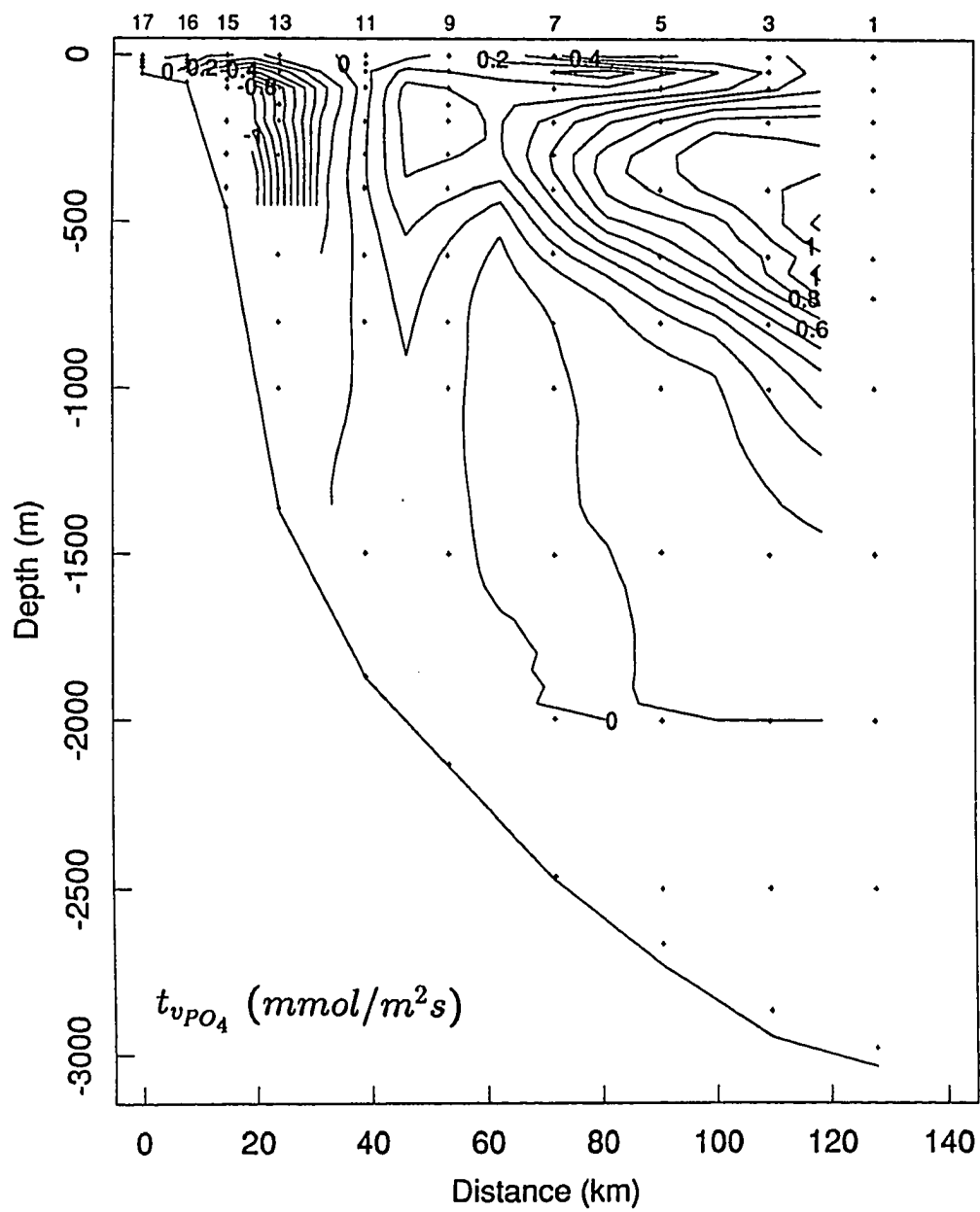


Figure 21 (continued)

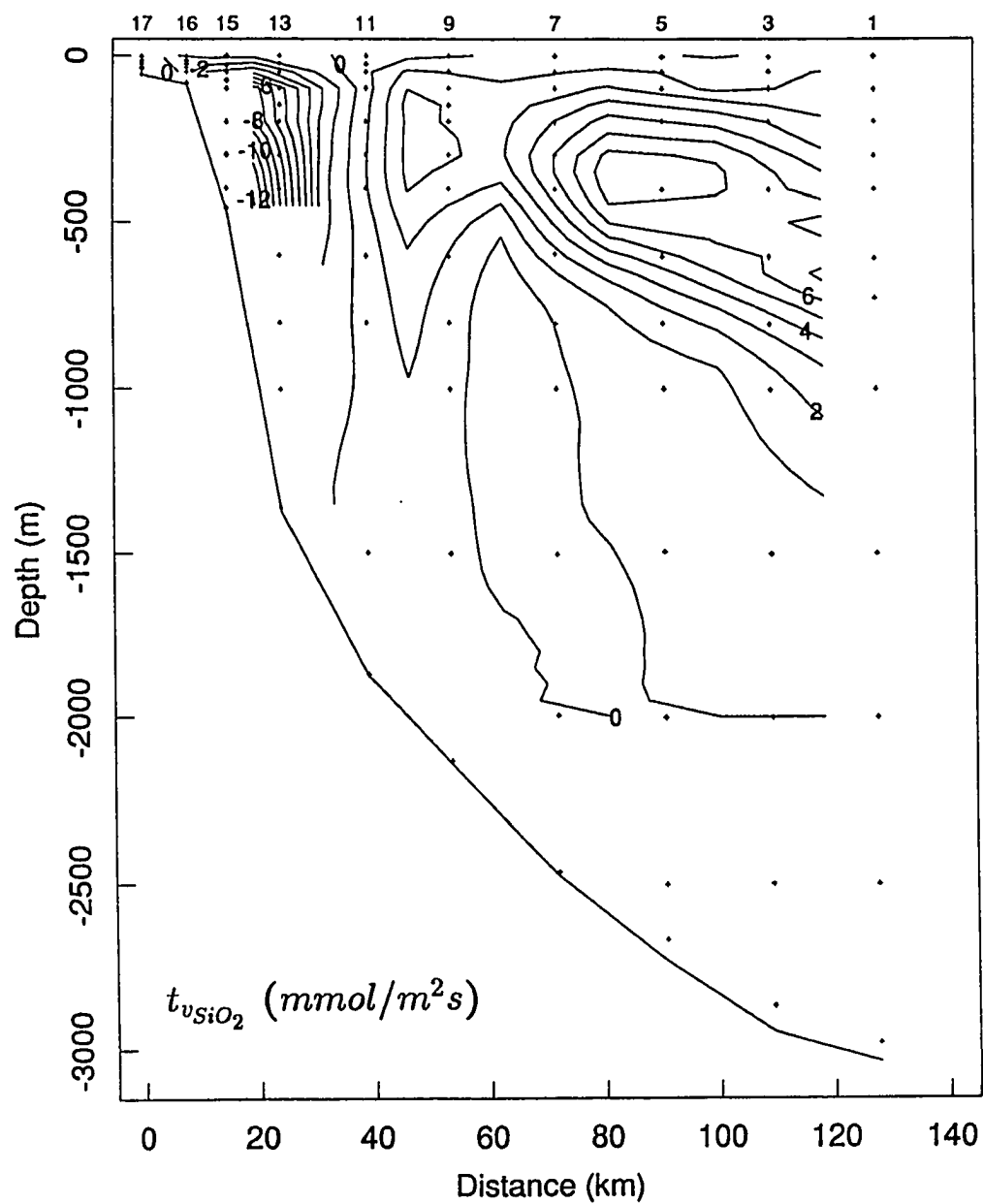


Figure 21 (continued)

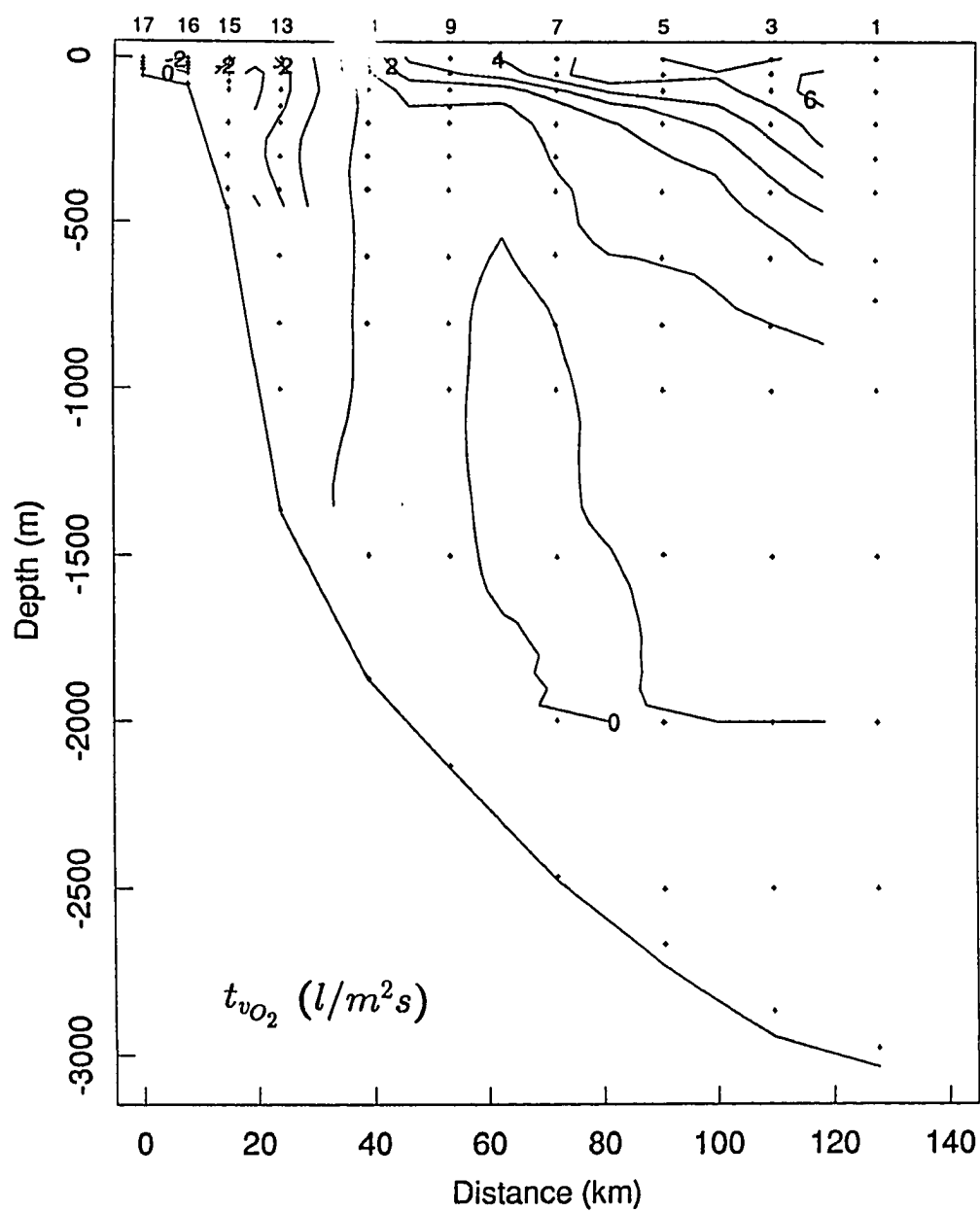


Figure 21 (continued)

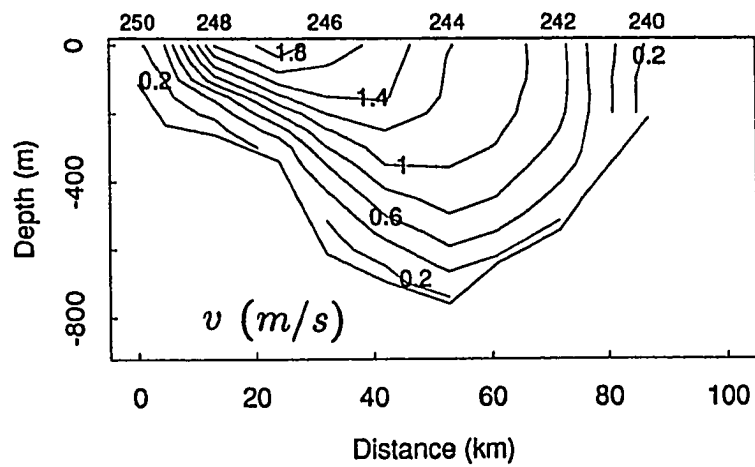


Figure 22. Velocity, and nitrate, phosphate, silicate and DO fluxes in section 24N.

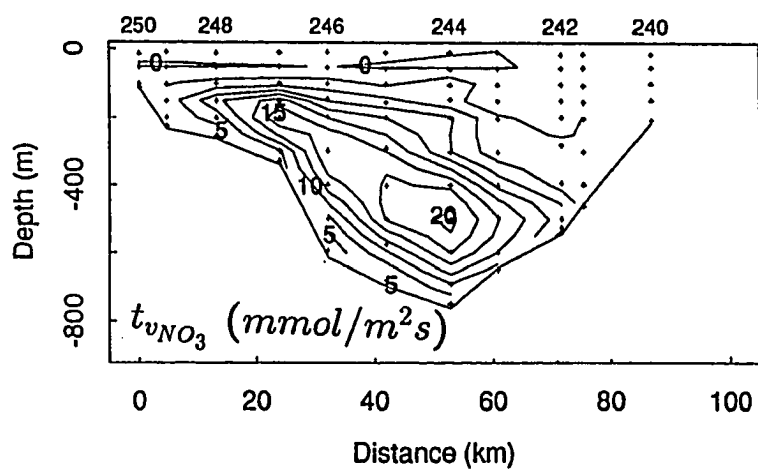


Figure 22 (continued)

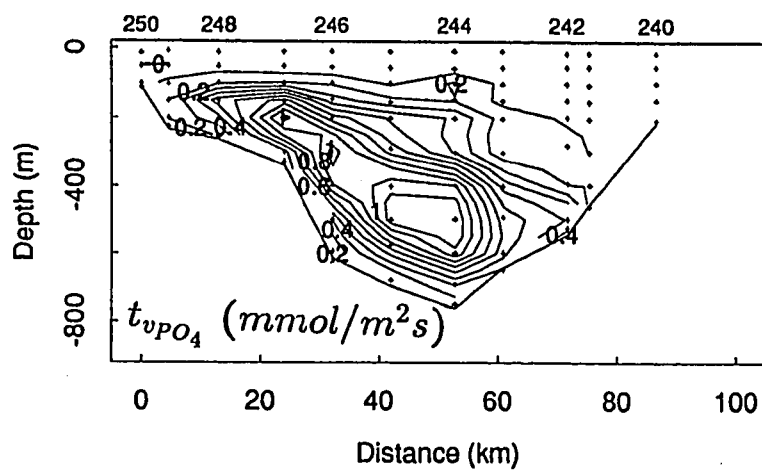


Figure 22 (continued)

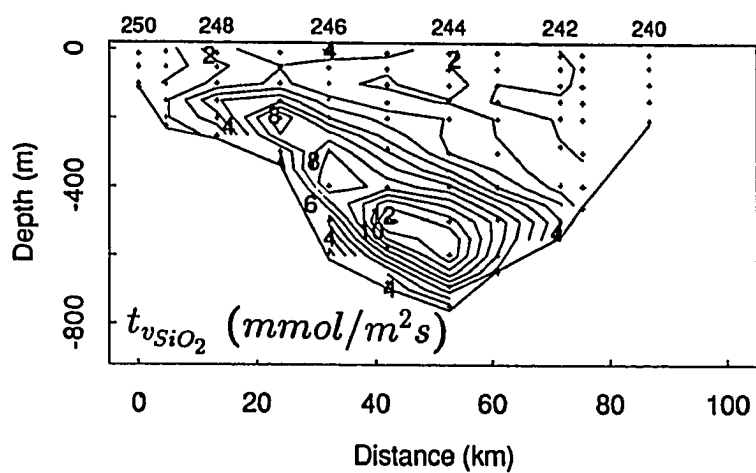


Figure 22 (continued)

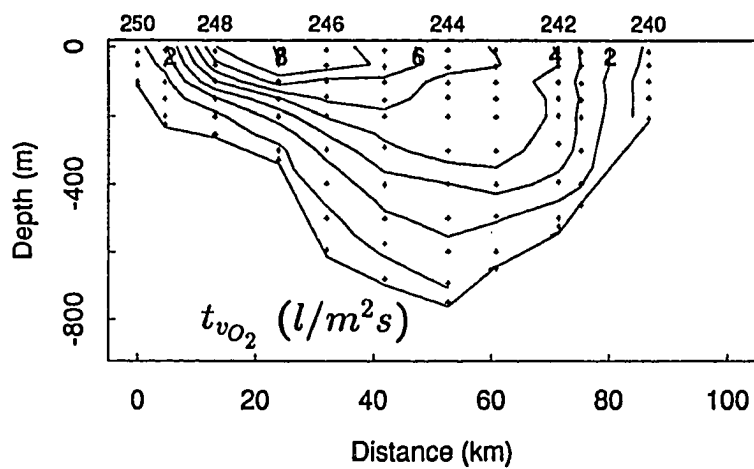
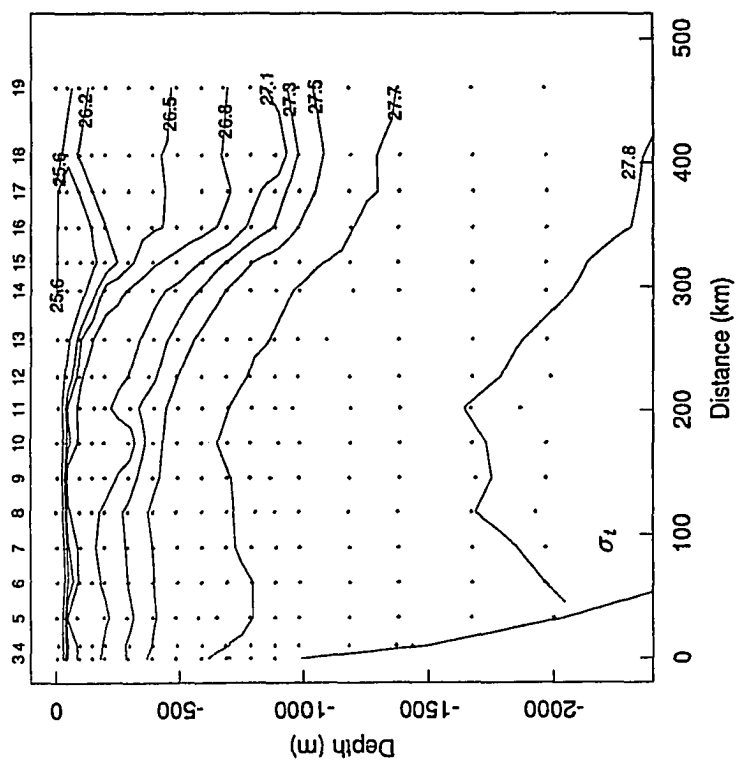


Figure 22 (continued)

Figure 23. Density (σ_t), velocity, nitrate concentration, and nitrate, phosphate, silicate and DO fluxes in section 36N, down to 2000 *m*.



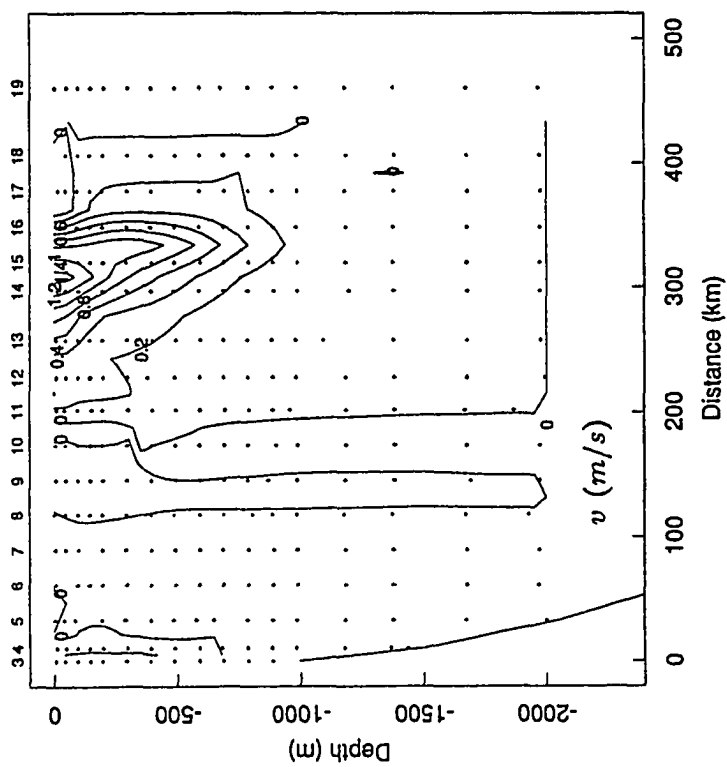


Figure 23 (continued)

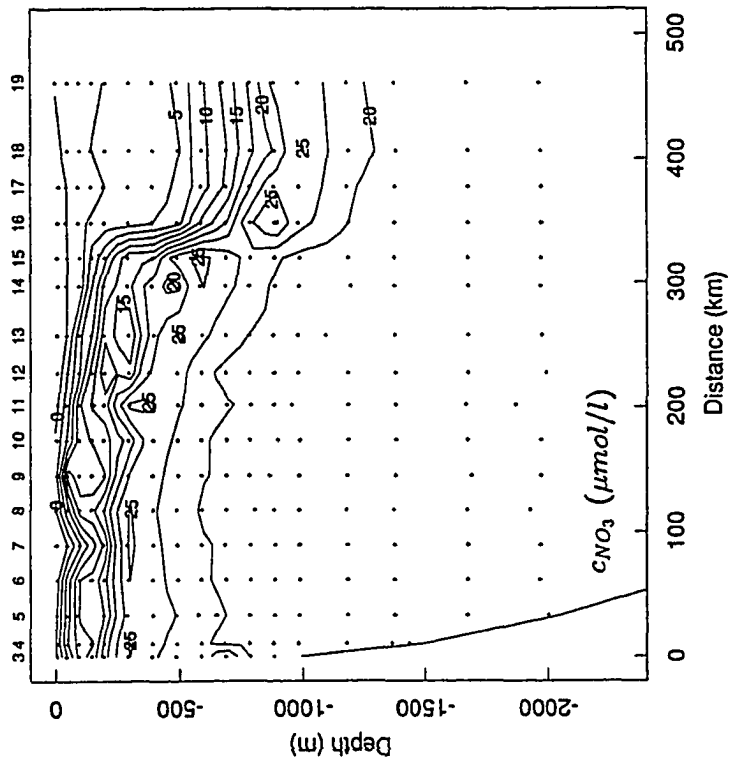


Figure 23 (continued)

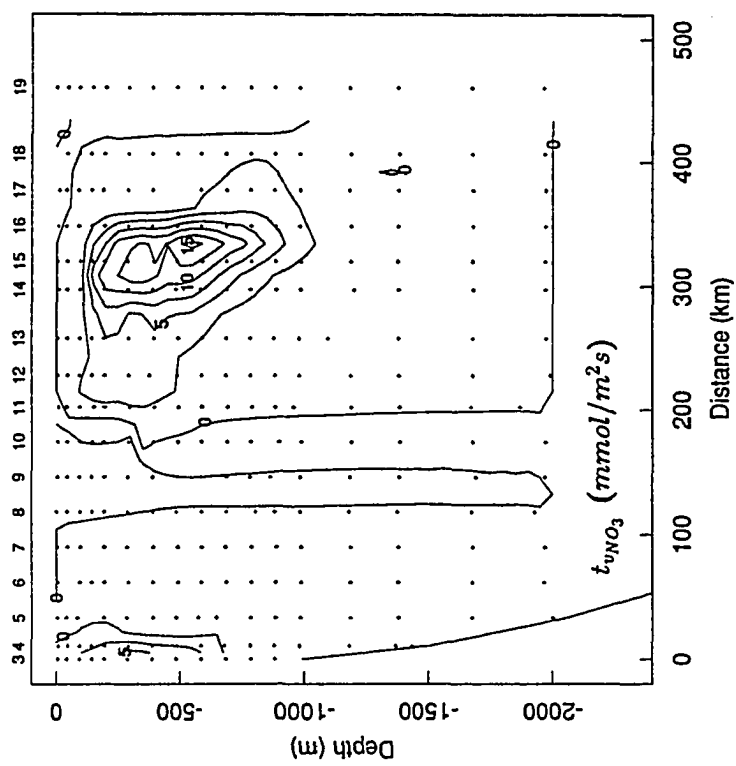


Figure 23 (continued)

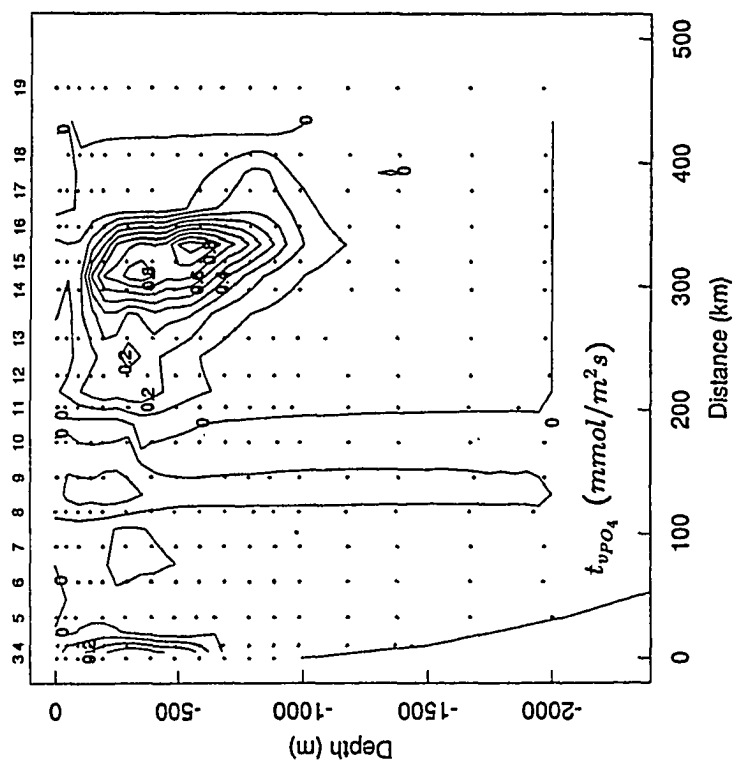


Figure 23 (continued)

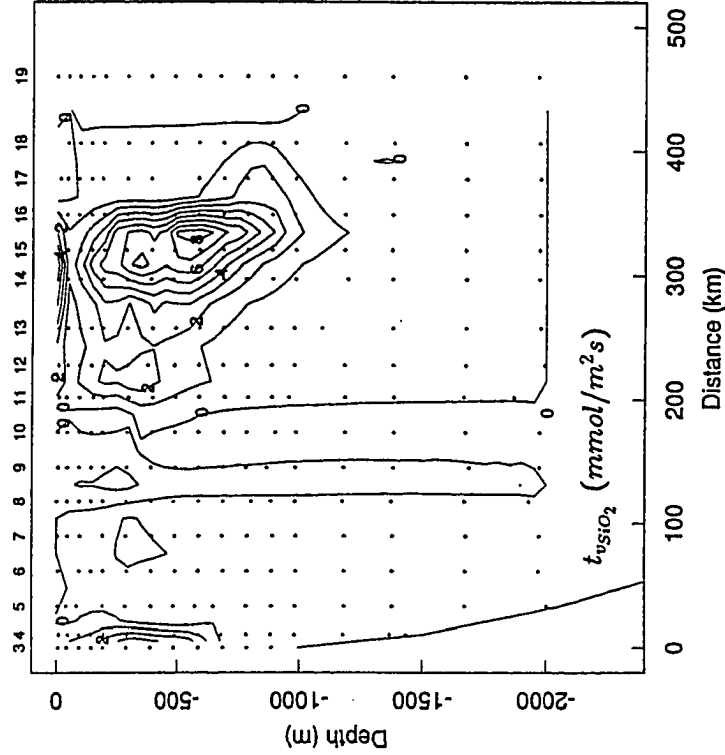


Figure 23 (continued)

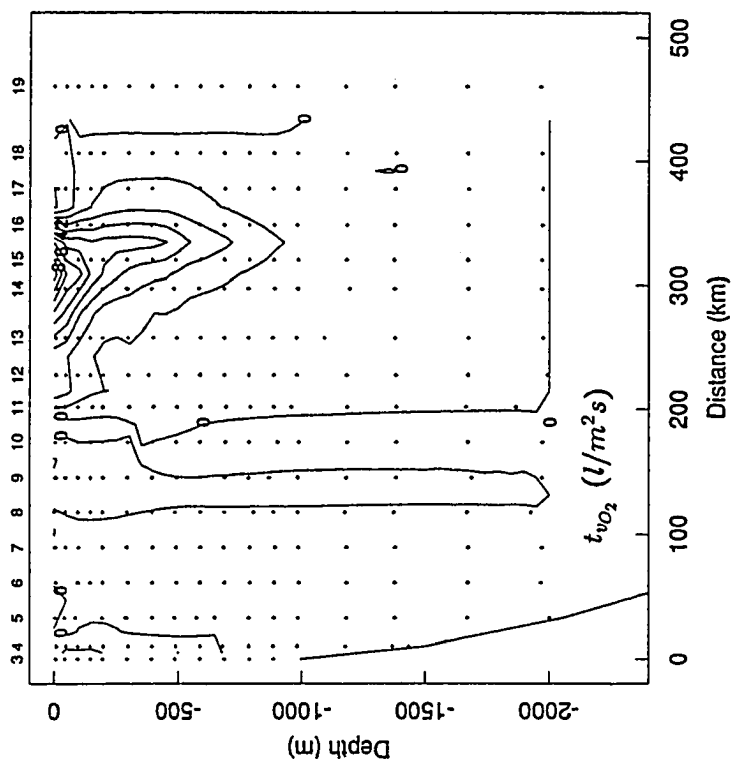
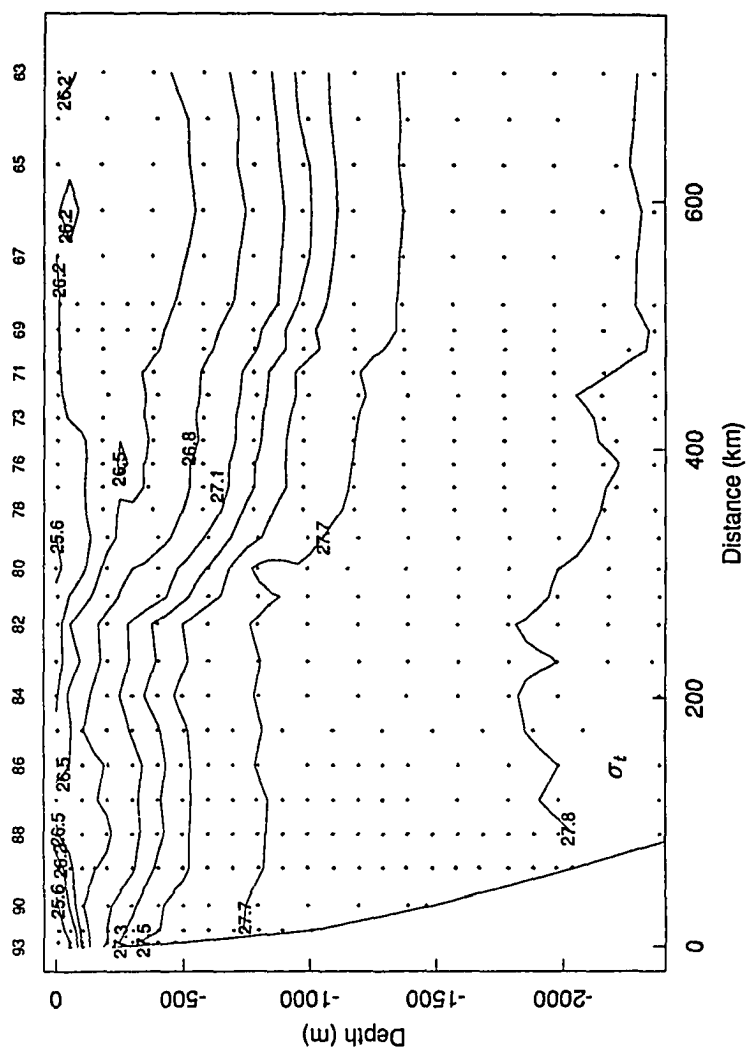


Figure 23 (continued)

Figure 24. Density (σ_t), velocity, nitrate concentration, and nitrate, phosphate, silicate and DO fluxes in section 64W, down to 2000 *m*.



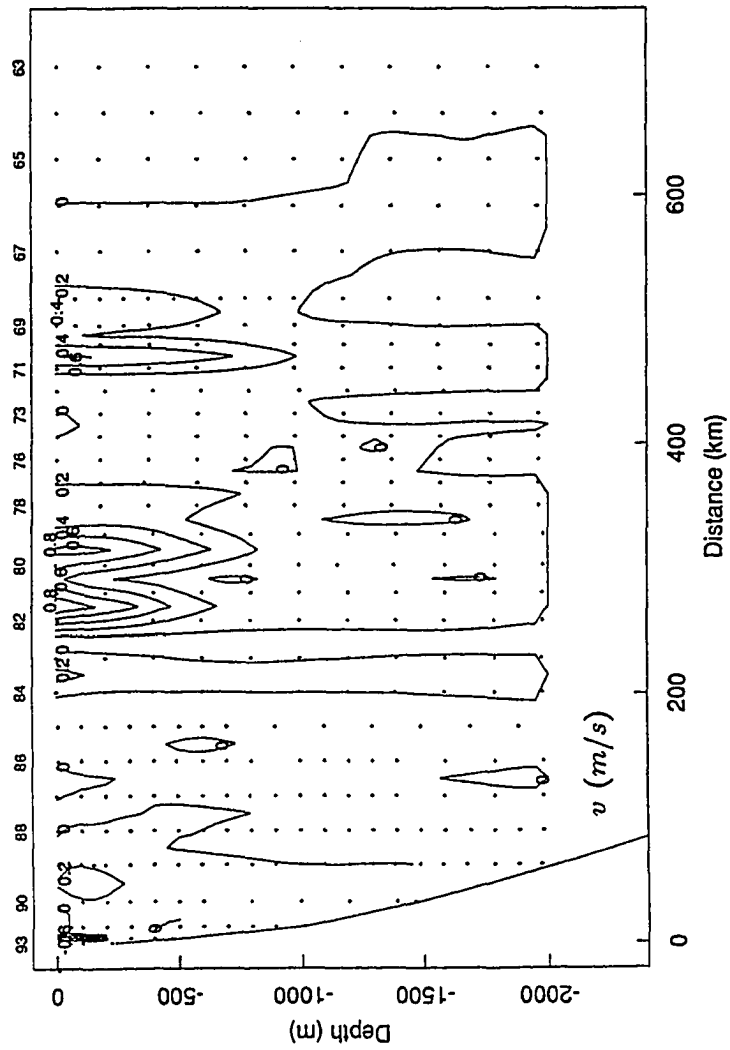


Figure 24 (continued)

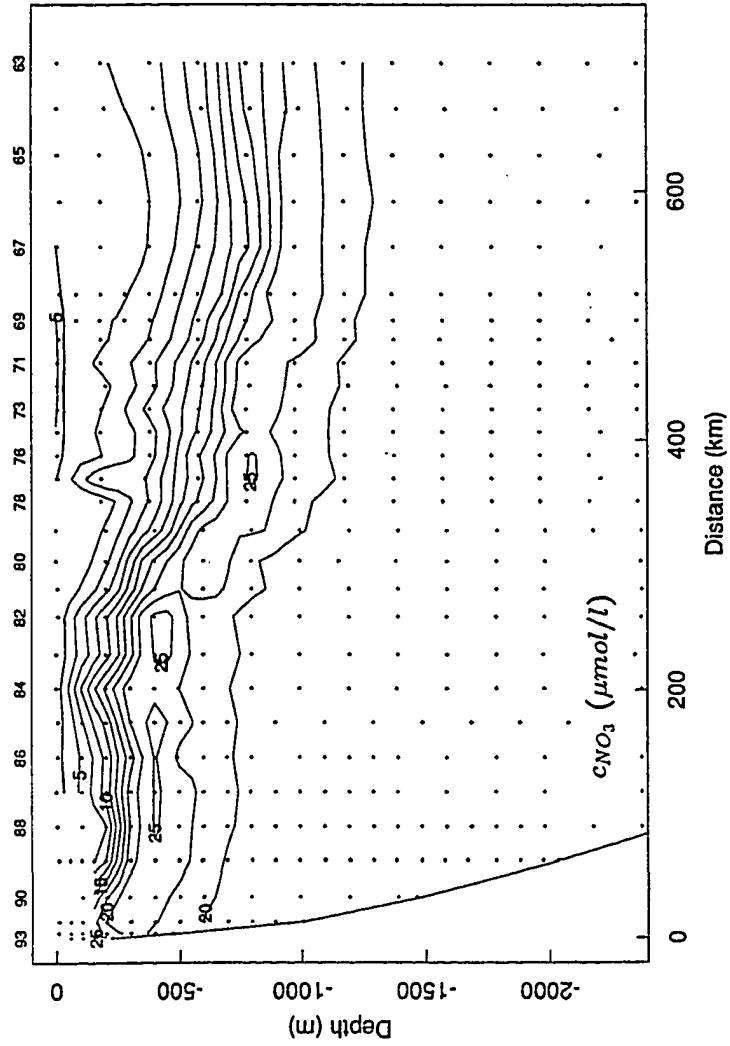


Figure 24 (continued)

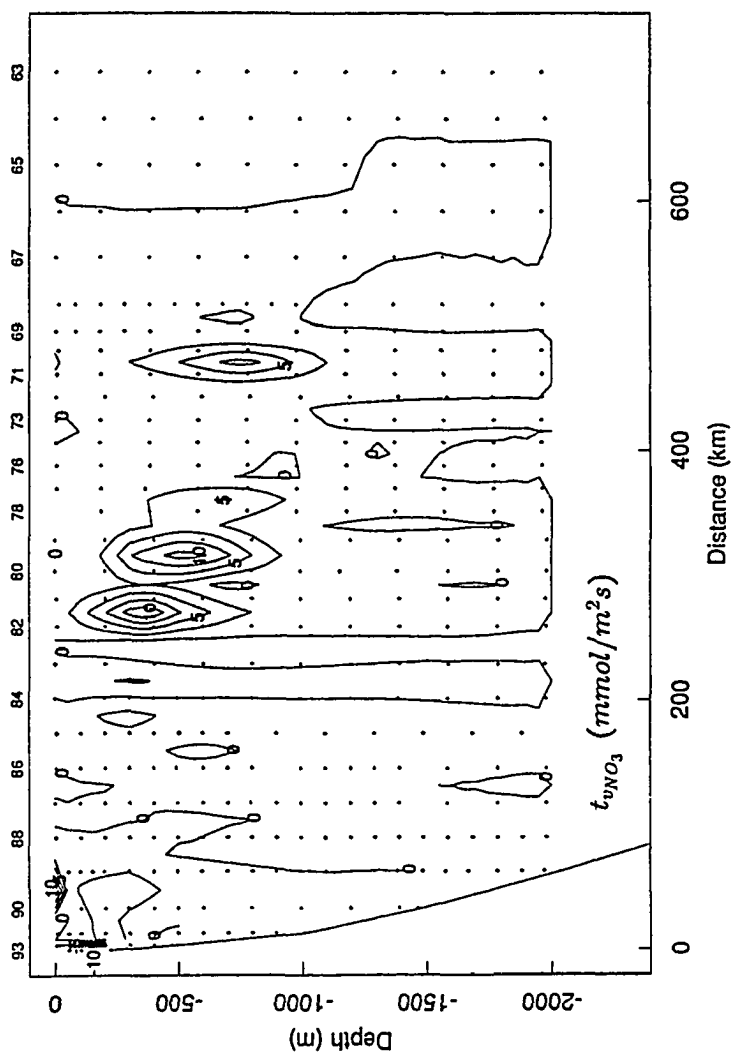


Figure 24 (continued)

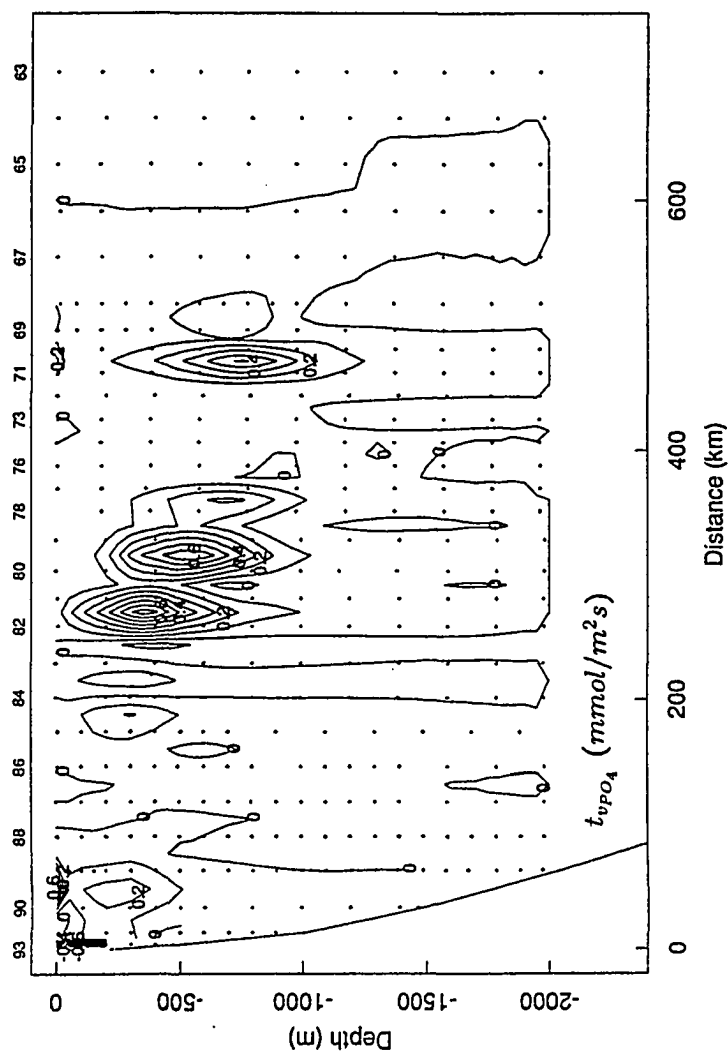


Figure 24 (continued)

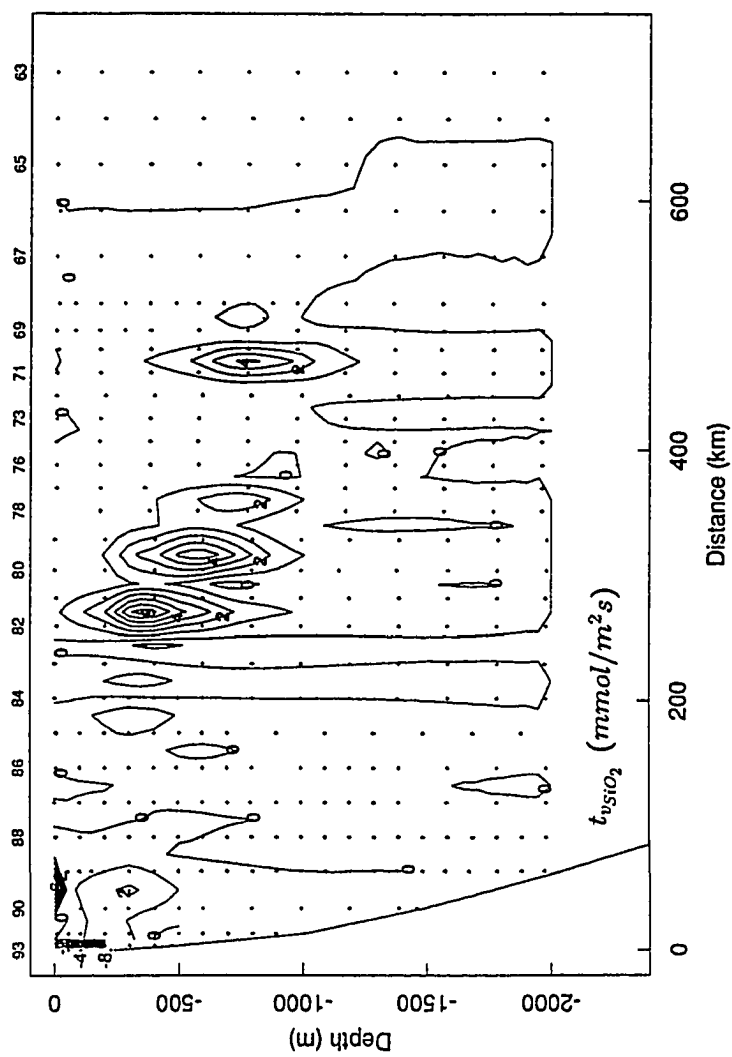


Figure 24 (continued)

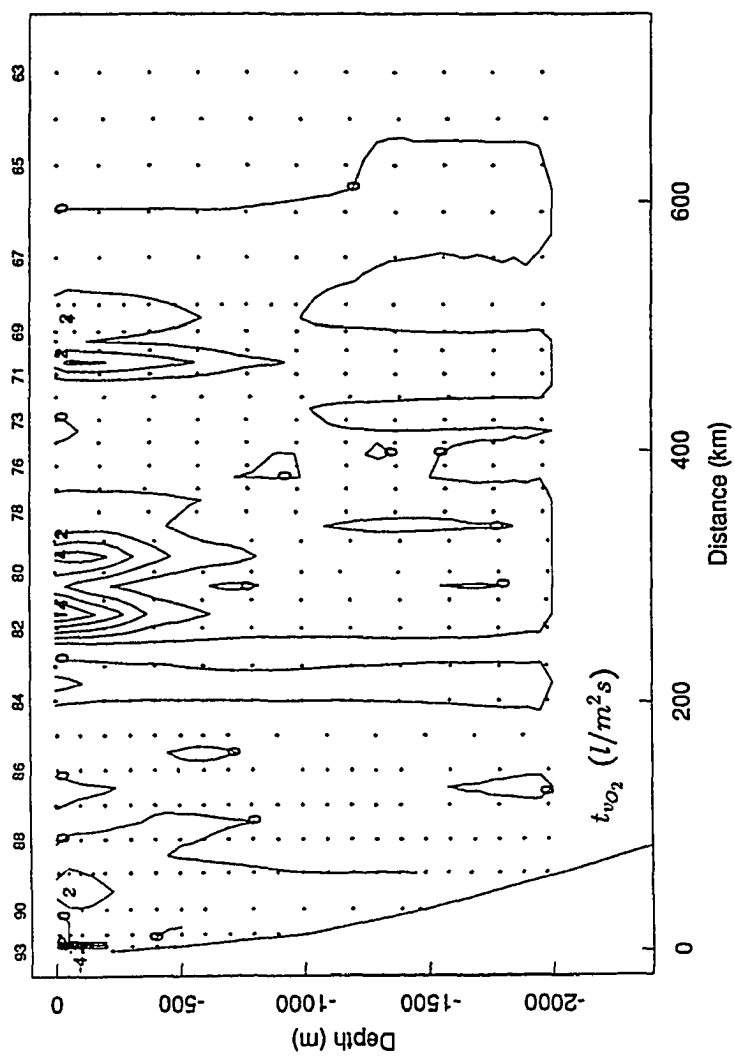
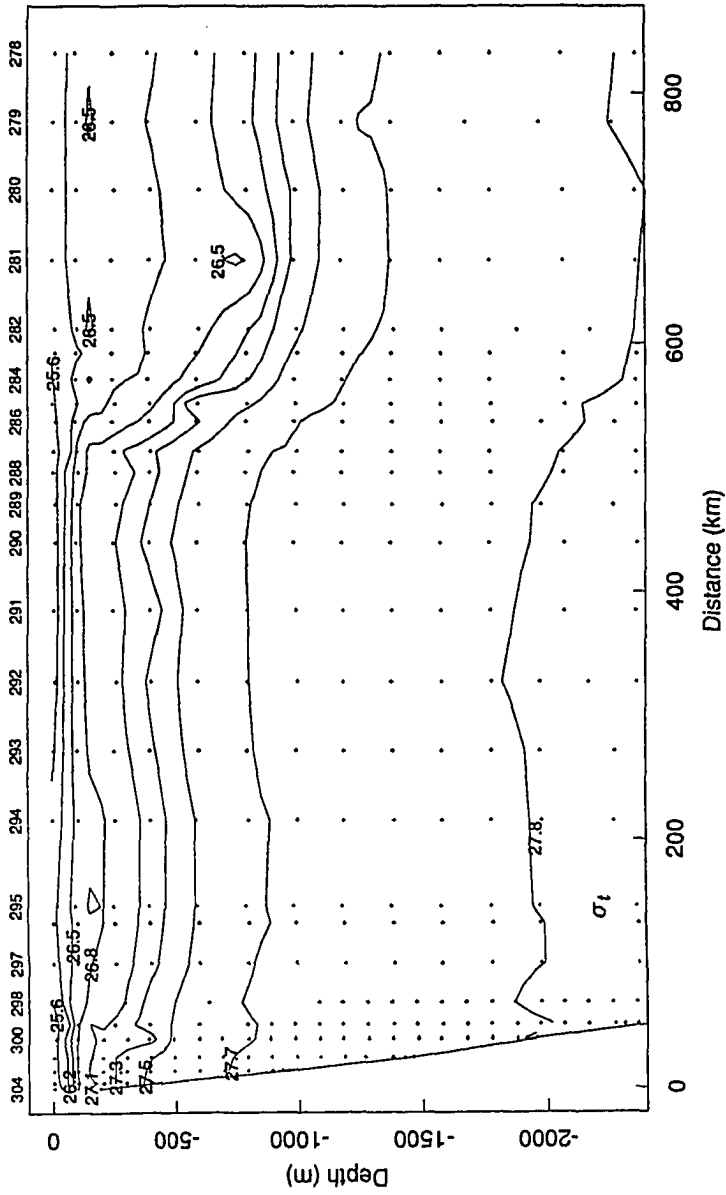


Figure 24 (continued)

Figure 25. Density (σ_t), velocity, nitrate concentration, and nitrate, phosphate, silicate and DO fluxes in section 53W, down to 2000 *m*.



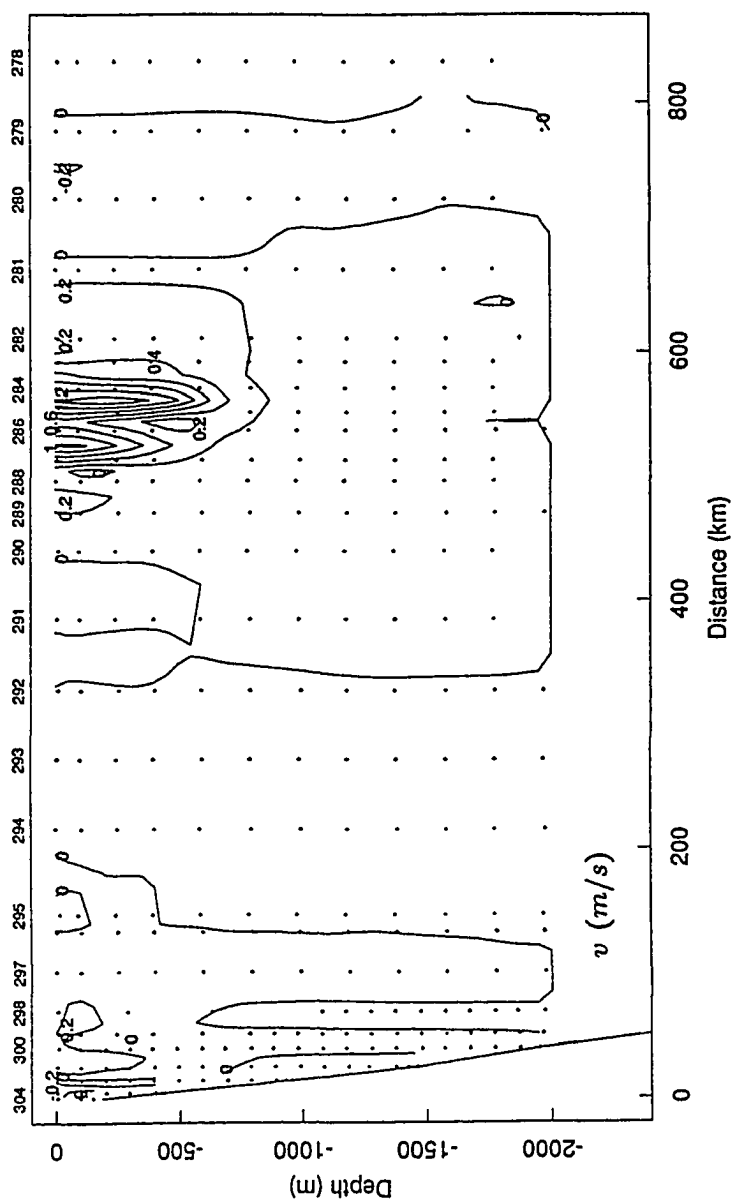


Figure 25 (continued)

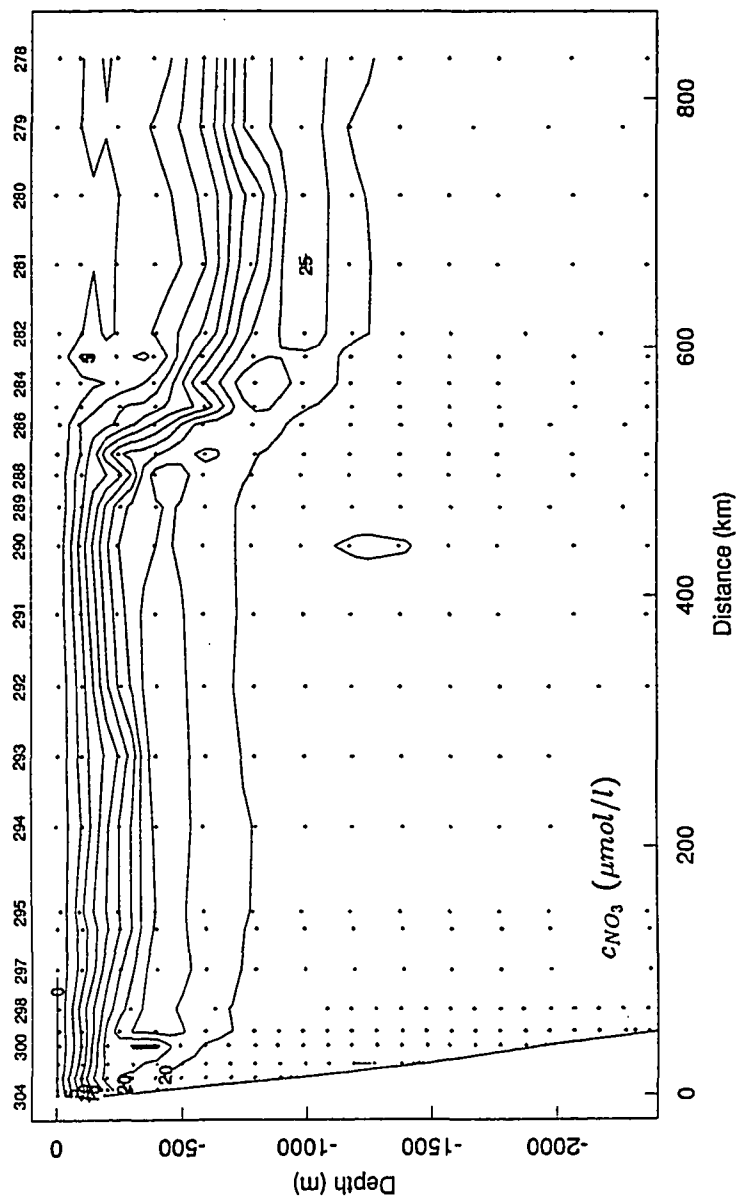


Figure 25 (continued)

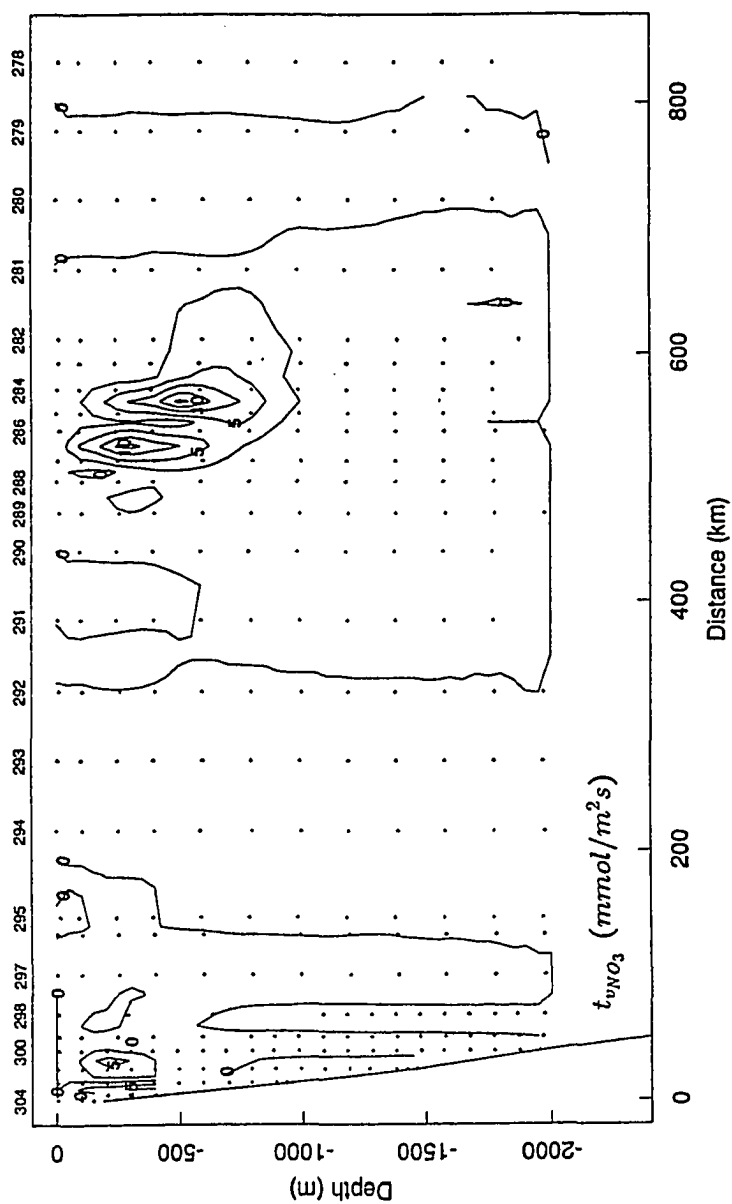


Figure 25 (continued)

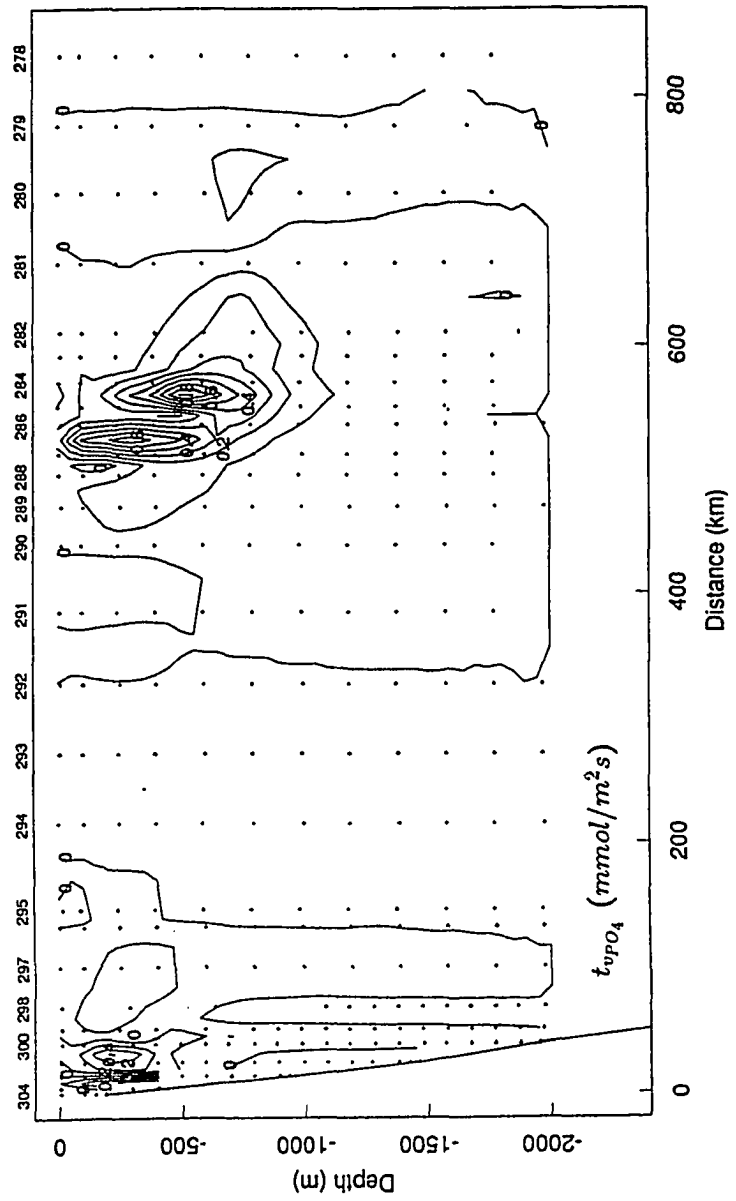


Figure 25 (continued)

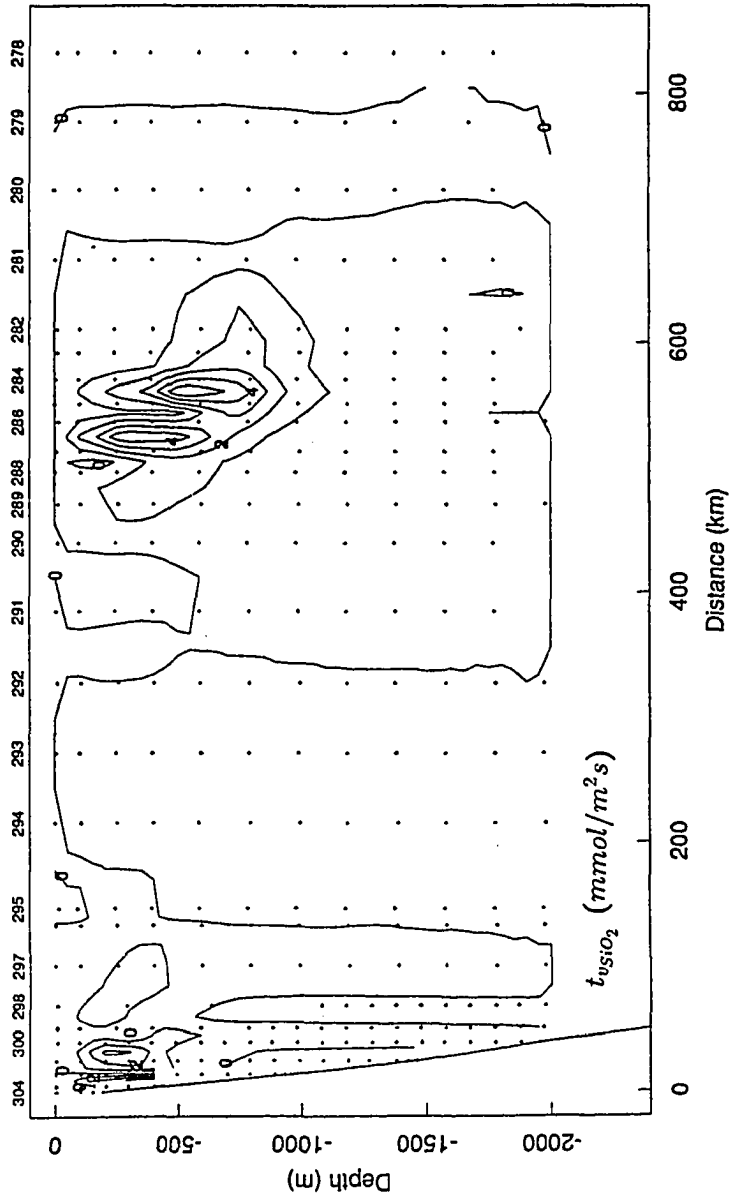


Figure 25 (continued)

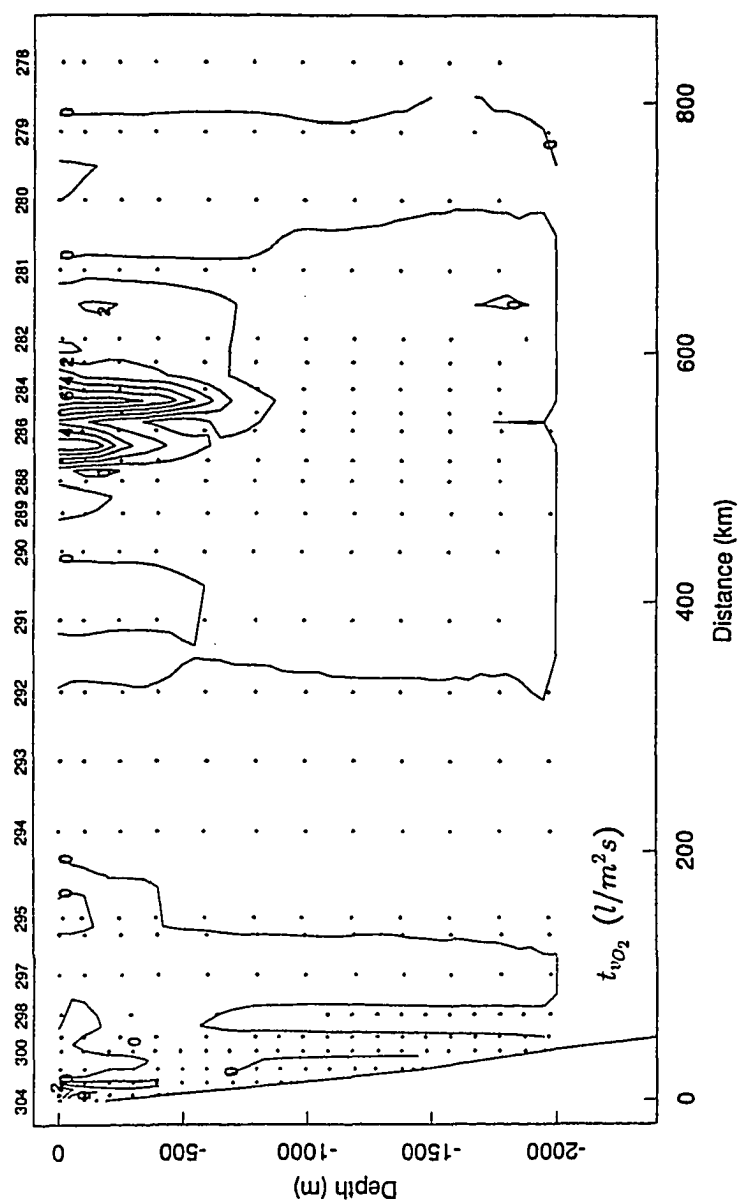
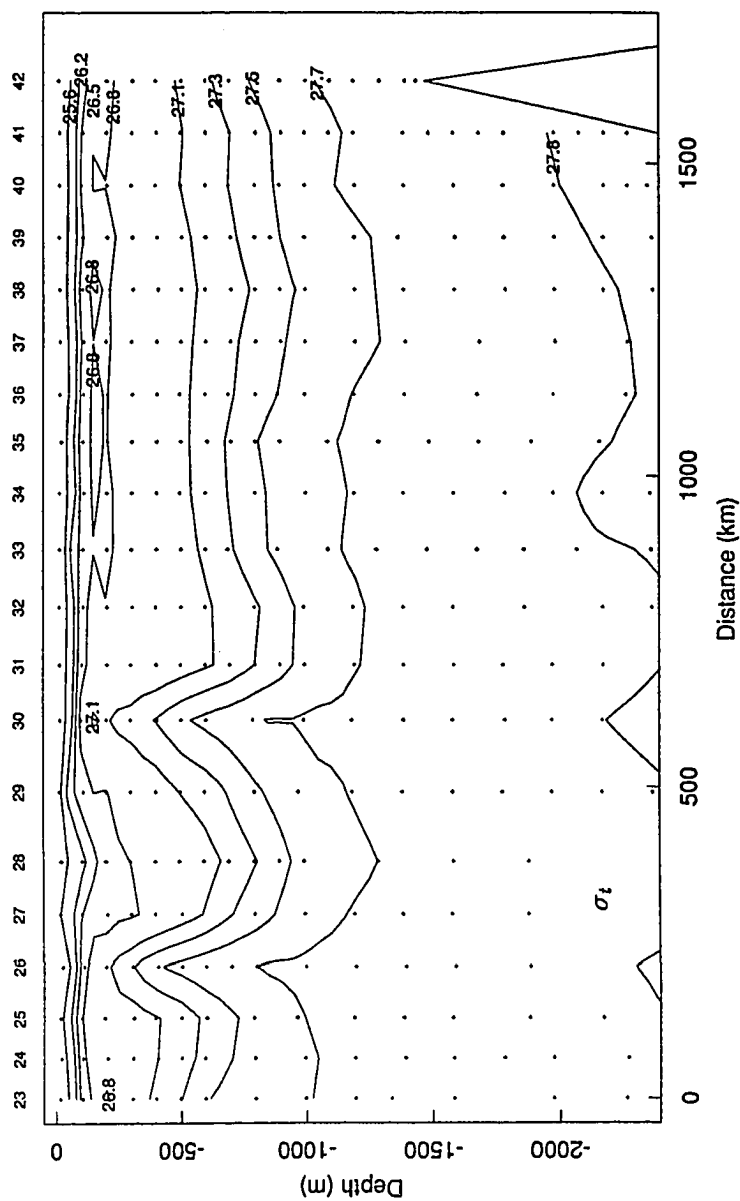


Figure 25 (continued)

Figure 26. Density (σ_t), velocity, nitrate concentration, and nitrate, phosphate, silicate and DO fluxes in section 35W, down to 2000 *m*.



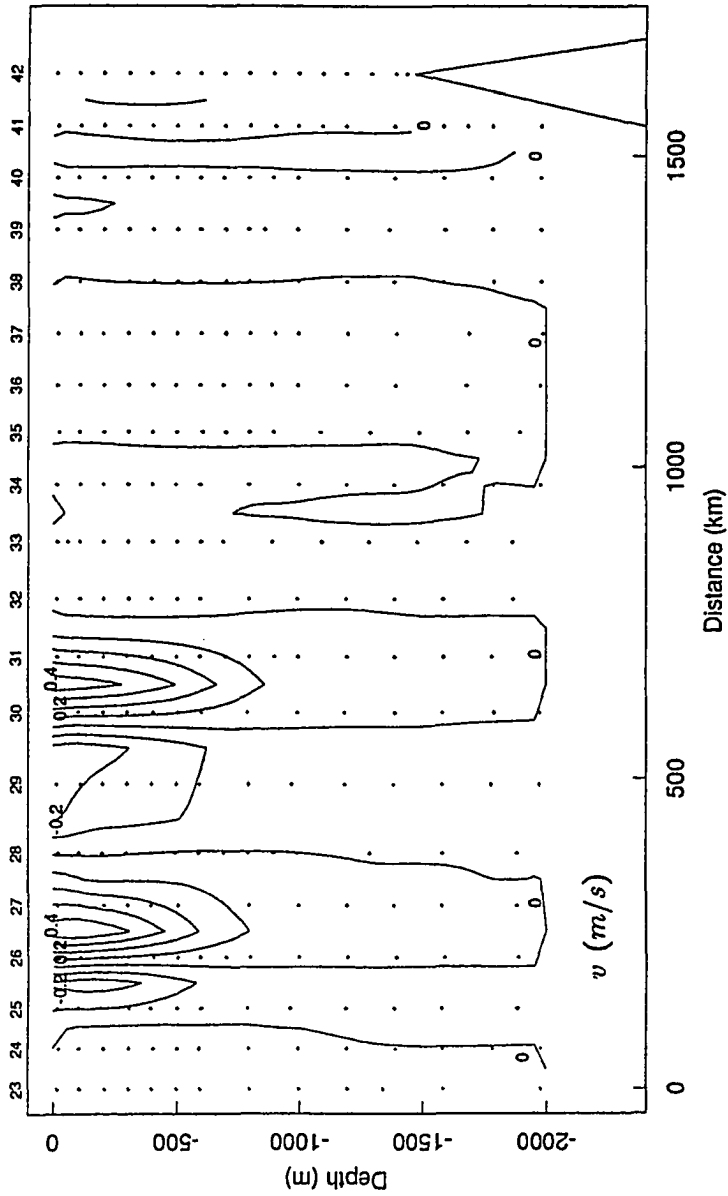


Figure 26 (continued)

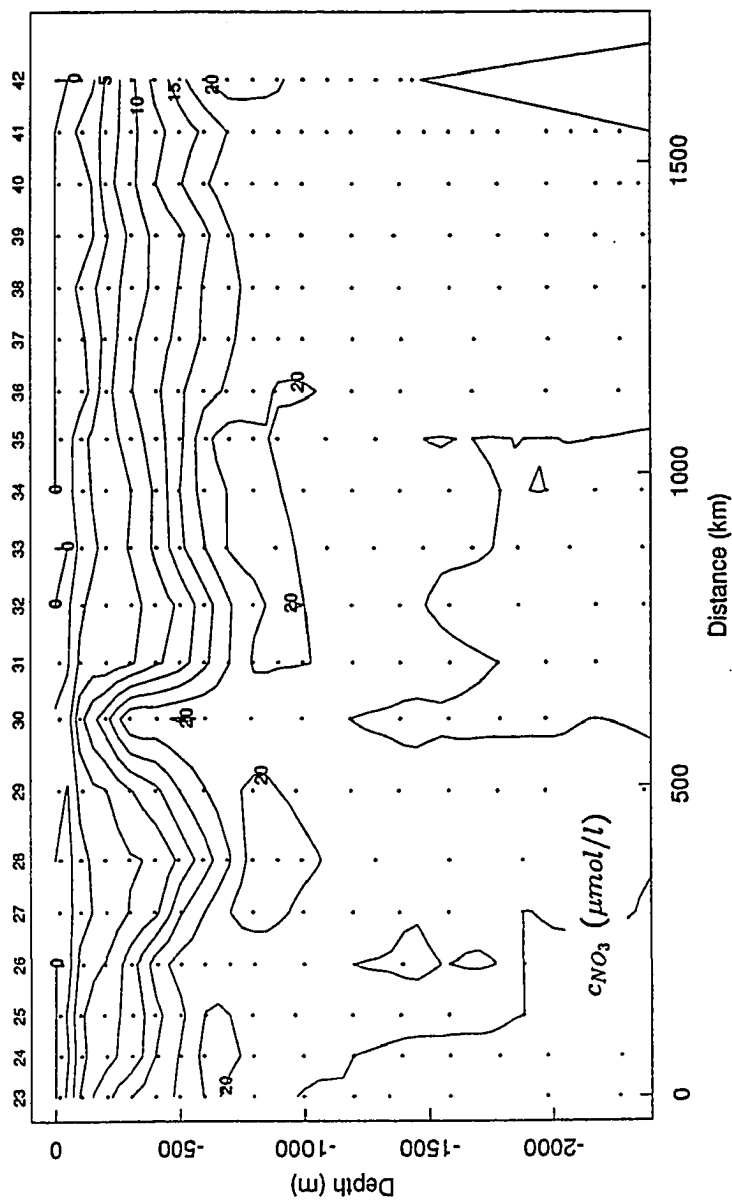


Figure 26 (continued)

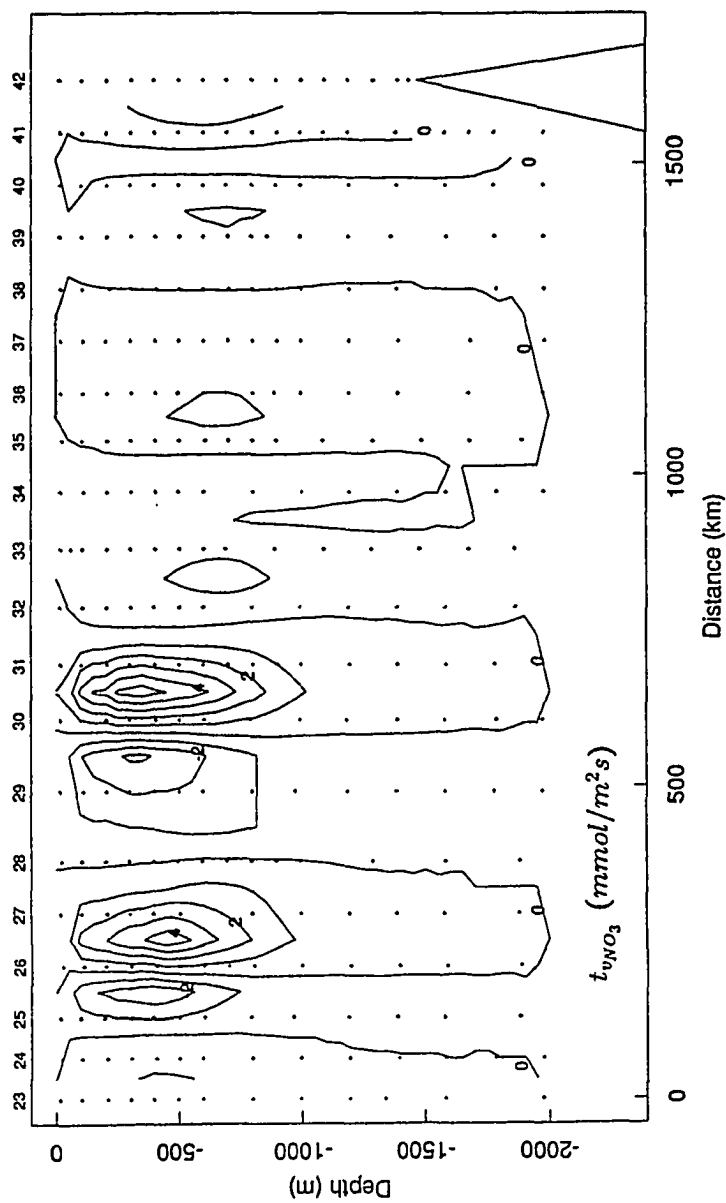


Figure 26 (continued)

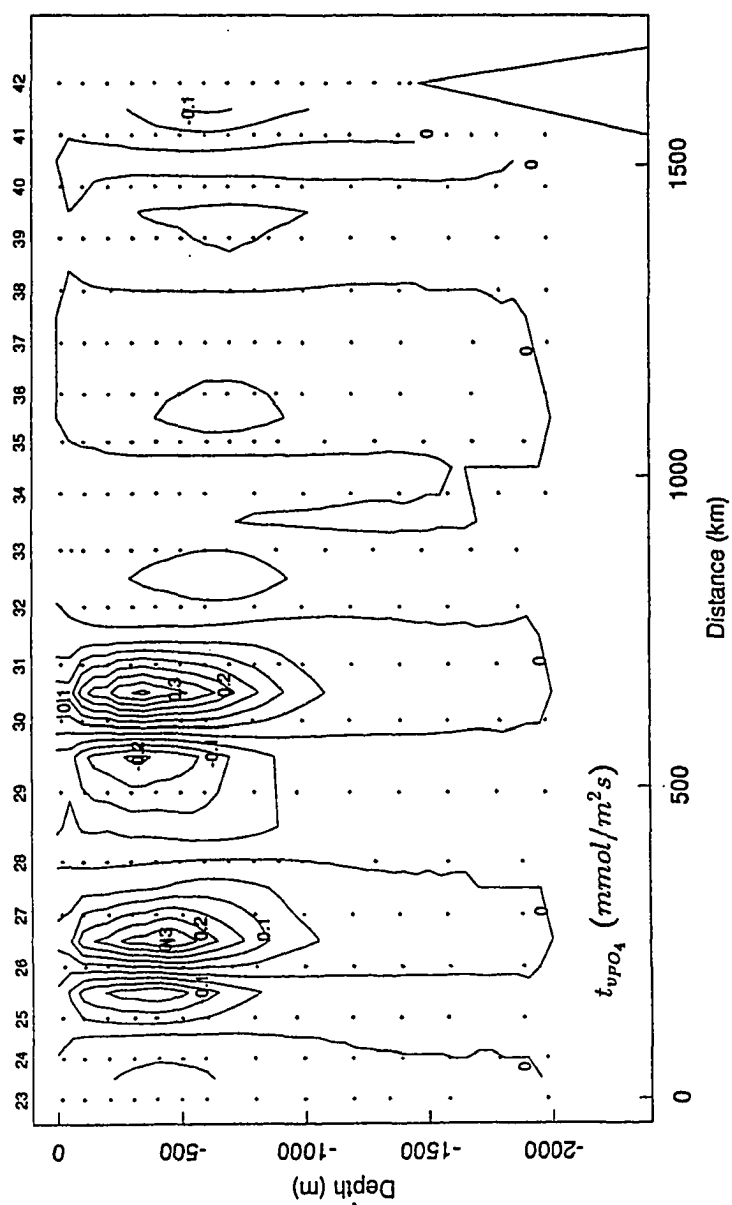


Figure 26 (continued)

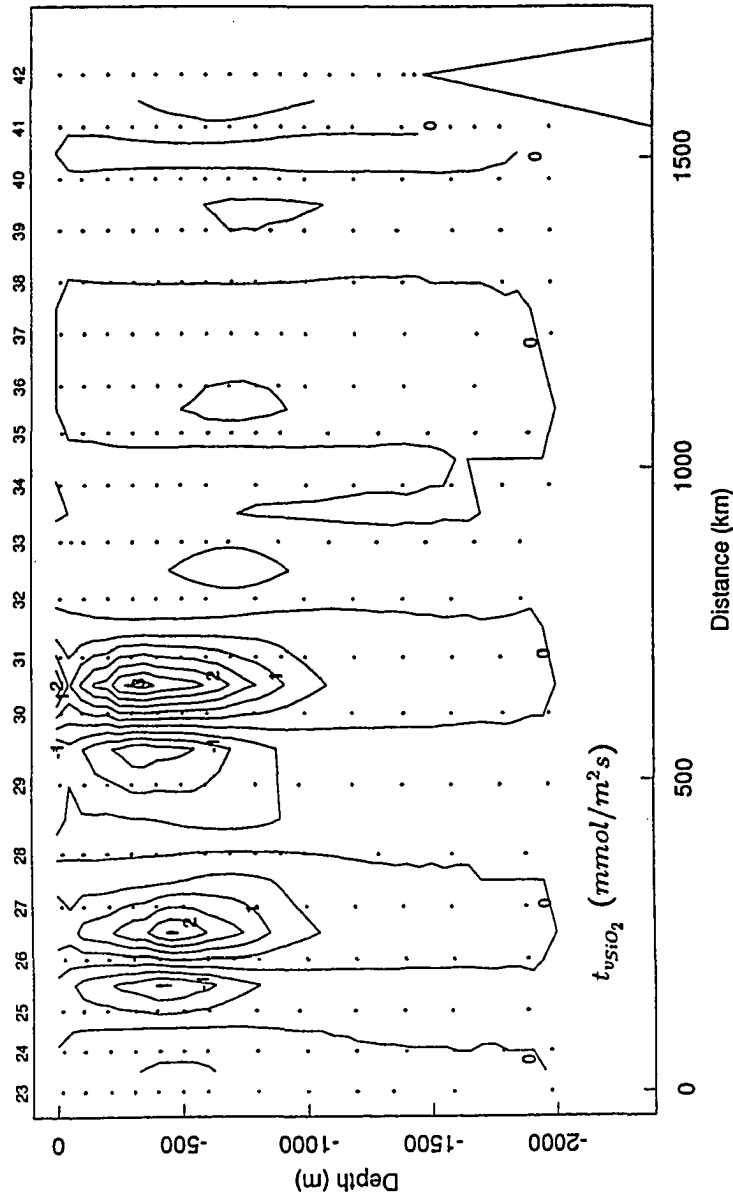


Figure 26 (continued)

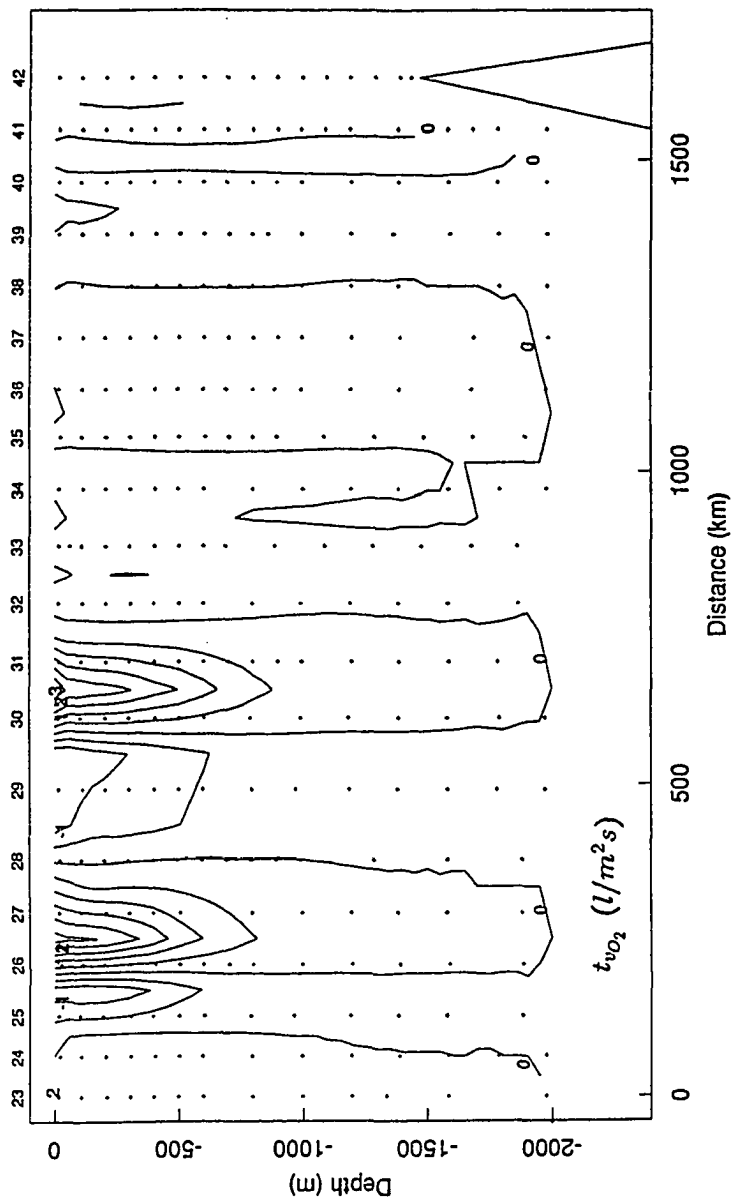


Figure 26 (continued)

and a maximum located in the mid-thermocline, centered near $\sigma_t = 27.3$. The distribution of DO has a maximum in the surface layers and a minimum near the $26.8\sigma_t$ -isopycnal, after which it increases again.

The $27.1 - 27.7\sigma_t$ -stratum corresponds to the nutrient maximum and DO minimum concentrations in the mid and upper thermocline (Riley 1951), the nutrient bearing stratum of the North Atlantic Ocean (Csanady 1990b). In all cases the nutrient flux contours define a Nutrient Stream, or region of high nutrient flux associated with the Gulf Stream system. The core of the Nutrient Stream is located in the upper portion of the nutrient bearing stratum ($26.2 < \sigma_t < 27.3$), centered at about 500 m depth, below and slightly offshore of the high-velocity core of the Gulf Stream. The Nutrient Stream is identifiable in all sections, although downstream of section 36N it has several branches, and at section 35W also reverse transport of significant magnitude. Flux intensity is greatest in the Florida Straits and declines monotonically downstream (except for DO which has similar magnitudes at sections 24N and 36N).

Fig. 10 indicates the position of the Nutrient Stream, estimated from the five sections that encompass the whole Gulf Stream. The contours of the Nutrient Stream in the figure correspond to flanking nutrient flux values of $(2.5, 0.2, 1)\text{ mmol } (NO_3, PO_4, SiO_2)\text{ m}^2\text{ s}^{-1}$, which roughly coincide with velocity contours of 0.2 m s^{-1} and DO flux contours of $1\text{ l m}^{-2}\text{ s}^{-1}$. The irrigation of the Nutrient Stream from the western boundary into the North Atlantic Ocean suggests that it may play a similar role as arteries in a living being, if one adopts the philosophy of Lovelock (1979).

The continuity of properties along isopycnal surfaces is evident in Figs. 21 to

26. There is one qualification, however, illustrated in Figs. 27 and 28: nutrient (nitrate in Fig. 27) and DO concentration contours in a σ_t -distance map show significant departures from the general horizontal trend at the location of the Nutrient Stream. Up to $\sigma_t = 27.0$, i.e. in the lower and mid-thermocline layers, the nutrient and DO concentrations are seen to be almost a function of density alone. In lighter layers the concentration shows a maximum for nutrient and a minimum for DO at stations 15 and 16, just seaward of the high-velocity core of the Gulf Stream. One possible interpretation for this is mixing between the upper thermocline and surface waters, a transfer of nutrient-rich and DO-poor thermocline waters into the nutrient-depleted and DO-rich surface layers. It is important to note that a considerable number of data points show the nutrient maximum and DO minimum in the light layers of the Gulf Stream. However, variations shoreward from this maximum (e.g., near $x = 150 \text{ km}$) are mostly artifacts of the contouring scheme and should be ignored.

4.2 Changes in water mass and nutrient transports

We turn now to calculate total and partial water and nutrient transports by the Gulf Stream. The area integral of the velocity gives the water transport, in units of sverdrups. The total water transport by the Gulf Stream, V , is obtained by integrating over the area of the whole Stream. The transport that takes place between two isopycnals, V_i , can be obtained by integrating over the area of the Stream bounded by these isopycnals. The total transport can also be expressed as the summation of all the partial transports between consecutive isopycnal surfaces, with the upper and lower limits defined as the sea surface ($z = 0$) and the lowest

Figure 27. Nitrate concentration, c_{NO_3} , in section 36N as a function of σ_t and cross-stream distance.

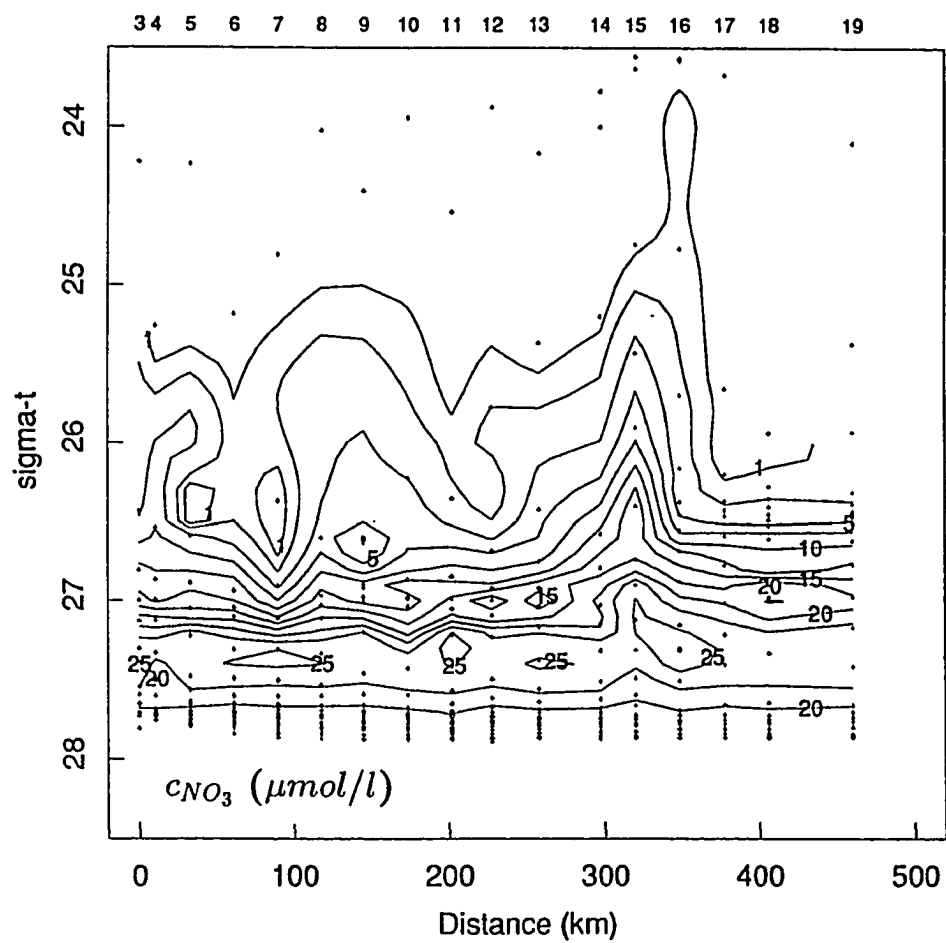
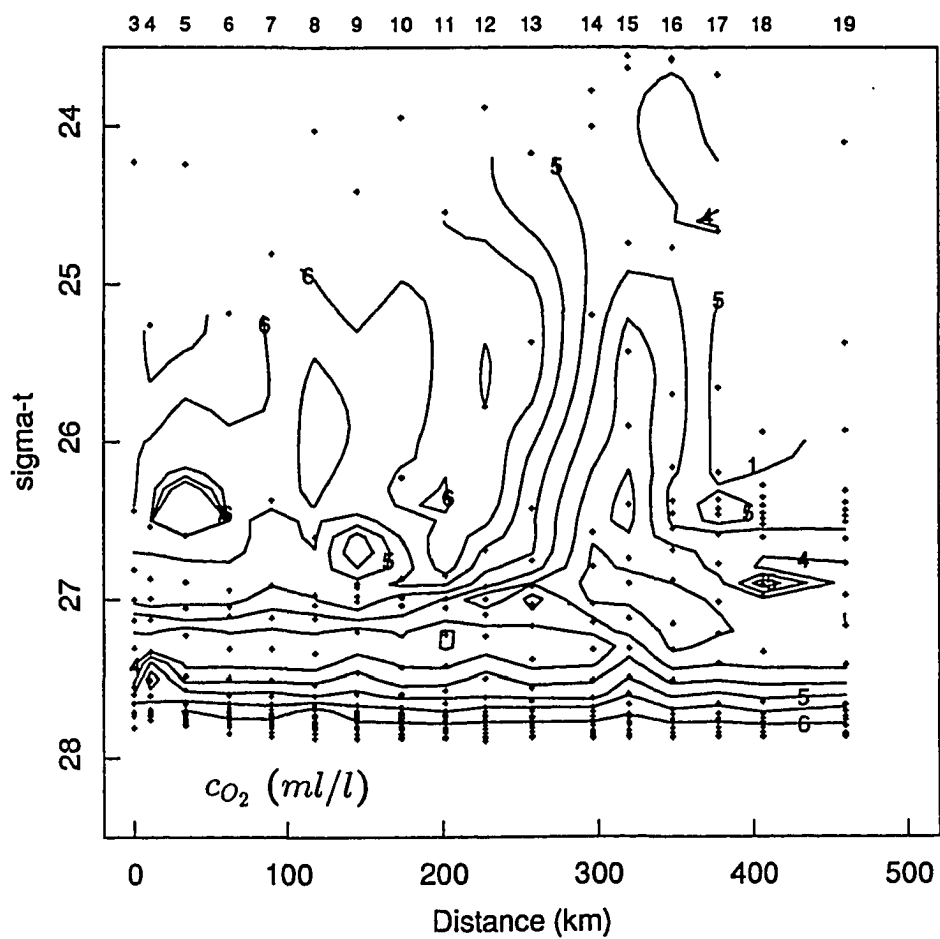


Figure 28. DO concentration, c_{O_2} , in section 36N as a function of σ_t and cross-stream distance.



isopycnal ($z = -h(x)$):

$$\begin{aligned} V &= \int_A v dA = \int_{-h}^0 \int_0^L v dx dz \\ &= \sum_{i=1}^{N-1} \int_{z_{i+1}}^{z_i} \int_0^L v dx dz = \sum_{i=1}^{N-1} V_i, \end{aligned} \quad (2)$$

where the depths of the isopycnals are given by $z_i \equiv z(\sigma_{ti}, x)$, and N is the number of isopycnal surfaces used in partitioning the Gulf Stream. The topmost surface is the sea surface and the lowest isopycnal is the assumed surface of no motion. The cross-stream limits $x = 0$ and $x = L$ are chosen as to include all significant baroclinic transport by the Gulf Stream.

Similarly, the area integral of the nutrient flux gives the nutrient transport, T_v , with typical units of $kmol s^{-1}$ ($l s^{-1}$ for DO). Again we can express the nutrient transport by the whole Nutrient Stream as the summation of all partial transports between consecutive isopycnals:

$$\begin{aligned} T_v &= \int_A c v dA = \int_{-h}^0 \int_0^L c v dx dz \\ &= \sum_{i=1}^{N-1} \int_{z_{i+1}}^{z_i} \int_0^L c v dx dz = \sum_{i=1}^{N-1} T_{vi}. \end{aligned} \quad (3)$$

The nutrient and water transports for each layer may be related through

$$T_{vi} = \bar{c}_i V_i, \quad (4)$$

where \bar{c}_i is a mean, velocity weighted, concentration for the layer. This concentration may be related to the mean layer concentration, c_i , as

$$\begin{aligned} \bar{c}_i &= \frac{\int_{z_{i+1}}^{z_i} \int_0^L c v dx dz}{\int_{z_{i+1}}^{z_i} \int_0^L v dx dz} \\ &\simeq \frac{\int_{z_{i+1}}^{z_i} \int_0^L c dx dz}{\int_{z_{i+1}}^{z_i} \int_0^L dx dz} = c_i, \end{aligned} \quad (5)$$

with the approximation holding if the layers are thin enough and the velocity is a relatively slowly varying function of depth. In the limit of a layer with infinitesimal small thickness equation (4) becomes expression (1) for nutrient flux. For the cross-shelf direction we can define similar quantities (U , U_i , T_u , T_{ui}), with the important difference that they cannot be directly calculated but instead they have to be inferred.

Brewer and Dyrssen (1987) estimates for the nitrate and phosphate transport were obtained using only one station with nutrient data, in combination with Niiler and Richardson (1973) velocity measurements. Their estimates compare rather well with ours, obtained from 11 stations in section 24N (see Table 1). Our values are slightly larger, the difference being partially due to the fact that our estimate for water mass transport is larger than the value used by Brewer and Dyrssen (1987) (we used Niiler and Richardson's summer velocity field, while Brewer and Dyrssen apparently used their annual mean velocities).

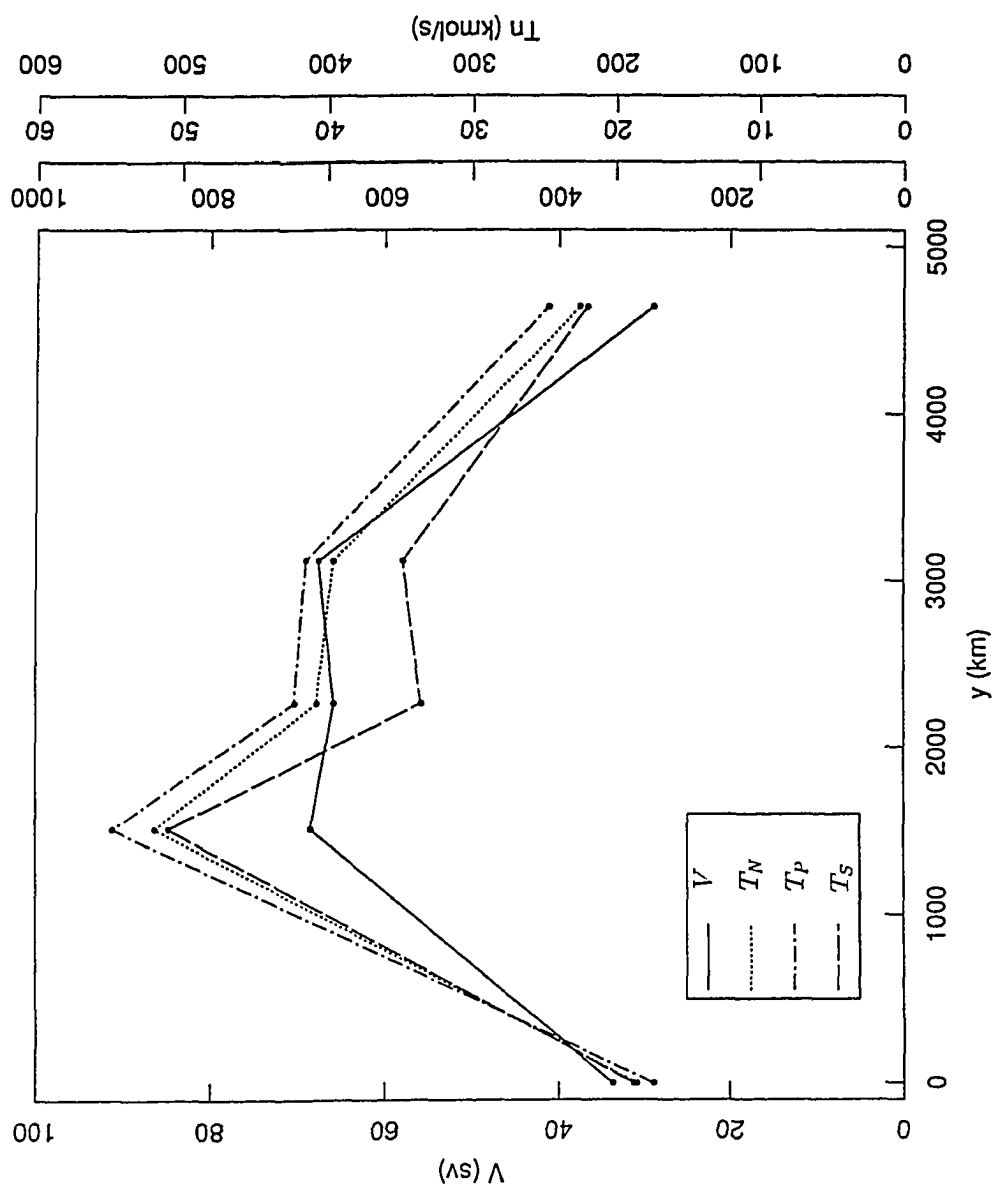
The water mass and nutrient transports across section 24N may be compared with the (partial) transports across section 7S, also in Table 1. It is noteworthy that while the water transport shows only a 12% increase, the nutrient transport roughly increase by a factor of two. The increase in nutrient transport appears even more striking if we recall that section 7S actually recorded the passage of only a portion of the Gulf Stream.

Fig. 29 shows the changes in total water and nutrient transports by the Gulf Stream, for the five complete sections. The total nutrient transport peaks at section 36N. Total nutrient transport at this section is 863 kmol s^{-1} for NO_3 , 54.7 kmol s^{-1} for PO_4 , and 508 kmol s^{-1} for SiO_2 . This figure shows that although

Section	V	T_v			
		NO_3	PO_4	SiO_2	DO
FS	29.5	292	16.4	-	109
24N	33.7	309	17.4	187	131
7S	38.2	530	39.7	301	152

Table 1. Total water mass (sverdrups), nutrient ($kmol\ s^{-1}$), and DO ($lm^{-2}s^{-1}$) transports across the Florida Straits according to Brewer and Dyrssen (1987) and our calculations (FS and 24N, respectively). Also shown are the partial transports going across section 7S.

Figure 29. Variation of total water mass and nutrient transports with along-stream distance. The three scales in the right margin correspond to nitrate, phosphate, and silicate transport, respectively.



it may be conjectured that much of the nutrient transport recirculates, a large fraction of it undoubtedly reaches the subpolar gyre.

In addition to the above total transports, we have also calculated the transports of water mass, nutrients and DO, in a succession of overlying layers, using the above expressions for V_i and $T_{v,i}$. The layers chosen are between the sea surface and the $\sigma_t = 25.6$ isopycnal surface, and between pairs of the isopycnals, $\sigma_t = 25.6$, 26.2, 26.5, 26.8, 27.1, 27.3, 27.5, 27.7, and 27.8. The isopycnal $\sigma_t = 27.8$ approximately coincides with the 2000 m assumed level of no motion. The isopycnals chosen divide the cross section of the Gulf Stream into strips of roughly similar depth. The top three strips are in what Worthington (1976) called the warm water, the next two upper thermocline water, the two below that mid-thermocline water, and the last two lower-thermocline water. Down to the mid-thermocline, the layers considered by Sarmiento et al. (1982) were nearly the same as ours, although their choice was based on equal surface outcropping areas in winter.

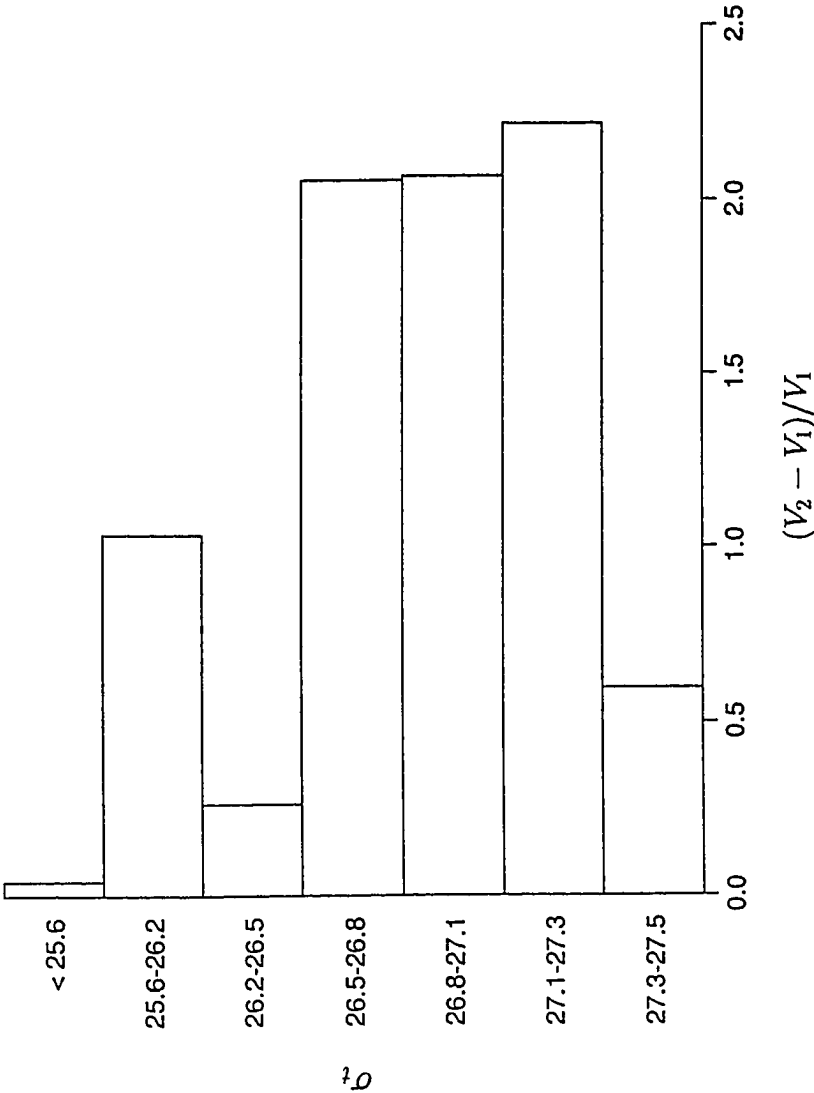
Table 2 contains V_i and $T_{v,i}$ for nitrate, phosphate, silicate and DO, in all the isopycnal layers mentioned, for sections 24N and 36N. As is well known, the baroclinic water mass transport of the Gulf Stream roughly doubles between these two sections. Nutrient transport, however, is seen to treble, and the increase in DO transport is also larger than that for the water mass transport. This relatively large increase in nutrient transport is partially due to along-isopycnal inflow from the Sargasso Sea on the deeper layers ($\sigma_t > 27.5$), which are not present in the Florida Straits section. We may see in section 36N that these layers have nutrient and DO concentrations higher than the overall values (see Table 2; for example, for nitrate the deep layers have a concentration of $19.25 \mu\text{mol l}^{-1}$, while the over-

Table 2. Total and partial water mass (sverdrups), nutrient ($kmol s^{-1}$) and DO ($lm^{-2}s^{-1}$) transports, and nutrient ($\mu mol l^{-1}$) and DO ($ml l^{-1}$) concentrations in sections 24N and 36N.

all mean concentration is of $16.92 \mu\text{mol l}^{-1}$). Hence, we may expect that their contribution to the total nutrient transport will be greater than their contribution to the total water mass transport. However, the differences in these concentrations are less than 20%, and by themselves cannot explain the much larger change in nutrient transport (a factor of three) when compared with the water transport (a factor of two). Furthermore, they can neither explain why the increase in nutrient transport is so different from the increase in DO transport.

To find an answer to these questions we need to look at the increase in water mass and nutrient transport over the shallower (surface and upper-thermocline) layers. As in the deeper layers, these changes are attributed to along-isopycnal inflow from the Sargasso Sea. Expressed as a fraction of the upstream water transport, the increase in V in the various layers range from 0 to 200%, with a pronounced broad maximum between the $\sigma_t = 26.5$ and 27.3 isopycnal surfaces (Fig. 30). Notice that these increases are generally of the same order as the 'upstream' transport at section 24N, and therefore dwarf any errors in the transport estimates. As may be seen in Fig. 30, most of the water mass transport increase occurs in the upper thermocline layers ($26.5 < \sigma_t < 27.3$). Because these are the layers constituting the nutrient bearing stratum, the predominance of this inflow helps explaining the much greater than proportionate increase of nutrient transport in section 36N. Since this stratum is poor in oxygen, this also explains why the increase in DO transport is not comparable to the increase in nutrient transport.

Figure 30. Relative increase between sections 24N and 36N of water mass transport in isopycnal layers.



Chapter 5. Water Mass and Nutrient Balances

*Trifles make perfection, and perfection
is no trifle.*

Michelangelo Buonarroti (1475-1564)

The above explanation for the relatively large increase in nutrient over water mass transport (as due to inflow from the Sargasso Sea), is borne out in a general way by an examination of the nutrient transport changes, but there are some important discrepancies. In this chapter we use the nutrients as a tracer in order to quantify the processes taking place between sections 24N and 36N, that may be responsible for these discrepancies. In order to do so we require the changes in water and nutrient transport to be at least of the same order as the input through the Florida Straits. A very small change is not significant when compared with the temporal variability of the transports. An increase much larger than the inflow through the upstream section, contains insufficient information on the upstream conditions.

5.1 Nutrient anomalies

Let an 'advective' concentration be defined by

$$c_a = \frac{T_{n2} - T_{n1}}{V_2 - V_1}, \quad (6)$$

where the numeric subscripts 1 and 2 refer to the upstream and downstream sections, respectively. If inflow took place strictly along isopycnals, the advective

concentration would equal some weighted mean of the concentrations c_{n1} and c_{n2} (which only differ by about 10%, so that c_{n2} is a reasonable approximation to the concentration of the inflow). As long as the increases in both mass transport and nutrient transport in a given layer are of the order as the upstream transports, any major differences between c_a and c_{n2} are significant and require an explanation. An advective concentration much larger than the layer concentration implies excess nutrient supply, the opposite difference a deficiency.

Excluding the uppermost layer and the two bottom layers from consideration (because the $\Delta V/V_1$ ratio is too small or too large for this argument), significant excess nutrient supply is found in the layers above the $\sigma_t = 26.8$ isopycnal, deficiency below (see Table 2). Combining all the layers above this isopycnal into a single 'surface' stratum, and all those down to $\sigma_t = 27.5$ into a 'thermocline' stratum, one finds a weighted average c_a about twice c_{n2} in the surface stratum, a 15% deficiency in the thermocline stratum. Expressed in terms of nitrate transport, the increase in the surface stratum is 160 kmol s^{-1} , only half of which is explained by the isopycnal inflow. In the thermocline, the increase is 230 kmol s^{-1} , in place of 265 kmol s^{-1} if the inflow were isopycnal. Table 2 shows similar differences for the other nutrients. As may be expected, the exact amount of the smaller discrepancy in the thermocline scatters more, its average over the three nutrients being 17%.

For the deep layers the mean and advective concentration for the nutrients and DO show good agreement, as it is expected for recirculating water input taking place exclusively along the isopycnals. However, the DO results for the topmost layer suggest the existence of an important extra source of DO. This source can only be the air-sea interface, and causes DO to be a non-conservative quantity, not

only due to biological factors (which are reasonably well known, but are estimated below to be negligible) but also because of air-sea flux. Hence, DO is not included in the remaining discussion.

5.2 A kinematic model for water and nutrient balances

The ‘excess’ nutrient transport observed in the surface stratum, and the concentration anomalies over the Nutrient Stream suggest two-way exchange, and possibly one-way mass transfer, of thermocline waters into the surface stratum. A two-box model of the Gulf Stream between sections 24N and 36N (Fig. 31) can be used to estimate the rates of these diapycnal transfer processes. Given the large nutrient transport increases, nutrient utilization is legitimately ignored in the mass balances (see discussion below). The large water mass transport, and the large increase in this transport, makes it realistic to suppose steady state (ignoring ‘storage’ of water between sections) and to neglect any exchange with the continental margin. The water mass and nutrient balances for the surface and thermocline strata are then:

$$\Delta V_s = U_s + W, \quad (7)$$

$$\Delta T_s = c_s U_s + c_t W + (c_t - c_s)E, \quad (8)$$

$$\Delta V_t = U_t - W, \quad (9)$$

$$\Delta T_t = c_t U_t - c_t W - (c_t - c_s)E. \quad (10)$$

where the ΔV are increases in water mass transport, the ΔT increases in nutrient transport, U_s and U_t are inflows from the surface and thermocline strata, W is one-way transfer, and E is two-way exchange. These equations are readily solved for the four unknowns U_s , U_t , W and E . In the next chapters we will argue that

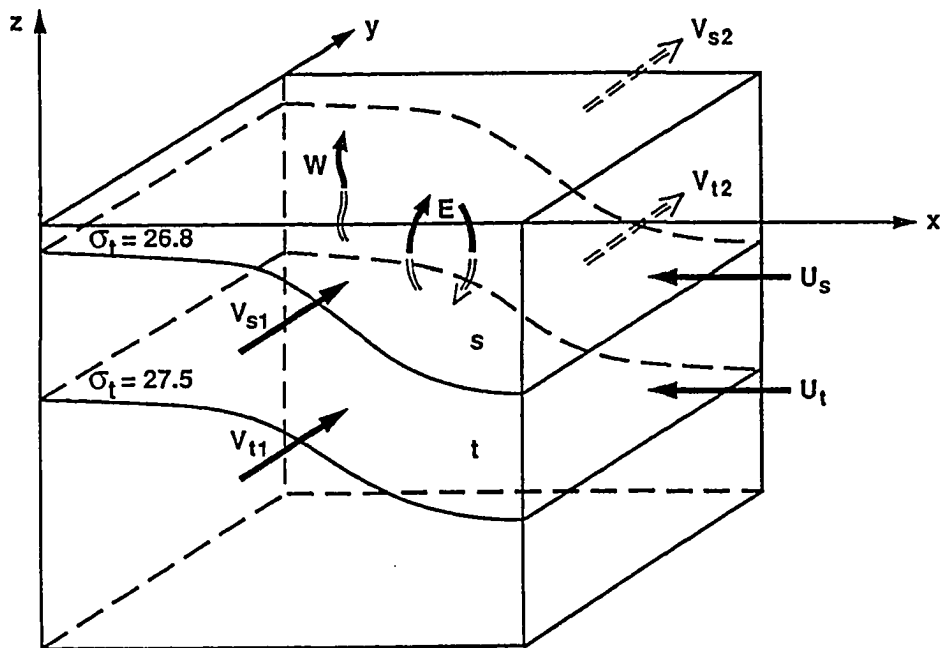


Figure 31. Schematic representation of the main elements for the two-box model of the Gulf Stream between sections 24N and 36N.

both W and E may be explained in terms of the divergence of the Reynolds density flux.

The neglect of nutrient utilization may be readily justified by empirical data obtained in the South Atlantic Bight. Yoder et al. (1983) quote new production rates at the edge of the continental shelf, implying nitrate utilization at the rate of $2.3 \times 10^{-6} \text{ kmol m}^{-2} \text{ d}^{-1}$, similar to rates used by Walsh et al. (1988), $3 - 5 \times 10^{-6} \text{ kmol m}^{-2} \text{ d}^{-1}$, in a numerical model of production in the Mid-Atlantic Bight. Supposing a utilization rate of $3 \times 10^{-6} \text{ kmol m}^{-2} \text{ d}^{-1}$ over a 100-km-wide strip between sections 24N and 36N (1500 km apart) gives a nitrate transport loss of 5 kmol s^{-1} , or 3% of the calculated increase in transport in the surface layer, which is certainly at the noise level. To utilize hundreds of kmol s^{-1} at the empirical utilization rates would take an area the size of the subtropical gyre. Therefore, utilization is important for the balance of nutrients between whole transoceanic sections (as discussed by Brewer and Dyrssen, 1987, for such a section at 24°N), but not between sections of an intense Nutrient Stream.

5.3 Recirculation and mixing

Equations (2), (3), (5) and (7) to (10) may be applied separately to the nitrate, phosphate and silicate transport, yielding three sets of estimates for water mass inflow and mixing. These are shown in Table 3. While the estimates scatter somewhat (especially for W), they all show similar inflow into the surface and thermocline strata, upward one-way transfer, and significant two-way exchange. Realistic values, with error bars, are as follows (all in sverdrups):

Nutrient	U_s	U_t	W	E
NO_3	11.53	15.04	2.38	2.17
PO_4	9.62	16.95	4.29	1.19
SiO_2	13.44	13.12	0.47	3.53

Table 3. Estimates for inflow and mixing water mass transports (sverdrups) between sections 24N and 36N, obtained from the two-box model.

$$U_s = 12 \pm 1.5,$$

$$U_t = 15 \pm 1.9,$$

$$W = 2.4 \pm 1.9,$$

$$E = 2.4 \pm 1.2.$$

The along-stream distance between the two sections is about 1500 km, so that the overall one-way transfer and two-way exchange rates (per unit length of the Stream) are $1.6 m^2 s^{-1}$, with fairly wide error bars. Distributed over the 80-km width of the Stream the corresponding mixing coefficients are both about $2 \times 10^{-5} m s^{-1}$. An upwelling velocity of similar magnitude characterizes equatorial upwelling (Wyrski 1981). Fig. 32 is a schematic representation of the overall mass transfer rates, off the Mid-Atlantic Bight, according to the values calculated above. Csanady and Hamilton's (1988) estimate, for the mass transfer rate to the shallower layers in the continental slope, is also included in this figure.

Water mass and nitrate transports in different strata of all five sections are shown in Table 4 (with $\sigma_t < 25.6$ included in the surface stratum). Between sections 36N-64W and 64W-53W there is little inflow or outflow; from 53W to 35W there is large outflow from the surface stratum and inflow into the thermocline. Application of the above box model to those section pairs cannot be justified because the $\Delta V/V$ requirement is not met, and indeed it leads to erratic results.

5.4 Estimates of mean transports

We finish this chapter by obtaining some gross estimates of the mean nitrate transport (surface to 2000 m) by the Nutrient Stream, and its distribution among the surface, thermocline and deep stratum. Similar calculations may be easily

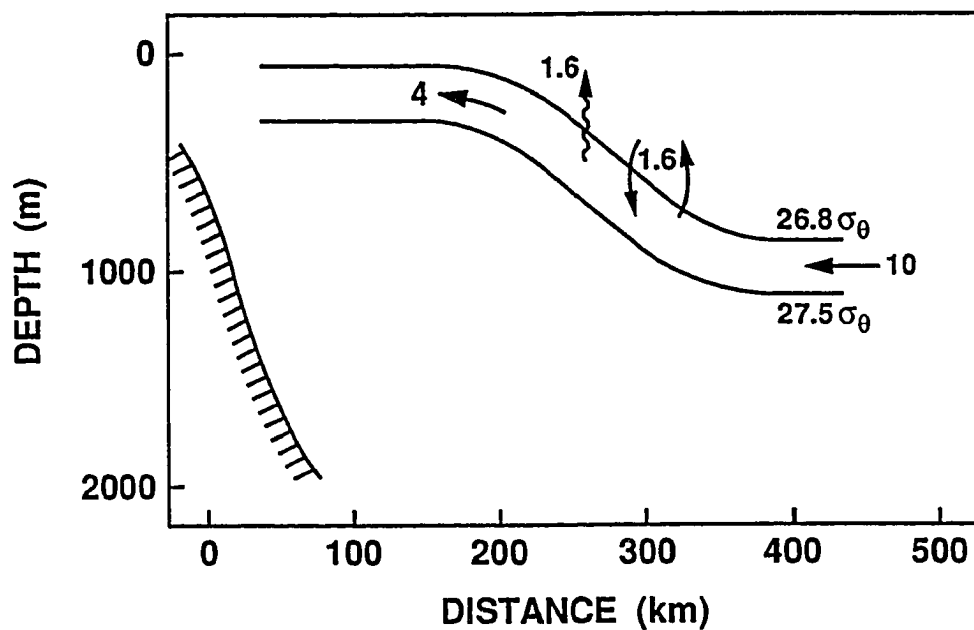


Figure 32. Schematic illustration of the overall mass transfer rates (in units of m^2s^{-1}), off the Mid-Atlantic Bight.

Section	24N	36N	64W	53W	35W
V_s	25.78	39.69	40.87	43.86	4.48
V_t	7.62	20.28	18.54	17.57	21.05
V_d	0.25	8.53	6.44	6.18	3.49
T_{vs}	115.5	273.9	187.8	220.8	17.5
T_{vt}	187.0	418.5	362.3	314.7	292.6
T_{vd}	6.3	170.4	128.0	123.5	65.4

Table 4. Water mass (sverdrups) and nitrate transports ($kmol\ s^{-1}$) in the surface s ($\sigma_t < 26.8$), thermocline t ($26.8 < \sigma_t < 27.5$), and deep strata d ($27.5 < \sigma_t < 27.8$) of sections 24N, 36N, 64W, 53W, and 35W.

extended to the other nutrients, but they will not be shown here. Given the number of approximations used in obtaining these values, we are actually more interested in assessing how sensitive along-isopycnal inflow, one-way transfer and two-way exchange are to possible errors in our along-stream transport estimates. We find that the mean along-isopycnal input is likely to be considerably larger than the previously calculated values, but one-way and two-way mixing are presumably nearly the same.

Niiler and Richardson (1973) and Worthington (1976) have studied the water mass transport variability in the Gulf Stream across the Florida Straits and the Mid-Atlantic Bight, respectively. For the Florida Straits, Niiler and Richardson (1973) estimated a mean water mass transport of 29.5 sverdrups with a mean annual variability of 8.2 sverdrups and total variability between 19 and 38 sverdrups. From Worthington's (1976, Table 10) summary of sections for the Mid-Atlantic Bight, we may estimate the mean water mass transport (referred to the 2000 *m* level) as 77.5 sverdrups, with a standard deviation of 7.1 sverdrups and maximum variability between 63 and 90 sverdrups. Both Niiler and Richardson (1973) and Worthington's (1976) results show large seasonal and interannual variability. Further, similarly large transport variations occur within a season of a particular year, presumably due to mesoscale features. Hence, it is not surprising to observe that sections 24N and 36N, despite being only two and a half months apart, do reflect these differences. Our calculated values for these sections, 33.7 and 68.5 sverdrups are 14% larger and 12% smaller than Niiler and Richardson (1973) and Worthington's (1976) mean values, respectively, but well within their observed variability.

As a first approximation, we may assume that the partial changes in water transport, as well as the partial and total changes in nutrient transport, are proportionally the same as the changes in the total water transport. Under this condition, and using Niiler and Richardson's (1973) value (29.5 sverdrups) for the mean water transport, we estimate the total nitrate transport across section 24N to be 270 kmol s^{-1} . The partial contributions from each stratum [surface, thermocline and deep] for this section are estimated to be [22.6, 6.7 and 0.3] sverdrups for water mass transport and [100, 163 and 5] kmol s^{-1} for nitrate transport.

We may follow a similar procedure for section 36N, now using Worthington's (1976) mean water mass transport (68.5 sverdrups). In this manner, we estimate the total mean nitrate transport across section 36N to be 976 kmol s^{-1} , and the partial contributions from each stratum [surface, thermocline and deep] to be [44.9, 23.0 and 9.6] sverdrups for water mass transport and [310, 473 and 192] kmol s^{-1} for nitrate transport.

We can now calculate the values for mean advective cross-stream inflow and diapycnal mixing, based on the above mean values for the surface and thermocline along-stream water mass and nitrate transports. Application of the kinematic model with these values leads to cross-stream isopycnal water transports of 19.2 and 19.4 sverdrups in the surface and thermocline strata, respectively, about 50% larger than the values obtained in last section. However, the one-way transfer and two-way exchange values remain almost unchanged (less than a 5% change.)

Chapter 6. Equations in Isopycnic Coordinates

The naturalist differs from the mathematician in that he considers things clothed, whereas the mathematician considers them as bare of any visible material.

Aristotle (B.C. 384-322)

In the last two chapters we used isopycnic coordinates in several ways. First, the presence of nutrient anomalies in the distance- σ_t plane suggested the possibility of exchange between isopycnal layers. Second, the separation of the total water mass and nutrient transports into partial transports by a finite number of isopycnal layers, allowed us to examine the origin of the changes in the structure of the transports. Finally, a kinematic model was built based on simple water mass and nutrient continuity arguments, which gave us an estimate of the intensity of overall diapycnal mixing between the Florida Straits and the Mid-Atlantic Bight.

Our results in the last chapter pointed to the existence of two processes responsible for exchange of water between the upper-thermocline and surface strata of the Gulf Stream. The first process, one-way transfer (W), is responsible for the transfer of water from the upper thermocline into the surface stratum. The second process is two-way exchange (E) between both strata. The diapycnal velocity, which has to be responsible for both processes, may be expressed as the divergence of the Reynolds density flux. In the remainder of this work we will explore the

situation in which the Reynolds density flux is caused by small scale turbulence that has its origin in hydrodynamic instability, and we will show how it can lead to the second process, two-way exchange. In this case an appropriate parameter to estimate the degree of turbulence is the gradient Richardson number.

How do local instabilities and mixing develop? In this chapter we seek an answer with the help of the mass, momentum and vorticity equations in isopycnic coordinates, in the presence of diapycnal mixing. In particular, we show that large enough diapycnal convergence or divergence can control the separation between isopycnal layers, and drive the potential vorticity balance.

6.1 The ‘mean’ diapycnal velocity

Before reviewing the momentum and vorticity equations in isopycnic coordinates we must define what we mean by ‘time-mean’ density surfaces and what are the corresponding diapycnal and entrainment velocities. In the cartesian (x, y, z) system, with velocity components (u, v, w) , the instantaneous diapycnal velocity, w_ρ , is defined as the material tendency for density:

$$w_\rho = \frac{D\rho}{Dt} = \frac{\partial\rho}{\partial t} + u\frac{\partial\rho}{\partial x} + v\frac{\partial\rho}{\partial y} + w\frac{\partial\rho}{\partial z}, \quad (11)$$

where $D/Dt \equiv \partial/\partial t + u\partial/\partial x + v\partial/\partial y + w\partial/\partial z$ is the material change operator in cartesian coordinates.

The mass conservation equation in cartesian coordinates is

$$\frac{\partial\rho}{\partial t} + \frac{\partial(u\rho)}{\partial x} + \frac{\partial(v\rho)}{\partial y} + \frac{\partial(w\rho)}{\partial z} = \nabla \cdot \mathbf{M}, \quad (12)$$

where \mathbf{M} is the molecular density flux vector. In an incompressible fluid and in the absence of diabatic heating or molecular diffusion, this equation is equivalent to $w_\rho = 0$.

It is reasonable to suppose that the time scale of instabilities developing in regions with significant mixing is much shorter than the time scale of significant displacements of the boundary current. Over the latter time scale, the fast unstable motions may be regarded as turbulence, giving rise to the conventional Reynolds fluxes of density. In this conceptual framework, the slowly changing ‘mean’ density field $\tilde{\rho}$ is viewed as the stochastic average over a large number of realizations, or more practically, a time-mean taken over the long-time scale. Fast motions distorting a given density isopleth, ρ , are removed by time-averaging the depths taken by that isopleth over the long-time scale, for each x and y , to give $\tilde{z} = z(x, y, \rho = \tilde{\rho})$.

With this conceptual model in mind, we decompose the density and velocity fields into fast (primed) and slow (tilded) motions: $\rho = \tilde{\rho} + \rho'$, $u = \tilde{u} + u'$, $v = \tilde{v} + v'$, $w = \tilde{w} + w'$. Taking the mean over the long-time scale, the mass-conservation equation becomes

$$\begin{aligned}\tilde{w}_\rho &\equiv \frac{\partial \tilde{\rho}}{\partial t} + \tilde{u} \frac{\partial \tilde{\rho}}{\partial x} + \tilde{v} \frac{\partial \tilde{\rho}}{\partial y} + \tilde{w} \frac{\partial \tilde{\rho}}{\partial \tilde{z}} \\ &= \nabla \cdot \tilde{\mathbf{M}} - \left[\left(\frac{\partial}{\partial x} (\overline{u'\rho'}) + \frac{\partial}{\partial y} (\overline{v'\rho'}) + \frac{\partial}{\partial \tilde{z}} (\overline{w'\rho'}) \right) \right] \equiv -\nabla \cdot \tilde{\mathbf{G}},\end{aligned}\quad (13)$$

having assumed incompressibility. The vector $\tilde{\mathbf{G}}$ results from the contribution of the mean molecular ($\tilde{\mathbf{M}}$) and turbulent ($\tilde{\mathbf{F}}$) density flux vectors, $\tilde{\mathbf{G}} = \tilde{\mathbf{F}} - \tilde{\mathbf{M}}$. The (mean) turbulent density flux vector, or Reynolds density flux, has components $\tilde{\mathbf{F}} \equiv (\tilde{F}_x, \tilde{F}_y, \tilde{F}_z) \equiv (\overline{u'\rho'}, \overline{v'\rho'}, \overline{w'\rho'})$. In the atmosphere vertical density flux may be due both to diabatic heating (latent heat release and radiation flux divergence) and mixing, but in the ocean (except in the uppermost 10 m or so) the contribution from diabatic heating (or cooling) is negligible.

The diapycnal velocity, w_ρ , defined in the (x, y, ρ) system, can be further

related to the vertical velocity, w , in the vertical coordinate (x, y, z) system, as follows

$$w = \frac{\partial z}{\partial t} + u \frac{\partial z}{\partial x} + v \frac{\partial z}{\partial y} + w_\rho \frac{\partial z}{\partial \rho}. \quad (14)$$

In the long-time mean systems $z' = 0$ and $w_\rho = \tilde{w}_\rho$, so an equivalent relation holds,

$$\begin{aligned} \tilde{w} &= \frac{\mathcal{D}\tilde{z}}{\mathcal{D}t} = \frac{\partial \tilde{z}}{\partial t} + \tilde{u} \frac{\partial \tilde{z}}{\partial x} + \tilde{v} \frac{\partial \tilde{z}}{\partial y} + \tilde{w}_\rho \frac{\partial \tilde{z}}{\partial \tilde{\rho}} \\ &\equiv \frac{d\tilde{z}}{dt} + \tilde{w}_\rho \frac{\partial \tilde{z}}{\partial \tilde{\rho}} \equiv \frac{d\tilde{z}}{dt} + \tilde{w}_e, \end{aligned} \quad (15)$$

where $\mathcal{D}/\mathcal{D}t \equiv \partial/\partial t + \tilde{u} \partial/\partial x + \tilde{v} \partial/\partial y + \tilde{w}_\rho \partial/\partial \tilde{\rho}$, expresses the material change as seen from the long-time mean isopycnal coordinate system. The contributions to the mean vertical velocity are $d\tilde{z}/dt \equiv (\partial/\partial t + \tilde{u} \partial/\partial x + \tilde{v} \partial/\partial y) \tilde{z}$, which is the result of the local vertical motion of the mean isopycnals plus the vertical component of motion along the mean isopycnal surfaces, and $\tilde{w}_e \equiv \tilde{w}_\rho \tilde{J} \equiv \tilde{w}_\rho \partial \tilde{z} / \partial \tilde{\rho}$, the mean entrainment velocity which is directly related with the mean Reynolds density flux divergence through the mean Jacobian.

6.2 Isopycnal equations with diapycnal mixing

Consider now the mass and momentum equations in isopycnal coordinates, in the presence of diapycnal velocities. For simplicity, hereafter we will refer to the diapycnal gradients of the diapycnal velocity simply as diapycnal divergence (or convergence), to the diapycnal gradients of the horizontal velocity as diapycnal velocity gradients, and to any along-isopycnal gradient as an epipycnal gradient, with equivalent notation for all other quantities.

To obtain the dynamical equations, in the presence of a ‘mean’ diapycnal velocity \tilde{w}_ρ , we write down the mass and momentum balances in a fluid element

of sides dx , dy and $Jd\tilde{\rho}$. Consistency with the previous discussion dictates the use of ‘mean’ isopycnal surfaces, $\tilde{\rho}$. Hereafter, except where indicated, the diapycnal velocities and isopycnal layers will always be the above discussed ‘mean’ values. Furthermore, when referring to ‘overall’ quantities, a much longer time-average (over many long-time scales) will be implied. The equations, dropping tildes, are (Dutton 1976)

$$\frac{\partial(Ju)}{\partial t} + \frac{\partial(Ju^2)}{\partial x} + \frac{\partial(Juv)}{\partial y} + \frac{1}{\rho} \frac{\partial(\rho Juw_\rho)}{\partial \rho} - fJv = -\frac{1}{\rho} \left[\frac{\partial(Jp)}{\partial x} + \frac{\partial}{\partial \rho} \left(p \frac{\partial z}{\partial x} \right) \right] + JA, \quad (16)$$

$$\frac{\partial(Jv)}{\partial t} + \frac{\partial(Juv)}{\partial x} + \frac{\partial(Jv^2)}{\partial y} + \frac{1}{\rho} \frac{\partial(\rho Jvw_\rho)}{\partial \rho} + fJu = -\frac{1}{\rho} \left[\frac{\partial(Jp)}{\partial y} + \frac{\partial}{\partial \rho} \left(p \frac{\partial z}{\partial y} \right) \right] + JB, \quad (17)$$

$$\frac{\partial p}{\partial \rho} + \rho Jg = 0, \quad (18)$$

$$\frac{\partial J}{\partial t} + \frac{\partial(Ju)}{\partial x} + \frac{\partial(Jv)}{\partial y} + \frac{1}{\rho} \frac{\partial(\rho Jw_\rho)}{\partial \rho} = C. \quad (19)$$

A and B are the resultant horizontal components of all dissipative forces, including Reynolds stresses and molecular friction, and C is the result of the horizontal Reynolds mass fluxes and molecular diffusion. In these equations all derivatives are taken along isopycnals, i.e. with the density ρ constant. Equations (16) and (17) are the horizontal momentum equations, equation (18) is the hydrostatic equation and equation (19) is the mass conservation equation.

Dividing through by J and using the mass-conservation equation, the horizontal momentum balances can be rewritten in their ‘acceleration’ form as

$$\frac{du}{dt} + w_\rho \frac{\partial u}{\partial \rho} - fv = -\frac{\partial \phi}{\partial x} + A, \quad (20)$$

$$\frac{dv}{dt} + w_\rho \frac{\partial v}{\partial \rho} + fu = -\frac{\partial \phi}{\partial y} + B, \quad (21)$$

where $\phi = p/\rho + gz$ is the Montgomery potential (Montgomery 1937). This differs from the non-diffusive result (Csanady 1989) in the presence of terms containing w_ρ .

The mass conservation equation (19) may be rewritten as the material tendency of $j = \rho J$,

$$\frac{\mathcal{D}j}{\mathcal{D}t} = -j \left(\frac{\partial u}{\partial x} + \frac{\partial v}{\partial y} \right) - j \frac{\partial w_\rho}{\partial \rho} + \rho C. \quad (22)$$

where $\mathcal{D}/\mathcal{D}t$ is the material derivative in isopycnic coordinates, as defined in equation (15). This relation shows that j , which is proportional to the separation between adjacent isopycnals, changes due to convergence (or divergence) of the flow in the epipycnal and diapycnal directions. If epipycnal convergence and horizontal Reynolds mass flux can be neglected (see Section 12), equation (12) reduces to

$$\frac{1}{j} \frac{\mathcal{D}j}{\mathcal{D}t} \simeq -\frac{\partial w_\rho}{\partial \rho}. \quad (23)$$

6.3 Vorticity balance

The vorticity equation in isopycnic coordinates, derived from the cross-product of the acceleration form of the momentum equations, may be written as

$$\frac{\partial \zeta}{\partial t} + \frac{\partial [u(\zeta + f)]}{\partial x} + \frac{\partial [v(\zeta + f)]}{\partial y} = S, \quad (24)$$

where $\zeta = \partial v/\partial x - \partial u/\partial y$ is the diapycnal component of the relative vorticity (the difference between this and the vertical component being that here the derivatives are taken along isopycnals). The source term, S , is given by

$$\begin{aligned} S &\equiv \frac{\partial}{\partial x} \left(B - w_\rho \frac{\partial v}{\partial \rho} \right) + \frac{\partial}{\partial y} \left(w_\rho \frac{\partial u}{\partial \rho} - A \right) \\ &= \left(\frac{\partial w_\rho}{\partial y} \frac{\partial u}{\partial \rho} - \frac{\partial w_\rho}{\partial x} \frac{\partial v}{\partial \rho} \right) + \left(\frac{\partial B}{\partial x} - \frac{\partial A}{\partial y} \right) - w_\rho \frac{\partial \zeta}{\partial \rho} \end{aligned}$$

$$\equiv T_i + T_o - w_\rho \frac{\partial \zeta}{\partial \rho}, \quad (25)$$

where $T_i = (\partial w_\rho / \partial y)(\partial u / \partial \rho) - (\partial w_\rho / \partial x)(\partial v / \partial \rho)$ and $T_o = \partial B / \partial x - \partial A / \partial y$.

Following Dutton (1976, p. 341), T_i may be interpreted as tilting of horizontal vorticity by writing

$$\begin{aligned} \frac{\partial w_\rho}{\partial y} \frac{\partial u}{\partial \rho} &= \frac{\partial w_\rho}{\partial y} \left(\eta + \frac{\partial w_\rho}{\partial x} \right), \\ \frac{\partial w_\rho}{\partial x} \frac{\partial v}{\partial \rho} &= \frac{\partial w_\rho}{\partial x} \left(\frac{\partial w_\rho}{\partial y} - \xi \right), \end{aligned} \quad (26)$$

where η and ξ are the horizontal components of relative vorticity in isopycnic coordinates, $\xi = \partial w_\rho / \partial y - \partial v / \partial \rho$ and $\eta = \partial u / \partial \rho - \partial w_\rho / \partial x$. Hence, T_i can be rewritten as

$$T_i = \left(\frac{\partial w_\rho}{\partial y} \frac{\partial u}{\partial \rho} - \frac{\partial w_\rho}{\partial x} \frac{\partial v}{\partial \rho} \right) = \left(\eta \frac{\partial w_\rho}{\partial y} + \xi \frac{\partial w_\rho}{\partial x} \right). \quad (27)$$

This shows that in the presence of epipycnal gradients of the diapycnal velocity, the horizontal relative vorticities, ξ and η , are converted into relative diapycnal vorticity, ζ .

With this partition, equations (24) and (25) reveal that changes in the vorticity on an isopycnal are caused by the tilting of horizontal relative vorticity, T_i , torque by eddy stresses, T_o , and advection of the diapycnal vorticity gradient, $w_\rho \partial \zeta / \partial \rho$. An alternative form of this equation may be obtained by adding this last contribution to the local change and epipycnal advection terms. Then we obtain a vorticity tendency equation in the (x, y, ρ) system (Staley, 1960)

$$\frac{\mathcal{D}(\zeta + f)}{\mathcal{D}t} = -(f + \zeta) \left(\frac{\partial u}{\partial x} + \frac{\partial v}{\partial y} \right) + T_i + T_o, \quad (28)$$

with $\mathcal{D}/\mathcal{D}t$ as defined in equation (15). This tells us that the material change of the absolute vorticity is due to horizontal convergence or divergence, tilting of horizontal vorticity and torque by eddy stresses.

Equation (24) may also be written as a flux potential vorticity equation

$$\frac{\partial(jq)}{\partial t} + \frac{\partial(ujq)}{\partial x} + \frac{\partial(vjq)}{\partial y} = T_i + T_o - w_\rho \frac{\partial \zeta}{\partial \rho}, \quad (29)$$

with the potential vorticity q defined as

$$q = \frac{\zeta + f}{j}. \quad (30)$$

The implications of this equation, for the behavior of q as a tracer, have been discussed by Haynes and McIntyre (1987, 1990). Since the terms on the right-hand side of equation (29) may be written as the epipycnal divergence of a source term (equation 25), they argued that the amount of q between adjacent isopycnals, or “potential vorticity substance” jq , can only change through epipycnal transport. However, as Haynes and McIntyre point out, q itself may change due to dilution or concentration of potential vorticity substance through diapycnal mass transfer.

For the analysis of data it is convenient to use the potential vorticity tendency equation. With the help of equation (19), the vorticity equation (24) may be transformed into

$$\frac{dq}{dt} = \frac{S}{j} + \frac{q}{j} \frac{\partial}{\partial \rho}(jw_\rho), \quad (31)$$

or, equivalently, as the material tendency of potential vorticity in the (x, y, ρ) system

$$\frac{\mathcal{D}q}{\mathcal{D}t} = \frac{T_i}{j} + \frac{T_o}{j} + q \frac{\partial w_\rho}{\partial \rho}. \quad (32)$$

In neither of these two expressions has the right-hand side the form of an epipycnal divergence, meaning that q may indeed change through processes other than epipycnal transport. In particular, the last equation tells us that the potential vorticity of a fluid parcel changes not only due to tilting of horizontal vorticity

and torque by eddy stresses, but also due to diapycnal transfer associated with diapycnal divergence (or convergence). If T_i/j and T_o/j are relatively small (see Chapter 9), equation (32) may be approximated by

$$\frac{1}{q} \frac{\mathcal{D}q}{\mathcal{D}t} \simeq \frac{\partial w_\rho}{\partial \rho}. \quad (33)$$

Equations (22) and (32) may be related, through the definition of potential vorticity, as follows

$$\frac{1}{q} \frac{\mathcal{D}q}{\mathcal{D}t} = -\frac{1}{j} \frac{\mathcal{D}j}{\mathcal{D}t} + \frac{1}{\zeta + f} \frac{\mathcal{D}(\zeta + f)}{\mathcal{D}t}. \quad (34)$$

This equation states that the relative change in potential vorticity is due to contributions from relative changes in both j and $\zeta + f$. If diapycnal mixing is locally dominant then we should be able to use the approximations (23) and (33) for the left-hand side and the first term of the right-hand side, respectively. Hence, for these approximations to be correct we require the contribution from the relative change in absolute vorticity in equation (34) to be small compared with the contribution from the relative change in j .

Chapter 7. Dynamical Analysis of Section 36N

*The true philosophers, the lovers of
the true, should not be irritated,
but knowing to have erroneously
thought, would thank who showed to
them the very true.*

Galileo Galilei (1564-1642)

Here we start to apply the isopycnic formulation, as developed in the last chapter, to section 36N. We look for confirmation in the dynamics, of what the kinematics suggested: large local diapycnal velocities. First, we show that the Richardson numbers in the Nutrient Stream may locally reach critical values, which points to shear-mixing as the source of vertical Reynolds density flux. Then we establish that anomalies in the Jacobian and potential vorticity fields overlap, as expected if diapycnal divergence controls the potential vorticity balance.

7.1 The Jacobian and the Richardson number

In Fig. 33 we present the distribution of j in isopycnic coordinates ¹ which, because of the small variations of ρ , closely resembles that of J , and is an index of separation between adjacent isopycnals. Several distinct domains are apparent, also recognizable in Fig. 19. The most extensive domain encompasses Sargasso Sea and Gulf Stream thermocline layers, where j is relatively large, about $10^6 m$ in the upper thermocline and still larger values below. Another extensive domain

¹ According to convention, hereafter J and j -values shown are absolute values.

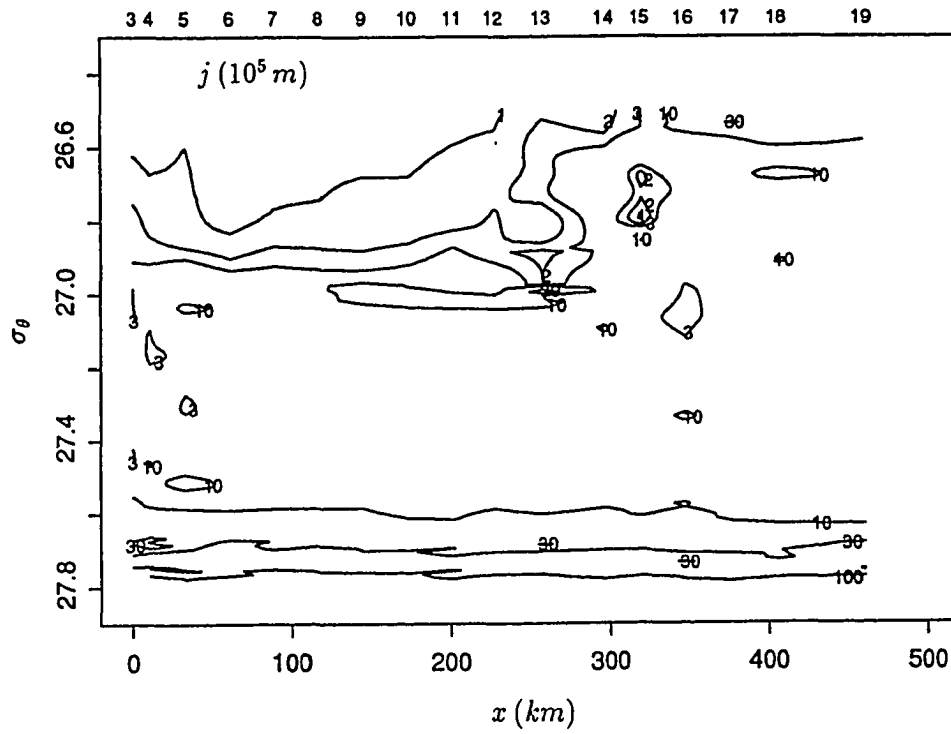


Figure 33. Separation index, $j = \rho J$, in section 36N.

represents the near-surface stratified layers within the Slope Sea and shelf waters, with j -values of order $10^5 m$. Just underneath this region a band of large j values is seen, about $1-3 \times 10^6 m$, representing the residue of the winter pycnostad. Finally, a small but distinct domain, of relatively low j values, below $3 \times 10^5 m$, appears at the location of the Nutrient Stream. This is the domain of interest for our present study. Since the corresponding domain is not easy to identify in Fig. 19, Fig. 34 shows an enlargement of the σ_θ distribution in cartesian coordinates for the area of interest. On it we have hatched the regions with j less than $3 \times 10^5 m$, for $\sigma_\theta > 26.5$. Our domain of interest is confined to those areas hatched between stations 13 and 17. In these regions the vertical distance between adjacent isopycnals is relatively small, although this does not stand out in a depth versus distance plot.

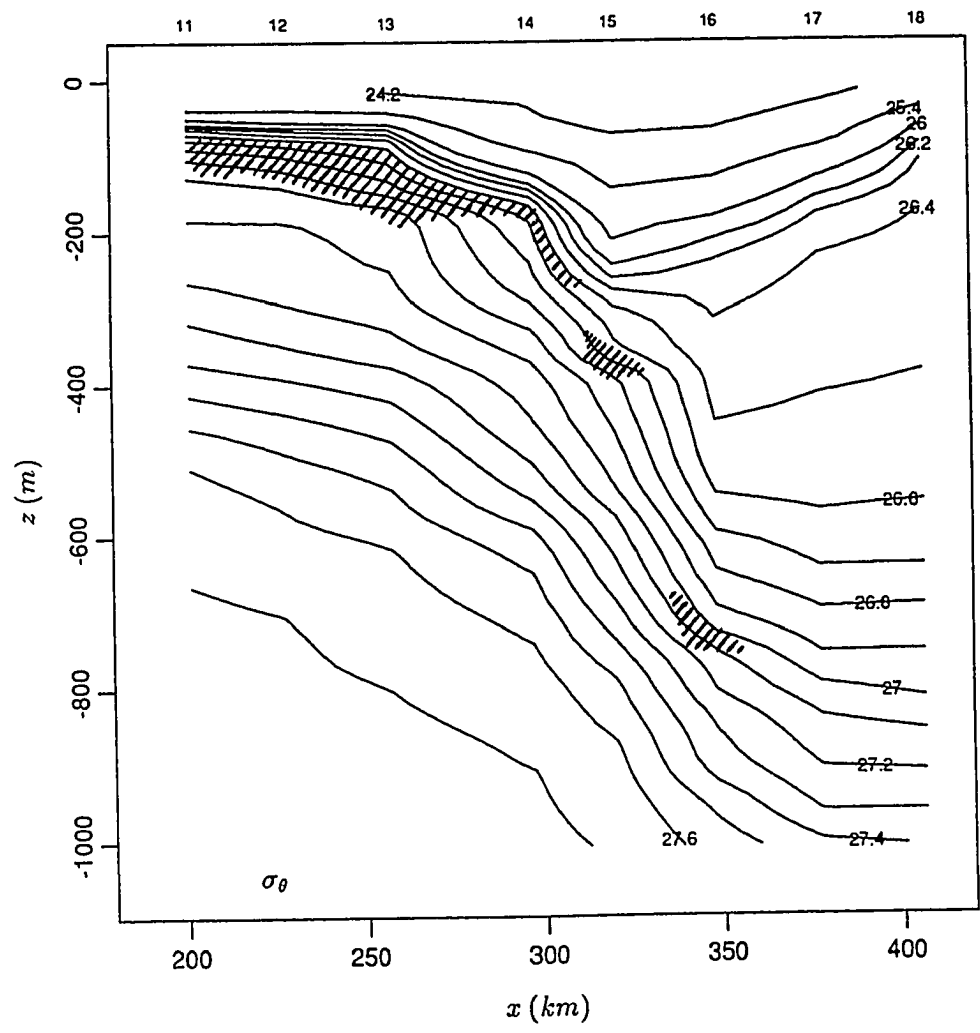
As a next step in our analysis, we calculated the distribution of the Montgomery potential (Fig. 35). The Montgomery potential, ϕ , is calculated from the anomaly of the dynamic pressure referenced to the lower σ_θ surface, $\sigma_\theta(z = z_r) \equiv \sigma_r$, as

$$\phi = \frac{p}{\rho} + gz = g(D_r - z\theta), \quad (35)$$

where p is the pressure and g is the gravitational acceleration. The anomaly of the dynamic height, D_r , is calculated as $D_r = \int_{z_r}^z \theta dz$. The density anomaly θ is defined as $\rho = \rho_r(1 - \theta)$, where $\rho_r = \rho(z_r)$ is the reference density. It is obtained as $\theta = (\sigma_r - \sigma_\theta)/(1000 + \sigma_r)$.

The original (Montgomery 1937), and most common usage, for the Montgomery potential requires that the reference isopycnal surface coincides with a level surface, which is taken as the level of no motion. In practice this may not be the case, for which reason we have used the above version for the Montgomery

Figure 34. Sigma-theta, σ_θ , for the top 1000 m of the Gulf Stream in section 36N. For $\sigma_\theta > 26.5$, the areas corresponding to $j < 3 \times 10^5 m$ have been hatched.



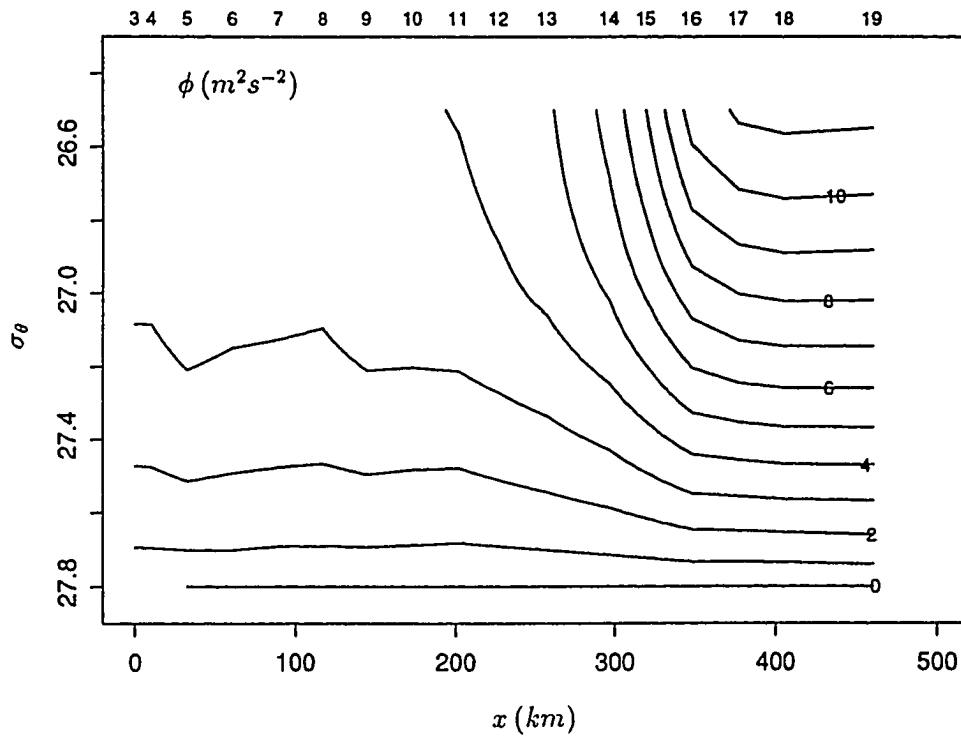


Figure 35. Montgomery potential, ϕ , referred to the $27.8\sigma_\theta$ -surface, in section 36N.

function (Buscaglia 1971). This version allows us to use the geostrophic approximation (from equation 20),

$$fv \simeq \frac{\partial \phi}{\partial x}, \quad (36)$$

to calculate the along-stream geostrophic velocity relative to a reference lower isopycnal. We chose this surface to be $\sigma_r = 27.8$, which we also assume as the level of no motion. The velocity field obtained in this manner is shown in Fig. 36. The Montgomery potential distribution in our section compares well with Bower et al.'s (1985) results for three sections located some 500 km further NE (notice, however, that there is a difference of a g factor in these definitions).

From the depth and geostrophic velocity distributions we estimate the (gradient) Richardson number, Ri , as follows:

$$Ri = \frac{g \frac{\partial \rho}{\partial z}}{\rho \left(\frac{\partial v}{\partial z} \right)^2} = \frac{gJ}{\rho \left(\frac{\partial v}{\partial \rho} \right)^2}. \quad (37)$$

A number of theoretical investigations have shown the existence of a critical Ri value, Ri_c , below which mixing is supposed to develop. The value of Ri_c depends on the flow under consideration but ranges from zero to 0.25, the latter value applying to unbounded parallel shear flow (for reviews see Miles 1986, Fernando 1991). The first equality in equation (37) defines Ri in cartesian coordinates, the second its equivalent in isopycnic coordinates. The second definition shows that Ri diminishes with J (isopycnals close together) and with increasing diapycnal gradients of the horizontal velocity. This is contrary to the intuitive idea that Ri should increase with static stability (decreasing J). The key factor is the velocity gradient: if the diapycnal gradient of the horizontal velocity remains constant then the Richardson number decreases with increasing static stability.

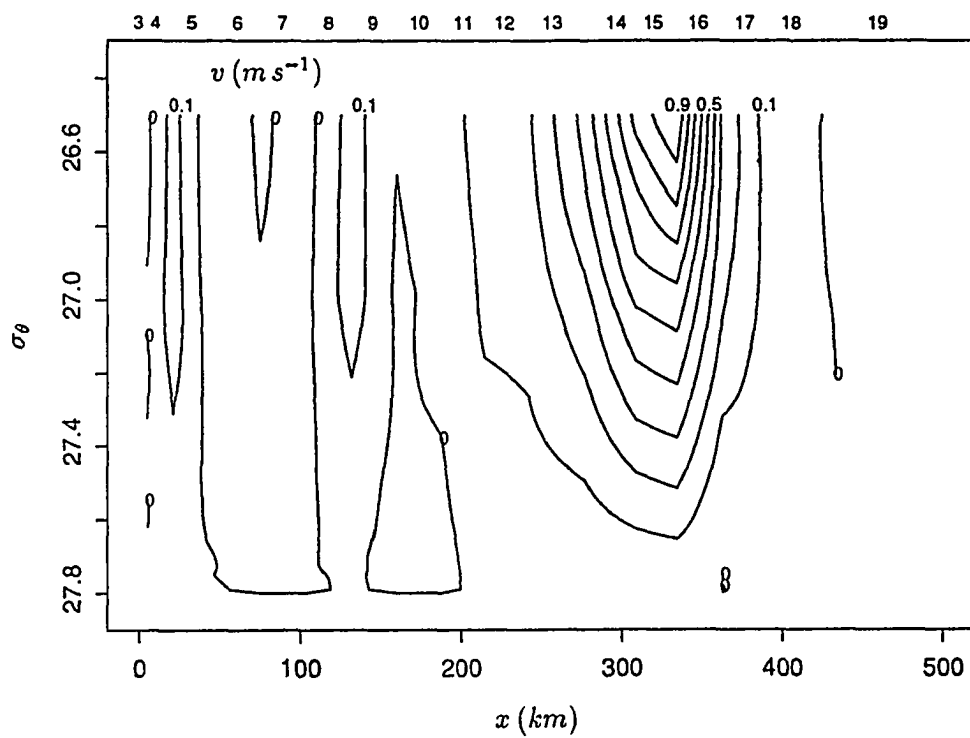


Figure 36. Along-stream geostrophic velocity, v , referred to the $27.8 \sigma_\theta$ -surface, in section 36N.

The Ri distribution ² in section 36N is shown in Fig. 37, with relatively large Ri values (> 40) everywhere except between stations 13 and 17, the position of the Gulf Stream. The regions with minima Ri values (< 5) are found in the upper thermocline of the Gulf Stream, the location of the Nutrient Stream. Recall that these values, apparently well above critical, are obtained with the 16 m -smoothed and subsequently interpolated values. This was done in order to remove the inversions in the density field, but it also has the effect of reducing the gradients in highly stratified regions, increasing J and presumably Ri . Additionally, the neglect of the ageostrophic velocity contribution is probably another reason why Ri , as calculated, may be an overestimated index of dynamical stability. The results nevertheless show that shear-instability is most likely to occur in the Nutrient Stream, if anywhere. Nakao (1977) also found a layer of minimum, but supercritical, Ri values (using data vertically separated by $20 - 100\text{ m}$), which appeared to be associated to the upper thermocline layers of the Kuroshio.

The appearance of mixed-regions and inversions in the potential density field, although disturbing to the isopycnic formulation, is a necessary part of the instability and mixing processes to which we have referred. It is unavoidable that any mixing reduces stratification (increases J), and creates well-mixed regions and local inversions in time and space if Kelvin-Helmholtz instabilities and billows are responsible for this process (Thorpe 1973, 1987). Smoothing and interpolation of the data considerably modifies the local z values, the large extent of this change being related to the similar vertical sizes of the well-mixed regions ($\sim 20\text{ m}$) and the smoothing interval (16 m). The substantial effect of smoothing on these regions may be appreciated in Fig. 18, where both unsmoothed and smoothed density

² As usual, throughout this work we always present absolute Ri values.

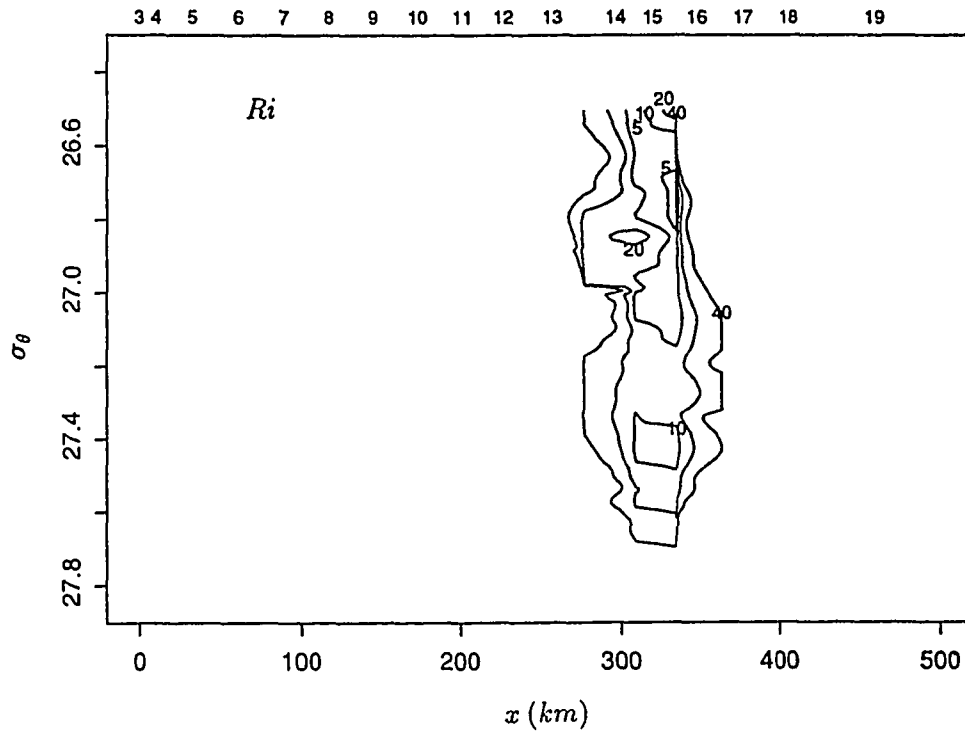


Figure 37. Richardson number, Ri , in section 36N.

profiles are shown for a portion of station 15.

That the observed minimum smoothed Ri values indicate the existence of locally much smaller, near critical Ri , is supported by the following argument. Equations (35) and (36) yield the thermal wind equation in isopycnic coordinates:

$$f \frac{\partial v}{\partial \rho} = \frac{g}{\rho} \frac{\partial z}{\partial x}. \quad (38)$$

Substitution in equation (37) then approximates Ri in isopycnic coordinates by

$$Ri = \left(\frac{f}{g} \right)^2 \frac{\rho^2 J}{\left(\frac{\partial z}{\partial x} \right)^2}. \quad (39)$$

Equation (39) shows that Ri depends directly on J and inversely on the square of the horizontal depth gradient. Vertically averaging smooths the density field, and subsequent interpolation to sigma-theta surfaces produces a smoothed depth field and reduces the minima in J . Fig. 38 shows the 2 m -averaged original (which we call ‘unsmoothed’) j distribution in vertical coordinates, for the region of the Gulf Stream. In this figure we present contour lines only for 10^0 and 10^3 units (10^5 and 10^8 m), which correspond to well-stratified and well-mixed regions, respectively. The large variability of this field reflects mainly the existence of numerous well-mixed thin layers (of about 10 – 20 m). The effect of smoothing in reducing this variability is clear if we compare this figure with Fig. 33, where we presented the j field obtained from the smoothed data (in isopycnic coordinates). This reduction in the range of the Jacobian is brought out even more clearly by Fig. 39, which presents $J = j/\rho$ as a function of density, for both the smoothed and unsmoothed cases (the data are from stations 14, 15, and 16, within the Gulf Stream). In this figure we may also observe how smoothing eliminates the negative Jacobian values and increases the absolute minima.

Figure 38. Separation index, $j = \rho J$, for the top 1000 m of the Gulf Stream, from the unsmoothed density field in section 36N. 0 stands for 10^0 units ($10^5 m$), and 3 for 10^3 units ($10^8 m$).

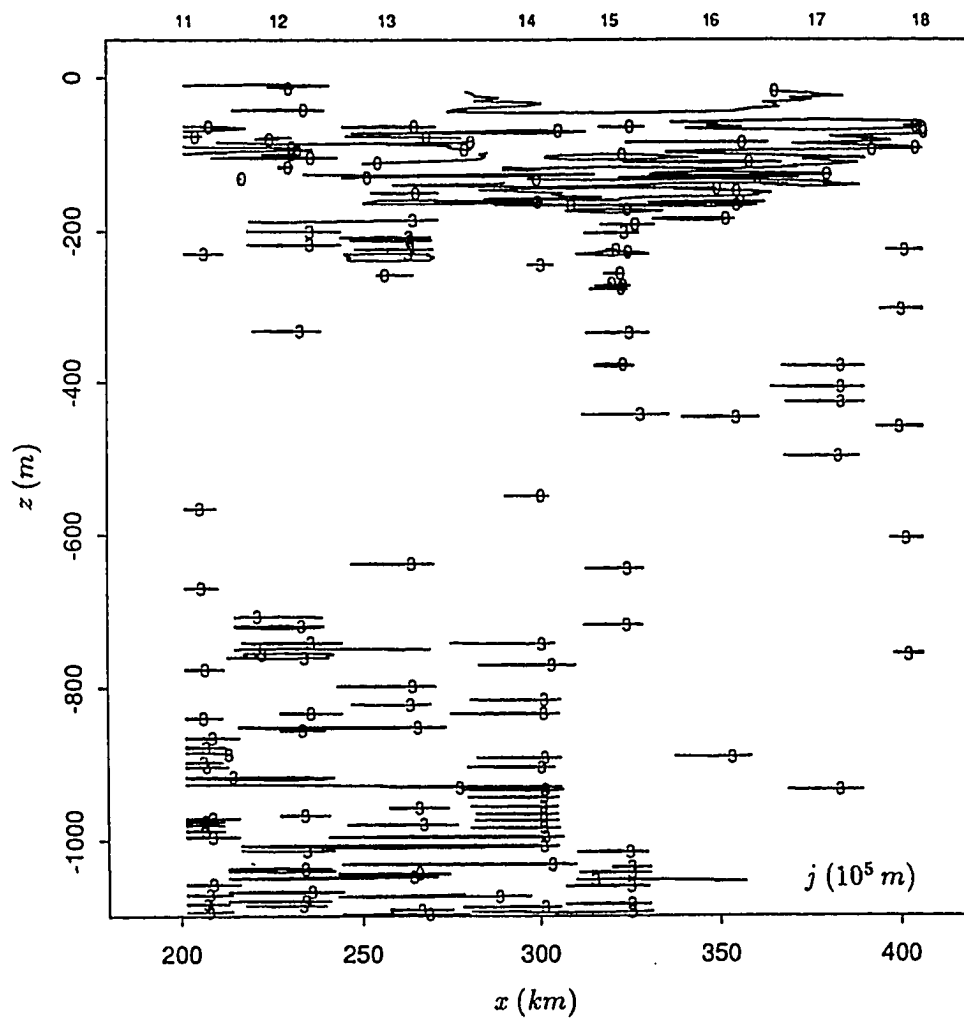
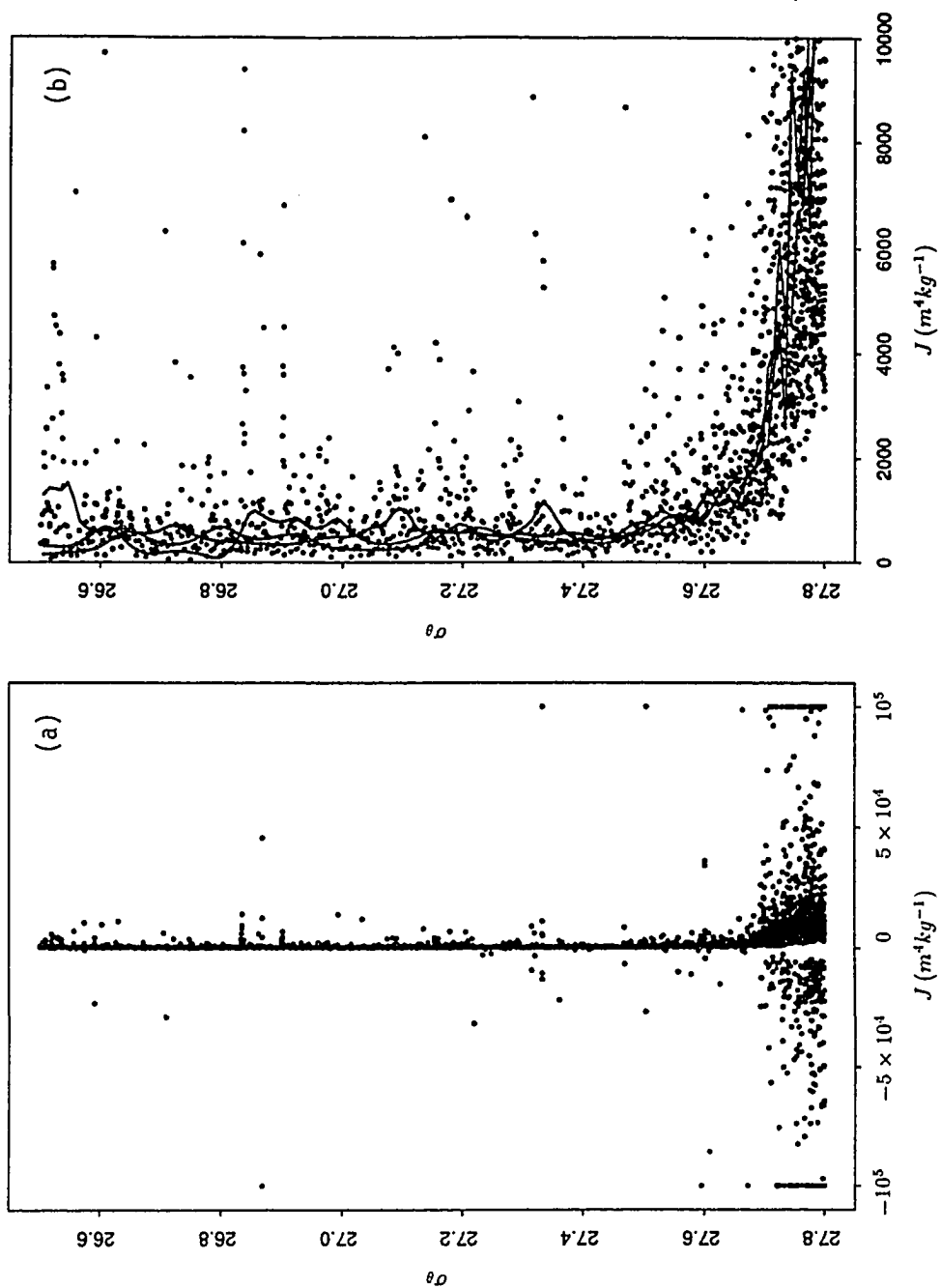


Figure 39. J as a function of σ_θ , for both the smoothed and unsmoothed density fields, in section 36N (the data for this figure is from stations 14, 15, and 16). (a) Complete range of values for the unsmoothed data, with absolute values greater than $10^5 \text{ m}^4 \text{ kg}^{-1}$ being replaced by this limit. (b) Detail of the region with Jacobian values between 0 and $10^4 \text{ m}^4 \text{ kg}^{-1}$; each of the three solid lines corresponds to the smoothed field for a different station, the dots correspond to the unsmoothed values.

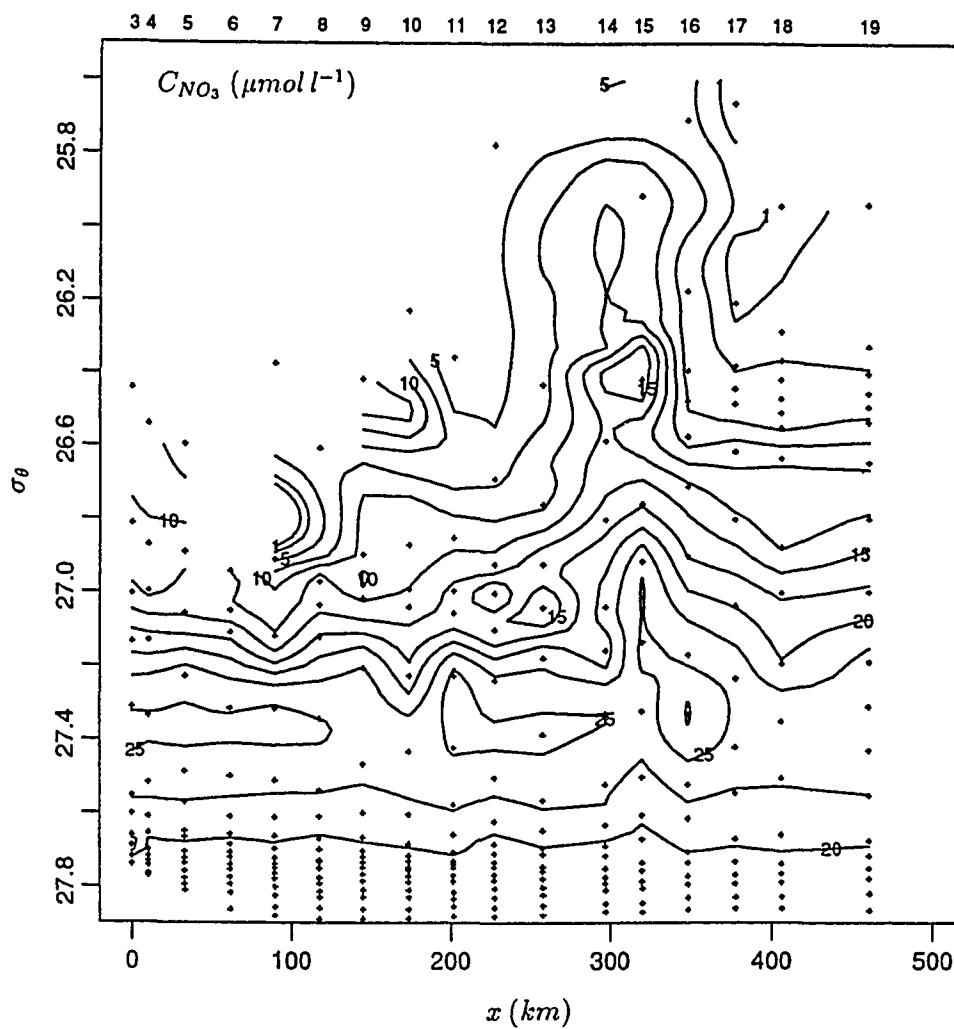


The effect of smoothing on the diapycnal velocity gradients is likely to be smaller in view of the thermal wind equation (38). This equation says that the diapycnal gradient of the geostrophic velocity is equivalent to the epipycnal cross-stream gradient of the depth field. Since there is no clear reason to anticipate that $\partial z/\partial x$ changes rapidly with ρ , we may expect that the effect of smoothing on this quantity is small. Additional support for this idea will arise from the results of a simple model for diapycnal mixing, presented in Chapter 9.

The idea of instability and mixing in the upper thermocline layers is also supported by the nutrient distribution along isopycnals, as already pointed out in Chapter 4. Fig. 40 shows the nitrate distribution for section 36N, this figure being essentially the same as Fig. 27 above, but with σ_θ replacing σ_t . The nitrate concentration is roughly constant along isopycnals in the lower layers, up to the $27.0\sigma_\theta$ -surface. Above that, the concentration isopleths depart from the horizontal at the location of the Gulf Stream, which we interpreted as a signature of mixing and upward entrainment. This idea is consistent with nutrient excess and deficiency in the surface and thermocline layers, respectively, and it was confirmed by balances of water mass and nutrient transports.

Similar nutrient anomalies have been reported earlier by Stefánsson and Atkinson (1971), for several sections across the Gulf Stream off the North Carolina coast. Fig. 7 reproduced from their work, shows large positive anomalies in the $25.0-26.6\sigma_t$ stratum and smaller, but significant, negative anomalies in the $27.0-27.5\sigma_t$ stratum. Stefánsson and Atkinson suggested that the positive anomalies are caused by waters of Caribbean origin, in accordance with Richards and Redfield (1955) earlier discussion for oxygen anomalies. However, this explanation cannot

Figure 40. Nitrate concentration, c_{NO_3} , in section 36N, as a function of σ_θ and cross-stream distance.



justify the negative nutrient anomalies. A complementary explanation, consistent with our previous calculations, is that the anomalies are caused by mixing.

7.2 Vorticity anomalies in the Nutrient Stream

Fig. 41 presents the distribution of the absolute vorticity, $\zeta + f$, in isopycnic coordinates. The vertical component of the relative vorticity has been approximated by $\zeta = \partial v / \partial x$, where v is the along-stream geostrophic velocity (Fig. 36). The planetary vorticity for this section is about $8.7 \times 10^{-5} \text{ s}^{-1}$. The figure reveals the cyclonic and anticyclonic sides of the Gulf Stream, with absolute vorticity larger (up to about $10 \times 10^{-5} \text{ s}^{-1}$) and smaller (down to nearly $6 \times 10^{-5} \text{ s}^{-1}$) than the planetary vorticity. However, the relative changes of absolute vorticity are clearly much smaller than those of the Jacobian, roughly one-third versus a factor of five.

Fig. 42 presents the distribution of the isopycnic potential vorticity q , as defined by equation (30).³ This is similar to the Jacobian distribution, and shows the same domains as described above. In particular, within the Nutrient Stream the potential vorticity attains relatively large values, above $3.5 \times 10^{-10} \text{ m}^{-1} \text{ s}^{-1}$, versus $10^{-10} \text{ m}^{-1} \text{ s}^{-1}$ for the surrounding waters. The range of variation is thus about a factor of three to five, slightly less than the range of the Jacobian.

The figures establish the existence of an anomalous region of relatively small j and large q , with extreme values in the core of the Nutrient Stream ($26.65 < \sigma_\theta < 26.8$). It is worthy to point out that this same q anomaly may also be seen in the results of Roemmich and Wunsch (1985), obtained using the same data set. They presented the potential vorticity on the $\sigma_\theta = 26.75$ isopycnal (their Fig. 15b,

³ Again, hereafter q -values shown have dropped the negative sign.

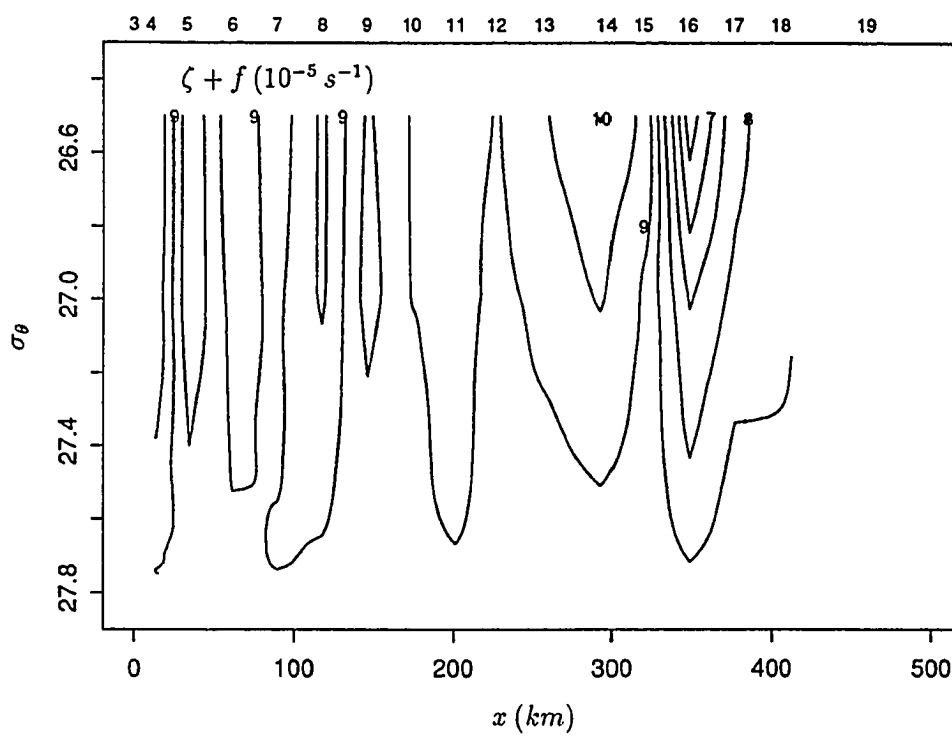


Figure 41. Absolute vorticity, $\zeta + f$, in section 36N. Planetary vorticity at this location is about $8.7 \times 10^{-5} s^{-1}$.

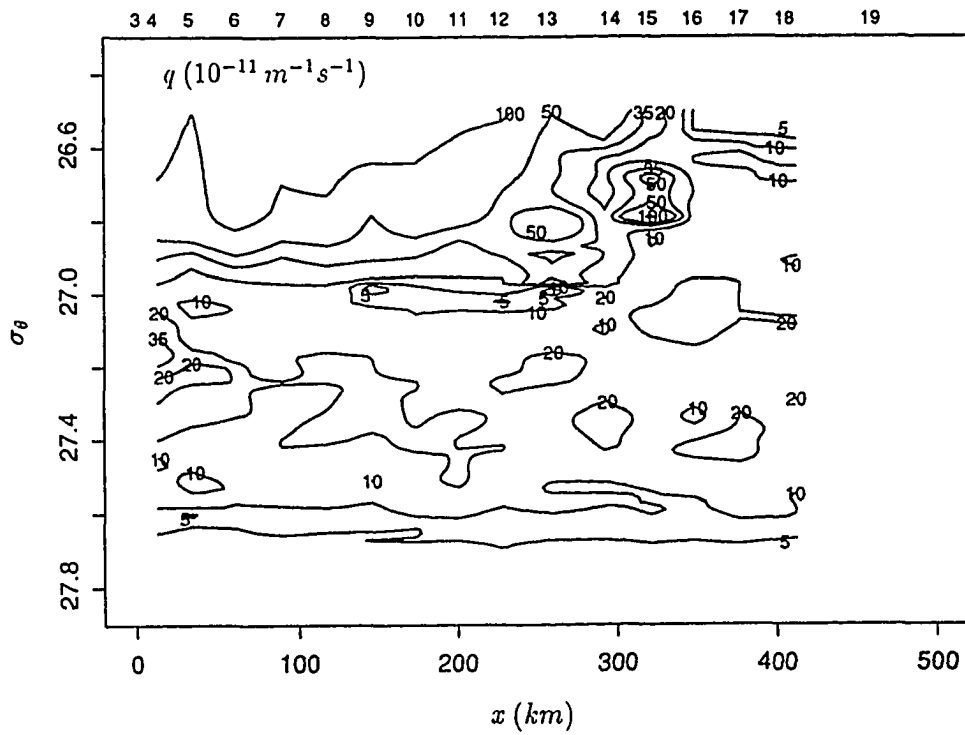


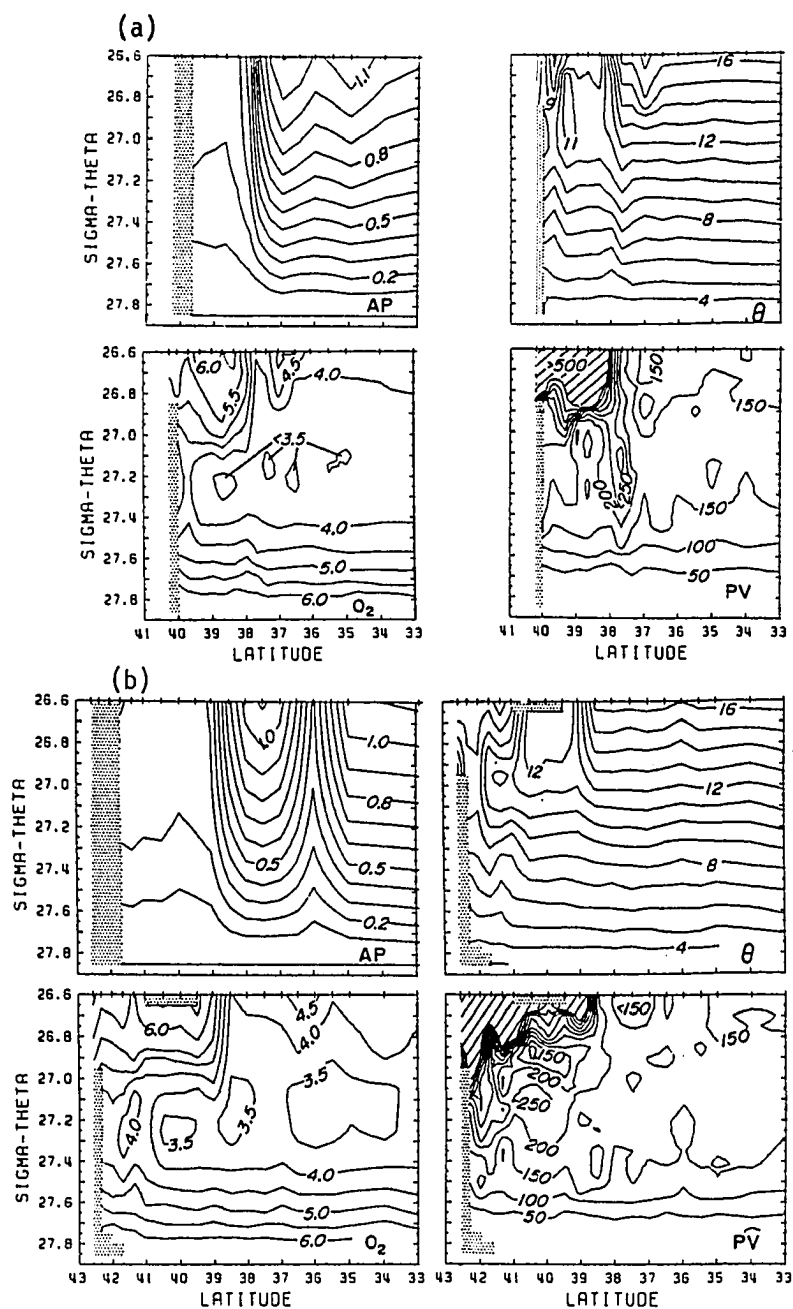
Figure 42. Potential vorticity, q , in section 36N.

not reproduced here), for the whole transatlantic section approximately along 36° N, of which ours is the western portion. Their results also show a striking intense peak of potential vorticity in the western end of the section. The magnitude of this peak ($\simeq 6 \times 10^{-10} \text{ m}^{-1} \text{ s}^{-1}$) is in good agreement with our estimates, and shows to be about five times larger than the background level in the interior of the subtropical gyre ($\simeq 1 - 1.5 \times 10^{-10} \text{ m}^{-1} \text{ s}^{-1}$). The narrow confines of the anomaly are such that it quickly becomes imperceptible in any spatially smoothed map (e.g. Roemmich and Wunsch 1985, Fig. 14b).

As discussed above (equations 22 to 33), diapycnal convergence or divergence may be directly related to the material changes of j and q whenever the other contributions are considerably smaller. The fact that the anomalies are present in both the j and q fields, but not in the absolute vorticity field, suggests that this is indeed the case (equation 34). However, at this point we cannot tell whether the diapycnal convergence is producing or removing the observed anomalies. We argue below that it is the inertial, nearly-inviscid, evolution of Gulf Stream meanders that causes instability (and low Ri numbers), which then leads to diapycnal convergence and mixing.

Also relevant to this discussion are the potential vorticity distributions calculated by Bower et al. (1985) and Leaman et al. (1989). Bower et al. (1985) showed these for several Gulf Stream sections. In all their sections, patches of anomalously large potential vorticity within the Nutrient Stream are apparent (Fig. 43). Leaman et al.'s (1989) sections do not show such anomalies, presumably because they are not individual surveys but were calculated by averaging an ensemble of a large number of surveys at the same location.

Figure 43. Montgomery potential AP (units of dynamic meters) referenced to $\sigma_\theta = 27.85$, potential temperature θ ($^{\circ}C$), dissolved oxygen O_2 ($ml\ l^{-1}$), and potential vorticity $PV = (f/\rho) \partial\rho/\partial z$ ($10^{-12} m^{-1}s^{-1}$), for four sections across the Gulf Stream. The longitudes of the sections are (a) $68^{\circ}30'W$, (b) $64^{\circ}30'W$, (c) $56^{\circ}30'W$, and (d) $54^{\circ}30'W$. Reproduced from Bower et al. (1985).



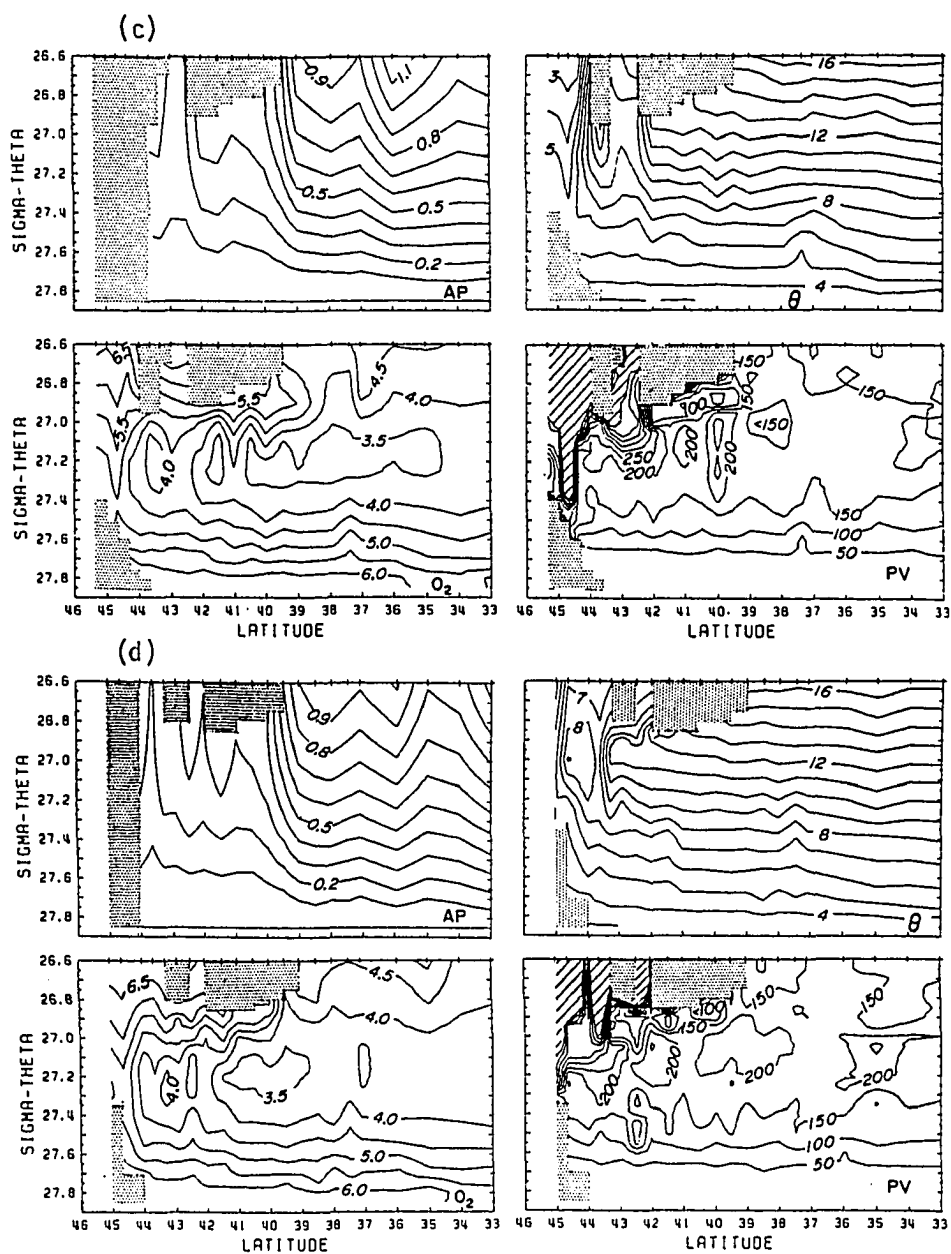


Figure 43 (continued)

Note that for equation (33) to be valid the absolute value of j cannot be too small. Some physical process is likely to set a limitation on the squeezing together of the isopycnals, the reduction of j . The appearance of small Ri numbers within the domain of small j (see Figs. 33 and 37) supports the idea that the limitation is due to hydrodynamic instability and mixing, once two isopycnal surfaces get too close. As discussed before, the distributions of j and Ri are expected to be roughly similar. The distribution of $(\partial v / \partial \rho)^2$ (Fig. 44) is anti-similar. Changes in the square of the diapycnal velocity gradient reinforce changes of j in modifying the Ri distribution.

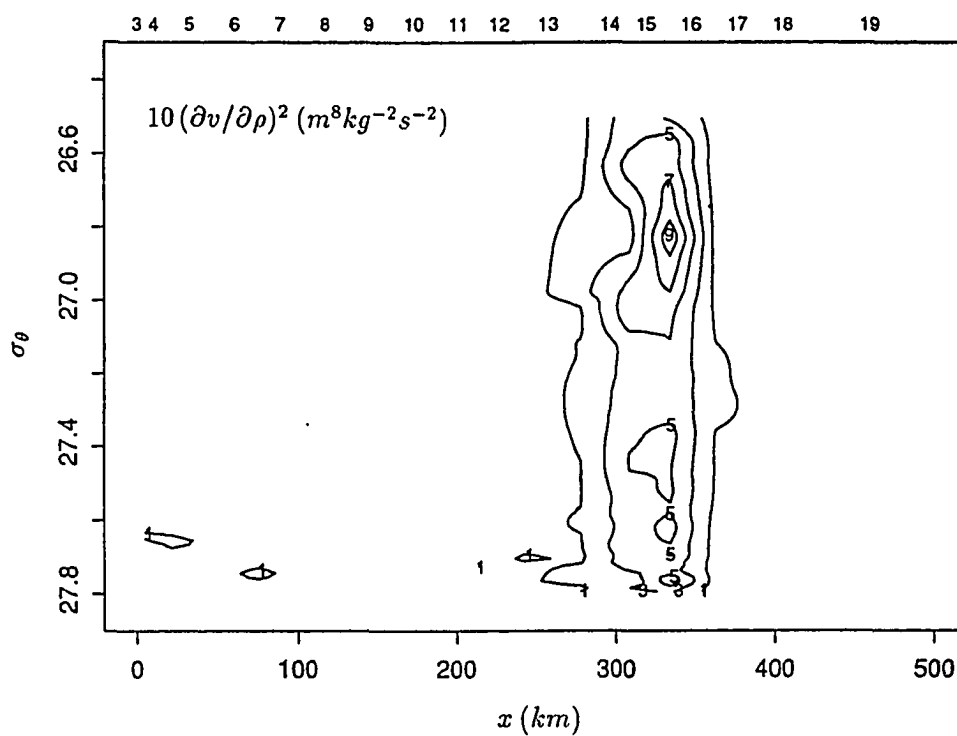


Figure 44. Square of the diapycnal velocity gradient, $(\partial v / \partial \rho)^2$, in section 36N.

Chapter 8. Diapycnal Fluxes of Mass and Potential Vorticity

*All our knowledge has its origin in
our perceptions.*

Leonardo da Vinci (1452-1519)

All art is but imitation of nature.

Seneca (B.C. 4?-A.D. 65)

Our purpose in the next two chapters is to further explore the causes and consequences of the diapycnal velocities. In this chapter we will concentrate on examining the causes. We start by obtaining an approximate expression for the diapycnal velocity, from a simple first-order closure model. Using published results, we express the eddy diffusivity in terms of the Richardson number.

We find that anomalous values in the Jacobian and the potential vorticity fields occur together with the maximum values of diapycnal convergence (or stretching of tightly packed isopycnals). This is consistent with previously noted evidence of small Richardson numbers, and suggests that we are observing the results of mixing triggered by hydrodynamical instability. The diapycnal velocities show alternating maxima and minima, suggesting that the overall result of instability-mixing is two-way exchange.

8.1 Estimating the diapycnal velocity

In connection with surface mixed-layer deepening, a plethora of models have been proposed in the literature for calculating the diapycnal (entrainment) velocity (see reviews by Zilitinkevich et al. 1979, Deardorff 1983, Gaspar 1988, Fernando 1991). In these models the diapycnal velocity is often calculated from the buoyancy flux term in the turbulence kinetic energy equation. The leading terms in that equation are turbulent energy production and dissipation. The buoyancy flux term is typically about 3% of the leading terms. A relatively small error in the prediction of the leading terms therefore translates into a large error for the buoyancy flux, and for the diapycnal velocities. Fernando (1991) summarized laboratory and field data on entrainment in stratified shear flows, and showed that the observations do not support the models.

Here we make estimates of the diapycnal velocity using a first-order closure model similar to Munk and Anderson's (1948). The Reynolds density flux vector, \mathbf{F} , may be taken to be perpendicular to the 'mean' isopycnal surfaces and is approximated by its vertical component, $F_z = \overline{w'\rho'}$ (recall that we have dropped tildes from all mean quantities). F_z is parameterized using a spatially varying vertical density eddy diffusivity, K :

$$F_z = -K \frac{\partial \rho}{\partial z} = -\frac{K}{J}, \quad (40)$$

Therefore, neglecting the contribution from the (mean) molecular density flux vector, \mathbf{M} , equation (13) becomes

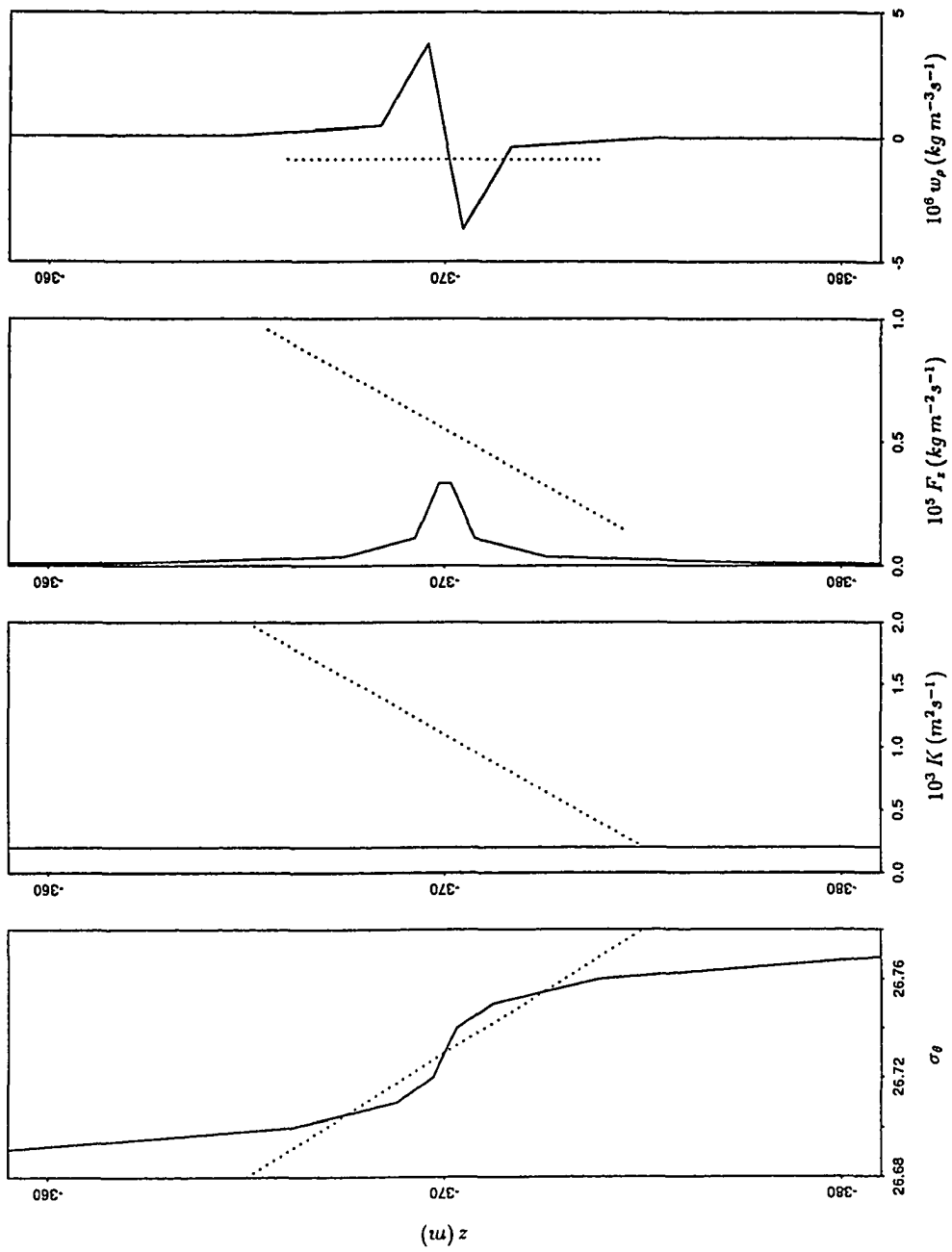
$$w_\rho \simeq -\frac{\partial F_z}{\partial z} = \frac{\partial}{\partial z} \left(\frac{K}{J} \right) = \frac{1}{J} \frac{\partial K}{\partial z} + K \frac{\partial^2 \rho}{\partial z^2} = \frac{1}{J^2} \frac{\partial K}{\partial \rho} - \frac{K}{J^3} \frac{\partial J}{\partial \rho}. \quad (41)$$

The entrainment velocity is related to the diapycnal velocity by $w_e = J w_\rho$ (equation 15).

Equation (41) shows that the diapycnal velocity may be thought of as arising from two terms: the vertical variation of the eddy diffusivity and uneven vertical distances between isopycnals equally spaced in σ_θ -space. The first term generates a diapycnal velocity in the direction of decreasing K (recall that J is negative), or equivalently, an entrainment velocity in the direction of increasing K (as discussed further in Csanady, 1990a). This agrees with the empirical findings that entrainment takes place in the direction of increasing turbulence (Turner 1973). The second contribution, which depends linearly on K , is due to continuity of vertical mass transfer, and differs from zero whenever the Jacobian changes with depth.

Fig. 45 is a representation of w_ρ for two idealized cases. In the first case (solid line) we consider an isolated highly stratified layer (similar to the feature centered at $\sigma_\theta \simeq 26.73$ in Fig. 18), and assume a constant density eddy diffusivity ($K = 2 \times 10^{-4} \text{ m}^2 \text{ s}^{-1}$), from which we calculate F_z and w_ρ using equations (40) and (41). In this case we observe the creation of two peaks in w_ρ , which cause convergent w_e . The result is water mass input into the tightly packed (stratified) isopycnal layers, which will tend to move them apart (reduce stratification). A succession of such events, with w_ρ irregularly reversing direction, will result in overall two-way exchange between adjacent isopycnal layers. Second (dotted line), we consider the case of constant linear stratification, with K changing linearly from $K(z = 375 \text{ m}) = 2 \times 10^{-4} \text{ m}^2 \text{ s}^{-1}$ to $K(z = 365 \text{ m}) = 2 \times 10^{-3} \text{ m}^2 \text{ s}^{-1}$, crudely simulating a source of turbulence in the surface layer just above. In this case the result is upward diapycnal one-way transfer. Note that the overall one-way transfer and two-way exchange coefficients, obtained in Chapter 5, are interpreted

Figure 45. Density, density eddy diffusivity, vertical Reynolds density flux, and diapycnal velocity, for two idealized situations leading to two-way exchange (solid line) and one-way transfer (dotted line).



as the result of the time-mean (over many long-time scales) entrainment velocity, $w_e = Jw_\rho$. Hence, in order to prevent confusion, in this work we have avoided calling one-way transfer as “entrainment”.

In general, K will depend both on external sources of turbulence and on the dynamical stability of the flow. To model small scale turbulence caused by hydrodynamic instability in stratified shear flow, the eddy diffusivity has to be expressed in terms of the Richardson number. In the meteorological literature there have been many suggestions of such a functional form for K . In oceanography, one early ansatz was Munk and Anderson’s (1948) relationship of the form $K = K_0(1 + \beta Ri)^{-3/2}$, with $\beta = 10/3$, and K_0 the density eddy diffusivity in neutral conditions. In the late 70’s, studies by James (1977, 1978), Boericke and Hogan (1977), Kao et al. (1977), Hamilton and Rattray (1978) and Foo (1981), all employed this kind of parameterization.

Gargett (1984) reviewed the various methods employed in the literature to estimate K and concluded that the most accurate and consistent representation portrays K as a decreasing function of the Vaisala frequency, N [$N^2 = (g/\rho)(d\rho/dz) = g/j$]. Sarmiento et al. (1976), using Radon profiles near the ocean floor, estimated K to be inversely proportional to N . Svensson (1980), using budget models with conservative tracers for a wide variety of estuarine and oceanic situations, estimated this dependence to be $K \propto N^{-1.2}$. A dependence of K on N alone may be valid for oceanic regions with negligible shear. For example, Armi (1979) examined the effects of epipycnal gradients in eddy diffusivity in a vertical advective-diffusive equation for density. He pointed out that the epipycnal gradients in K play the role of a horizontal advective velocity, and used the assumptions of dominant

boundary mixing and zero vertical velocity to obtain a dependence of the form $K \propto N^{-2}$. This result showed good agreement with observations at mid-depths. Note that such a relationship between K and N arises directly from equation (41) for zero diapycnal velocity (no vertical gradients in $\overline{w'\rho'}$). This is to be expected at mid-depths in the ocean, away from sources or sinks of turbulence, and for negligible shear. For this case equation (41) becomes

$$\frac{1}{K} \frac{\partial K}{\partial \rho} - \frac{1}{J} \frac{\partial J}{\partial \rho} = 0, \quad (42)$$

which results in Armi's dependence,

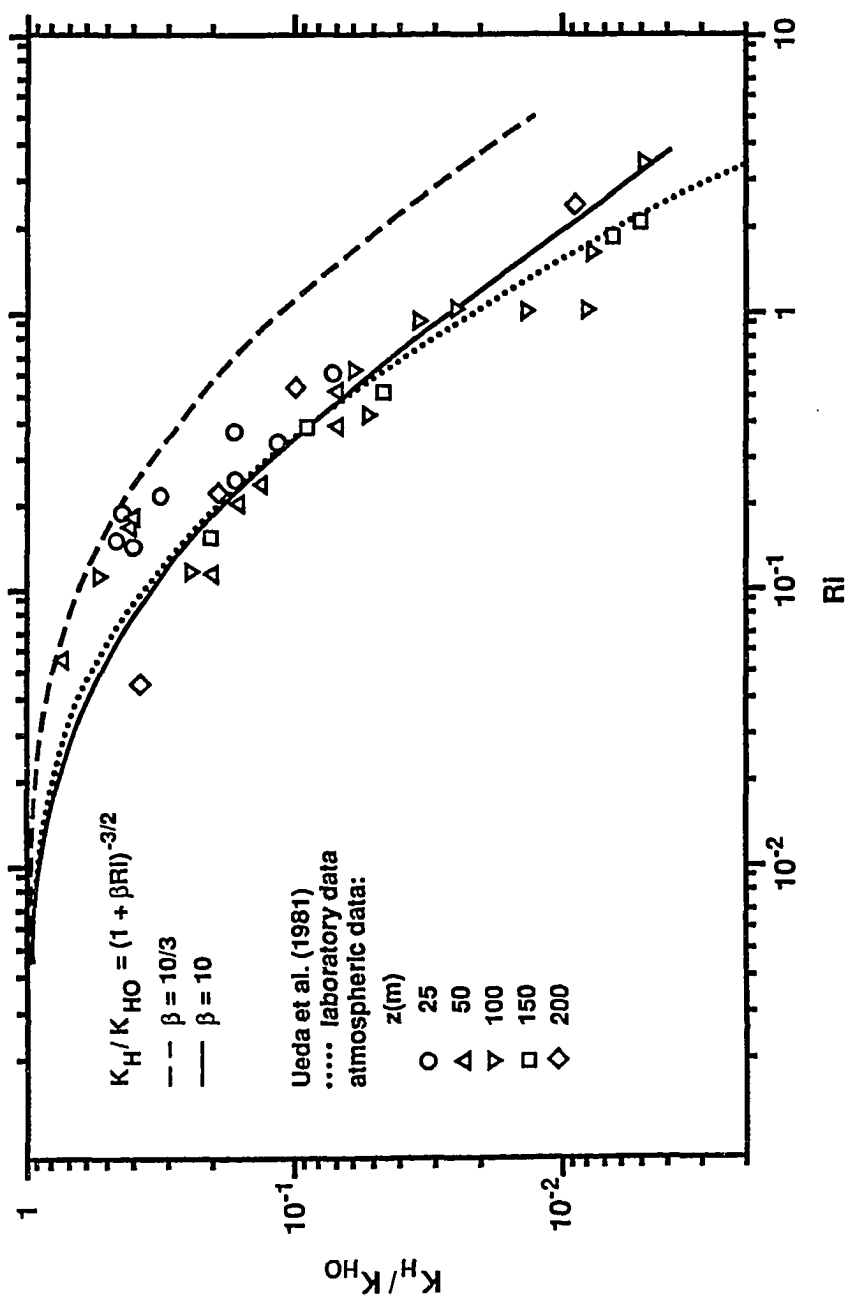
$$K = cJ = \frac{cg}{\rho N^2}, \quad (43)$$

where c is a constant of integration.

Peters et al. (1988), in a study of the equatorial undercurrent (where the shear is strong), found two different regimes of K -dependence on Ri . In the low Ri regime ($Ri < 0.3$), they found a nearly catastrophic decrease of K with Ri ($K \sim Ri^{-9}$). Such a relation is very appealing because it conforms to the theoretical critical Ri criterion. At higher Ri their $K(Ri)$ dependence closely resembles the Munk-Anderson formula. The work of Peters et al. (1988) is a remarkable pioneering investigation, but the authors warn that their indirect method of flux determination undermines the accuracy of the results.

For stratified flows with strong shear the comprehensive empirical study by Ueda et al. (1981) seems to offer the best basis for specifying the $K(Ri)$ relationship. Ueda et al. used observations in the atmospheric boundary layer above the surface layer, as well as data of Komori et al. (1983) for stratified open-channel flow. Fig. 46, modified from Ueda et al. (1981), shows the variation of the ratio

Figure 46. Variation of the ratio K_H/K_{H0} with Richardson number. Data reported by Ueda et al. (1981) for the atmospheric boundary layer are shown. The dotted line is Ueda et al.'s (1981) interpolation formula for laboratory data of Komori et al. (1983). The dashed and solid lines correspond to Munk and Anderson's (1948) expression with $\beta = 10/3$ and 10, respectively.



K_H/K_{H0} with Ri , where K_H is the heat diffusivity and K_{H0} is the heat diffusivity in neutral conditions. The data points are from direct measurements in the atmospheric boundary layer, the different symbols indicating the distance above the surface. The dotted line represents an interpolation formula derived by Ueda et al. (1981) from the laboratory data of Komori et al. (1983). The formula is a modification of Ellison's (1957) suggestion for the relation between vertical eddy diffusivity and eddy viscosity. Ueda et al. (1981) state that their results are consistent with Deardorff's (1967), taken far from the surface, where direct boundary effects are not important.

Ueda et al. (1981) suggest that for large Ri the ratio K_H/K_{H0} decreases approximately as Ri^{-2} . However, we have plotted over this figure Munk and Anderson's (1948) relation, both with $\beta = 10/3$ (dashed line), as they suggested, and with $\beta = 10$ (solid line). The $\beta = 10/3$ value indeed gives too small a decrease of the ratio K_H/K_{H0} with Ri , but the value $\beta = 10$ gives an approximation to the data which is as good as the one proposed by Ueda et al. (1981). Since considerable evidence indicates that for large Ri the eddy diffusivity should decrease as $Ri^{-3/2}$ (Turner 1986), we have chosen this Ri dependence. Hence, assuming that the heat and salt eddy diffusivity are the same and equal to the density eddy diffusivity K , we obtain the following parameterization in terms of Ri and the density eddy diffusivity in neutral conditions K_0 :

$$K = K_0(1 + 10Ri)^{-3/2}. \quad (44)$$

With this result, equation (41) for the diapycnal velocity becomes

$$w_\rho = \frac{K_0}{J^2(1 + 10Ri)^{3/2}} \left[\frac{10}{(1 + 10Ri)} \frac{dRi}{d\rho} + \frac{1}{J} \frac{dJ}{d\rho} \right]. \quad (45)$$

We now need an estimate for K_0 . In their pioneering study, Munk and Anderson (1948) employed unrealistically high K_0 values, as large as $0.1 \text{ m}^2 \text{ s}^{-1}$. A great deal of variation, however, still characterizes K values recently reported in the literature. Review papers by Moum and Osborn (1986), Eriksen (1987), Gibson (1987) and Gregg (1987) quote K values ranging from 10^{-6} to $10^{-4} \text{ m}^2 \text{ s}^{-1}$. Hopfinger (1987), in another review, has the upper bound as $10^{-3} \text{ m}^2 \text{ s}^{-1}$.

Gregg and Sanford (1980) estimated maximum K values consistently below $10^{-4} \text{ m}^2 \text{ s}^{-1}$ for the Sargasso Sea, and one order of magnitude smaller in the Gulf Stream. Hogg et al. (1982) obtained, for the deep ocean, $K \simeq 3 - 4 \times 10^{-4} \text{ m}^2 \text{ s}^{-1}$. Lietzke and Lerman (1975) and Smethie (1980), for small embayments, found $K \simeq 4 \times 10^{-4} \text{ m}^2 \text{ s}^{-1}$. Gargett (1984) summarized a number of studies that give values as large as $10^{-3} \text{ m}^2 \text{ s}^{-1}$. However, her best estimate was $K \simeq 2 - 3 \times 10^{-4} \text{ m}^2 \text{ s}^{-1}$, for the depth range of $4 - 5 \text{ km}$.

The eddy diffusivity at Ri-critical conditions has to be close to the maximum K values reported. Accordingly, we have chosen $K_0 = 2.6 \times 10^{-3} \text{ m}^2 \text{ s}^{-1}$. Using this value in equation (44) we obtain $K(Ri = 0.25) = 4 \times 10^{-4} \text{ m}^2 \text{ s}^{-1}$.

8.2 Diapycnal velocities and diapycnal convergence

Equation (45) provides the basis for estimating w_ρ from the J and Ri distributions previously calculated. From w_ρ we can also determine w_e and $\partial w_\rho / \partial \rho$. For generality, and since the exact value of K_0 is unknown, these quantities are expressed in terms of K_0 . We give the results as multiples of K_0 , as well as actual values with our best choice of K_0 ($2.6 \times 10^{-3} \text{ m}^2 \text{ s}^{-1}$). For simplicity we omit the units of the former but we give the units for the latter.

Fig. 47 shows a few contours of the distribution of w_ρ in section 36N. Solid

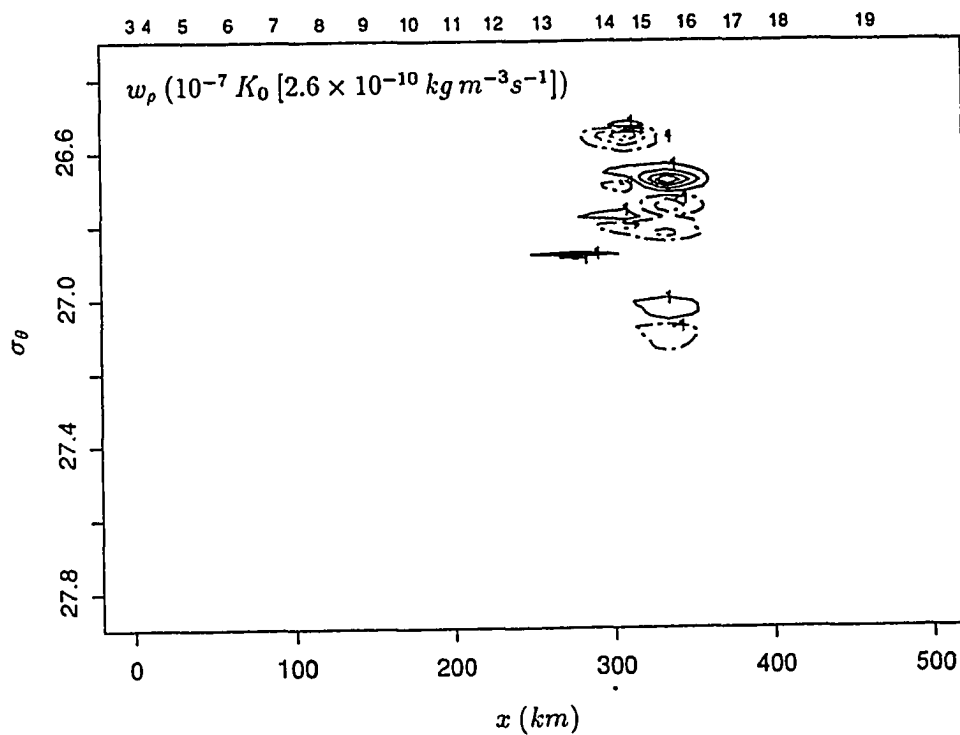


Figure 47. Diapycnal velocity, w_ρ , in section 36N. Solid and dashed lines refer to positive and negative values, respectively. Only the contours with $(\pm) 10^{-7} K_0 [2.6 \times 10^{-10} \text{ kg m}^{-3} \text{ s}^{-1} \simeq 2.6 \times 10^{-10} \sigma_\theta \text{ s}^{-1}]$ are labeled. Additional contours, changing by $(\pm) 2 \times 10^{-7} K_0 [5.2 \times 10^{-10} \text{ kg m}^{-3} \text{ s}^{-1} \simeq 5.2 \times 10^{-10} \sigma_\theta \text{ s}^{-1}]$, are shown.

and dashed lines refer to positive and negative values, respectively. In this figure we have labeled only the contours with $(\pm)10^{-7}K_0$ [$2.6 \times 10^{-10} kg m^{-3} s^{-1} \simeq 2.6 \times 10^{-10} \sigma_\theta s^{-1}$]. Additional contours changing by $(\pm)2 \times 10^{-7}K_0$ [$5.2 \times 10^{-10} kg m^{-3} s^{-1} \simeq 5.2 \times 10^{-10} \sigma_\theta s^{-1}$] are also shown, but they have not been labeled in order to avoid overlapping numbers. The main purpose of the figure is to show the total absence of significant values except in the upper-thermocline layers of the Gulf Stream. Similar results hold for w_e and $\partial w_\rho / \partial \rho$, shown in Figs. 48 and 49, respectively.

It is important at this point to establish the location of the Nutrient Stream in section 36N, in isopycnal coordinates. This is done with the help of Fig. 50, where we present the nitrate flux field. In this figure the small crosses indicate the location of the nutrient data. These data have been interpolated to σ_θ -surfaces separated by 0.01 intervals, for the offshore positions where the geostrophic velocity was calculated, using a smooth bivariate interpolant. The nitrate flux is then calculated using equation (1). Values greater than $10 mmol m^{-2} s^{-1}$ in this figure occur in the $26.6 < \sigma_\theta < 27.2$ range, with maximum values close to $15 mmol m^{-2} s^{-1}$ near the $\sigma_\theta = 26.8$ isopycnal. Another smaller maximum, located in the $26.2 < \sigma_\theta < 26.55$ range (see Fig. 23), only exhibits its deepest portion in this figure. Recall that the $\sigma_\theta = 26.8$ isopycnal surface defined the separation between the anomalous nutrient concentration values, with excess above and deficiency below it. It also corresponds to the location of the large patchy diapycnal velocities, as shown in the last figures. It is natural then to propose that this distribution of diapycnal velocities is responsible for the nutrient anomalies, in agreement with our discussion in Chapter 5. We show next that it is also responsible for the anomalies in

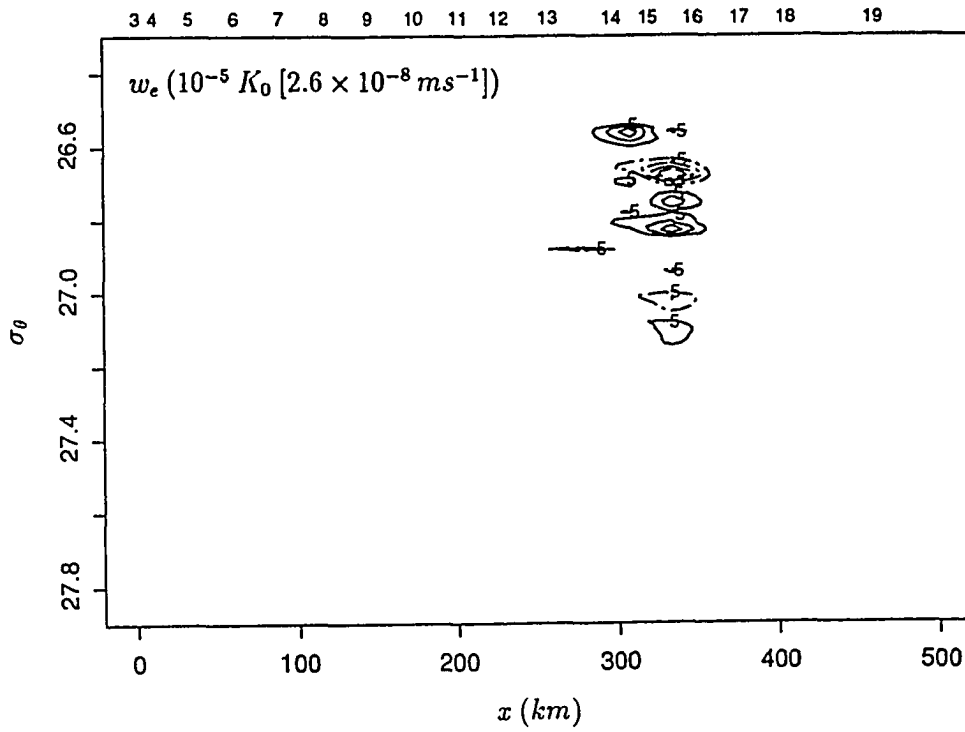


Figure 48. Entrainment velocity, w_e , in section 36N. Solid and dashed lines refer to positive and negative values, respectively. Only the contours with $(\pm) 5 \times 10^{-5} K_0$ [$1.3 \times 10^{-7} m s^{-1}$] are labeled. Additional contours, changing by $(\pm) 5 \times 10^{-5} K_0$ [$1.3 \times 10^{-7} m s^{-1}$], are shown.

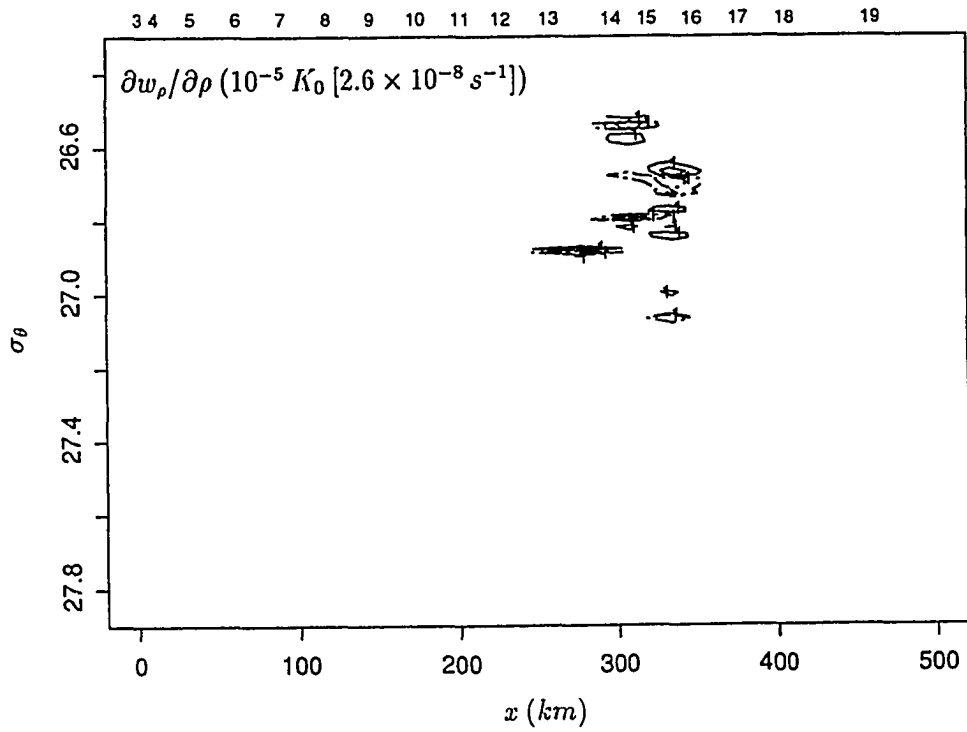


Figure 49. Diapycnal divergence, $\partial w_\rho / \partial \rho$, in section 36N. Solid and dashed lines refer to positive and negative values, respectively. Only the contours with $(\pm) 10^{-5} K_0 [2.6 \times 10^{-8} s^{-1}]$ are labeled. Additional contours, changing by $(\pm) 10^{-5} K_0 [2.6 \times 10^{-8} s^{-1}]$, are shown.

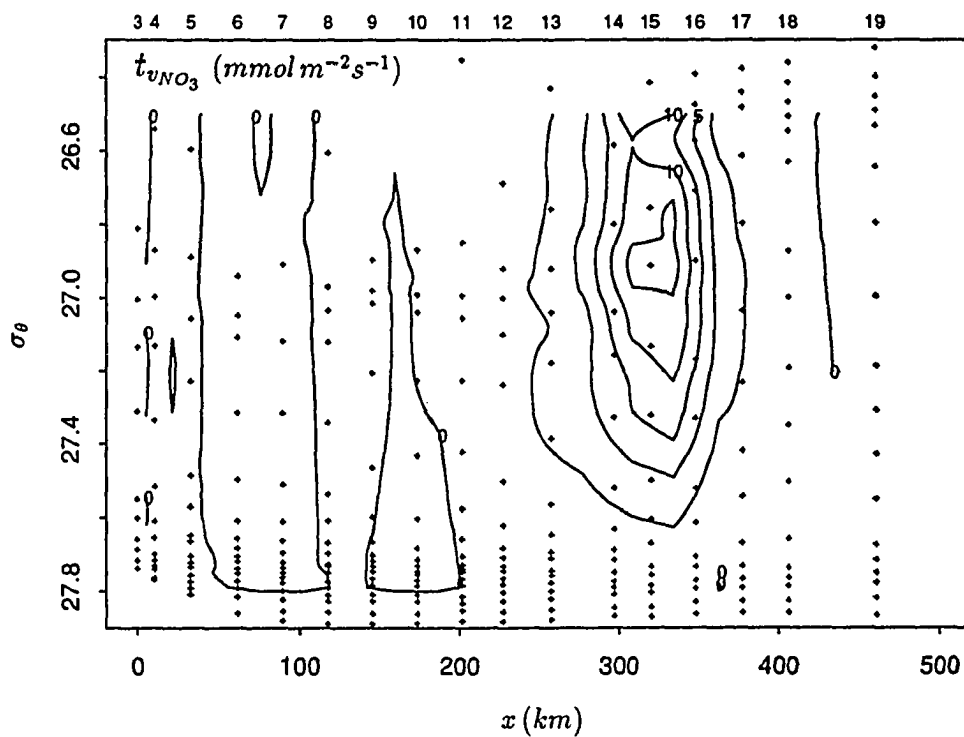


Figure 50. Nitrate flux in isopycnal coordinates (compare with Fig. 23), defining the location of the lower portion of the Nutrient Stream.

the Jacobian and the potential vorticity.

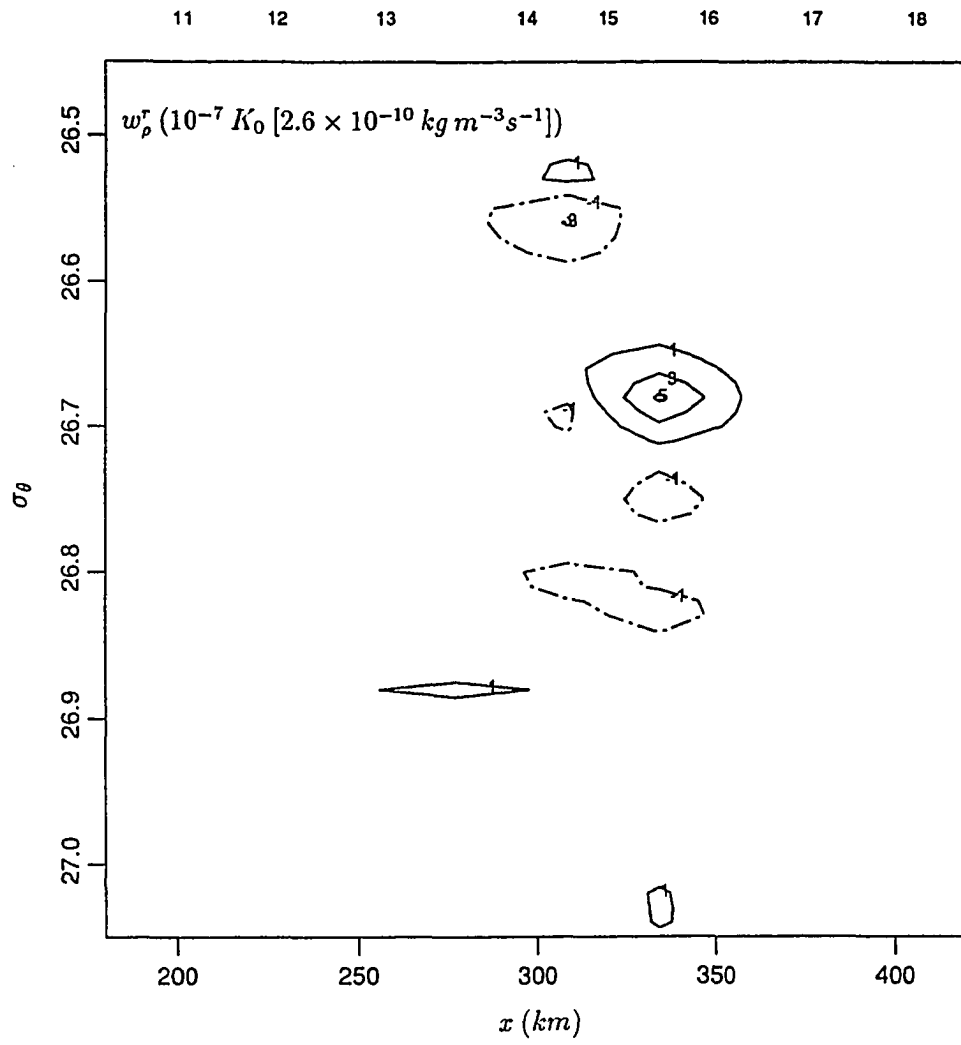
In Figs. 51 and 52 we enhance the results for the diapycnal velocity, in the region corresponding to the Nutrient Stream. Fig. 51 contours separately the two contributions to w_ρ in equation (45), while Fig. 52 shows their combined result. The first contribution to w_ρ (first term on the right-hand side of equations 41 or 45) depends on the diapycnal gradient of Ri ; we denote this contribution by the superscript r , w_ρ^r . The second contribution depends on the diapycnal gradient of J ; it is denoted with the superscript j , w_ρ^j . Contour intervals are in units of $10^{-7}K_0$ [about $2.6 \times 10^{-10} \sigma_\theta s^{-1}$]. Solid and dashed lines refer to positive and negative values, respectively.

A striking feature in these figures is their patchy character. A patch of positive values usually alternates with a patch of negative values, of similar size, both of about the same magnitude. The diapycnal extension of the patches varies, but does not exceed about $0.05 \sigma_\theta$. Within the Nutrient Stream the directions of w_ρ^r and w_ρ^j agree everywhere. The maximum contribution from the term depending on the Ri variation is roughly twice that from the term depending on the J variation.

Figs. 53 and 54 present the corresponding w_e and $\partial w_\rho / \partial \rho$ distributions for the same enhanced region. In these figures the contours are labeled in units of $10^{-4}K_0$ [$2.6 \times 10^{-7} m s^{-1}$] and $10^{-5}K_0$ [$2.6 \times 10^{-8} s^{-1}$], respectively. Solid and dashed lines refer to positive and negative values. Again, the patchy nature of the fields is evident. With our best estimate, $K_0 = 2.6 \times 10^{-3} m^2 s^{-1}$, we find absolute maximum values for w_ρ , w_e and $\partial w_\rho / \partial \rho$, of about $2.6 \times 10^{-9} \sigma_\theta s^{-1}$, $6.6 \times 10^{-7} m s^{-1}$, and $1.1 \times 10^{-7} s^{-1}$, respectively.

Recall that w_ρ (w_e) is the actual diapycnal (entrainment) velocity, not an

Figure 51. Contributions to the diapycnal velocity (equation 45), w_ρ^r and w_ρ^j , within the Nutrient Stream in section 36N. Solid and dashed lines refer to positive and negative values, respectively.



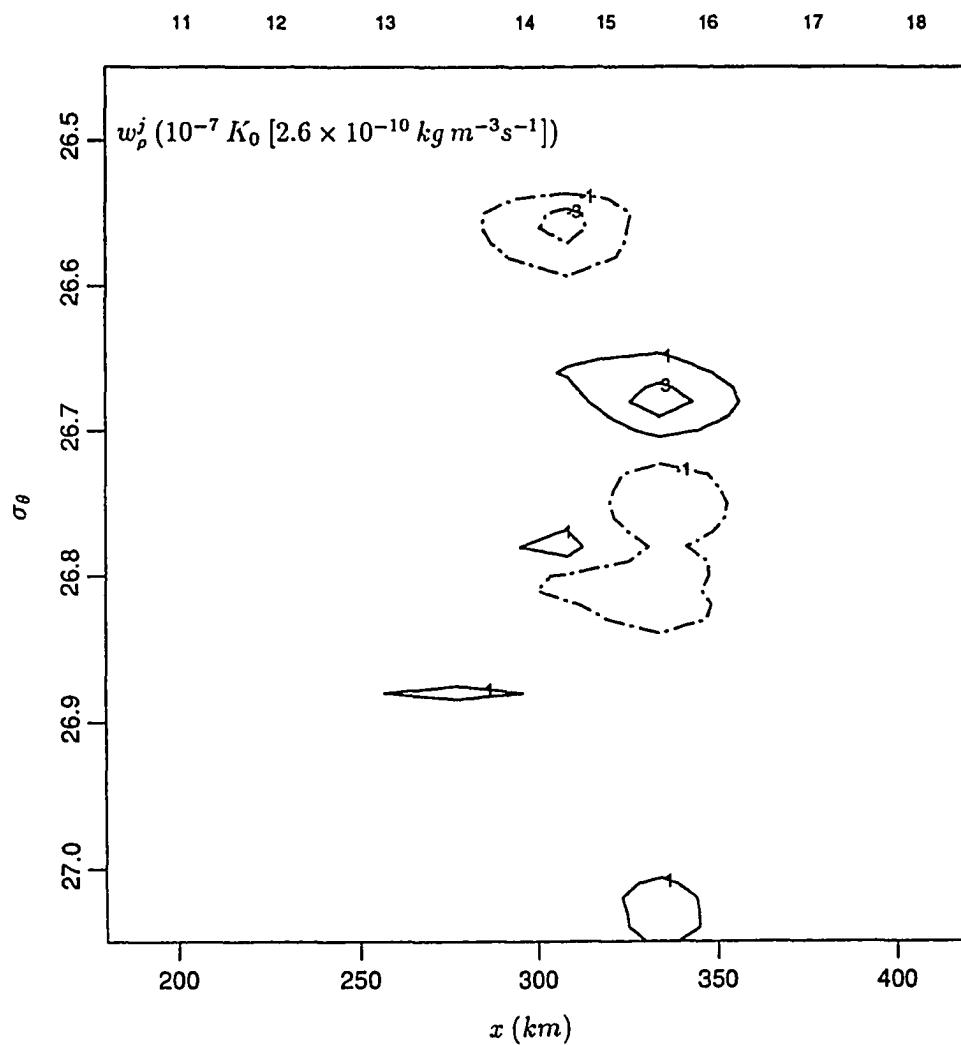


Figure 51 (continued)

Figure 52. Diapycnal velocity, w_ρ , within the Nutrient Stream in section 36N. Solid and dashed lines refer to positive and negative values, respectively.

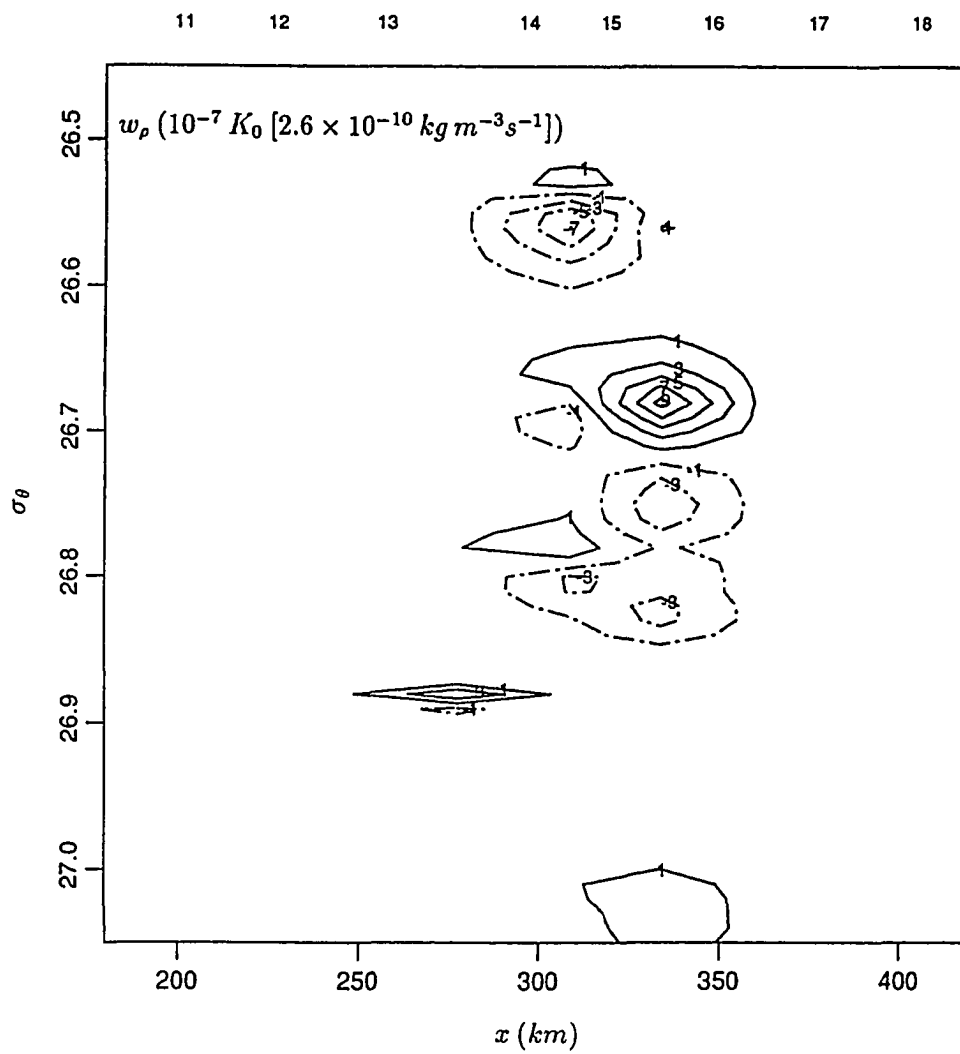


Figure 53. Entrainment velocity, w_e , within the Nutrient Stream in section 36N. Solid and dashed lines refer to positive and negative values, respectively.

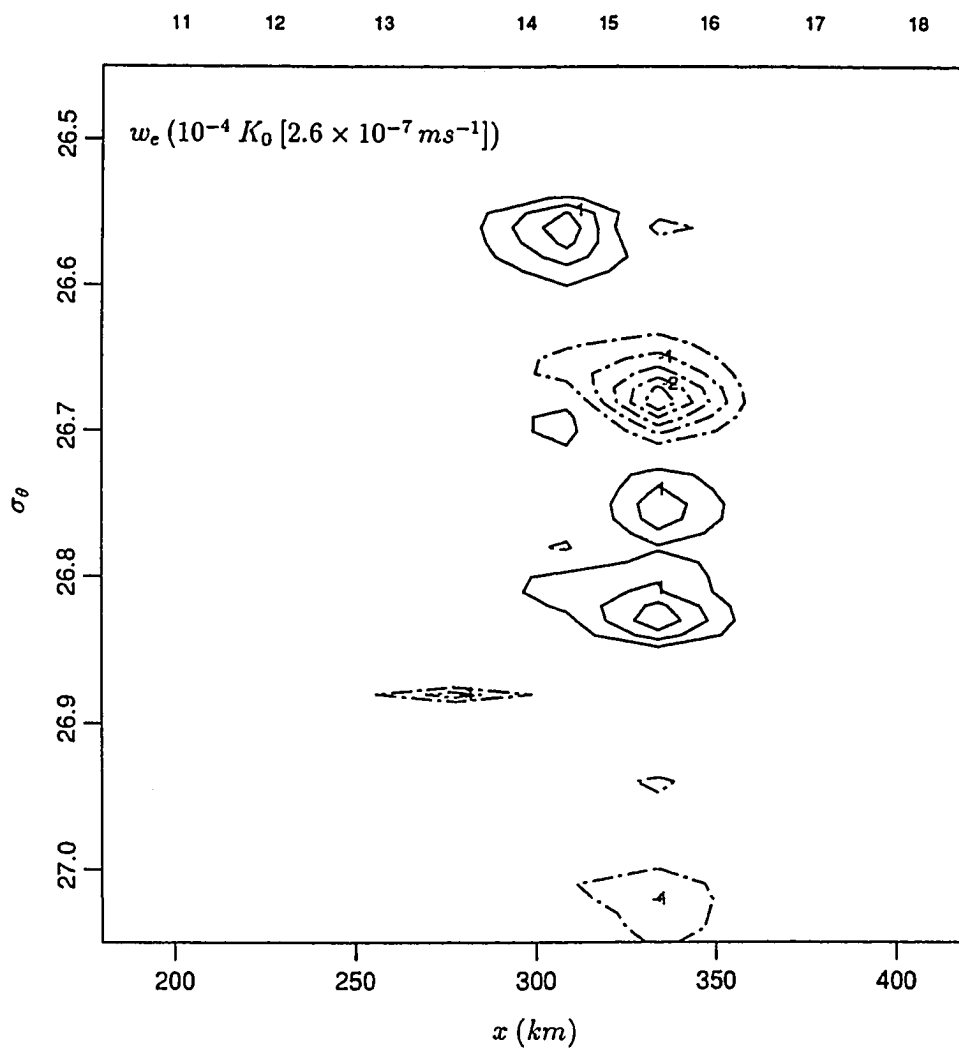
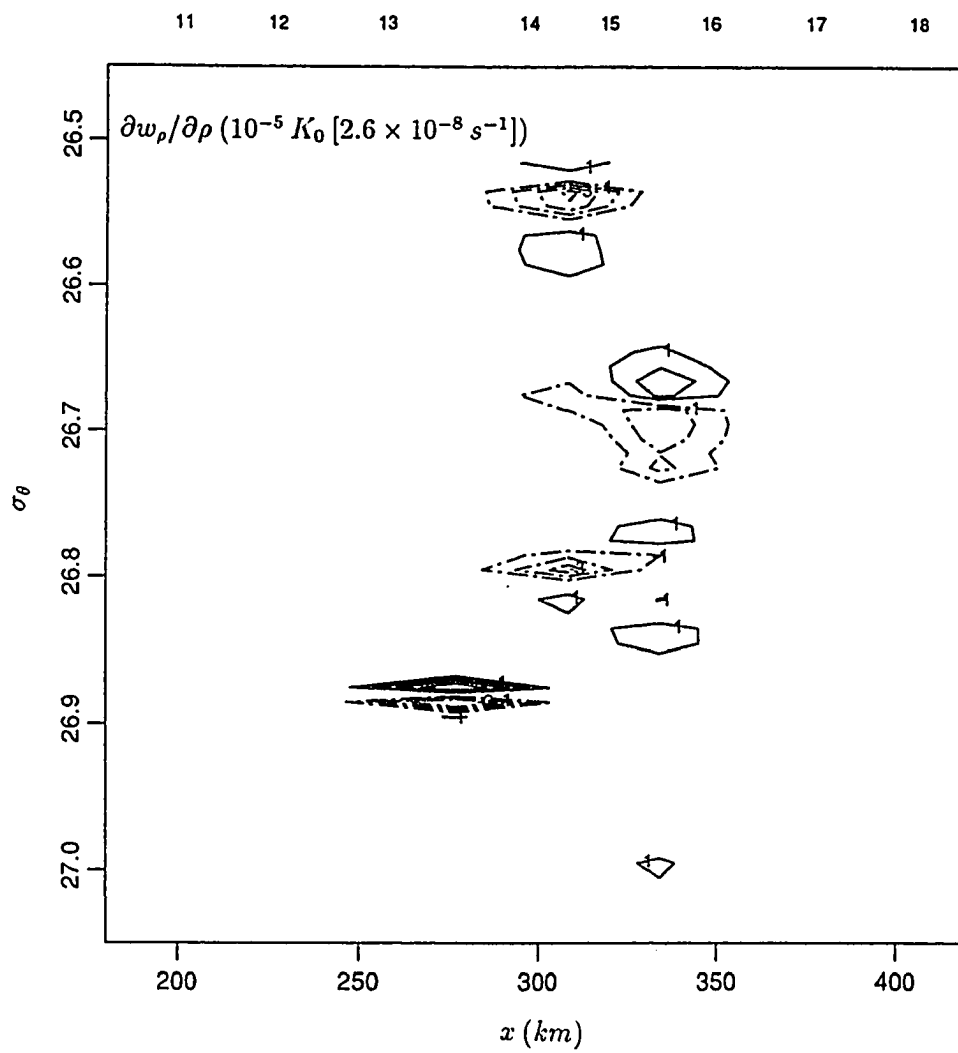


Figure 54. Diapycnal divergence, $\partial w_\rho / \partial \rho$, within the Nutrient Stream in section 36N. Solid and dashed lines refer to positive (divergence) and negative (convergence) values, respectively.



epipycnal contribution to the total vertical velocity. The above values are certainly much smaller than those we obtained in Chapter 5, by about two orders of magnitude, but this is likely the result of smoothing. We showed earlier that smoothing the depth field, z (in isopycnic coordinates), has a large effect on the Jacobian, and hence on the Richardson number. Equation (45) shows that smoothing also must have a large effect on the diapycnal velocity. This is clear if we realize that this expression not only includes a high power of J (and Ri), but it also includes $dJ/d\rho$ (and $dRi/d\rho$). Figs. 38 and 39 indeed showed that the unsmoothed J -values can change very rapidly in the diapycnal direction.

We may now compare the $\partial w_\rho / \partial \rho$ field with the distribution of j and q . In view of equation (23), if the calculated $\partial w_\rho / \partial \rho$ field is the result of the observed j distribution, then any strong signal in $\partial w_\rho / \partial \rho$ must be related to an anomaly in the j distribution. In Fig. 55 we present an enhancement of the j field for the Nutrient Stream region, with the same spatial scaling as the previous figures. A comparison of this figure with Fig. 54 shows that the location of the local negative maxima of $\partial w_\rho / \partial \rho$ (between stations 14 and 16, centered at about $\sigma_\theta = 26.7$ and 26.8 ; also near $\sigma_\theta = 26.55$ at station 14), correspond to minima in j . This supports the hypothesis that large diapycnal convergence is associated with mixing between tightly packed isopycnals. Similar agreement exists for the q field (see Fig. 42, its enhancement is not shown here).

Fig. 56 shows the distribution of the eddy diffusivity, K , as calculated using equation (44). Maximum values of K , of about $0.005K_0$ [$1.3 \times 10^{-5} m^2 s^{-1}$], are found in the Nutrient Stream. This value is one order of magnitude larger than those used by Orlanski and Cox (1973) in a model of western boundary currents.

Figure 55. Separation index, $j = \rho J$, within the Nutrient Stream in section 36N.

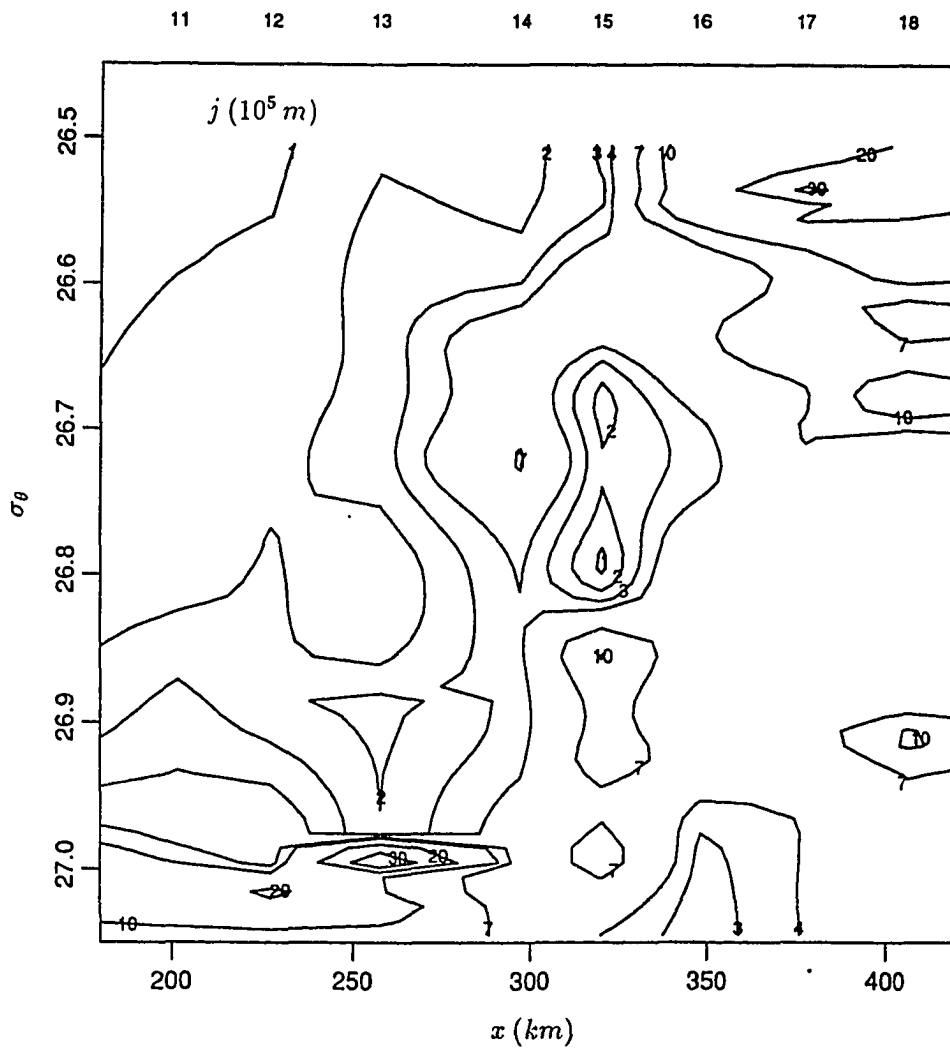
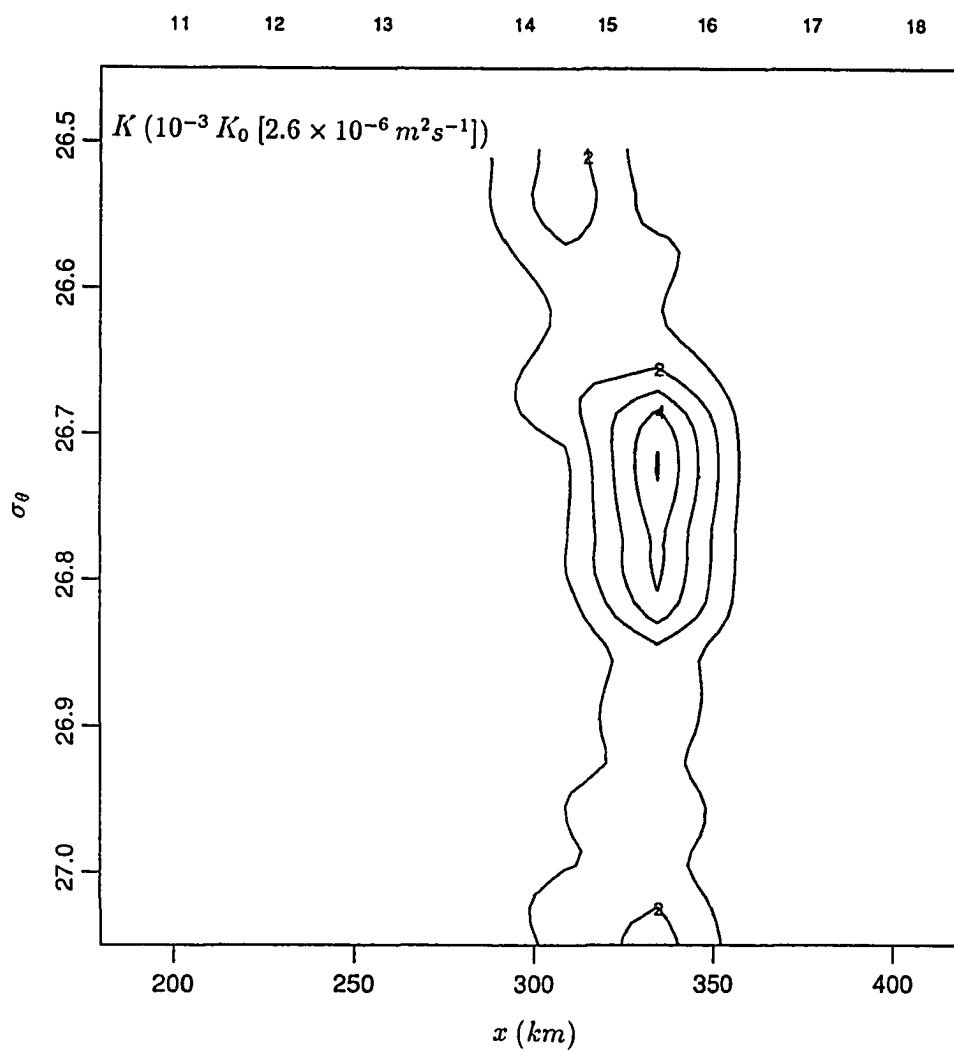


Figure 56. Density eddy diffusivity, K , within the Nutrient Stream
in section 36N.



However, it is almost certainly an underestimate, obtained from the smoothed field.

Chapter 9. Two-Way Exchange

Experience never errs; it is only your judgements that err by promising themselves effects such as are not caused by your experiments.

Leonardo da Vinci (1452-1519)

In this chapter we turn our attention to the consequences of the diapycnal transfer of mass in highly stratified, but dynamically unstable, regions. The fine structure of the density field exhibits numerous ‘staircases’. Our formula for the diapycnal velocity allows us to construct a simple model to simulate the creation of ‘treads’ on the staircase (or mixed regions) in previously subcritical regions. The diapycnal velocities arising from the model are large enough to support our previous estimate for the two-way exchange coefficient in the Nutrient Stream.

9.1 Frontogenesis and mixing

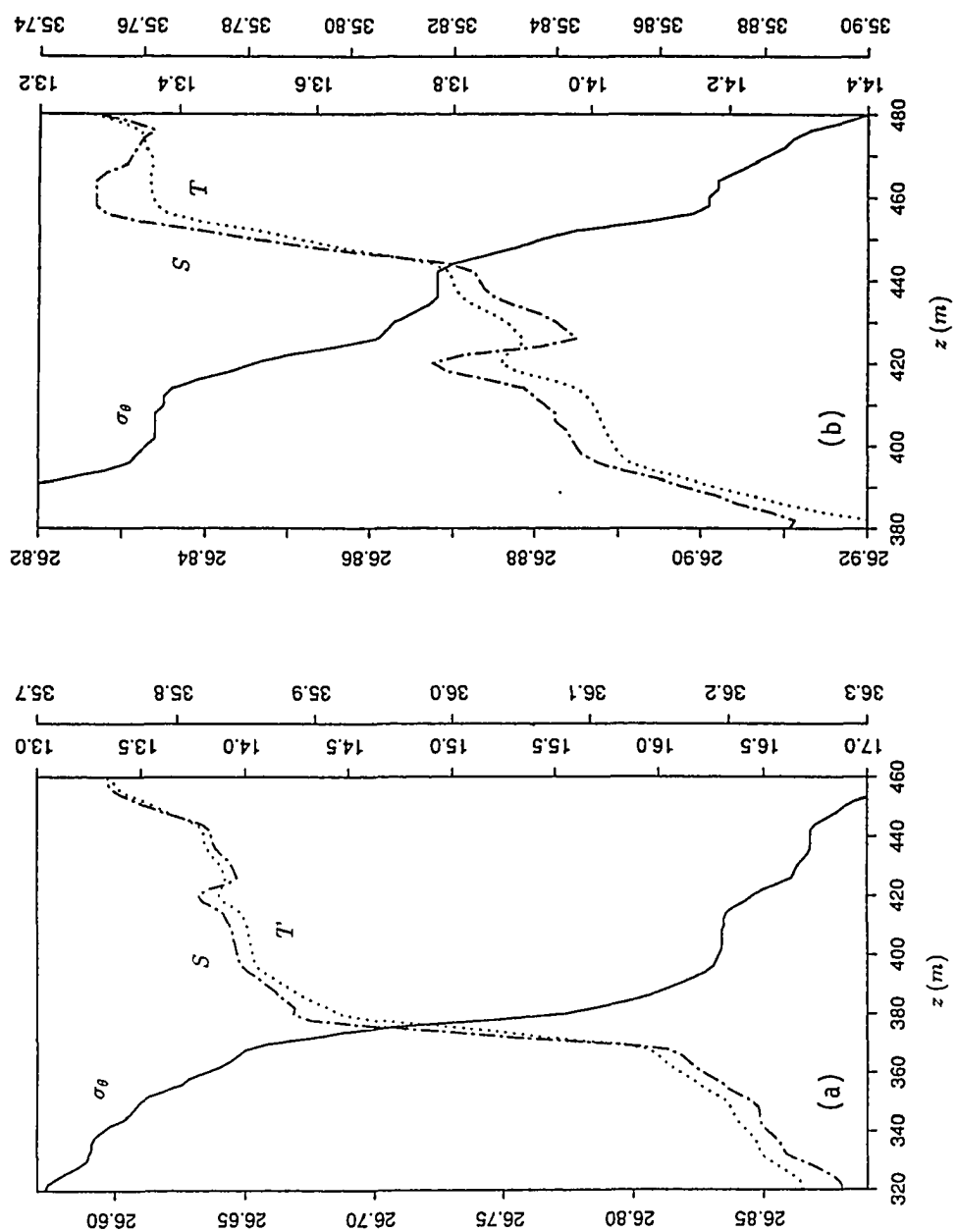
It is reasonable to suppose that large diapycnal velocities are the manifestation of intermittent mixing events, triggered by subcritical Ri values, associated with increased horizontal and decreased diapycnal depth gradients (increased horizontal and vertical density gradients, in vertical coordinates). The generation of such strong gradients, or frontogenesis, has long been known to occur in atmospheric jet stream waves (Newton 1954, Staley 1960, Palmén and Newton 1969, Newton 1978). In the jet stream the density gradients are reduced between a crest

and the subsequent trough, while they increase after the trough. Similarly, we may anticipate that the separation between adjacent isopycnal layers is likely to be reduced during some phase of the Gulf Stream meanders. During the shrinking of the isopycnal layers, or frontogenetical stage, the Jacobian decreases (and the potential vorticity increases, corresponding to the “dynamic frontogenesis” discussed by Bleck et al., 1988). During this stage the diapycnal velocity gradient should also increase (through the thermal-wind relation) and create subcritical Ri regions. This is consistent with the observations of Bane et al. (1981), in the Gulf Stream off the South-Atlantic Bight, that the intensification of the horizontal velocity in meanders is accompanied by an increase of the vertical velocity gradient.

An expanded view of the density profile within the Nutrient Stream helps in the visualization of regions prone to mixing. Fig. 18 shows the original (unsmoothed) $2m$ -averaged temperature, salinity and density data, for station 15 which cuts across the Nutrient Stream. Inversions in temperature and salinity are evident. However, the inversions are density-compensating, and the density distribution is staircase-like. In Fig. 18, well-mixed layers (treads in the staircase) are found near the $\sigma_\theta \simeq 26.60$ and 27.15 layers, best defined in the $26.8 < \sigma_\theta < 27.0$ range. This figure also shows the smoothed and interpolated density-depth profile. The highly stratified region is still apparent in this smoothed representation, but the small-scale treads disappear (see also Figs. 33 and 38 for the separation index j). This is because the interpolation to σ_θ -surfaces cannot show well-mixed regions.

In Fig. 57 we show the enhancement of two contrasting regions. Fig. 57a pre-

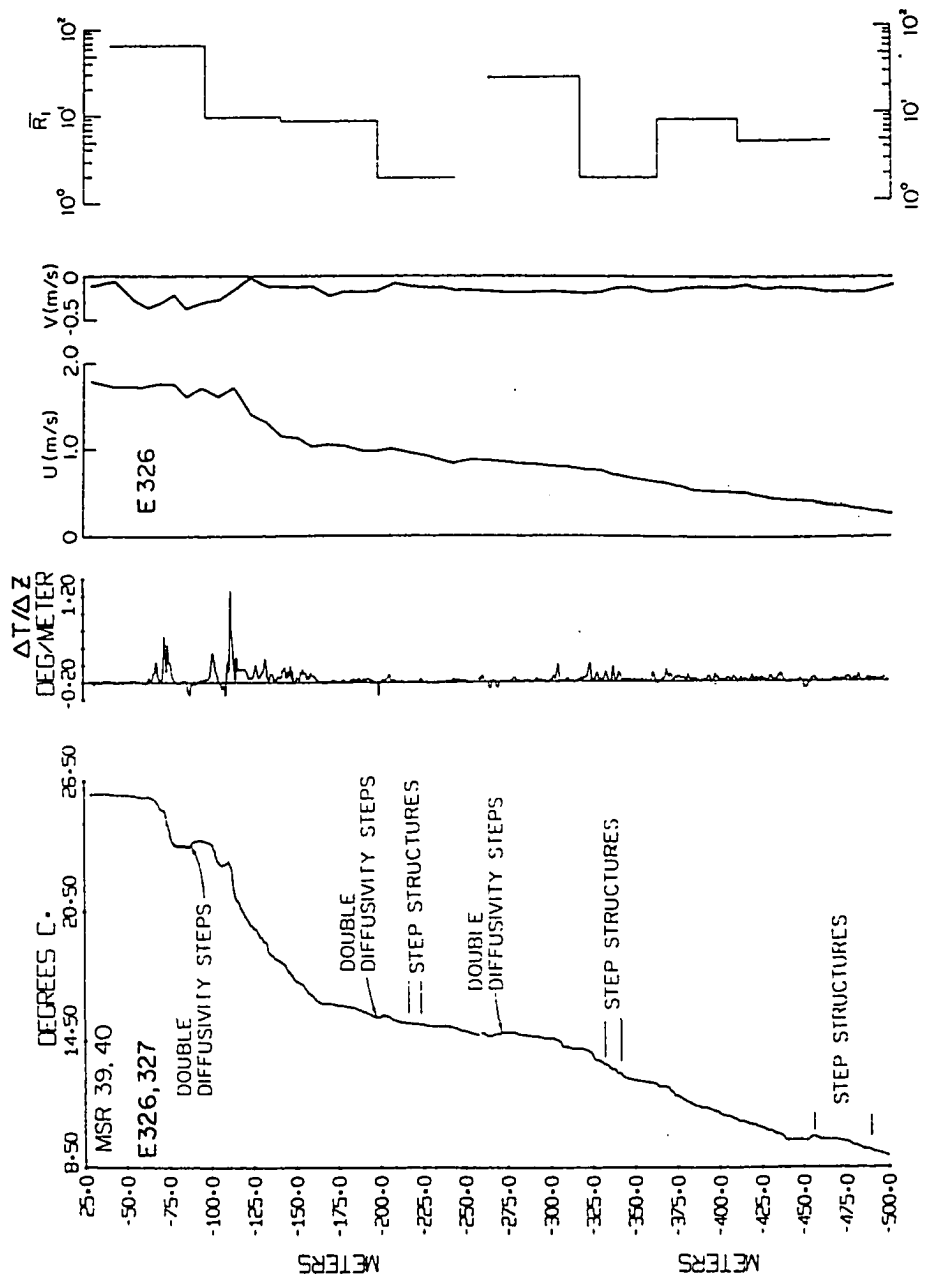
Figure 57. Details of the temperature, salinity and sigma-theta profiles, using the unsmoothed data of station 15 (see Fig. 18). (a) A highly stratified region centered at $\sigma_\theta = 26.73$, and (b) the underlying step-like structure.



sents the highly stratified region centered at $\sigma_\theta = 26.73$, responsible for anomalously small Jacobians. Fig. 57b shows the step-like structure immediately below this region (on a vertical scale three times larger). The temperature and salinity inversions in the latter figure may be interpreted as signatures of vertical overturning activity. The density scale of the small j regions ('risers' in the staircase) is variable, with a maximum of about $0.15 \sigma_\theta$. The vertical thickness of these stratified regions is about 20 m , about the same as reported for the thermocline (Toole and Schmitt 1987, Marmorino 1987, see also Itsweire et al. 1989). Adjacent to the minima in j we find well-mixed regions (treads). Their length scale is also of about 20 m .

The step-like density structure in the Nutrient Stream resembles those attributed to double-diffusive intrusions (for reviews see Turner 1973, and Garrett 1982). Gregg and Sanford (1980) reported several meters thick temperature stepped structures in the upper thermocline of the Gulf Stream (Fig. 58), and interpreted them to be predominantly caused by salt-fingering. Their calculated 50 m -averaged Richardson numbers were supercritical; however, this may have been caused by vertical averaging, as discussed earlier. Other studies, however, have held intermittent turbulent shear-mixing responsible for staircase structures (Kullenberg et al. 1974, Gregg et al. 1986, Marmorino 1987, Toole and Schmitt 1987). Gregg et al. (1986) reported step-like density structures in a diffusively stable thermocline, which they ascribed to the breaking of near-inertial internal waves. They found dissipation to vary in the vertical, with alternating high and low values in adjacent layers. Their results suggest that the start and the end of a burst of high dissipation may be associated with 10 m -averaged subcritical Rich-

Figure 58. High resolution temperature and temperature gradient in a station taken near the middle of the Gulf Stream, at about $38^{\circ}N$, $69^{\circ}W$. Also shown are the horizontal velocities (vertical resolution of about 8 m) and the 50 m -averaged Richardson numbers (adapted from Gregg and Sanford 1980).



ardson numbers (their Figs. 9a and 11, not reproduced here). Kundu and Beardsley (1991), analyzing upwelling on the west coast of the United States, found near-critical Ri numbers in the upwelled main thermocline associated with high vertical mean shear. They speculated on the existence of thin interface layers with subcritical Ri numbers, while mean measured values were above critical. Critically stable regions have been reported in the equatorial undercurrent by Chereskin et al. (1986), Toole et al. (1987) and Peters et al. (1988), and in the main oceanic thermocline by Eriksen (1978). Eriksen (1987) also reported Ri values in the seasonal thermocline to be frequently subcritical, at times when diapycnal mixing appeared to be intense.

Instability and mixing in the upper-thermocline layers of section 36N were first suggested by the nutrient distributions, confirmed later by the dynamic anomalies and diapycnal velocities calculated from the smoothed depth field. Further evidence is given by the isopycnic distribution of $\overline{w'\rho'} = K/J$, w_ρ and $\partial w_\rho / \partial \rho$ between stations 15 and 16 of section 36N, where the latter quantities are calculated using equation (45) (Fig. 59). In general, the maxima in the vertical Reynolds density flux are associated with the spreading of the isopycnals, the largest value centered at $\sigma_\theta = 26.73$, the location of the minimum of j in Fig. 33 and 55 (the minimum of Ri in Fig. 37).

Some support for the idea of frontogenesis followed by mixing comes from work by Arnøe et al. (1990). Fig. 60, adapted from their paper, shows the temperature distribution (dashed lines; solid lines are for $T = 15$ and 18°C) and the regions of enhanced phytoplankton, zooplankton and small animal concentration (shaded regions), for two transects across the Gulf Stream. The top illustration is a trans-

Figure 59. Vertical Reynolds density flux, diapycnal velocity and its diapycnal gradient, as calculated from the smoothed data of stations 15 and 16, within the Nutrient Stream in section 36N. The dotted line is the calculated $\overline{w'\rho'} = K/J$ distribution, and the dashed and solid lines are the corresponding w_ρ and $\partial w_\rho / \partial \rho$ profiles.

Stations 15-16

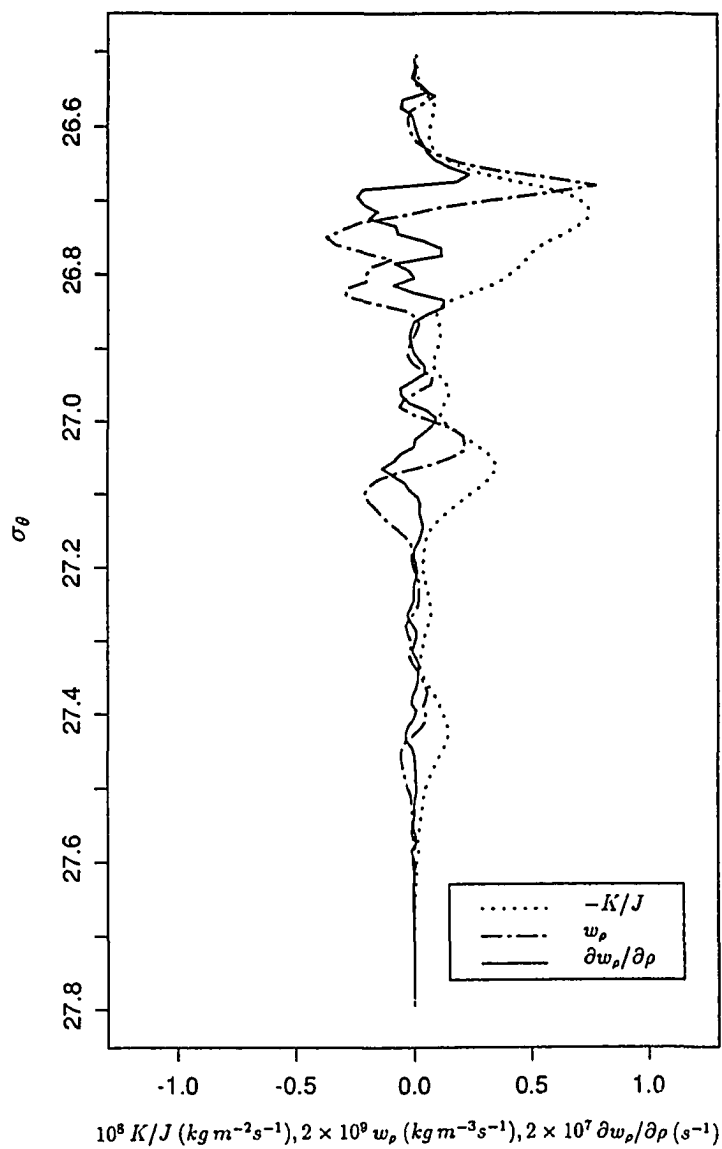
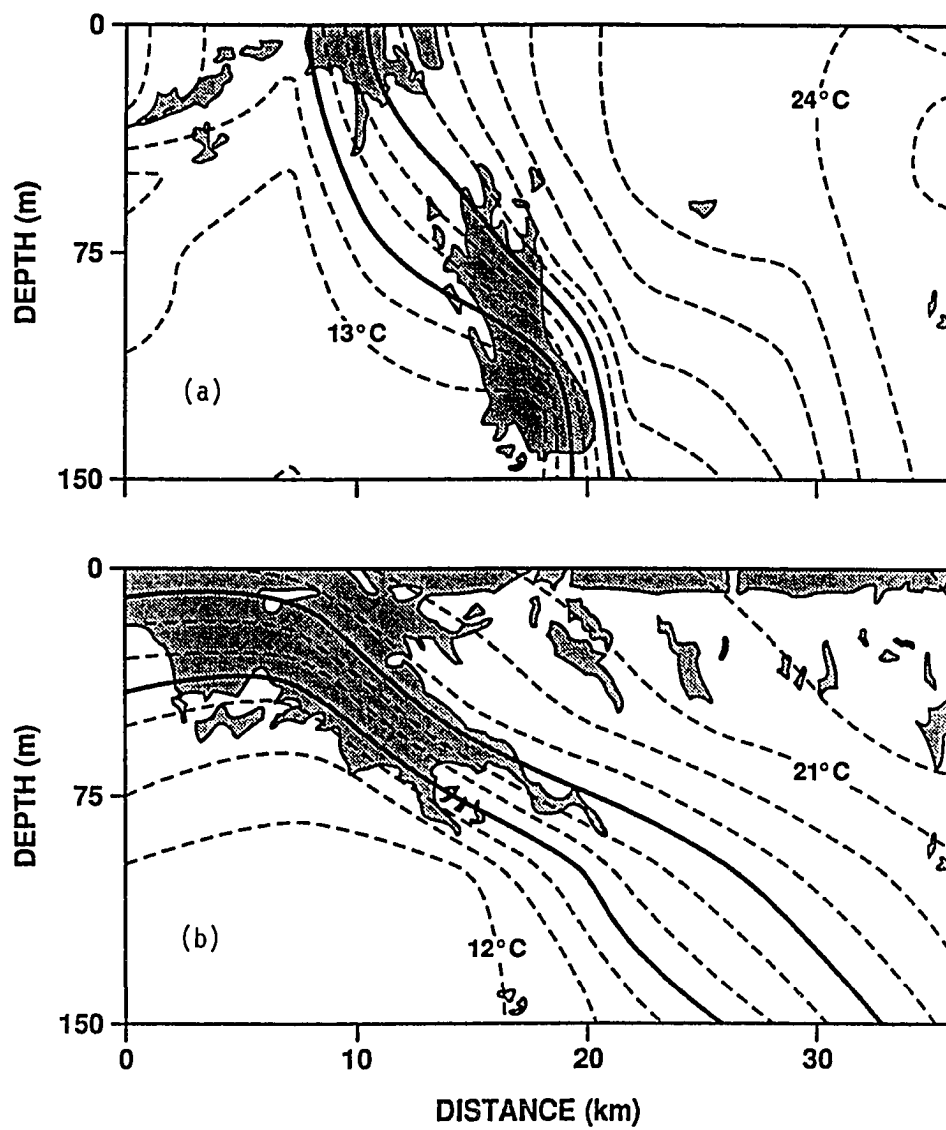


Figure 60. Temperature distribution (dashed lines; solid lines are for $T = 15$ and 18°C) and regions with high phytoplankton concentration (shaded areas) for two nearby transects across the Gulf Stream (adapted from Arnone et al. 1990). The transect in (a) was approximately taken across the inflection point between a crest and the subsequent trough, the transect in (b) was taken slightly before the subsequent crest.



ect similar to ours in that it was taken near the inflection point between the crest and following trough of a meander. The bottom figure comes from a transect taken slightly before the crest of the next meander. Arnone et al. (1990) pointed out that the downward and upward movements of phytoplankton (used as a tracer) show shrinking (convergence) and stretching (divergence) of the isopycnal layers, in agreement with Bower's (1989) calculations of convergence-divergence from the movement of isopycnal floats. The transects also show the spread of phytoplankton across isothermal layers, which may be used as an indicative of diapycnal mixing. Using the two isotherms, $T = 15$ and 18°C , for guidance, it may be noted that phytoplankton is somewhat broader in the transect taken near the inflection point.

9.2 A simple model of diapycnal mass transfer

In order to explain some of the observed features in the distribution of the diapycnal velocity, we have constructed a simple model of the vertical Reynolds density flux, $F_z = \overline{w'\rho'}$, within the Nutrient Stream. We wish to explore the effects of localized subcritical Ri numbers, associated with small Jacobians and large diapycnal velocity gradients caused by frontogenesis. The corresponding vertical Reynolds density flux distribution has a maximum on some isopycnal of the upper thermocline, say $\sigma_m = 26.73$. We idealize this by a hyperbolic secant-distribution:

$$\overline{w'\rho'} = \delta \text{sech} \left[\frac{(\sigma_\theta - \sigma_m)}{\beta_1} \right], \quad (46)$$

where $\delta \equiv \overline{w'\rho'}_{max}$, and β_1 is the scale, in σ_θ units, of the mixing region.

The vertical Reynolds density flux can be related to the Jacobian with the

help of equations (40), (44) and (37),

$$\overline{w'\rho'} = \frac{K_0(1 + 10Ri)^{-3/2}}{J} = \frac{K_0}{(1 + 10AJ)^{3/2}J}, \quad (47)$$

where A is :

$$A \equiv \frac{Ri}{J} = \left(\frac{g}{\rho}\right) \left(\frac{\partial v}{\partial \rho}\right)^{-2}, \quad (48)$$

and J again denotes the absolute value of the Jacobian.

Since we don't have estimates of $\partial v/\partial \rho$ for the unsmoothed density field we assume the minimum (subcritical) Ri value to be $Ri_s = 0.2$, at the center of the mixing region. We estimate the center J_s value from Fig. 27a, as $J_s = 60 m^4 kg^{-1}$. The first equality in equation (47) (with $K_0 = 2.6 \times 10^{-3} m^2 s^{-1}$) then gives $\delta = 8.3 \times 10^{-6} kg m^{-3} s^{-1}$. Equation (48) gives $A = 0.0033 kg m^{-4}$, and $\partial v/\partial \rho = 1.7 m^4 kg^{-1} s^{-1}$. This last value is not much larger than the maximum value ($1 m^4 kg^{-1} s^{-1}$, see Fig. 44) estimated from the smoothed density field, as expected from our discussion in Chapter 7. As a first approximation, we assume that the calculated velocity gradient is constant, and use equation (48) to obtain the Jacobian corresponding to $Ri_c = 0.25$, $J_c = Ri_c/A = 75 m^4 kg^{-1}$.

The value for β_1 is estimated (again from Fig. 57a) to be $0.025 \sigma_\theta$ -units. The vertical Reynolds density flux distribution given by equation (46) (with the previously estimated δ and β_1), is shown in Fig. 61a, together with the values of w_ρ and $\partial w_\rho/\partial \rho$, calculated from $w_\rho = -\partial(\overline{w'\rho'})/\partial z$ (equation 41). The maxima of w_ρ and $\partial w_\rho/\partial \rho$ are approximately $5 \times 10^{-6} kg m^{-3} s^{-1}$ and $5 \times 10^{-4} s^{-1}$, respectively. The maxima for w_e , estimated as $w_e = J_c w_\rho$, is $4 \times 10^{-4} m s^{-1}$.

The J distribution can now be calculated from equation (47), with the result shown by the solid line in Fig. 62a. It shows a region of $J < J_c$ around the

Figure 61. Simple model for the vertical Reynolds density flux, $\overline{w'\rho'}$, at the location of the Nutrient Stream, both (a) before and (b) after mixing. The dotted line is the hypothetical $\overline{w'\rho'}$ distribution, the dashed and solid lines are the corresponding w_ρ and $\partial w_\rho/\partial \rho$ profiles.

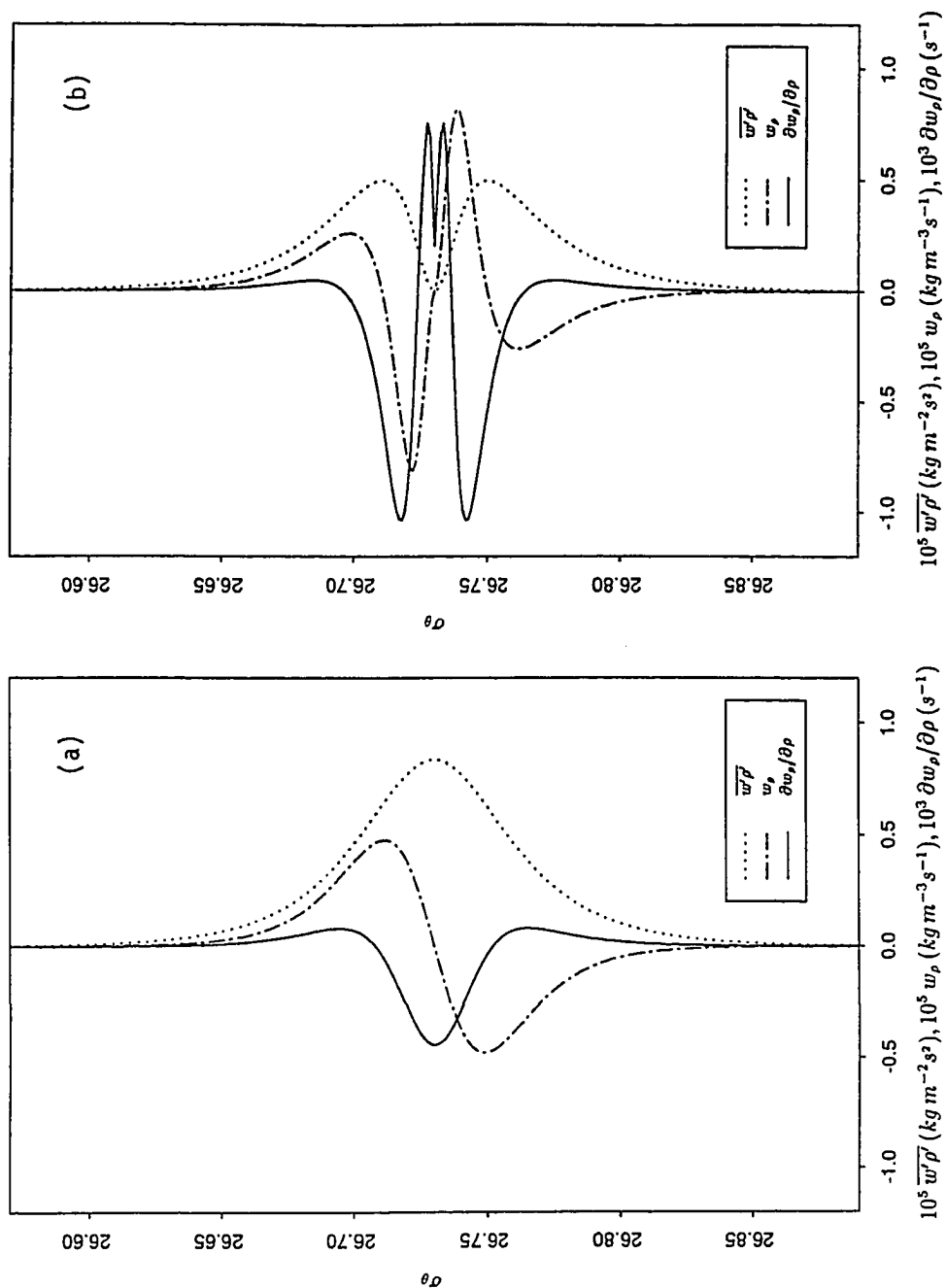
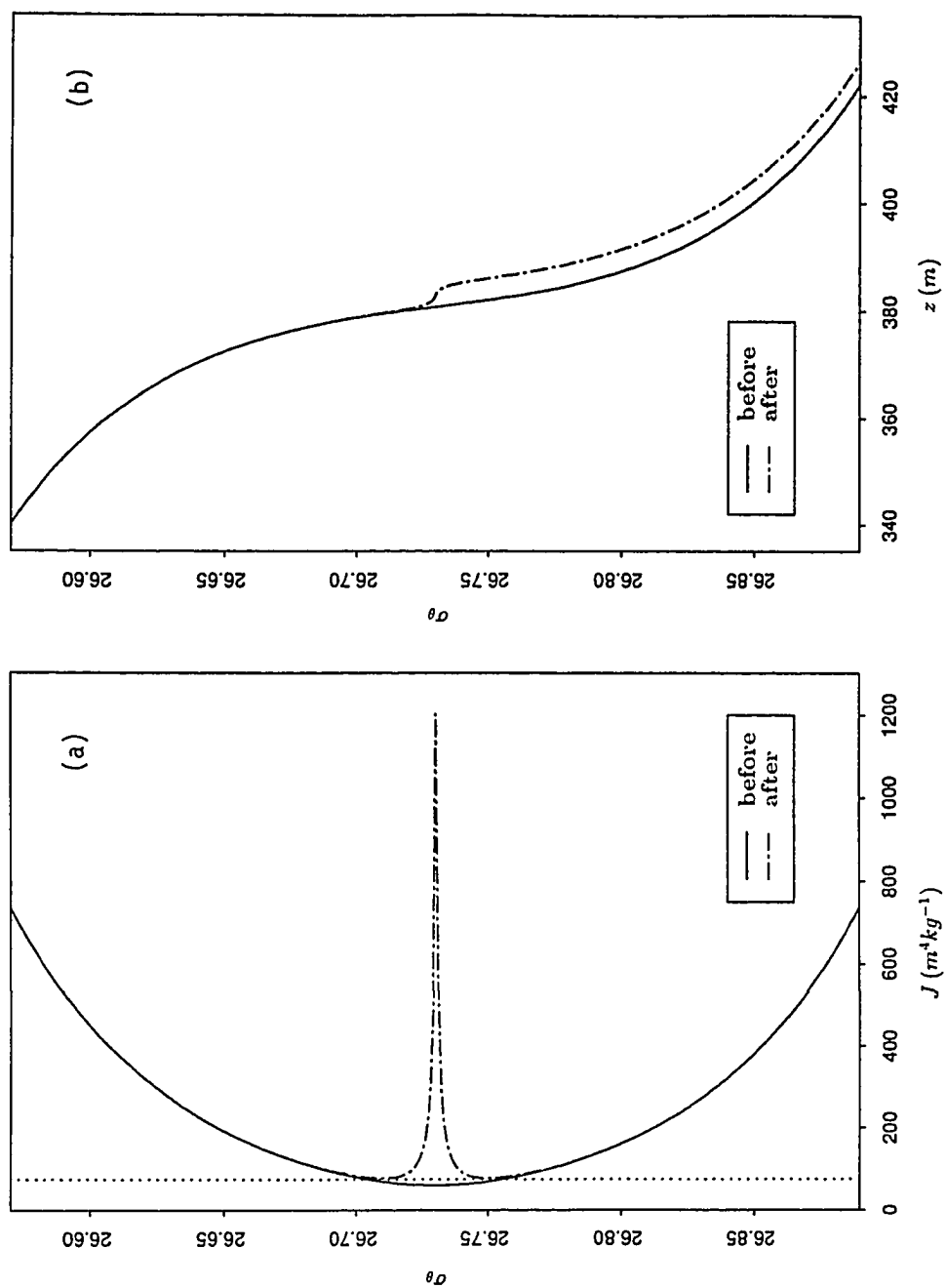


Figure 62. (a) Jacobian, J , and (b) depth, z , profiles corresponding to the original (before mixing, solid line) and modified (after mixing, dotted-dashed line) vertical Reynolds density flux $\overline{w'\rho'}$. The dotted vertical line in the Jacobian distribution indicates the value of J_c .



minimum, J_s . From an upper reference level, $\sigma_\theta(z = 270\text{ m}) = 26.58$, the J -distribution can be integrated to give the density-depth variation shown in Fig. 62b (solid line).

The most important result of these calculations is the large diapycnal convergence in the region of maximum vertical Reynolds density flux (see again Fig. 61a). The convergence must push apart the well packed isopycnal layers, and compress the layers at the edges of the mixing region. In the central region, convergence reduces density fluctuations, eventually to zero once the layer is well-mixed, so that the density flux also drops to zero. Large enough convergence may generate secondary mixing events at the edges of the original mixing region. The modified density flux distribution, after secondary mixing at the edges, can be modeled by subtracting a second hyperbolic secant from the original one, of nearly the same amplitude, $\delta' = 0.999 \times 1.1 \times 10^{-5} \text{ kg m}^{-2} \text{ s}^{-1}$, the factor of 0.999 ensuring that no singularity develops. The second hyperbolic secant is taken to be narrower ($\beta_2 < \beta_1$), affecting only the region with $J < J_c$. The resulting distribution is

$$\overline{w'\rho'} = \delta \text{sech} \left[\frac{(\sigma_\theta - \sigma_m)}{\beta_1} \right] - \delta' \text{sech} \left[\frac{(\sigma_\theta - \sigma_m)}{\beta_2} \right]. \quad (49)$$

This, together with the corresponding w_ρ and $\partial w_\rho / \partial \rho$ distributions, is shown in Fig. 61b. Following localized mixing, additional patches of positive and negative values of w_ρ and $\partial w_\rho / \partial \rho$ have been created.

With the modified $\overline{w'\rho'}$, we can again solve for J to obtain the results shown by the dotted-dashed line in Fig. 62a. The subcritical J values have now disappeared, and a large peak in J has developed in their place. As before, we can calculate the modified density-depth variation (dotted-dashed line in Fig. 62b). This shows the creation of a well-mixed region, a step in the density profile resembling those

seen in Fig. 57b.

Comparing Fig. 61 with Fig. 59 (see also Fig. 18), one sees evidence of “primary” mixing in the observations. Large mixed layers (corresponding to a succession of smaller well-mixed layers in the unsmoothed representation) may be postulated to have developed centered at about $\sigma_\theta = 26.6$, 26.9 and 27.3. Well stratified layers, produced through instability and diapycnal convergence in the adjacent layers, may be postulated to be centered at $\sigma_\theta = 26.73$ and 27.08. In these cases the large peaks in the vertical Reynolds density flux, attributable to instability-mixing, are accompanied by side-lobes of high diapycnal velocity, and opposing peaks of diapycnal convergence. The much smaller amplitude of the observed quantities is presumably due to the smoothing of the depth distribution.

A rough estimate of how long mixing episodes may last can be obtained from equation (23) for the material tendency of j . For constant $\partial w_\rho / \partial \rho$, along a material trajectory this equation has a solution of the form

$$j \simeq j_0 \exp \left(-\frac{\partial w_\rho}{\partial \rho} t \right). \quad (50)$$

With a value for $\partial w_\rho / \partial \rho$ of $O(10^{-4} \text{ s}^{-1})$, we find that the anomaly in j (a factor of five) would disappear in a few hours. Such a short time-scale points at the ephemeral nature of any individual dynamical anomaly in the Nutrient Stream, and is consistent with our earlier assumption that mixing occurs in periods much shorter than the movements of the boundary current.

We showed earlier (Fig. 51) that the two terms in equation (45), w_ρ^r and w_ρ^j , have the same sign in their contribution to w_ρ . This is because the direction of decreasing absolute value of J (positive w_ρ^j) is also the direction of increasing diapycnal velocity gradients and decreasing Ri (positive w_ρ^r). The resulting diapyc-

cnal convergence forces the isopycnals apart, increasing J . As the layers widen, the Richardson number goes well above critical. The result of this event is the generation of mixed, step-like, layers. With local values for w_e of $O(10^{-4} \text{ m s}^{-1})$, and a time scale of several hours, we may estimate that during each mixing event a few meters of water are transferred into the subcritical (well-stratified) layers. After many mixing events, occurring at different times and positions of the upper-thermocline, the aggregate result is two-way exchange between layers of the Nutrient Stream. To sustain this process, the isopycnal layers must be drained or replenished through epipychnal divergence/convergence. One possible mechanism for this is through the correlation of layer depth and cross-stream velocity, or horizontal Reynolds mass flux (the “peristaltic pumping” suggested by Csanady, 1989), which is comprised under the C term in equation (9). Based on energy considerations, Csanady showed that this flux has to be necessarily convergent (negative) in the upper thermocline layers of a western boundary current.

9.3 Estimates of tilting and torque terms

To support the validity of the above model estimates, it is important to establish that shear-induced mixing, and not tilting of horizontal vorticity or torque by external forces, dominates the vorticity balance within the Nutrient Stream, ie. we must show the accuracy of approximations (23) and (33). Table 5 summarizes our estimates for various quantities in section 36N within the Nutrient Stream, both from the smoothed density data (upper row) and from the above simple model of diapycnal mass transfer (lower row). Let us first look at the estimates from the

Table 5. Estimates for quantities involved in maximum contributions to the vorticity balance, within the Nutrient Stream. The upper row gives the results as calculated from the smoothed density data. The lower row gives the estimates as obtained from our simple model of diapycnal mass transfer.

	j (m)	q ($m^{-1}s^{-1}$)	$\partial w_z / \partial z$ ($kg\,m^{-4}s^{-1}$)	$\partial v / \partial \rho$ ($m^4kg^{-1}s^{-1}$)	K (m^2s^{-1})	$T_i / (jg)$ (s^{-1})	$T_w / (jg)$ (s^{-1})	$T_{ab} / (jg)$ (s^{-1})	w_p ($kg\,m^{-3}s^{-1}$)	w_s ($m\,s^{-1}$)	$\partial w_s / \partial \rho$ (s^{-1})
16 m-smoothed mixing model	2×10^3 7.5×10^4	5×10^{-10} 1.2×10^{-9}	1.1×10^{-13} 2×10^{-10}	1 1.7	1.3×10^{-5} 4×10^{-4}	1.1×10^{-9} 4×10^{-6}	2.1×10^{-11} 6×10^{-8}	- 1.9×10^{-7}	2.6×10^{-9} 5×10^{-6}	6.6×10^{-7} 4×10^{-4}	1.1×10^{-7} 5×10^{-4}

smoothed density data. The tilting term in equation (32) may be estimated as

$$\frac{T_i}{jq} \simeq -\frac{1}{jq} \frac{\partial w_\rho}{\partial x} \frac{\partial v}{\partial \rho}. \quad (51)$$

Using the numbers in the upper row of Table 5, we may calculate the maximum absolute value of the tilting term to be $T_i/(jq) \simeq 1.1 \times 10^{-9} \text{ s}^{-1}$. Similarly, the torque term may be estimated as

$$\frac{T_o}{jq} \simeq \frac{1}{jq} \frac{\partial B}{\partial x} \sim \frac{A_v}{jq} \frac{\partial}{\partial x} \left(\frac{\partial^2 v}{\partial z^2} \right) + \frac{A_h}{jq} \frac{\partial}{\partial x} \left(\frac{\partial^2 v}{\partial x^2} \right), \quad (52)$$

where A_v and A_h are the vertical and horizontal eddy viscosity coefficients. Let us call the first term on the right, depending on A_v , $T_{ov}/(jq)$, and the second, depending on A_h , $T_{oh}/(jq)$. The along-stream velocity, cross-stream length and depth scales can be set as 1 m s^{-1} , 25 km and 500 m , respectively. Using these scales, and assuming $A_v \simeq K$ and $A_h \simeq 300 \text{ m}^2 \text{ s}^{-1}$ (Bower et al. 1985, Boudra and Chassignet 1988), we obtain $T_{ov}/(jq) = 2.1 \times 10^{-11} \text{ s}^{-1}$ and $T_{oh}/(jq) = 1.9 \times 10^{-7} \text{ s}^{-1}$. Note that only the first value is entered in the upper row in Table 5, which lists the vertically smoothed estimates. The second value, which depends solely on epipycnal gradients, is not affected by smoothing, and is entered only in the second row, along with the estimates using the unsmoothed data (see below): it would clearly not be appropriate to compare it with the highly damped estimates of the first row. The maximum value of $\partial w_\rho / \partial \rho$ for the smoothed density field is $1.1 \times 10^{-7} \text{ s}^{-1}$ (Fig. 54). This value is much larger than both tilting and the contribution of vertical eddy diffusion to the torque.

The second row of Table 5 lists the estimates obtained from the idealized model discussed in the previous section, with the help of the above scales. The maximum tilt and torque contributions to the potential vorticity equation are now

several orders of magnitude larger than those in the first row. However, they are still considerably smaller than our new estimate for the diapycnal convergence, $5 \times 10^{-4} \text{ s}^{-1}$. The next term in size is tilting of horizontal vorticity, two orders of magnitude smaller.

The importance of the diapycnal term in equation (32) may be further highlighted by comparing it with the relative change of planetary vorticity due to advection, $(v/f)(\partial f/\partial y)$. For $v = 1 \text{ m s}^{-1}$ this term is $2.1 \times 10^{-7} \text{ s}^{-1}$, three orders of magnitude smaller than the maximum diapycnal divergence. This indicates that, within the Nutrient Stream, localized stretching or shrinking can indeed dominate vorticity changes. The situation is different for the vertically smoothed values, however, with both terms being of similar magnitude. This shows that what appears as little vertical averaging (a 16 m running filter), produces a large reduction in the local values of diapycnal divergence or convergence.

The contribution of epipycnal divergence to the potential vorticity balance (see equations 22 and 44) was estimated by Bower (1989) from the initial and final position of RAFOS floats, under the assumption that potential vorticity is conserved along an isopycnal trajectory. This allowed Bower to calculate the epipycnal divergence from the relative change in absolute vorticity. Here we have shown that within the Nutrient Stream this assumption is generally incorrect, with Jacobian anomalies being considerably larger than those of the absolute vorticity. The RAFOS floats are designed for self-adjusting compressibility (Bower and Rossby, 1989) and cannot follow diapycnal mixing. Nevertheless, Bower's estimates, obtained from an ensemble of trajectories which presumably average out the local effects of diapycnal mixing, are likely to be of the correct order of magnitude. The

mean values she obtained for epipycnal divergence are about $(\pm) 5 \times 10^{-7} s^{-1}$. Again, these epipycnal estimates must be compared with those from our model for the unsmoothed density field. In doing so we see that the epipycnal divergence is three orders of magnitude smaller than the estimated maximum contribution from the diapycnal convergence.

Finally, the horizontal Reynolds mass flux contribution to the potential vorticity balance may be estimated using Csanady's (1989) parameterization for the horizontal Reynolds mass flux in a western boundary current. This is based on the idea that the velocity and depth fluctuations must be proportional to the characteristic mean velocity (v_m) and layer depth in the current, $\overline{u'j'} \sim \alpha j v_m$, where $\alpha \simeq 0.0025$. With these values for the core of the Nutrient Stream we obtain $\overline{u'j'} \sim 10^{-11} s^{-2}$, and the appropriate term for comparison in equation (32) is $\overline{u'j'} \partial q / \partial x \sim 10^{-7} s^{-1}$. This term is again much smaller than the diapycnal term for the unsmoothed model. This result could have been expected in view of equation (34), which shows that the horizontal Reynolds mass flux must be related with the horizontal Reynolds stresses. Hence, its contribution should not be larger than the $T_o/(jq)$ term discussed above.

Chapter 10. The Upper Level Atmospheric Jet Stream Analogy

*What is your language, oh, Sea?
The language of eternal quest.
What language is your answer, oh, Sky?
The language of eternal silence.*
Rabindranath Tagore (1861-1941)

The similarity of tropospheric jet streams to oceanic currents has long been appreciated (Iselin 1950, Rossby 1951). Newton (1978) compared the dimensions and volume transport profiles of the jet stream to those of the Gulf Stream. The similarity he found in volume transport profile is remarkable, where the ratio of typical dimensions ranges from 1, for shear-related quantities, to 30, for horizontal size and velocity. Newton also noted that Gulf Stream meanders are dynamically similar to jet stream waves. He suggested that isentropic convergence, intensified diapycnal velocity gradients and downwelling at the troughs of jet stream and their counterparts at ridges, should be mirrored in the Gulf Stream. Many of these features can now indeed be identified, as shown in recent studies by Bower (1989) and Bower and Rossby (1989).

The upper level frontal systems have been held responsible for mixing of tropospheric and stratospheric air masses. In the 50's and 60's this generated much interest in connection with the fate of radioactivity released by nuclear testing in the stratosphere. Later, attention turned to the transfer of chlorofluoromethanes from the troposphere to the stratosphere. In the ocean, western boundary currents

play a similar role in the exchange of water masses of the continental margins with the ocean interior. The desire to understand that process was initially the principal motivation for our work.

Among the studies of the 70's on the upper level jet stream, those relevant to the present work are Shapiro (1976, 1978) and Gidel and Shapiro (1979). A review is given in Keyser and Shapiro (1986), see also Keyser and Rotunno (1990). Shapiro (1976) reported potential vorticity anomalies in the upper level jet stream and, in order to explain them, postulated an appropriate distribution of vertical Reynolds potential temperature flux (Fig. 63). Later, in order to support his ideas Shapiro (1978) showed the distributions of Ri and q in the upper level atmospheric jet stream (Fig. 64).

A comparison of Fig. 64 with Figs. 37 and 42 shows compelling similarity between the Ri and q anomalies in the jet stream and the Gulf Stream. The main difference between the two potential vorticity distributions arises because the jet stream has shear layers both above and below the level of maximum wind, while in western boundary currents the maximum velocity usually occurs near the water surface. Hence, in the oceanic case the vertical Reynolds density flux distribution, $\overline{w'\rho'}$, is similar to the lower half of the (negative) vertical Reynolds potential temperature flux, $-\overline{w'\theta'}$, shown in Fig. 63b. The vertical density flux is zero at the sea surface if air-sea fluxes of heat and salt vanish, not because the velocity has a maximum as in the case of the jet stream.

Shapiro's concept of the mechanism responsible for the anomalies differs from ours. His approach is based on the following approximate relations in isentropic coordinates, with potential temperature θ as the vertical coordinate (Shapiro 1976,

Figure 63. Shapiro's (1976) representation of turbulence in upper level atmospheric jet stream systems. (a) Regions of clear-air turbulence in the vicinity of the jet stream are stippled; the solid and dashed lines are contours of potential temperature and wind speed, respectively. (b) The postulated vertical Reynolds potential temperature flux, $\overline{w'\theta'}$, is shown as a function of height; the crosses indicate observed values.

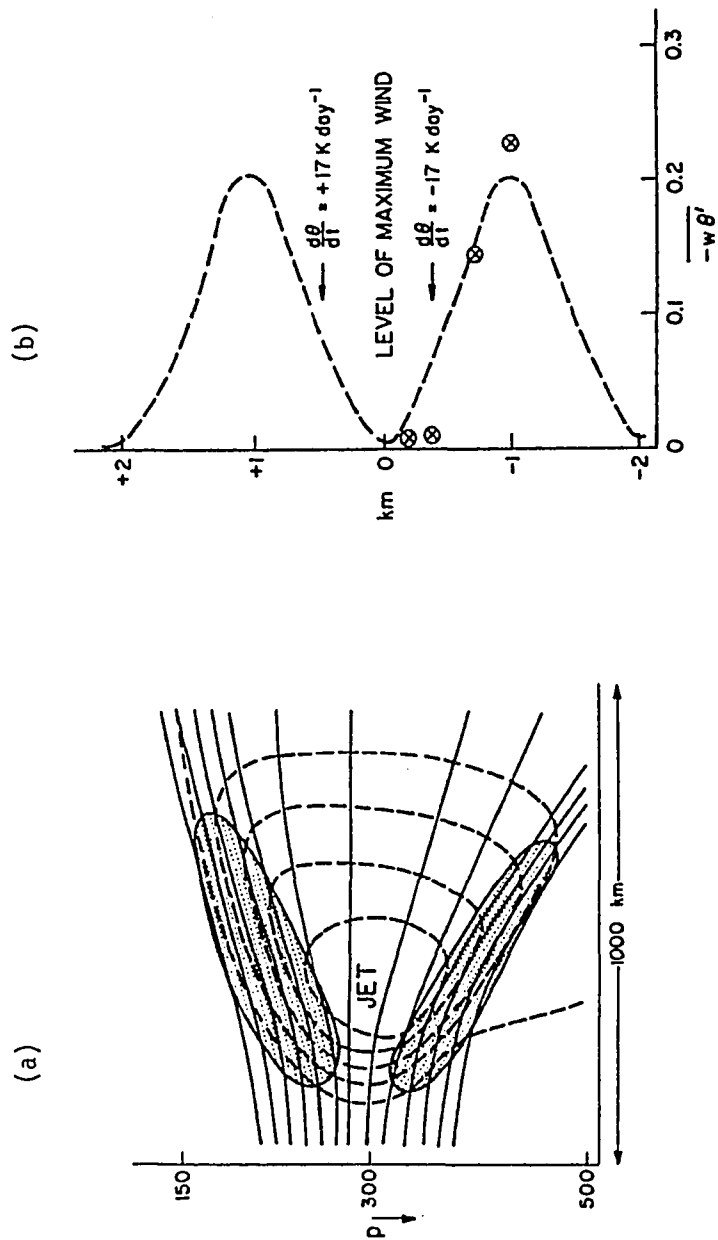
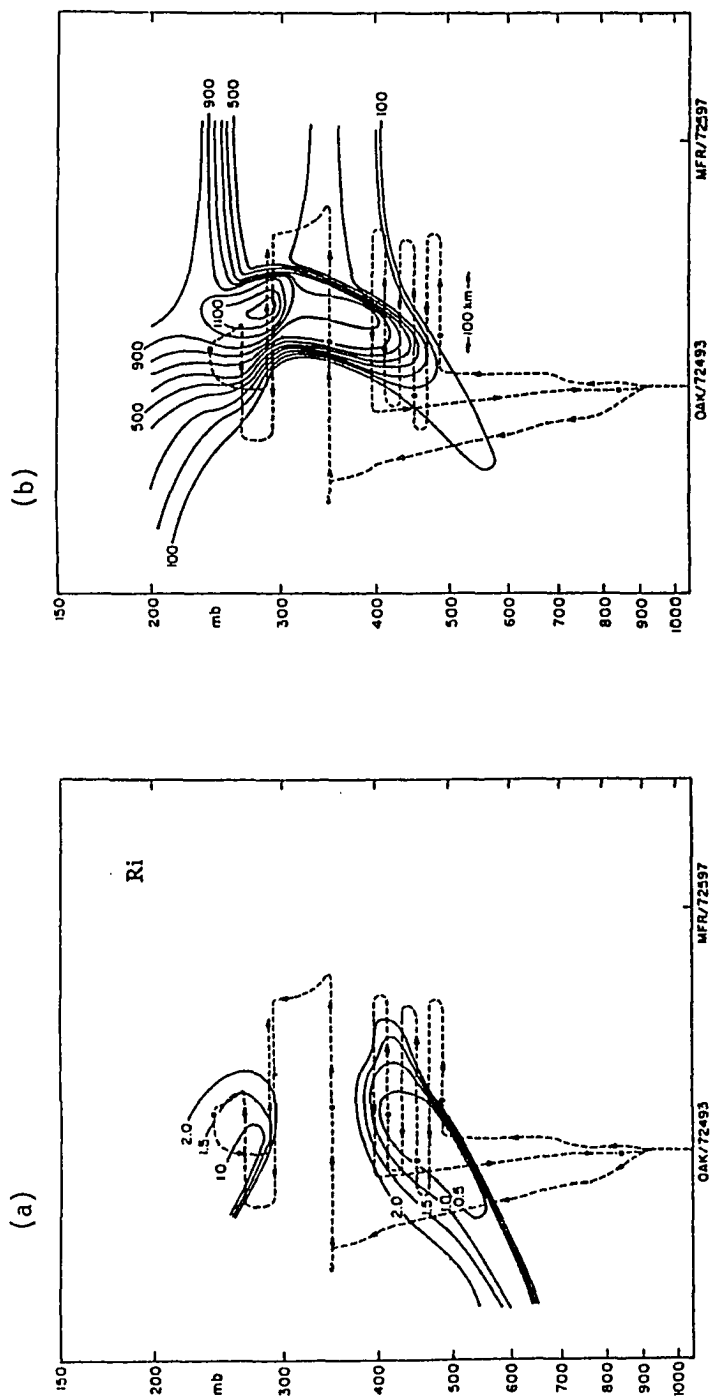


Figure 64. (a) Richardson number and (b) potential vorticity (units of $10^{-7} K s^{-1} mb^{-1}$), in isobaric coordinates, for a section across the upper level atmospheric jet stream system (reproduced from Shapiro 1978). The dashed line indicates the flight path taken during the observations.



equations 8 and 7):

$$\frac{d}{dt} \left[(\zeta + f) \frac{\partial \theta}{\partial p} \right] \simeq (\zeta + f) \frac{\partial}{\partial p} \left(\frac{d\theta}{dt} \right), \quad (53)$$

and

$$\frac{d\theta}{dt} \simeq -\frac{\partial}{\partial z} \overline{w'\theta'}, \quad (54)$$

where d/dt is identical to $\mathcal{D}/\mathcal{D}t$ but with θ replacing ρ . Shapiro suggested that high potential vorticity anomalies are produced at the level of maximum wind, through mixing by clear-air-turbulence. He said that this inhibits the vertical spreading of the isentropes during frontogenesis, required in a cyclonic shear zone by conservation of potential vorticity.

The last two equations, together with the potential temperature flux distribution postulated by Shapiro (Fig. 63b), indeed suggest that a region of high potential vorticity may be generated at the level of maximum wind.⁴ However, from the same argument, regions of low potential vorticity should arise at the maxima in vertical shear, the two maxima of $-\overline{w'\theta'}$ in Fig. 63b. This is not the case in Fig. 64b, with q being large precisely where, according to Shapiro's criterion, it should be small.

Equations (53) and (54) are essentially the same as our equations (33) and $w_\rho \simeq -\partial(\overline{w'\rho'})/\partial z$ (see equation 41). Equation (33) may be rewritten as

$$\frac{\mathcal{D}}{\mathcal{D}t} \left[\frac{(\zeta + f)}{\rho} \frac{\partial \rho}{\partial z} \right] \simeq \frac{(\zeta + f)}{\rho} \frac{\partial w_\rho}{\partial z}. \quad (55)$$

Note that equations (53) and (55) are equivalent, except for the density, ρ , which (55) retains inside the material derivative. This difference arises from the definitions of potential vorticity used by Shapiro and here (the terms between brackets

⁴ Note again that we talk in terms of absolute values, actually $(\zeta + f) \partial \theta / \partial p$ is negative and $\partial / \partial p (d\theta / dt)$ is a negative maximum at the level of maximum wind.

in equations (53) and (55), respectively). Equation (55) can actually be rewritten as (53) with the appearance of additional terms, which Shapiro assumed to be negligible besides the diapycnal divergence term. Note also that equation (53) has the derivatives with respect to pressure, while equation (55) has them with respect to depth, which compensates for θ and ρ increasing in opposite vertical directions (in particular, $\overline{w'\theta'}$ is negative and $\overline{w'\rho'}$ positive).

Our interpretation is that mixing is triggered by the dense packing of isopycnals (regions of low J and high q values) during frontogenesis, while the diapycnal velocity gradients are maintained or perhaps even increased. From this point of view the low J (and high q) values are the results of frontogenesis, and mixing that reduces the anomalies is the consequence. As we have argued above, a simple model as well as observations support this point of view. Figs. 54 and 55 show that anomalously small j (high q) values are associated with diapycnal convergence, not divergence as Shapiro's ideas would imply. The same point of view underlies the analyses by Roach (1970) and Browning et al. (1970) of atmospheric jet streams, who assumed that a critical Ri number limits the vertical spacing between isentropes during frontogenesis.

One way to reconcile the q distribution in the Gulf Stream with Shapiro's observations for the jet stream is to note that in Fig. 64b there could actually be two distinct maxima of q , if the single maximum were an artifice of contouring over the relatively poorly sampled level of maximum wind. This would then agree with two observed separate minima in Ri (Fig. 64a). In this manner, the similarity between one-half of the upper level frontal system and the western boundary frontal system would be complete.

Chapter 11. Conclusions

*Love is an ocean. Its waves are troubled
by the winds. It has no port or shore.
The Lover perished on this ocean,
and with him his torments perished,
and the work of his fulfillment began.*

Ramón Llull (1232-1316)

To sum up the work in this dissertation, the original objective was to throw light on the transport of nutrients by a western boundary current. The first part of the work, therefore, analyzed the distribution of nutrient transport among different isopycnal layers of the Gulf Stream, and how this distribution changes along the Stream. Solid evidence emerged from this analysis for upward one-way transfer and two-way exchange between the upper layers of the thermocline and the surface layer. Richardson number instability, associated with frontogenesis in Gulf Stream meanders, seemed the most likely mechanism to produce mixing. A theoretical analysis of the vorticity balance of the boundary current, allowing for diapycnal mass transfer, yielded clues on the necessary conditions for dominant diapycnal mixing. Detailed examination of dynamical anomalies in a Gulf Stream hydrographic cross section revealed clear signatures of instability induced mixing, and established the importance of diapycnal mass transfer.

The results of the nutrient transport analysis reinforce and characterize Brewer and Dyrssen's (1987) idea that the Gulf Stream is a major source of nutrients for

the North Atlantic. A Nutrient Stream flows under the Gulf Stream and the North Atlantic Current, carrying a very large supply of nutrients northeastward (of the order of 10^3 kmol s^{-1} of nitrate and proportional amounts of other nutrients). It occupies the upper-thermocline layers, with its core centered around the $26.8\sigma_\theta$ -isopycnal surface, at depths of about 500 m. Only about a third of the supply comes through the Florida Straits, the rest from the Sargasso Sea thermocline, arriving between the Straits and the Mid-Atlantic Bight. The water transport from the subtropical gyre into the western boundary is dominated by inflow from the thermocline. Because the upper thermocline is the principal nutrient bearing stratum, the inflow from there into the Nutrient Stream is responsible for the large increase in nutrient transport.

The proximity of the Nutrient Stream to the surface already suggests the likelihood of nutrients reaching the surface layers. Mass and nutrient balances of individual isopycnal layers shows evidence not only for thermocline-surface mass exchange, but also net upward (diapycnal) one-way transfer. Our estimate for the overall rate (per unit length of the Stream) of one-way transfer plus two-way exchange from the thermocline to the surface layers, $3.2 \text{ m}^2 \text{ s}^{-1}$, is similar to the estimate of western boundary upwelling, about $4 \text{ m}^2 \text{ s}^{-1}$, obtained by Csanady and Hamilton (1988). The source for these processes must be along-isopycnal inflow from the upper thermocline, at a rate of some $10 \text{ m}^2 \text{ s}^{-1}$.

Isopycnic coordinates are powerful in the analysis of anomalies produced by diapycnal mass transfer. Anomalies may occur in the distribution of tracers, such as nutrients, and in dynamical quantities that control the structure of the flow, such as the Jacobian or potential vorticity. In a Gulf Stream section off the Mid-

Atlantic Bight we find substantial anomalies in all these quantities, at the location of the Nutrient Stream. The anomalies coexist with small (but not subcritical) Richardson numbers, calculated from smoothed data. The raw data show much sharper gradients, but also density inversions, which have to be eliminated in order to define the isopycnic coordinate system. It is reasonable to suppose, however, that unsmoothed Richardson numbers are locally and temporally subcritical.

We establish theoretically that coincident anomalies of small Jacobian and large potential vorticity imply dominant diapycnal convergence (divergence), causing thicker (thinner) isopycnal layers. The diapycnal velocity is calculated from the vertical gradient of the Reynolds density flux, parameterized in terms of the Jacobian and the Richardson number. This model demonstrates that diapycnal convergence is responsible for the observed anomalies in Jacobian and potential vorticity.

An important concept arising from our analysis is Ri -control of mixing in the Nutrient Stream. According to this concept, adjacent isopycnal surfaces can only approach one another to a certain point, at which Ri becomes critical. Instability then creates well-mixed regions, or steps, in the density-depth profile. A simple model of diapycnal mass transfer, associated with mixing in unstable layers, is able to reproduce the observed steps.

High and low J regions are responsible for the patchy character of the diapycnal velocity field in the Nutrient Stream. This field, consisting of alternating positive and negative diapycnal velocities, causes localized diapycnal divergences and convergences (with packing and spreading of the isopycnals). Thus diapycnal velocities are not only a passive result of the diapycnal distribution of the hori-

zontal velocities and of the small-scale structure of the layers, but are responsible for modifying this structure and the distribution of potential vorticity.

We hypothesize that frontogenesis in meanders causes a reduction of the Jacobian and an increase in the diapycnal gradients of the horizontal velocities, which occasionally takes the Richardson number below its critical value. This produces mixing between adjacent layers of fluid, raising or lowering isopycnal surfaces. The (temporal and spatial) aggregate result is two-way water exchange between adjacent layers of the Nutrient Stream. Our crude estimate for the maximum entrainment velocity is $4 \times 10^{-4} \text{ m s}^{-1}$. This is large enough to account for the overall two-way exchange coefficient between the upper-thermocline and the surface layers, calculated from mass and nutrient balances ($2 \times 10^{-5} \text{ m s}^{-1}$).

Diapycnal divergence and convergence can locally dominate the potential vorticity balance within the Nutrient Stream, the relevant term being three orders of magnitude greater than the contribution from the planetary vorticity gradient. On the other hand, vertical averaging over even relatively short distances (16 m) rapidly reduces the calculated diapycnal convergence, to the point where its effect on the vorticity balance is of the same order as planetary vorticity. Its importance in the overall potential vorticity balance is a question that must be left open.

The resemblance between the present work and Shapiro's (1976, 1978) analysis of the upper level atmospheric jet stream (Shapiro 1976, 1978) is noteworthy. However, the interpretation of the two sets of observations is different. In our model frontogenesis is the origin of the anomalies, and mixing, once a critical Ri is attained, is their consequence, while according to Shapiro the anomalies are the result of mixing by clear-air-turbulence.

We may conclude that diapycnal mixing in the Nutrient Stream is responsible for water exchange between nutrient-rich upper-thermocline layers and nutrient-depleted surface layers. This is likely to be a mechanism of prime importance in sustaining productivity in the Gulf Stream region, and possibly over the northern North Atlantic.

Bibliography

- Armi, L., 1979: Effects of variations in eddy diffusivity on property distributions in the oceans. *J. Mar. Sci.*, **37**, 515-530.
- Arnone, R. A., R. W. Nero, J. M. Jech, and I. de Palma, 1990: Acoustic imaging of biological and physical processes within Gulf Stream meanders. *Eos Trans. Amer. Geophys. Union*, **71**, 982.
- Atkinson, L. P., T. N. Lee, J. O. Blanton, and G. Paffenhöfer, 1987: Summer upwelling on the southeastern continental shelf of the U.S.A. during 1981. Hydrographic observations. *Prog. Oceanogr.*, **19**, 231-266.
- Bane, J. M., Jr., D. A. Brooks, and K. R. Lorenson, 1981: Synoptic observations of the three-dimensional structure and propagation of Gulf Stream meanders along the Carolina continental margin. *J. Geophys. Res.*, **86**, 6411-6425.
- Bane, J. M., Jr., O. B. Brown, R. H. Evans, and P. Hamilton, 1988: Gulf Stream remote forcing of shelfbreak currents in the Mid-Atlantic Bight. *Geophys. Res. Letters*, **15**, 405-407.
- Barret, J. R., and W. Schmitz, 1971: Transport float measurements and hydrographic station data from three sections across the Gulf Stream near 67°W, R. V. Crawford Cruise 168, June-July 1968. W. H. O. I. Reference No. 71-66.
- Bleck, R., R. Onken, and J. D. Woods, 1988: A two-dimensional model of mesoscale frontogenesis in the ocean. *Quart. J. R. Met. Soc.*, **114**, 347-371.
- Boericke, R. R., and J. M. Hogan, 1977: An X-Z hydraulic/thermal model for estuaries. *J. Hydraul. Div.*, **103**, 19-37.
- Bolin, B., A. Björkström, K. Holmén, and B. Moore, 1983: The simultaneous use of tracers for ocean circulation studies. *Tellus*, **35**, 206-236.
- Bolin, B., A. Björkström, K. Holmén, and B. Moore, 1987: On inverse methods for combining chemical and physical oceanographic data: A steady state analysis of the Atlantic Ocean. Report CM-71, Department of Meteorology, Stockholm.
- Boudra, D. B., and E. P. Chassignet, 1988: Dynamics of Agulhas retroflexion and ring formation in a numerical model. Part I: the vorticity balance. *J. Phys. Oceanogr.*, **18**, 280-303.
- Bower, A. S., 1989: Potential vorticity balances and horizontal divergence along particle trajectories in Gulf Stream meanders east of Cape Hatteras. *J. Phys. Oceanogr.*, **19**, 1669-1681.
- Bower, A. S., and T. Rossby, 1989: Evidence of cross-frontal exchange processes in the Gulf Stream based on isopycnal RAFOS float data. *J. Phys. Oceanogr.*, **19**, 1177-1190.
- Bower, S. A., H. T. Rossby, and J. L. Lillibridge, 1985: The Gulf Stream - Barrier

- or blender? *J. Phys. Oceanogr.*, 15, 24-32.
- Brewer, P. G., and Dyrssen, D., 1987: Ocean chemical fluxes across $25^{\circ}N$ in the Atlantic Ocean. Discussion paper prepared for the International GOFS Meeting, Paris, February 17-20.
- Brooks, D. A., and J. M. Bane, Jr., 1981: Gulf Stream fluctuations and meanders over the Onslow Bay upper continental slope. *J. Phys. Oceanogr.*, 11, 247-256.
- Brooks, D. A., and J. M. Bane, Jr., 1983: Gulf Stream meanders off North Carolina during Winter and Summer 1979. *J. Geophys. Res.*, 88, 4633-4650.
- Brown, O. B., R. H. Evans, J. W. Brown, R. H. Gordon, R. C. Smith, and K. S. Baker, 1984: Blooming off the U. S. East Coast: A satellite description. In *Global ocean flux study*, National Academy Press, Washington, pp. 67-84.
- Brown, O., R. Evans, R. Watts, C. Casagrande, P. Hamilton, W. Boicourt, G. Csanady, 1987: Study of physical processes on the U.S. Mid-Atlantic Continental Slope and Rise. SAIC Report No. 86/7539&129, MMS Report No. 87-0024, 506 pp.
- Browning, K. A., T. W. Harrold, and J. R. Starr, 1970: Richardson number limited shear zones in the free atmosphere. *Quart. J. R. Met. Soc.*, 96, 40-49.
- Buscaglia, J. L., 1971: On the circulation of the intermediate water in the Southwestern Atlantic Ocean. *J. Mar. Res.*, 29, 245-255.
- Chereskin, T. K., J. N. Moum, P. J. Stabero, D. R. Caldwell, C. A. Paulson, L. A. Regier, and D. Halpern, 1986: Time scale variability at $140^{\circ}W$ in the equatorial Pacific. *J. Geophys. Res.*, 91, 12887-12897.
- Cox, M. D., 1985: An eddy-resolving numerical model of the ventilated thermocline. *J. Phys. Oceanogr.*, 15, 1312-1234.
- Csanady, G. T., 1979: The pressure field along the western margin of the North Atlantic. *J. Geophys. Res.*, 84, 49905-4915.
- Csanady, G. T., 1989: Energy dissipation and upwelling in a western boundary current. *J. Phys. Oceanogr.*, 19, 462-473.
- Csanady, G. T., 1990a: Mixing in coastal regions. In *The sea: ocean engineering science*, Volume 9, B. Le Mehaute and D. M. Hanes (eds.), John Wiley and Sons, New York, 593-629.
- Csanady, G. T., 1990b: Physical basis of coastal productivity. The SEEP and MASAR experiments. *Eos Trans. Amer. Geophys. Union*, 71, 1060-1061 and 1064-1065.
- Csanady, G. T., and P. Hamilton, 1988: Circulation of slopewater. *Cont. Shelf Res.*, 8, 565-624.
- Deardorff, J. W., 1967: Empirical dependence of the eddy coefficient for heat upon stability above the lowest 50 m. *J. Appl. Met.*, 6, 631-643.
- Deardorff, J. W., 1983: A multi-limit mixed-layer entrainment formulation. *J. Phys. Oceanogr.*, 13, 988-1002.
- Defant, A., 1937: C. G. Rossby, Dynamik stationärer ozeanischen Ströme im Lichte der experimentellen Strömungslehre. *Ann. der Hydrogr. und Mar. meteorologie*, pp. 57-68.

- Dutton, J. A., 1976: *The ceaseless wind*, McGraw-Hill, New York, 579 pp.
- Ekman, V. W., 1939: Neuere Ergebnisse und Probleme zur Theorie der Konvektionsströme in Meere. Gerlands Beiträge zur Geophysik, Suppl. 4, Ergebnisse der Kosmischen Physik IV, 74 pp., Leipzig.
- Ellison, T. H., 1957: Turbulent transport of heat and momentum from an infinite rough plane. *J. Fluid Mech.*, 2, 456-466.
- Eriksen, C. C., 1978: Measurements and models of fine structure, internal gravity waves and wave breaking in the deep ocean. *J. Geophys. Res.*, 83, 2989-3009.
- Eriksen, C. C., 1987: Observations of the seasonal cycle of upper ocean structure and the roles of advection and diapycnal mixing. *J. Geophys. Res.*, 92, 5354-5368.
- Esaias, W. E., G. C. Feldman, C. R. McClain, and J. A. Elrod, 1986: Monthly satellite-derived phytoplankton pigment distribution for the North Atlantic basin. *Eos Trans. Am. Geophys. Union*, 67, 835-837.
- Fernando, H. J. S., 1991: Turbulent mixing in stratified fluids. *Annu. Rev. Fluid Mech.*, 23, 455-493.
- Fofonoff, N. P., 1981: The Gulf Stream system. In *Evolution of physical oceanography*, B. A. Warren (ed.), MIT Press, Cambridge.
- Foo, E., 1981: A two-dimensional diabatic isopycnic model-simulating the coastal upwelling front. *J. Phys. Oceanogr.*, 11, 604-626.
- Fuglister, F. C., 1963: Gulf Stream '60. *Progress Oceanogr.*, 1, 265-373.
- Fuglister, F., 1972: Cyclonic rings formed in the Gulf Stream, 1965-1966. In *Studies in physical oceanography - A tribute to Georg Wüst in his 80th birthday*, A. Gordon (ed.), Gordon and Breach, 137-168.
- Gargett, A. E., 1984: Vertical eddy diffusivity in the ocean interior. *J. Mar. Res.*, 42, 359-393.
- Garrett, C., 1982: On the parameterization of diapycnal fluxes due to double-diffusive intrusions. *J. Phys. Oceanogr.*, 12, 952-959.
- Gaspar, P., 1988: Modeling the seasonal cycle of the upper ocean. *J. Phys. Oceanogr.*, 18, 161-180.
- Gibson, C. H., 1987: Fossil turbulence and intermittency in sampling oceanic mixing processes. *J. Geophys. Res.*, 92, 5383-5404.
- Gidel, L. T., and M. A. Shapiro, 1979: The role of clear air turbulence in the production of potential vorticity in the vicinity of upper tropospheric jet stream-frontal systems. *J. Atmos. Sci.*, 36, 2125-2138.
- Gregg, M. C., 1987: Diapycnal mixing in the thermocline: A review. *J. Geophys. Res.*, 92, 5249-5286.
- Gregg, M. C., and T. B. Sanford, 1980: Signatures of mixing from the Bermuda Slope, the Sargasso Sea and the Gulf Stream. *J. Phys. Oceanogr.*, 10, 105-127.
- Gregg, M. C., E. A. D'Asaro, T. J. Shay, and N. Larson, 1986: Observations of persistent mixing and near-inertial internal waves. *J. Phys. Oceanogr.*, 16, 856-885.
- Halkin, D., and T. Rossby, 1985: The structure and transport of the Gulf Stream

- at 73°W. *J. Phys. Oceanogr.*, 15, 1439-1452.
- Hamilton, P., and M. Rattray, Jr., 1978: A numerical model of the depth-dependent wind-driven upwelling circulation on a continental shelf. *J. Phys. Oceanogr.*, 8, 437-457.
- Haynes, P. H., and M. E. McIntyre, 1987: On the evolution of vorticity and potential vorticity in the presence of diabatic heating and frictional or other forces. *J. Atmos. Sci.*, 44, 828-841.
- Haynes, P. H., and M. E. McIntyre, 1990: On the conservation and impermeability theorems for potential vorticity. *J. Atmos. Sci.*, 47, 2021-2031.
- Holland, W. R., T. Keffer, and P. B. Rhines, 1984: Dynamics of the oceanic general circulation: the potential vorticity field. *Nature*, 308, 698-705.
- Hogg, N., P. Biscaye, W. Gardner, and W. J. Schmitz, Jr., 1982: On the transport and modification of Antarctic Bottom Water in the Vema Channel. *J. Mar. Res.*, 40 (Suppl.), 231-263.
- Hopfinger, E. J., 1987: Turbulence in stratified fluids: A review. *J. Geophys. Res.*, 92, 5287-5303.
- Iselin, C. O'D., 1950: Some common characteristics of the Gulf Stream and the atmospheric jet stream. *Trans. N. Y. Acad. Sci., Ser. II*, 13, 84-86.
- Itsweire, E. C., T. R. Osborn, and T. P. Stanton, 1989: Horizontal distribution and characteristics of shear layers in the seasonal thermocline. *J. Phys. Oceanogr.*, 19, 301-320.
- James, I. D., 1977: A model on the annual cycle of temperature in a frontal region of the Celtic Sea. *Estuarine Coastal Mar. Sci.*, 5, 339-353.
- James, I. D., 1978: A note on the circulation induced by a shallow-sea front. *Estuarine Coastal Mar. Sci.*, 7, 197-202.
- Jenkins, W. J., 1980: Tritium and ^3He in the Sargasso Sea. *J. Mar. Res.*, 38, 533-569.
- Jenkins, W. J., 1987: ^3H and ^3He in the Beta Triangle: observations of gyre ventilation and oxygen utilization rates. *J. Phys. Oceanogr.*, 17, 763-783.
- Kao, T. W., C. Park, and H. Pao, 1977: Buoyant surface discharge and small-scale oceanic fronts: A numerical study. *J. Geophys. Res.*, 82, 1747-1752.
- Kawase, M., and J. L. Sarmiento, 1985: Nutrients in the Atlantic thermocline. *J. Geophys. Res.*, 90, 8961-8979.
- Keffer, T., 1985: The ventilation of the world's oceans: maps of the potential vorticity field. *J. Phys. Oceanogr.*, 15, 509-523.
- Keyser, D., and R. Rotunno, 1990: On the formation of potential-vorticity anomalies in upper-level jet-front systems. *Mon. Wea. Rev.*, 118, 1914-1921.
- Keyser, D., and M. A. Shapiro, 1986: A review of the structure and dynamics of upper-level frontal zones. *Mon. Wea. Rev.*, 114, 452-499.
- Kirwan, A. D., 1963: Circulation of Antarctic Intermediate Water deduced through isentropic analysis. Reference No. 63-34F, Texas A & M University, College Station, Texas, 34 pp.
- Kirwan, A. D., Jr., G. McNally and J. Coehlo, 1976: Gulf Stream kinematics inferred from a satellite-tracked drifter. *J. Phys. Oceanogr.*, 6, 750-755.

- Komori, S., H. Ueda, F. Ogino, and T. Mizushima, 1983: Turbulence structure in stably stratified open-channel flow. *J. Fluid. Mech.*, 130, 13-26.
- Kullenberg, G., C. R. Murthy, and H. Westerberg, 1974: Vertical mixing characteristics in the thermocline and hypolimnion regions of Lake Ontario (IFYGL). *Proc. 17th Conf. Great Lakes Res.*, 425-434.
- Kundu, P. K., and R. C. Beardsley, 1991: Evidence of a critical Richardson number in moored measurements during the upwelling season off Northern California. *J. Geophys. Res.*, 96, 4855-4868.
- Leaman, K. D., E. Johns, and T. Rossby, 1989: The average distribution of volume transport and potential vorticity with temperature at three sections across the Gulf Stream. *J. Phys. Oceanogr.*, 19, 36-51.
- Leetma, A., and A. F. Bunker, 1978: Updated charts of the mean annual wind stress, convergences in the Ekman layers, and Sverdrup transports in the North Atlantic. *J. Mar. Res.*, 36, 311-322.
- Leetma, A., P. Niiler, and H. Stommel, 1977: Does the Sverdrup relation account for the Mid-Atlantic circulation? *J. Mar. Res.*, 35, 1-10.
- Levine E. R., D. N. Connors, P. C. Cornillon, and H. T. Rossby, 1986: Gulf Stream kinematics along an isopycnal float trajectory. *J. Phys. Oceanogr.*, 16, 1317-1328.
- Lietzke, T. A., and A. Lerman, 1975: Effects of bottom relief in two-dimensional oceanic eddy diffusion models. *Earth Planet. Sci. Letters*, 24, 337-344.
- Lovelock, J. E., 1979: *Gaia. A new look at life on earth*. Oxford University Press, Oxford, 157 pp.
- Luyten, J., and H. Stommel, 1986: Gyres driven by combined wind and buoyancy flux. *J. Phys. Oceanogr.*, 16, 1551-1560.
- Luyten, J., J. Pedlosky, and H. Stommel, 1983: The ventilated thermocline. *J. Phys. Oceanogr.*, 13, 292-309.
- Marmorino, G. O., 1987: Observations of small-scale mixing processes in the seasonal thermocline. Part II: Wave breaking. *J. Phys. Oceanogr.*, 17, 1348-1355.
- McDowell, S., P. Rhines, and T. Keffer, 1982: North Atlantic potential vorticity and its relation to the general circulation. *J. Phys. Oceanogr.*, 12, 1417-1436.
- Miles, J., 1986: Richardson's criterion for the stability of stratified shear flow. *Phys. Fluids*, 29, 3470-3471.
- Montgomery, R. B., 1937: A suggested method for representing gradient flow in isentropic surfaces. *Bull. Am. Met. Soc.*, 18, 210-212.
- Montgomery, R. B., 1938: Circulation in upper layers of Southern North Atlantic deduced with use of isentropic analysis. *Papers Phys. Oceanogr. Meteorol.*, 6, 1-55.
- Moum, J. N., and T. R. Osborn, 1986: Mixing in the main thermocline. *J. Phys. Oceanogr.*, 16, 1250-1259.
- Munk, W. H., 1950: On the wind-driven ocean circulation. *J. Meteorol.*, 7, 79-93.
- Munk, W. H., and E. R. Anderson, 1948: Notes on a theory of the thermocline. *J. Mar. Res.*, 7, 276-295.

- Nakao, T., 1977: Oceanic variability in relation to fisheries in the East China Sea and the Yellow Sea. *J. Faculty Mar. Sci. Technology*, 11, 199-367.
- Newton, C. W., 1954: Frontogenesis and frontolysis as a three-dimensional process. *J. Meteorol.*, 11, 449-461.
- Newton, C. W., 1978: Fronts and wave disturbances in Gulf Stream and atmospheric jet stream. *J. Geophys. Res.*, 83, 4697-4706.
- Niiler, P. N., and W. S. Richardson, 1973: Seasonal variability of the Florida current. *J. Mar. Res.*, 31, 144-167.
- NSF/NASA, 1989: Ocean color from space. U. S. Global Ocean Flux Study Office, Woods Hole Oceanographic Institution, Woods Hole.
- Orlanski, J., and M. D. Cox, 1973: Baroclinic instability in ocean currents. *Geophys. Fluid Dyn.*, 4, 297-332.
- Palmén, E., and C. E. Newton, 1969: *Atmospheric circulation systems*. Academic Press, New York, 603 pp.
- Parr, A. E., 1938: On the validity of the dynamic topographic method for the determination of ocean current trajectories. *J. Mar. Res.*, 1, 119-132.
- Peters, H., M. C. Gregg, and J. M. Toole, 1988: On the parameterization of equatorial turbulence. *J. Geophys. Res.*, 93, 1199-1218.
- Redfield, A. C., 1936: An ecological aspect of the Gulf Stream. *Nature*, 138, 1013.
- Reid, J. L., Jr., 1965: *Intermediate waters of the Pacific Ocean*. The Johns Hopkins Oceanographic Studies, vol. 2, Johns Hopkins University Press, Baltimore, 85 pp.
- Rhines, P. B., and W. Y. Young, 1982a: A theory of wind-driven circulation. I. Mid-ocean gyres. *J. Marine Res.*, 40, 559-596.
- Rhines, P. B., and W. Y. Young, 1982b: Homogenization of potential vorticity in planetary gyres. *J. Fluid Mech.*, 122, 347-368.
- Richards, A. F., and A. C. Redfield, 1955: Oxygen-density relationships in the western North Atlantic. *Deep-Sea Res.*, 2, 182-199.
- Richardson, P. L., J. F. Price, W. B. Owens, W. J. Schmitz, H. T. Rossby, A. M. Bradley, J. R. Valdes, and D. C. Webb, 1981: North Atlantic subtropical gyre: SOFAR floats tracked by moored listening stations. *Sci.*, 213, 435-437.
- Riley, G. A., 1951: Oxygen, phosphate and nitrate in the Atlantic Ocean. *Bull. Bingham Oceanogr. Collection*, 13, 1-125.
- Riley, G. A., 1975: Further examination of the relation between biological productivity and physical oceanographic processes in the shelf and slope waters south of Long Island. Unpublished manuscript, Brookhaven National Laboratory, 18 pp.
- Roach, W. T., 1970: On the influence of synoptic development on the production of high level turbulence. *Quart. J. R. Met. Soc.*, 96, 413-429.
- Roemmich, D., and C. Wunsch, 1985: Two transatlantic sections: meridional circulation and heat flux in the subtropical North Atlantic Ocean. *Deep-Sea Res.*, 32, 619-644.
- Rossby, C. G., 1936: Dynamics of steady ocean currents in the light of experimen-

- tal fluid mechanics. *Papers Phys. Oceanogr. Meteorol.*, 5, 1-43.
- Rossby, C. G., 1951: On the vertical and horizontal concentration of momentum in air and ocean currents. *Tellus*, 3, 15-27.
- Rossby, H. T., E. R. Levine, and D. N. Connors, 1985: The isopycnal Swallow float - A simple device for tracking water parcels in the ocean. *Progress Oceanogr.*, 14, 511-525.
- Sarmiento, J. L., 1983: A tritium box model of the North Atlantic thermocline. *J. Phys. Oceanogr.*, 13, 1269-1274.
- Sarmiento, J. L., H. W. Feely, W. S. Moore, A. E. Bainbridge, and W. S. Broecker, 1976: The relationship between vertical eddy diffusion and buoyancy gradient in the deep sea. *Earth Planet. Sci. Lett.*, 32, 357-370.
- Sarmiento, J. L., C. G. Rooth, and W. Roether, 1982: The North Atlantic tritium distribution in 1972. *J. Geophys. Res.*, 87, 8047-8056.
- Schlitzer, R., 1988: Modeling the nutrient and carbon cycles of the North Atlantic. 1. Circulation, mixing coefficients and heat fluxes. *J. Geophys. Res.*, 93, 10699-10723.
- Schlitzer, R., 1988: Modeling the nutrient and carbon cycles of the North Atlantic. 2. New production, particle fluxes, CO_2 gas exchange, and the role of organic nutrients. *J. Geophys. Res.*, 94, 12781-12794.
- Seiwell, H. R., 1934: The distribution of oxygen in the western basin of the North Atlantic. *Pap. Phys. Oceanogr. Meteor.*, 3, 1-86.
- Shapiro, M. A., 1976: The role of turbulent heat flux in the generation of potential vorticity in the vicinity of upper-level jet stream systems. *Mon. Wea. Rev.*, 104, 892-906.
- Shapiro, M. A., 1978: Further evidence of the mesoscale and turbulent structure of upper level jet stream-frontal zone system. *Mon. Wea. Rev.*, 106, 1100-1111.
- Shaw, P. T., and H. T. Rossby, 1984: Towards a Lagrangian description of the Gulf Stream. *J. Phys. Oceanogr.*, 14, 528-540.
- Smethie, W. M., Jr., 1980: Estimation of vertical mixing rates in fjords using naturally occurring Radon-222 and salinity as tracers. *Fjord oceanography*, H. J. Freeland, D. M. Framer and C. D. Levings (eds.), Plenum Press, New York, 241-249.
- Spain, P., F., D. L. Dorson, and H. T. Rossby, 1981: PEGASUS: A simple, acoustically-tracked velocity profiler. *Deep-Sea Res.*, 228, 1553-1567.
- Staley, D. O., 1960: Evaluation of potential-vorticity changes near the tropopause and the related vertical motions, vertical advection of vorticity, and transfer of radioactive debris from stratosphere to troposphere. *J. Meteor.*, 17, 591-620.
- Stefánsson, U., and L. P. Atkinson, 1971: Nutrient-density relationships in the western North Atlantic between Cape Lookout and Bermuda. *Limnol. Oceanogr.*, 16, 51-59.
- Stommel, H., 1948: The westward intensification of wind-driven ocean currents. *Trans. Am. Geophys. Union*, 99, 202-206.
- Stommel, H., 1958: *The Gulf Stream: a physical and dynamical description*. Uni-

- versity of California Press, Berkeley, and Cambridge University Press, London, 202 pp.
- Stommel, H., 1965: *The Gulf Stream: a physical and dynamical description*. 2nd ed., University of California Press, Berkeley, and Cambridge University Press, London, 248 pp.
- Stommel, H., 1979: Determination of water mass properties of water pumped down from the Ekman layer to the geostrophic flow below. *Proc. Natl. Acad. Sci. USA*, 76, 3051-3055.
- Stommel, H., and F. Schott, 1977: The beta spiral and the determination of the absolute velocity field from hydrographic station data. *Deep-Sea Res.*, 24, 325-329.
- Stommel, H., and K. Yoshida (eds.), 1972: *Kuroshio: its physical aspects*. University of Tokyo Press, Tokyo, 517 pp.
- Stommel, H., P. Niiler, and D. Anati, 1978: Dynamic topography and recirculation of the North Atlantic. *J. Mar. Res.*, 36, 449-468.
- Svensson, T., 1980: Tracer measurement of mixing in the deep water of a small stratified sill fjord. In *Fjord oceanography*, H. J. Freeland, D. M. Framer and C. D. Levings (eds.), Plenum Press, New York, 233-240.
- Thiele, G., and J. L. Sarmiento, 1990: Tracer dating and ocean ventilation. *J. Geophys. Res.*, 95, 9377-9391.
- Thorpe, S. A., 1973: Experiments on instability and turbulence in a stratified shear flow. *J. Fluid Mech.*, 61, 731-751.
- Thorpe, S. A., 1987: Transitional phenomena and the development of turbulence in stratified fluids: A review. *J. Geophys. Res.*, 92, 5231-5248.
- Toole, J. M., and R. W. Schmitt, 1987: Small-scale structures in the north-west Atlantic sub-tropical front. *Nature*, 327, 47-49.
- Toole, J. M., H. Peters, and M. C. Gregg, 1987: Upper ocean shear and density variability at the equator during Tropic Heat. *J. Phys. Oceanogr.*, 17, 1397-1406.
- Tsuchiya, M., 1968: *Upper waters of the intertropical Pacific Ocean*. The Johns Hopkins Oceanographic Studies, vol. 4, Johns Hopkins University Press, Baltimore, 50 pp.
- Turner, J. S., 1973: *Buoyancy effects in fluids*. Cambridge University Press, Cambridge, 367 pp.
- Turner, J. S., 1986: Turbulent entrainment: the development of the entrainment assumption, and its application to geophysical flows. *J. Fluid Mech.*, 173, 431-471.
- Ueda, H., S. Mitsumoto, and S. Komori, 1981: Buoyancy effects on the turbulent transport processes in the lower atmosphere. *Quart. J. R. Met. Soc.*, 107, 561-578.
- Veronis, G., 1969: On theoretical models of the thermohaline circulation. *Deep-Sea Res.*, 16 (Suppl.), 301-323.
- Veronis, G., 1988: Circulation driven by winds and surface cooling. *J. Phys. Oceanogr.*, 18, 1920-1932.

- von Arx, W. S., 1962: *An introduction of physical oceanography*. Addison-Wesley, London.
- Walsh, J. J., D. A. Dieterle, and M. B. Meyers, 1988: A simulation analysis of the fate of phytoplankton within the Mid-Atlantic Bight. *Cont. Shelf Res.*, 8, 757-787.
- Watts, D. R., 1983: Gulf Stream variability. In *Eddies in marine science*, A. R. Robinson (ed.), SpringerVerlag, Berlin, 114-144.
- Welander, P., 1959: An advective model of the ocean thermocline. *Tellus*, 11, 309-318.
- Worthington, L. V., 1954: Three detailed cross-sections of the Gulf Stream. *Tellus*, 6, 116-123.
- Worthington, L. V., 1976: *On the North Atlantic circulation*. The Johns Hopkins Oceanographic Studies, vol. 6, Johns Hopkins University Press, Baltimore, 110 pp.
- Wunsch, C., 1978: The North Atlantic general circulation west of 50°W determined by inverse methods. *Rev. Geophys. Space Physics*, 16, 583-620.
- Wyrtki, K., 1981: An estimate of equatorial upwelling in the Pacific. *J. Phys. Oceanogr.*, 11, 1205-1214.
- Yentsch, C. S., 1974: The influence of geostrophy on primary production. *Tethys*, 6, 111-118.
- Yoder, J. A., L. A. Atkinson, S. S. Bishop, E. E. Hofmann, and T. N. Lee, 1983: Effect of upwelling on phytoplankton productivity of the outer southeastern United States continental shelf. *Cont. Shelf Res.*, 1, 385-404.
- Zilitinkevich, S. S., D. K. Chalikov, and Yu. D. Resnyanskiy, 1979: Modelling the oceanic upper layer. *Oceanol. Acta*, 2, 219-240.

Autobiographical Statement

José Luis Pelegrí Llopart

Personal Data

I was born on November 12, 1957, in Caracas, Venezuela. My parents are Catalan, hence I have both Spanish and Venezuelan nationalities. I married Mónica García Pérez in 1983, we have two daughters, Ana and Laura.

Formal Education

M.Sc. Oceanography, December 1984, Oregon State University, Corvallis, U.S.A.

M.Sc. Physical Oceanography, June 1980, University of Wales, Bangor, Great Britain.

Licenciatura Physics, June 1978, Universidad Simón Bolívar, Caracas, Venezuela.

Publications

Pelegrí, J. L., and G. T. Csanady, 1992: Diapycnal mixing in western boundary currents. Submitted to *J. Geophys. Res.*

Pelegrí, J. L., and J. R. Richman, 1992: On the role of shear mixing during transient coastal upwelling. *Cont. Shelf. Res.*, in press.

Pelegrí, J. L., and G. T. Csanady, 1991: Nutrient transport and mixing in the Gulf Stream. *J. Geophys. Res.*, 96, 2577-2583.

Pelegrí, J. L., 1988: Tidal fronts in estuaries. *Estuar. Coastal Shelf Sci.*, 27, 45-60.

Pelegrí, J. L., and P. Masciángoli, 1987: Método analítico para la determinación de la marea en canales. *Rev. Tec. Intevep*, 7, 59-68.

Pelegrí, J. L., 1986: Simulación numérica de afloramientos costeros. In "II Simposio sobre Aplicaciones del Método de los Elementos Finitos en Ingeniería", Barcelona, Spain, 3, B85-B100.

Villoria, C., J. L. Pelegrí, and P. Masciángoli, 1986: Operational Experiences and Innovations in the Venezuelan Oil Industry Oceanographic and Meteorological Data Gathering Program. In: "International Symposium for Marine Data Systems 1986", New Orleans, U.S.A., 232-238.

Pelegrí, J. L., and D. Padrón, 1986: Algunas características del régimen de corrientes en la plataforma continental al norte de la Península de Paria. *Bol. Inst. Oceanogr. Venezuela Univ. Oriente*, 26, 35-53.

Pelegrí, J. L., and R. G. Avila, 1986: Las mareas como sistemas cooscilantes en los Golfos de Venezuela y Paria. *Rev. Tec. Intevep*, 6, 1-15.

Cooper, C., G. F. Ortega, and J. L. Pelegrí, 1981: Numerical solution of currents generated by hurricanes. *Rev. Tec. Intevep*, 1, 9-18.

Communications and Reports

11 communications (abstract or unpublished paper) at meetings and 20 technical reports.

Appointments and Positions

Graduate Research Assistant, Old Dominion Univ. (since 12-88).

Oceanographer, Inst. Tecnol. Venezolano Petróleo, Venezuela (06-80 to 10-88).

Oceanography Instructor, Inst. Univ. Tecnol. Mar, Venezuela (01-80 to 05-80).

Memberships

American Geophysical Union, American Meteorological Society.